NASA Technical Paper 1074

A Design Handbook for Phase Change Thermal Control and Energy Storage Devices

William R. Humphries
George C. Marshall Space Flight Center
Marshall Space Flight Center, Alabama
and
Edwin I. Griggs
Tennessee Technological University
Cookeville, Tennessee

National Aeronautics
and Space Administration
Scientific and Technical Information Office
1977

ACKNOWLEDGMENTS

The authors wish to recognize a number of contributors whose aid was instrumental in completing this work. Dr. John Bailey of North Carolina State University is due a special debt of gratitude for his extensive efforts in paraffin properties investigations, excerpts of which are given in Section II. Dr. Donald Pitts of Tennessee Technological University is due special recognition for his work during two summers at the Marsnail Space Flight Center, under the auspices of the American Society for Engineering Education. During this period he made valuable contributions to verification of nondimensional computer modeling and contributed to parametric studies given in Section IV. In addition, a number of graduate students at Tennessee Technolcgical University contributed to certain phases of this work, particularly to the large body of computer runs required to amass the data given in Section IV.

It should be noted that the entire study was made possible by sustaining research funds supplied by the Marshall Space Flight Center of the National Aeronautics and Space Administration through basic research and Skylab project funding and later by funds supplied from the Energy Research and Development Administration via the Solar Heating and Cooling Program Office of the Marshall Space Flight Center.

TABLE OF CONTENTS

		Page
I.	INTRODUCTION	1
	A. Definition	1
	B. Applications	2
	C. Phase Change Material	2
	D. Scope of Study	5
II.	PROPERTY DATA	6
	A. Sources, Availability, and Estimated Cost of Selected Paraffins	6
	B. Melting and Transition Temperatures	10
	C. Heat of Fusion and Heat of Transition	10
	D. Specific Heat	10
	E. Density	20
	F. Thermal Conductivity	20
	G. Viscosity	29
	H. Surface Tension	29
	I. Coefficient of Expansion	29
III.	TWO-DIMENSIONAL ANALYSIS OF A PHASE CHANGE DEVICE	37
	A. Introduction	37
	B. Physical Model	40
	C. Differential Formulation	43
	D. Finite Difference Formulation	47
IV.	GENERAL PARAMETRIC STUDY	62
	A. Introduction	62
	B. Scope and Definitions	62
	C. Results	65
	D. Examples	142
V.	RELATED TOPICS	146
	A. Filler	146
	B. Convection	148
	C. Example Application with a Nonuniform Thermal Boundary Condition	159
	APPENDIX A – PROPERTY APPENDIX	167
	APPENDIX B – THERMAL RESISTANCE VARIATION	192

TABLE OF CONTENTS (Concluded)

	Page
APPENDIX C – COMPUTER PROGRAM FOR EXAMPLE DESCRIBED IN SECTION V	197
APPENDIX D – COMPUTER PROGRAM USED TO FACILITATE THE EXPLICIT NUMERICAL STUDY	206
REFERENCES	233

LIST OF ILLUSTRATIONS

Figure	Title	Page
1.	Responses of a phase change device	3
2.	A phase change device	4
3.	Correlation of phase change temperature with number of carbon atoms in the chain	14
4.	Correlation of heat of fusion with number of carbon atoms in the chain	16
5.	Correlation of heat of transition with number of carbon atoms in the chain	17
6.	Example illustrating effect of composition of heats of phase change for hexadecane-octadecane binary system	17
7.	Specific heat versus temperature for $C_{11}H_{24}$, $C_{12}H_{26}$, and $C_{13}H_{28}$	18
8.	Specific heat versus temperature for $C_{14}H_{30}$, $C_{15}H_{32}$, and $C_{16}H_{34}$	19
9.	Specific heat versus temperature for $C_{25}H_{52}$	20
10.	Specific heat of tetradecane ($C_{14}H_{30}$)	21
11.	Specific heat of hexadecane ($C_{16}H_{34}$)	22
12.	Specific heat of octadecane ($C_{18}H_{38}$)	23
13.	Specific heat of eicosane ($C_{20}H_{42}$)	24
14.	Liquid phase density of several paraffins	26
15.	Density of tetradecane ($C_{14}H_{30}$)	27
16.	Density of hexadecane ($C_{16}H_{34}$)	27
17.	Density of octadecane ($C_{18}H_{38}$)	28
18.	Density of eicosane ($C_{20}H_{42}$)	28
19.	Thermal conductivity of tetradecane ($C_{14}H_{30}$)	30

LIST OF ILLUSTRATIONS (Continued)

Figure	Title	Page
20.	Thermal conductivity of hexadecane ($C_{16}H_{34}$)	31
21.	Thermal conductivity of octadecane ($C_{18}H_{38}$)	32
22.	Thermal conductivity of eicosane ($C_{20}H_{42}$) extrapolated from data for lower carbon number paraffins	33
23.	Correlation of thermal conductivity data for normal paraffins (C_nH_{2n+2})	34
24.	Absolute viscosity of paraffins $C_{11}H_{24}$ through $C_{20}H_{42}$ versus temperature	35
25.	Surface tension for $C_{11}H_{24}$ through $C_{20}H_{42}$	36
26.	General designations for nodes and connecting conductances	38
27.	Phase change device application selected for study	40
28.	Typical single cell of phase change device	41
29.	Symmetrical half-cell used in analysis	42
30.	Coordinate system and dimensions for fin	44
31.	Coordinate system and dimensions for base	45
32.	Nodal grid designation	47
33.	Latent energy storage per unit base area versus fin height for fin thickness of 0.0127 cm (0.005 in.)	66
34.	Latent energy storage per unit base area versus fin height for fin thickness of 0.0508 cm (0.02 in.)	67
35.	Latent energy storage per unit base area versus fin height for fin thickness of 0.127 cm (0.05 in.)	68
36.	Base temperature rise at the termination of melting versus W for H = 1.26 cm (0.5 in.) and S_2 = 0.127 cm (0.05 in.)	69
37.	Base temperature rise of the termination at melting versus W for H = 2.54 cm (1.0 in.) and S_2 = 0.127 cm (0.05 in.)	70

LIST OF ILLUSTRATIONS (Continued)

Figure	Title	Page
38.	Base temperature rise at the termination of melting versus W for H = 5.08 cm (2.0 in.) and S_2 = 0.127 cm (0.05 in.)	71
39.	Base temperature rise at the termination of melting versus W for H = 10.16 cm (4.0 in.) and S_2 = 0.127 cm (0.05 in.)	72
40.	Base temperature rise at the termination of melting versus W for H = 20.32 cm (8.0 in.) and S_2 = 0.127 cm (0.05 in.)	73
41.	Base temperature rise at the termination of melting versus W for H = 1.27 cm (0.5 in.) and S_2 = 0.0508 cm (0.02 in.)	74
42.	Base temperature rise at termination of melting versus W for H = 2.54 cm (1.0 in.) and S_2 = 0.0508 cm (0.02 in.)	75
43.	Base temperature rise at termination of melting versus W for H = 5.08 cm (2.0 in.) and S_2 = 0.0508 cm (0.02 in.)	76
44.	Base temperature rise at termination of melting versus W for H = 10.16 cm (4.0 in.) and S_2 = 0.0508 cm (0.02 in.)	77
45.	Base temperature rise at termination of melting versus W for H = 20.32 cm (8.0 in.) and S_2 = 0.0508 cm (0.02 in.)	78
46.	Base temperature rise at termination of melting versus W for H = 1.27 cm (0.5 in.) and S_2 = 0.0127 cm (0.005 in.)	79
47.	Base temperature rise at termination of melting versus W for H = 2.54 cm (1.0 in.) and S_2 = 0.0127 cm (0.005 in.)	80
48.	Base temperature rise at termination of melting versus W for H = 5.08 cm (2.0 in.) and S_2 = 0.0127 cm (0.005 in.)	81
49.	Base temperature rise at termination of melting versus W for H = 10.16 cm (4.0 in.) and S_2 = 0.0127 cm (0.005 in.)	82
50.	Base temperature rise at termination of melting versus W for H = 20.32 cm (8.0 in.) and S_2 = 0.0127 cm (0.005 in.)	83
51.	Base temperature rise at the termination of melting versus H' for $\dot{q}''$ = 1076.4 J/s-m^2 (341.4 Btu/h-ft^2) and S_2 = 0.0127 cm (0.005 in.)	84

LIST OF ILLUSTRATIONS (Continued)

Figure	Title	Page
52.	Base temperature rise at the termination of melting versus H for $\dot{q}'' = 1076.4$ J/s-m^2 (341.4 Btu/h-ft^2) and $S_2 = 0.0508$ cm (0.020 in.)	85
53.	Base temperature rise at the termination of melting versus H for $\dot{q}'' = 1076.4$ J/s-m^2 (341.4 Btu/h-ft^2) and $S_2 = 0.127$ cm (0.050 in.)	86
54.	Base temperature rise at the termination of melting versus H for $\dot{q}'' = 2152.8$ J/s-m^2 (682.9 Btu/h-ft^2) and $S_2 = 0.0127$ cm (0.005 in.)	87
55.	Base temperature rise at the termination of melting versus H for $\dot{q}'' = 2152.8$ J/s-m^2 (682.9 Btu/h-ft^2) and $S_2 = 0.0508$ cm (0.020 in.)	88
56.	Base temperature rise at the termination of melting versus H for $\dot{q}'' = 2152.8$ J/s-m^2 (682.9 Btu/h-ft^2) and $S_2 = 0.127$ cm (0.05 in.)	89
57.	Base temperature rise at the termination of melting versus H for $\dot{q}'' = 4305.6$ J/s-m^2 (1365.7 Btu/h-ft^2) and $S_2 = 0.0127$ cm (0.005 in.)	90
58.	Base temperature rise at the termination of melting versus H for $\dot{q}'' = 4305.6$ J/s-m^2 (1365.7 Btu/h-ft^2) and $S_2 = 0.0508$ cm (0.020 in.)	91
59.	Base temperature rise at the termination of melting versus H for $\dot{q}'' = 4305.6$ J/s-m^2 (1365.7 Btu/h-ft^2) and $S_2 = 0.127$ cm (0.050 in.)	92
60.	Base temperature rise at the termination of melting versus H for $\dot{q}'' = 6458.3$ J/s-m^2 (2048.6 Btu/h-ft^2) and $S_2 = 0.0127$ cm (0.005 in.)	93
61.	Base temperature rise at the termination of melting versus H for $\dot{q}'' = 6458.3$ J/s-m^2 (2048.6 Btu/h-ft^2) and $S_2 = 0.0508$ cm (0.020 in.)	94
62.	Base temperature rise at the termination of melting versus H for $\dot{q}'' = 6458.3$ J/s-m^2 (2048.6 Btu/h-ft^2) and $S_2 = 0.127$ cm (0.050 in.)	95

LIST OF ILLUSTRATIONS (Continued)

Figure	Title	Page
63.	Transient base temperature rise versus fraction of PCM melted for H = 1.27 cm (0.5 in.) and S_2 = 0.0127 cm (0.005 in.)	97
64.	Transient base temperature rise versus fraction of PCM melted for H = 1.27 cm (0.5 in.) and S_2 = 0.0508 cm (0.020 in.)	98
65.	Transient base temperature rise versus fraction of PCM melted for H = 1.27 cm (0.5 in.) and S_2 = 0.127 cm (0.05 in.)	99
66.	Transient base temperature rise versus fraction of PCM melted for H = 2.54 cm (1 in.) and S_2 = 0.0127 cm (0.005 in.)	100
67.	Transient base temperature rise versus fraction of PCM melted for H = 2.54 cm (1 in.) and S_2 = 0.0508 cm (0.020 in.)	101
68.	Transient base temperature rise versus fraction of PCM melted for H = 2.54 cm (1 in.) and S_2 = 0.127 cm (0.05 in.)	102
69.	Transient base temperature rise versus fraction of PCM melted for H = 5.08 cm (2 in.) and S_2 = 0.0127 cm (0.005 in.)	103
70.	Transient base temperature rise versus fraction of PCM melted for H = 5.08 cm (2 in.) and S_2 = 0.0508 cm (0.02 in.)	104
71.	Transient base temperature rise versus fraction of PCM melted for H = 5.08 cm (2 in.) and S_2 = 0.127 cm (0.05 in.)	105
72.	Transient base temperature rise versus fraction of PCM melted for H = 10.16 cm (4 in.) and S_2 = 0.0127 cm (0.005 in.)	106
73.	Transient base temperature rise versus fraction of PCM melted for H = 10.16 cm (4 in.) and S_2 = 0.0508 cm (0.02 in.)	107
74.	Transient base temperature rise versus fraction of PCM melted for H = 10.16 cm (4 in.) and S_2 = 0.127 cm (0.05 in.)	108
75.	Transient base temperature rise versus fraction of PCM melted for H = 20.32 cm (8 in.) and S_2 = 0.0127 cm (0.005 in.)	109
76.	Transient base temperature rise versus fraction of PCM melted for H = 20.32 cm (8 in.) and S_2 = 0.0508 cm (0.02 in.)	110

LIST OF ILLUSTRATIONS (Continued)

Figure	Title	Page
77.	Transient base temperature rise versus fraction of PCM melted for H = 20.32 cm (8 in.) and S_2 = 0.127 cm (0.05 in.)	111
78.	Time required for PCM to melt for $\dot{q}''$ = 1076.4 J/s-m^2 (341.4 Btu/h-ft^2) and S_2 = 0.0127 cm (0.005 in.)	112
79.	Time required for PCM to melt for $\dot{q}''$ = 1076.4 J/s-m^2 (341.4 Btu/h-ft^2) and S_2 = 0.0508 cm (0.02 in.)	113
80.	Time required for PCM to melt for $\dot{q}''$ = 1076.4 J/s-m^2 (341.4 Btu/h-ft^2) and S_2 = 0.127 cm (0.05 in.)	114
81.	Time required for PCM to melt for $\dot{q}''$ = 2152.8 J/s-m^2 (682.9 Btu/h-ft^2) and S_2 = 0.0127 cm (0.005 in.)	115
82.	Time required for PCM to melt for $\dot{q}''$ = 2152.8 J/s-m^2 (682.9 Btu/h-ft^2) and S_2 = 0.0508 cm (0.02 in.)	116
83.	Time required for PCM to melt for $\dot{q}''$ = 2152.8 J/s-m^2 (682.9 Btu/h-ft^2) and S_2 = 0.127 cm (0.05 in.)	117
84.	Time required for PCM to melt for $\dot{q}''$ = 4305.6 J/s-m^2 (1365.7 Btu/h-ft^2) and S_2 = 0.0127 cm (0.005 in.)	118
85.	Time required for PCM to melt for $\dot{q}''$ = 4305.6 J/s-m^2 (341.4 Btu/h-ft^2) and S_2 = 0.0508 cm (0.02 in.)	119
86.	Time required for PCM to melt and $\dot{q}''$ = 4305.6 J/s-m^2 (1365.7 Btu/h-ft^2) and S_2 = 0.127 cm (0.05 in.)	120
87.	Time required for PCM to melt for $\dot{q}''$ = 6458.3 J/s-m^2 (2048.6 Btu/h-ft^2) and S_2 = 0.0127 cm (0.005 in.)	121
88.	Time required for PCM to melt for $\dot{q}''$ = 6458.3 J/s-m^2 (2048.6 Btu/h-ft^2) and S_2 = 0.0508 cm (0.02 in.)	122
89.	Time required for PCM to melt for $\dot{q}''$ = 6458.3 J/s-m^2 (2048.6 Btu/h-ft^2) and S_2 = 0.127 cm (0.05 in.)	123
90.	Energy ratio versus heat flux density for W = 0.127 cm (0.05 in.) and S_2 = 0.0127 cm (0.005 in.)	124

LIST OF ILLUSTRATIONS (Continued)

Figure	Title	Page
91.	Energy ratio versus heat flux density for W = 0.127 cm (0.05 in.) and S_2 = 0.0508 cm (0.02 in.)	125
92.	Energy ratio versus heat flux density for W = 0.127 cm (0.05 in.) and S_2 = 0.127 cm (0.05 in.)	126
93.	Energy ratio versus heat flux density for W = 0.254 cm (0.1 in.) and S_2 = 0.0127 cm (0.005 in.)	127
94.	Energy ratio versus heat flux density for W = 0.254 cm (0.1 in.) and S_2 = 0.0508 cm (0.02 in.)	128
95.	Energy ratio versus heat flux density for W = 0.254 cm (0.1 in.) and S_2 = 0.127 cm (0.05 in.)	129
96.	Energy ratio versus heat flux density for W = 0.508 cm (0.2 in.) and S_2 = 0.0127 cm (0.005 in.)	130
97.	Energy ratio versus heat flux density for W = 0.508 cm (0.2 in.) and S_2 = 0.0508 cm (0.02 in.)	131
98.	Energy ratio versus heat flux density for W = 0.508 cm (0.2 in.) and S_2 = 0.127 cm (0.05 in.)	132
99.	Energy ratio versus heat flux density for W = 1.016 cm (0.4 in.) and S_2 = 0.0127 cm (0.005 in.)	133
100.	Energy ratio versus heat flux density for W = 1.016 cm (0.4 in.) and S_2 = 0.0508 cm (0.02 in.)	134
101.	Energy ratio versus heat flux density for W = 1.016 cm (0.4 in.) and S_2 = 0.127 cm (0.05 in.)	135
102.	Energy ratio versus heat flux density for W = 2.032 cm (0.8 in.) and S_2 = 0.0127 cm (0.005 in.)	136
103.	Energy ratio versus heat flux density for W = 2.032 cm (0.8 in.) and S_2 = 0.0508 cm (0.02 in.)	137
104.	Energy ratio versus heat flux density for W = 2.032 cm (0.8 in.) and S_2 = 0.127 cm (0.05 in.)	137

LIST OF ILLUSTRATIONS (Continued)

Figure	Title	Page
105.	Base temperature rise versus W for three different fusion temperatures and H = 1.27 cm (0.5 in.) and S_2 = 0.127 cm (0.05 in.)	139
106.	Base temperature rise versus W for three different fusion temperatures and H = 2.54 cm (1.0 in.) and S_2 = 0.127 cm (0.05 in.)	140
107.	Base temperature rise versus W for three different fusion temperatures and H = 5.08 cm (2.0 in.) and S_2 = 0.127 cm (0.05 in.)	141
108.	Silveston's experimental results in the neighborhood of instability in various liquids	149
109.	Region of influence of L/d on heat transfer	149
110.	Surface tension convection patterns	150
111.	Volume change driven flow patterns	152
112.	Heat transfer characteristics of Bénard cells	154
113.	Zero-g ullage configurations	155
114.	Comparison between predicted and measured fusion front location for an example melt run	158
115.	Physical model for heat transfer between a phase change device and a flowing fluid	161
116.	Nodal pattern for calculating bulk temperature of flowing fluid	163
117.	Example exit temperature variations for a sinusoidal temperature at inlet	165
B-1.	Physical model	192
B-2.	Simplified thermal network	193
B-3.	Variation of equivalent thermal resistance with height for a fin thickness of 0.0127 cm (0.005 in.)	194

LIST OF ILLUSTRATIONS (Concluded)

Figure	Title	Page
B-4.	Variation of equivalent thermal resistance with height for a fin thickness of 0.0508 cm (0.02 in.)	195
B-5.	Variation of equivalent thermal resistance with height for a fin thickness of 0.127 cm (0.05 in.)	196
D-1.	Skelton flow chart	224

LIST OF TABLES

Table	Title	Page
1.	Potential Suppliers of Selected Paraffins	7
2.	Capabilities of Potential Suppliers of Selected Paraffins	8
3.	Some Approximate Price Data for Selected Paraffins	9
4.	Melting and Transition Data for the Paraffins (C_nH_{2n+2}) Containing Eleven Through Thirty Carbon Atoms	11
5.	Fusion Temperature for Selected Paraffins	12
6.	Transition Temperatures for Certain Paraffins	13
7.	Comparison of Heat of Fusion for Several Grades of Selected Paraffins	15
8.	Comparison of Heat of Transition for Several Grades of Selected Paraffins	16
9.	Specific Heat Data for Certain Paraffins	25
10.	Thermal Conductivity of Selected Paraffins	29
11.	Volumetric Coefficient of Expansion (60°F/15.6°C)	37
12.	Computer Program for Base Exposed to a Constant Heat Flux Density	52
13.	Computer Program for Base Exposed to a Step Increase in Temperature	57
14.	PCM and Metal Properties Used in Computations	64
15.	Values of Geometric Variables and Heat Flux Density Chosen for the Numerical Study	64
16.	Some Reported Thermal Conductivity Values for the Solid Phase of Certain Paraffins in W/m-°C (Btu/h-ft-°F)	160

LIST OF TABLES (Continued)

Table	Title	Page
A-1.	Fusible Materials with a Heat of Fusion Greater than 185.96 kJ/kg (80 Btu/lb) Listed in Order of Increasing Melt Temperature from 4.4 to 65°C (40 to 150°F)	169
A-2.	Comparisons of Fusion Properties and Melt Temperature of Selected PCM's Reported in Reference 56	171
A-3.	Properties of Six PCM's Studied in Reference 57 with a Fusion Temperature Between 273 and 373 K	172
A-4.	Melt Temperatures of Fifteen Low Temperature PCM Candidates	173
A-5.	Four Low Temperature PCM's Recommended in Reference 57	174
A-6.	PCM's Used in Tests Reported in Reference 58	175
A-7.	Comparative Data on Waxes and Inorganic Hydrates	176
A-8.	Melting Temperature of Some Mixtures Investigated for Air Conditioning Thermal Energy Storage	177
A-9.	Melting Temperature and Heat of Fusion of Inorganic Salt Hydrates	178
A-10.	Melting Point, Heat of Fusion, and Latent Heat Density of Some Inorganic Hydrates	180
A-11.	Melting Temperature and Heat of Fusion of Some Inorganic Hydrate Eutectics	181
A-12.	Calorimetric Data for Some Organic Thermal Energy Storage Materials for Solar Heating	182
A-13.	Melting Temperature and Heat of Fusion of Organic Materials for Air Conditioning-Hydrocarbons and Halogenated Hydrocarbons	183
A-14.	Melting Point and Heat of Fusion for Some Organic Eutectics	184
A-15.	Melting Temperature and Heat of Fusion for Some Acetamide-Organic Eutectics and Compounds	185

LIST OF TABLES (Concluded)

Table	Title	Page
A-16.	PCM Data for Some Alcohols, Phenols, Aldehydes, Ketones, and Ethers	186
A-17.	PCM Data for Organic Acids and Miscellaneous Organics	187
A-18.	Calorimetric Data for Air Conditioning Organic Materials	188
A-19.	Melting Point and Heat of Fusion for Clathrates and Semi-Clathrates Melting Congruently Above 0°C (32°F)	189
A-20.	Melting Point for Organic-Inorganic Eutectics	190
C-1.	Computer Program Used to Compute Fluid Temperature Variation as it Flows Through a Phase Change Device	198
C-2.	Required Input Data for the Program Listed in Table C-1	203
C-3.	Description of Output Data from Program Listed in Table C-1	205

A DESIGN HANDBOOK FOR PHASE CHANGE THERMAL CONTROL AND ENERGY STORAGE DEVICES

I. INTRODUCTION

A. Definition

Phase change thermal control devices have been discussed extensively in the literature. These articles often refer to a device of this type by different names such as thermal capacitor, thermal flywheel, heat of fusion device, latent heat device, and fusible mass device. However, all these terms refer to a component which is used to either thermally control a medium or store energy by utilizing a material which undergoes a change of phase.

There are a number of phase change transformation classes given by Lorsch [1] as

- Solid-liquid transformations (melting/freezing) (e.g., melting or freezing of ice or water)
- Liquid-gas transformations (vaporization) (e.g., boiling of water)
- Solid-gas transformations (sublimation) (e.g., sublimation of solid carbon dioxide at atmospheric pressure, "dry ice")
- Solid-solid transformations (e.g., transition of the rhombic form of sulfur to the monoclinic form)
- Liquid-liquid transformations (e.g., the transformation occurring when two liquids are immisible such as water and phenol).

Very little energy is released or absorbed by liquid-liquid transformations, and it is questionable whether this is a true class of phase change. The liquid-liquid transformation is neglected in the remainder of this work. Liquid-gas and solid-gas transformation classes have large volume changes associated with them, a feature which requires heavy and complicated pressure vessels or special design features, such as internal bellows. For this reason, they also are not considered herein. Solid-liquid transformations are of great importance because most classes of materials undergo this type of transformation without exhibiting large volume changes while releasing or absorbing relatively large quantities of energy. The fourth transformation is also of interest because the energy exchange can be significant and a number of materials display this phenomenon in a temperature range near their melting point. Consequently, for the purpose of this document, phase change processes are limited to solid-liquid and solid-solid transformations.

B. Applications

There are a number of uses to which phase change devices have been applied. Some of these are:

- Thermal damping of oscillatory outputs (e.g., Skylab space radiator fluid outlet)
- Inhibition of thermal excursions (e.g., Lunar Roving Vehicle drive control electronics)
- Maintaining constant temperature (e.g., Pegasus III coating experiment-thermocouple reference)
- Energy storage (e.g., solar heating and cooling energy storage such as illustrated by the MIT house application)
- Control mechanisms (e.g., Skylab 40°F vernatherm valve)
- Temperature indication (e.g., mushroom thaw warning indicator).

Brief descriptions of most of these applications through 1973 are given by Humphries [2]. Figure 1 depicts thermal responses for the first three applications.

Typically, a phase change device is passive with no moving parts, consisting of an external housing and the phase change material (PCM), with or without interspersed filler material (Fig. 2). Usually this device is in intimate thermal contact with the medium which it is thermally controlling. Although shown in a simplified form, this device can be applied in an almost infinite number of geometrical configurations with a myriad of different filler configurations.

C. Phase Change Material

Studies have shown that to qualify as a good PCM the material should possess the following characteristics:

- High heat of fusion per unit mass and volume
- Proper melting point (or range).

Other property requisites, but not requirements, for a good PCM are:

- High thermal diffusivity
- High coefficient of thermal conductivity

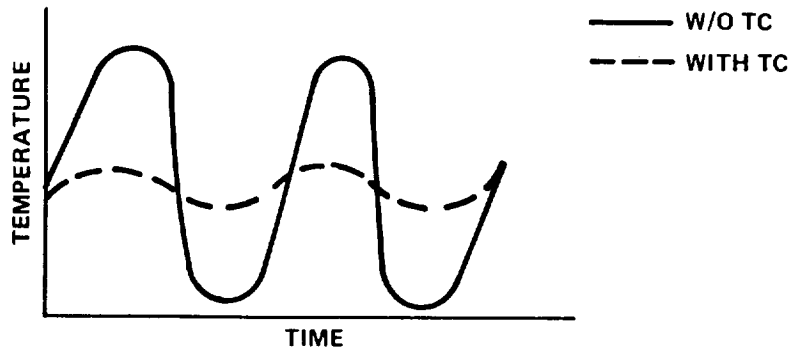

a. THERMAL DAMPING OF OSCILLATORY OUTPUTS

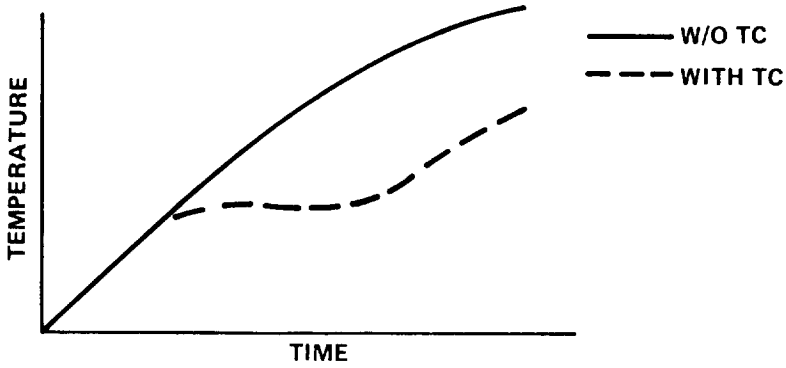

b. INHIBITING THERMAL EXCURSIONS

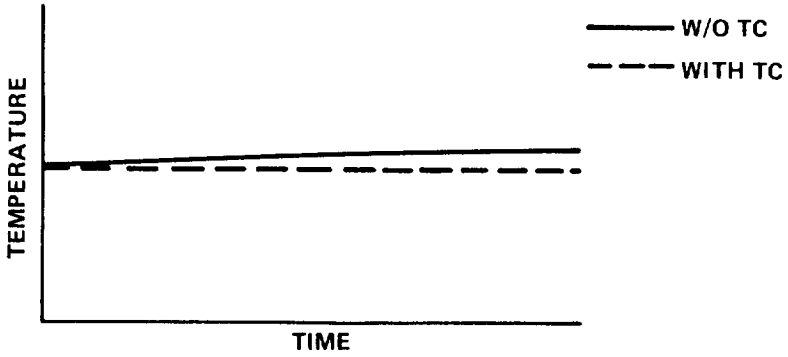

c. MAINTAINING CONSTANT TEMPERATURE

Figure 1. Responses of a phase change device.

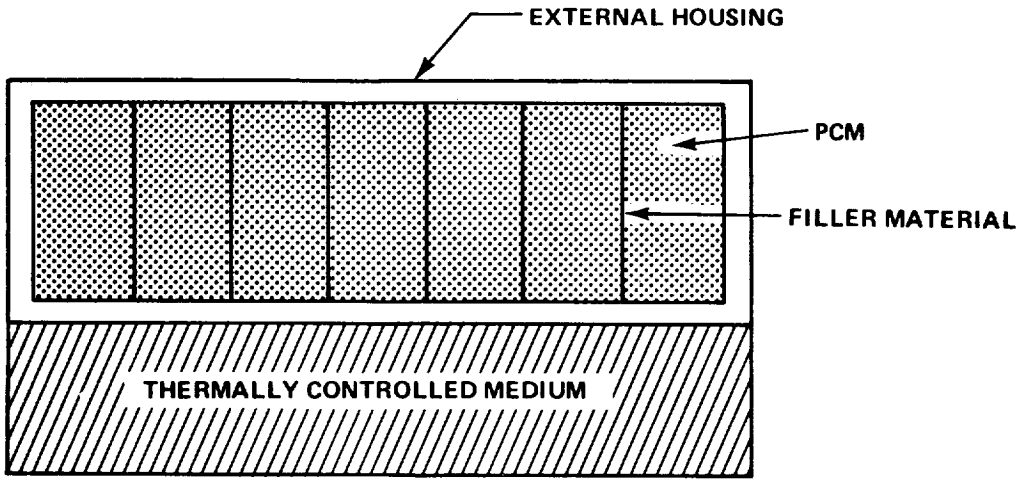

Figure 2. A phase change device.

- Noncorrosive
- Low coefficient of expansion
- High flash point
- Good wetting characteristics
- Minimum of void spaces (in solid-solid state)
- Stable
- Congruent phase change
- Little or no supercooling
- Relatively pure
- Nontoxic.

Economic factors of importance are:

- Low cost
- Present and future availability.

There are a number of classes of materials which have been investigated for use in phase change devices. Some of the more important are:

- Inorganic salt hydrates (e.g., glauber's salt $Na_2SO_4 \cdot 10H_2O$)
- Organic compounds (e.g., paraffins C_nH_{2n+2})
- Eutectics of the above (e.g., 88 mole percent acetic acid + 12 mole percent benzoic acid)
- Natural elements (e.g., sulphur, S)
- Water.

Of these materials, paraffins have been the most widely used, primarily in the space program.

D. Scope of Study

This section presents an overview of phase change devices; that is, it gives definitions, typical applications, and general limitations of this study. Section II presents PCM property data. Since most of the past devices have used paraffin as the PCM, Section II is primarily devoted to this class of materials. However, a large volume of nonparaffin data excerpted from other studies is given in the appendices. These data should allow the designer to use this document without resorting to time consuming literature searches for property data. Section III details the derivation and use of a nondimensional computer program. Section IV presents results of parametric studies performed using this nondimensional model. Using typical paraffin property data and thermal boundary conditions commensurate with earlier applications, optimum thermal design of the containment device is given parametrically. Examples for typical designs are given to illustrate use of these data. The intent of this study is to present sufficient data to allow the thermal designer to "short cut" time consuming analyses by either using the given numerical model and altering it to suit his application or, where possible, by using the parametric data directly. At a minimum, these data should allow the designer to get starting point estimates for his design. Section V outlines related topics. These topics include data which compare analytical and experimental results, discussing some of the discrepancies between the two. Section V also includes schemes for estimating convective effects. Other containment cases not covered by the examples used in Section IV are also given in Section V.

The reader should keep in mind that the treatment of phase change devices given in this document is limited to thermal aspects. As such, other topics of importance such as structural and material designs and selection are not addressed. Also, specialized subject matter such as the kinetics of the phase change process and chemical

phenomenon (e.g., supercooling, incongruent melting, and dendrite formation) are not discussed. Although convection analysis is discussed, details of convection stimulii such as buoyancy and surface tension forces are ignored. The reader is referred to survey reports by Grodzka [3,4] and a text by Chalmers [5] for information in these areas. Due to the large number of possible design configurations, this report addresses only typical and simplified schemes.

II. PROPERTY DATA

In several space-related applications of phase change devices, a paraffin has served as the PCM. Major emphasis in this section is given to those properties which are typically needed in a thermal design of selected paraffins. These include the melting temperature, transition temperature, heat of fusion, heat of transition, specific heat, density, thermal conductivity, viscosity, and coefficient of volume expansion.

Since hydrocarbon properties are dependent on purity, differences in reported property values may be directly related to differences in purity, a quantity often not specified.

Although this section is devoted to properties of paraffins, some of the properties of certain nonparaffins are presented in Appendix A. These have been extracted from several different references, and, in some cases, some paraffins and paraffin mixtures are included there also.

It is understood that the term paraffin generally denotes any of the saturated aliphatic hydrocarbons of the methane series C_nH_{2n+2}. Property data herein are principally limited, however, to those members of the family lying between n-Undecane ($C_{11}H_{24}$) and n-Triacontane ($C_{30}H_{62}$) because the corresponding range on melting temperature has included that of previously considered applications.

A. Sources, Availability, and Estimated Cost of Selected Paraffins

Table 1, which is based on a reported survey [6], shows a limited selection of companies and laboratories capable of supplying several selected paraffins in quantities adequate to be used in phase change devices. Also, the availability of Sunoco P-116 paraffin wax from the Sun Oil Co., C_{14}-C_{16} paraffin from Conoco, and a C_{15}-C_{16} paraffin mixture from Enjay is noted in Reference 1.

Information relative to type, grade, and physical property data availability from the suppliers listed in Table 1 is outlined in Table 2 based on a review [6] of their products.

TABLE 1. POTENTIAL SUPPLIERS OF SELECTED PARAFFINS[a]

Company	Address
American Petroleum Institute Standard Reference Materials	Carnegie-Mellon University Schenley Park Pittsburgh, Pennsylvania 15213
Aldrich Chemical Co., Inc.	940 West Saint Paul Avenue Milwaukee, Wisconsin 53233
Analabs Inc.	80 Republic Drive North Haven, Connecticut 06473
Chemical Sample Co.	4692 Kenny Road Columbus, Ohio 43221
Eastman (Kodak) Organic Chemicals	2400 Mt. Read Boulevard Rochester, New York 14650
Gallard-Schlesinger Chemical Manufacturing Corp.	584 Mineola Avenue Carle Place, New York 11514
The Humphrey Chemical Co.	Devine Street North Haven, Connecticut 06473
Lachat Chemicals Inc.	20200 Ashland Avenue Chicago Heights, Illinois 60411
Phillips Petroleum Co.	Bartlesville, Oklahoma 74004
Polysciences Inc.	Paul Valley Industrial Park Warrington, Pennsylvania 18976

a. From Table 9 of Reference 6.

The cost of paraffins is influenced significantly by purity, and it also varies considerably with source. The ultrahigh purity standard reference materials available from the American Petroleum Institute (API) cost $95 for a 5 ml unit [6]. Some price estimates for two grades of several paraffins are given in Table 3. All but the last three entries in Table 3 correspond to prices for relatively small quantities of reasonably high purity paraffins, probably made available for laboratory rather than large-scale commercial purposes. The last three entries denote some paraffin mixtures which can be obtained in large quantities.

TABLE 2. CAPABILITIES OF POTENTIAL SUPPLIERS OF SELECTED PARAFFINS[a]

Company	Ability to Supply Paraffin Hydrocarbons	Grades of Paraffin Hydrocarbon Available
American Petroleum Institute	Can be supplied	Ultrahigh purity
Aldrich Chemical Co., Inc.	Can be supplied	Only one grade available, unspecified purity
Analabs Inc.	Can be supplied	Only one grade available, purity specified greater than 99 percent
Chemical Sample Co.	Can be supplied	Several grades available
Eastman Organic Chemicals	Can be supplied	Only one grade available, unspecified purity
Gallard-Schlensinger Chemical Manufacturing	Does not manufacture paraffin hydrocarbons but can obtain them on request from other source	Only one grade available, unspecified purity
The Humphrey Chemical Co.	Can be supplied	Only one grade available, specified purity 99 percent
Lachat Chemical Inc.	Can be supplied	Only one grade available, specified purity 99 percent
Phillips Petroleum Co.	Can be supplied	Several grades available
Polysciences Inc.	Can be supplied as specialized items	Can provide materials at any purity level

a. From Table 10 of Reference 6.

TABLE 3. SOME APPROXIMATE PRICE DATA FOR SELECTED PARAFFINS

Material	Formula	Purity (percent)	Approximate[a] Unit Cost $/kg ($/lb)	Quantity kg (lb)	Reference
n-Nonane	C_9H_{20}	99	26.46 (12.00)	2.72 (6)	6
n-Nonane	C_9H_{20}	95	14.29 (6.48)	2.72 (6)	6
n-Decane	$C_{10}H_{22}$	99	16.26 (7.38)	2.77 (6.1)	6
n-Decane	$C_{10}H_{22}$	95	12.87 (5.84)	2.77 (6.1)	6
n-Undecane	$C_{11}H_{24}$	99	23.47 (10.65)	2.81 (6.2)	6
n-Undecane	$C_{11}H_{24}$	95	14.21 (6.44)	2.81 (6.2)	6
n-Dodecane	$C_{12}H_{26}$	99	16.45 (7.46)	2.86 (6.3)	6
n-Dodecane	$C_{12}H_{26}$	95	12.65 (5.74)	2.81 (6.2)	6
n-Tridecane	$C_{13}H_{28}$	99	34.99 (15.87)	2.86 (6.3)	6
n-Tridecane	$C_{13}H_{28}$	95	22.29 (10.11)	2.86 (6.3)	6
n-Tetradecane	$C_{14}H_{30}$	99	18.95 (8.59)	2.90 (6.4)	6
n-Tetradecane	$C_{14}H_{30}$	95	15.62 (7.09)	2.90 (6.4)	6
n-Pentadecane	$C_{15}H_{32}$	99	41.34 (18.75)	2.90 (6.4)	6
n-Pentadecane	$C_{15}H_{32}$	95	30.13 (13.67)	0.68 (1.5)	6
n-Hexadecane	$C_{16}H_{34}$	99	35.27 (16.00)	0.68 (1.5)	6
n-Hexadecane	$C_{16}H_{34}$	95	20.08 (9.11)	2.90 (6.4)	6
n-Heptadecane	$C_{17}H_{36}$	99	37.89 (17.19)	2.90 (6.4)	6
n-Heptadecane	$C_{17}H_{36}$	95	30.13 (13.67)	0.68 (1.5)	6
n-Octadecane	$C_{18}H_{38}$	99	18.65 (8.46)	2.95 (6.5)	6
n-Octadecane	$C_{18}H_{38}$	95	30.13 (13.67)	0.68 (1.5)	6
n-Nonodecane	$C_{19}H_{40}$	99	40.70 (18.46)	2.95 (6.5)	6
n-Nonodecane	$C_{19}H_{40}$	95	27.93 (12.67)	0.68 (1.5)	6
n-Eicosane	$C_{20}H_{42}$	99	26.05 (11.82)	2.99 (6.6)	6
n-Eicosane	$C_{20}H_{42}$	95	41.15 (18.67)	0.68 (1.5)	6
P-116 Paraffin		–	0.14 (0.065)	Not specified	1
C_{15}-C_{16} Paraffin mixture		–	0.11 (0.05)	4536 (10,000)	1
C_{14}-C_{16} Paraffin		–	0.11 (0.05)	Not specified	1

a. Prices shown are approximate based on 1974 publications. All but the last three entries shown in the table correspond to prices quoted for the small quantities indicated which, more than likely, are for laboratory applications and are not totally indicative for large commercial orders. Also, it should be noted that there is also variation in prices with supplier.

B. Melting and Transition Temperatures

Table 4 contains published [7,8] values of the melting and transition temperatures for the listed paraffins.

For commercial grades of paraffins, some variations in the phase change temperatures are to be expected. Impurities even tend to cause some difference in the melting and freezing temperatures. Some reported [6] experimental results which show the effect of purity on the fusion temperature for several grades of certain paraffins supplied by two manufacturers are given in the lower two segments of Table 5 together with the corresponding fusion temperature for the high purity paraffins available from API. Similar results and API data for solid-solid phase transition temperatures are given in Table 6.

For the seven paraffins listed in Tables 5 and 6, correlations of phase change temperatures corresponding to API data with the number of carbon atoms in the chain are shown in Figure 3.

C. Heat of Fusion and Heat of Transition

The energy values associated with solid-liquid and solid-solid transitions as published by API [7] or either by Timmermans [8] are also listed in Table 4. The effects of purity on these energy values based on comparisons between measurements [6] on two commercial grades (lower two segments of Tables 7 and 8) and values reported by the API for high purity paraffins are listed in Tables 7 and 8, respectively, for several paraffins.

For the seven paraffins listed in Tables 7 and 8, correlations of the heat of fusion and the heat of transition with the number of carbon atoms in the chain are shown in Figures 4 and 5, respectively, for the data available from API.

It is interesting to note also the effect of the mixing of two different paraffins on the heats of fusion and transition. As an example, the results reported [6] for a hexadecane-octadecane binary system are shown in Figure 6.

D. Specific Heat

The specific heat is temperature dependent in each phase with an increase in specific heat occurring with an increase in temperature. There is a change in specific heat between two phases. Data for all the paraffins listed in Table 4 have not been obtained. For some of the listed paraffins, specific heat data over a range of temperature are given in Reference 8. These have been plotted in Figures 7, 8, and 9. There are obvious gaps in the data in the vicinity of phase transitions. Data given in Reference 9 for $C_{14}H_{30}$, $C_{16}H_{34}$, $C_{18}H_{38}$, and $C_{20}H_{42}$ are shown in Figures 10 through 13, respectively.

TABLE 4. MELTING AND TRANSITION DATA FOR THE PARAFFINS (C_nH_{2n+2}) CONTAINING ELEVEN THROUGH THIRTY CARBON ATOMS

Name	Chemical Formula	Molecular Weight	Melting Temperature °C (°F)	Transition Temperature °C (°F)	Heat of Fusion kJ/kg (Btu/lb)	Heat of Transition kJ/kg (Btu/lb)
n-Undecane	$C_{11}H_{24}$	156.314	-25.6 (-14.1)	-36.6 (-33.8)	141.3 (60.8)	43.9 (18.9)
n-Dodecane	$C_{12}H_{26}$	170.341	- 9.6 (14.7)	None	210.5 (90.6)	None
n-Tridecane	$C_{13}H_{28}$	184.368	- 5.4 (22.3)	-18.2 (- 0.7)	154.8 (66.6)	41.6 (17.9)
n-Tetradecane	$C_{14}H_{30}$	198.395	5.9 (42.5)	None	229.9 (98.9)	None
n-Pentadecane	$C_{15}H_{32}$	212.422	10.0 (49.8)	- 2.3 (27.9)	163.7 (70.4)	43.2 (18.6)
n-Hexadecane	$C_{16}H_{34}$	226.449	18.2 (64.7)	None	228.9 (98.5)	None
n-Heptadecane	$C_{17}H_{36}$	240.476	22.0 (71.5)	11.1 (51.9)	168.3 (72.4)	45.5 (19.6)
n-Octadecane	$C_{18}H_{38}$	254.504	28.2 (82.7)	None	243.5 (104.7)	None
n-Nonadecane	$C_{19}H_{40}$	268.531	31.9 (89.4)	22.8 (72.9)	170.6 (73.4)	51.4 (22.1)
n-Eicosane	$C_{20}H_{42}$	282.558	36.4 (97.6)	36.2 (97.2)	247.3 (106.4)	None
n-Heneicosane	$C_{21}H_{44}$	296.585	40.2 (104.3)	32.5 (90.5)	160.8 (69.2)	52.2 (22.5)
n-Docosane	$C_{22}H_{46}$	310.612	44.0 (111.2)	43.0 (109.4)	157.6 (67.8)	90.8 (39.1)
n-Tricosane	$C_{23}H_{48}$	324.639	47.5 (117.5)	40.5 (104.9)	166.3 (71.5)	67.0 (28.8)
n-Tetracosane	$C_{24}H_{50}$	338.666	50.6 (123.1)	48.1 (118.6)	162.1 (69.7)	92.4 (39.8)
n-Pentacosane	$C_{25}H_{52}$	352.693	53.5 (128.3)	47.0 (116.6)	178.4 (76.7)	73.9 (31.8)
n-Hexadosane	$C_{26}H_{54}$	366.720	56.3 (133.3)	53.3 (127.9)	162.2 (69.8)	87.9 (37.8)
n-Heptacosane	$C_{27}H_{56}$	380.747	58.8 (137.8)	53.0 (127.4)	158.7 (68.3)	76.0 (32.7)
n-Octacosane	$C_{28}H_{58}$	394.774	61.4 (142.5)	58.0 (136.4)	163.7 (70.4)	89.8 (38.6)
n-Nonadosane	$C_{29}H_{60}$	408.802	63.4 (146.1)	58.2 (136.7)	161.7 (69.6)	72.7 (31.3)
n-Triacontane	$C_{30}H_{62}$	422.829	65.4 (149.7)	62.0 (143.6)	251.1 (108.0)	None

TABLE 5. FUSION TEMPERATURE FOR SELECTED PARAFFINS[a]

Material	Formula	Heating (Solid → Liquid) °C (°F)	Cooling (Liquid → Solid) °C (°F)	Purity (Mole Percent) or Grade
n-Undecane	$C_{11}H_{24}$	-25.74 (-14.05)	-25.74 (-14.05)	99.96 ± 0.03
n-Dodecane	$C_{12}H_{26}$	- 9.74 (14.74)	- 9.74 (14.74)	99.969 ± 0.025
n-Tridecane	$C_{13}H_{28}$	- 5.54 (22.30)	- 5.54 (22.30)	99.91 ± 0.06
n-Hexadecane	$C_{16}H_{34}$	18.02 (64.70)	18.02 (64.70)	99.90 ± 0.06 *
n-Octadecane	$C_{18}H_{38}$	28.03 (82.70)	28.03 (82.70)	99.90 ± 0.08
n-Nonadecane	$C_{19}H_{40}$	31.95 (89.80)	21.95 (89.80)	99.90 ± 0.08
n-Eicosane	$C_{20}H_{42}$	36.65 (98.20)	36.65 (98.20)	99.90 ± 0.08
n-Undecane	$C_{11}H_{24}$	-26.7 (-15.7)	-26.2 (-14.8)	99
n-Dodecane	$C_{12}H_{26}$	-11.7 (11.3)	-10.7 (13.1)	99
n-Tridecane	$C_{13}H_{28}$	- 6.2 (21.2)	- 6.0 (21.6)	99
n-Hexadecane	$C_{16}H_{34}$	18.9 (66.2)	18.4 (65.3)	99 **
n-Octadecane	$C_{18}H_{38}$	27.0 (80.8)	27.1 (81.0)	99
n-Nonadecane	$C_{19}H_{40}$	29.4 (85.1)	29.4 (85.2)	99
n-Eicosane	$C_{20}H_{42}$	35.7 (96.5)	35.1 (95.5)	99
n-Undecane	$C_{11}H_{24}$	-28.55 (-19.2)	-26.2 (-14.8)	99.75
n-Dodecane	$C_{12}H_{26}$	-11.35 (11.8)	-11.2 (12.2)	99
n-Tridecane	$C_{13}H_{28}$	- 7.35 (19.0)	- 7.2 (19.4)	99
n-Hexadecane	$C_{16}H_{34}$	18.9 (66.2)	18.6 (65.7)	99
n-Hexadecane	$C_{16}H_{34}$	11.0 (52.0)	12.9 (55.4)	95 ***
n-Octadecane	$C_{18}H_{38}$	26.6 (80.1)	26.4 (79.7)	95
n-Nonadecane	$C_{19}H_{40}$	31.4 (88.7)	32.4 (90.5)	95
n-Eicosane	$C_{20}H_{42}$	34.9 (95.0)	34.9 (95.0)	95
n-Eicosane	$C_{20}H_{42}$	32.4 (90.5)	32.9 (91.5)	(90)

a. Based on Tables 1 and 2 of Reference 6.

* Supplier A

** Supplier B

*** Supplier C

TABLE 6. TRANSITION TEMPERATURES FOR CERTAIN PARAFFINS[a]

Material	Heating (Solid → Solid) °C (°F)	Cooling (Solid → Solid) °C (°F)	Purity (Mole Percent) or Grade
n-Undecane	-36.6 (-33.5)	-36.6 (-33.5)	99.96 ± 0.03
n-Tridecane	-18.2 (- 0.4)	-18.2 (- 0.4)	99.91 ± 0.06 *
n-Nonadecane	22.8 (73.2)	22.8 (73.2)	99.90 ± 0.08
n-Undecane	-36.2 (-32.8)	-36.6 (-33.5)	99
n-Tridecane	-19.1 (2.0)	-18.2 (- 0.4)	99 **
n-Nonadecane	21.7 (71.2)	20.9 (69.8)	99
n-Undecane	-37.0 (-34.3)	-36.2 (-32.8)	99.75
n-Tridecane	-21.1 (- 5.65)	-19.2 (- 2.2)	99 ***
n-Nonadecane	20.5 (69.0)	20.9 (69.8)	95

a. Based on Tables 1 and 3 of Reference 6.

* Supplier A

** Supplier B

*** Supplier C

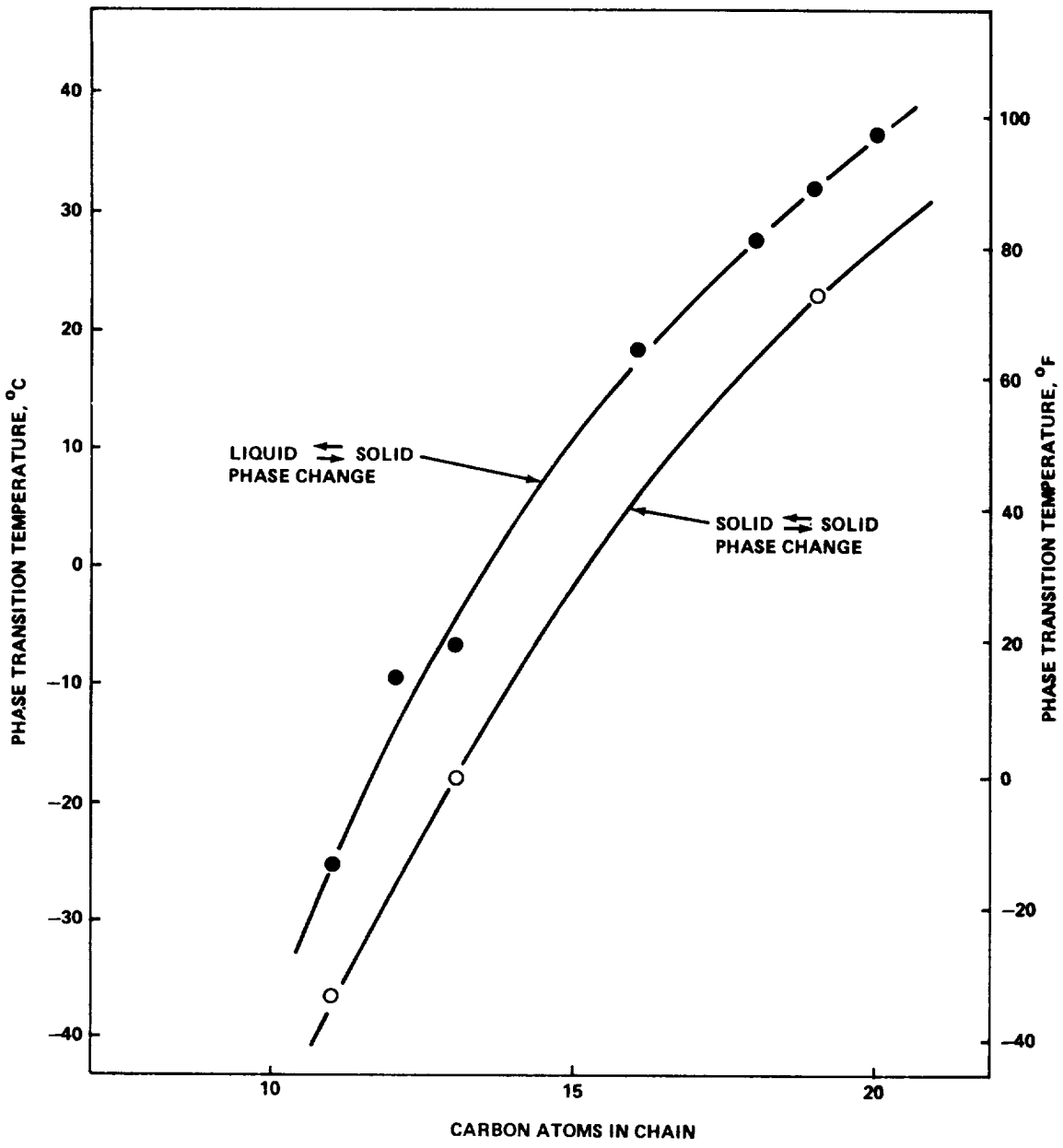

Figure 3. Correlation of phase change temperature with number of carbon atoms in the chain (from Fig. 1 of Reference 6).

TABLE 7. COMPARISON OF HEAT OF FUSION FOR SEVERAL GRADES OF SELECTED PARAFFINS

Material	Heating (Solid → Liquid) kJ/kg (Btu/lb)	Cooling (Liquid → Solid) kJ/kg (Btu/lb)	Purity (Mole %) or Grade	
n-Undecane	142 (61.2)	142 (61.2)	99.96 ± 0.03	*
n-Dodecane	216 (93.2)	216 (93.2)	99.969 ± 0.025	
n-Tridecane	154 (66.5)	154 (66.5)	99.91 ± 0.06	
n-Hexadecane	235 (101.5)	235 (101.5)	99.90 ± 0.06	
n-Octadecane	244 (105.0)	244 (105.0)	99.90 ± 0.08	
n-Nonadecane	187 (80.6)	187 (80.6)	99.90 ± 0.08	
n-Eicosane	248 (107.0)	248 (107.0)	99.90 ± 0.08	
n-Undecane	140 (60.4)	143 (61.7)	99	**
n-Dodecane	218 (94.0)	220 (94.9)	99	
n-Tridecane	145 (62.5)	159 (68.5)	99	
n-Hexadecane	237 (102.0)	235 (101.5)	99	
n-Octadecane	248 (107.0)	245 (105.6)	99	
n-Nonadecane	180 (77.5)	180 (77.5)	99	
n-Eicosane	249 (107.5)	245 (105.5)	99	
n-Undecane	142 (61.4)	141 (61.0)	99.75	***
n-Dodecane	218 (94.0)	212 (91.5)	99	
n-Tridecane	154 (66.2)	150 (64.8)	99	
n-Hexadecane	239 (103.0)	235 (101.5)	99	
n-Hexadecane	244 (105.0)	237 (102.0)	95	
n-Octadecane	243 (104.6)	242 (104.5)	95	
n-Nonadecane	182 (78.3)	179 (77.2)	95	
n-Eicosane	255 (110.0)	243 (104.8)	95	
n-Eicosane	241 (104.0)	234 (101.0)	90	

* Supplier A
** Supplier B
*** Supplier C

TABLE 8. COMPARISON OF HEAT OF TRANSITION FOR SEVERAL GRADES OF SELECTED PARAFFINS

Material	Heating (Solid → Solid) kJ/kg (Btu/lb)	Cooling (Solid → Solid) kJ/kg (Btu/lb)	Purity (Mole %) or Grade
n-Undecane	439 (18.9)	439 (18.9)	99.96 ± 0.03
n-Tridecane	416 (17.9)	416 (17.9)	99.91 ± 0.06 *
n-Nonadecane	514 (22.2)	514 (22.2)	99.90 ± 0.08
n-Undecane	409 (17.6)	405 (17.4)	99
n-Tridecane	433 (18.7)	470 (20.3)	99 **
n-Nonadecane	513 (22.1)	516 (22.3)	99
n-Undecane	403 (17.4)	422 (18.2)	99.75
n-Tridecane	403 (17.4)	406 (17.5)	99 ***
n-Nonadecane	495 (21.4)	499 (21.5)	95

* Supplier A
** Supplier B
*** Supplier C

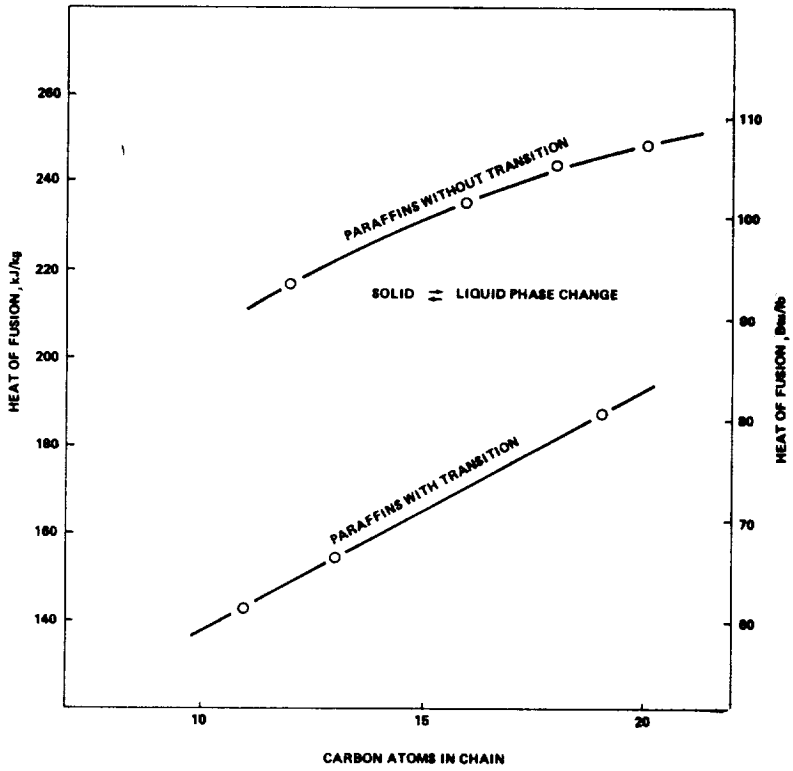

Figure 4. Correlation of heat of fusion with number of carbon atoms in the chain [from Fig. 5(a) of Reference 6].

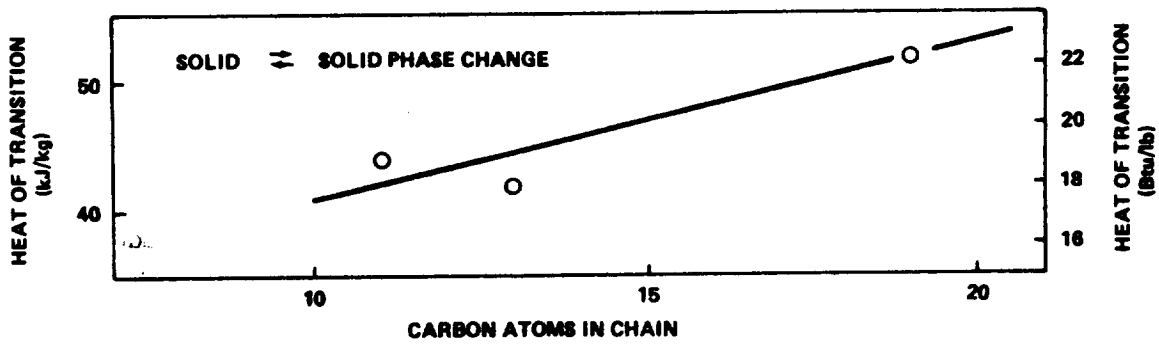

Figure 5. Correlation of heat of transition with number of carbon atoms in the chain [from Fig. 5(b) of Reference 6].

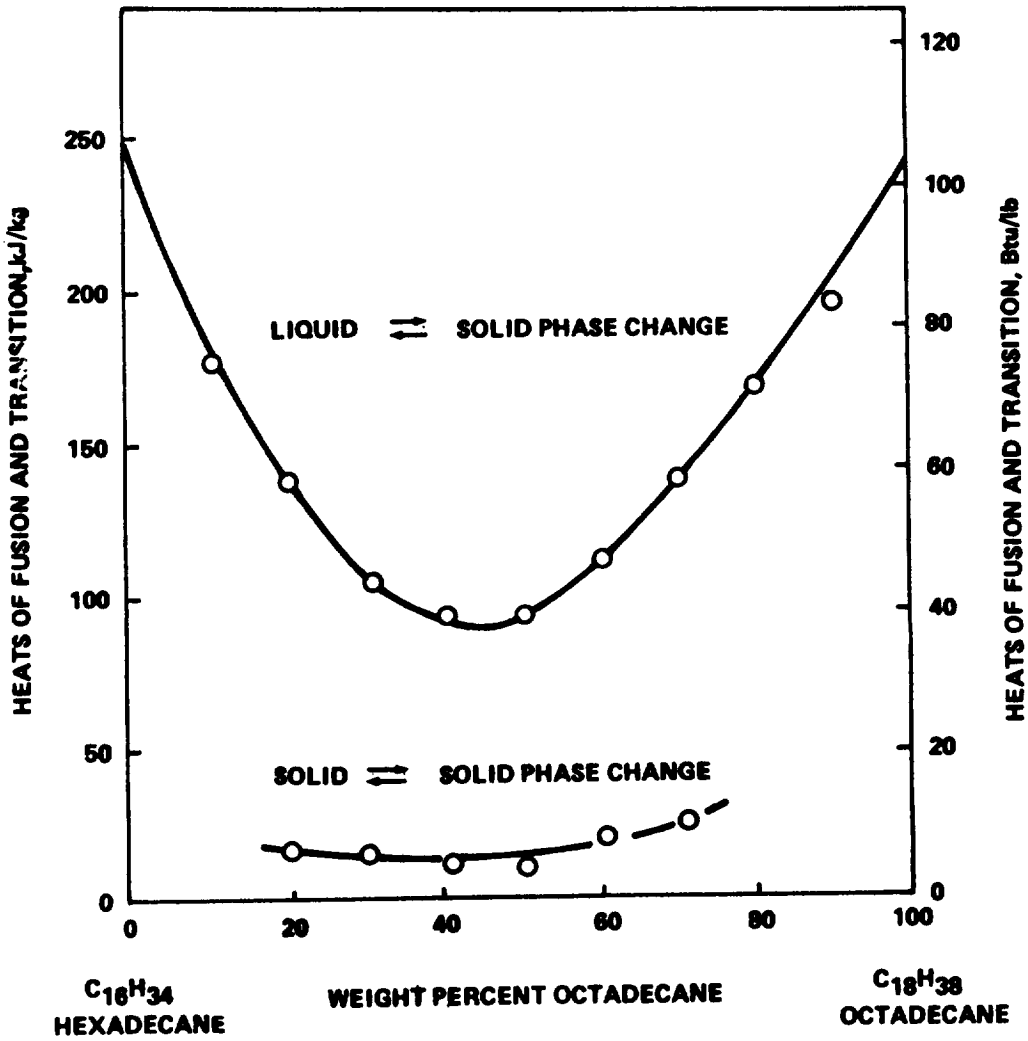

Figure 6. Example illustrating effect of composition of heats of phase change for hexadecane-octadecane binary system (from Fig. 29 of Reference 6).

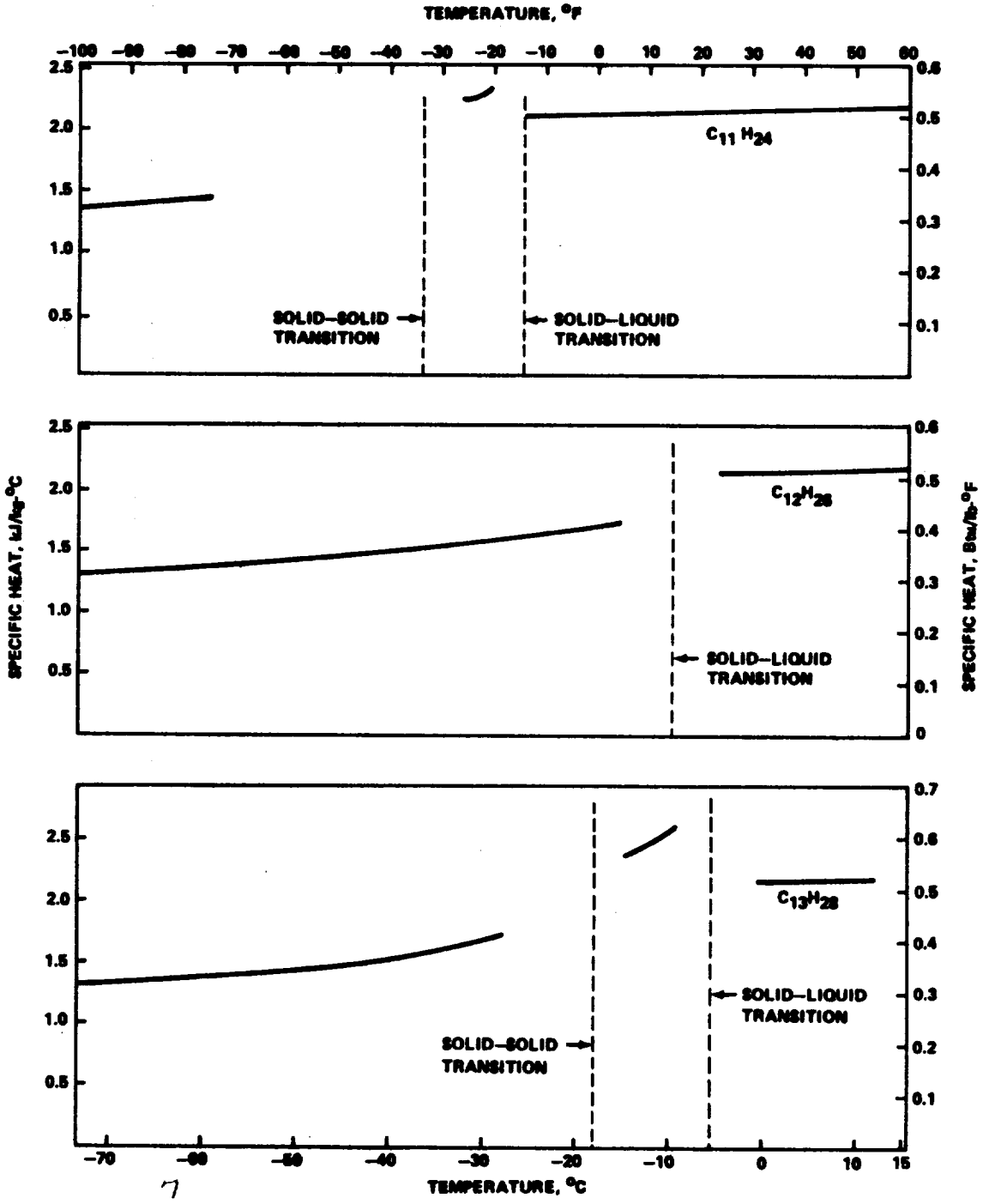

Figure 7. Specific heat versus temperature for $C_{11}H_{24}$, $C_{12}H_{26}$, and $C_{13}H_{28}$ (based on data given in Reference 8).

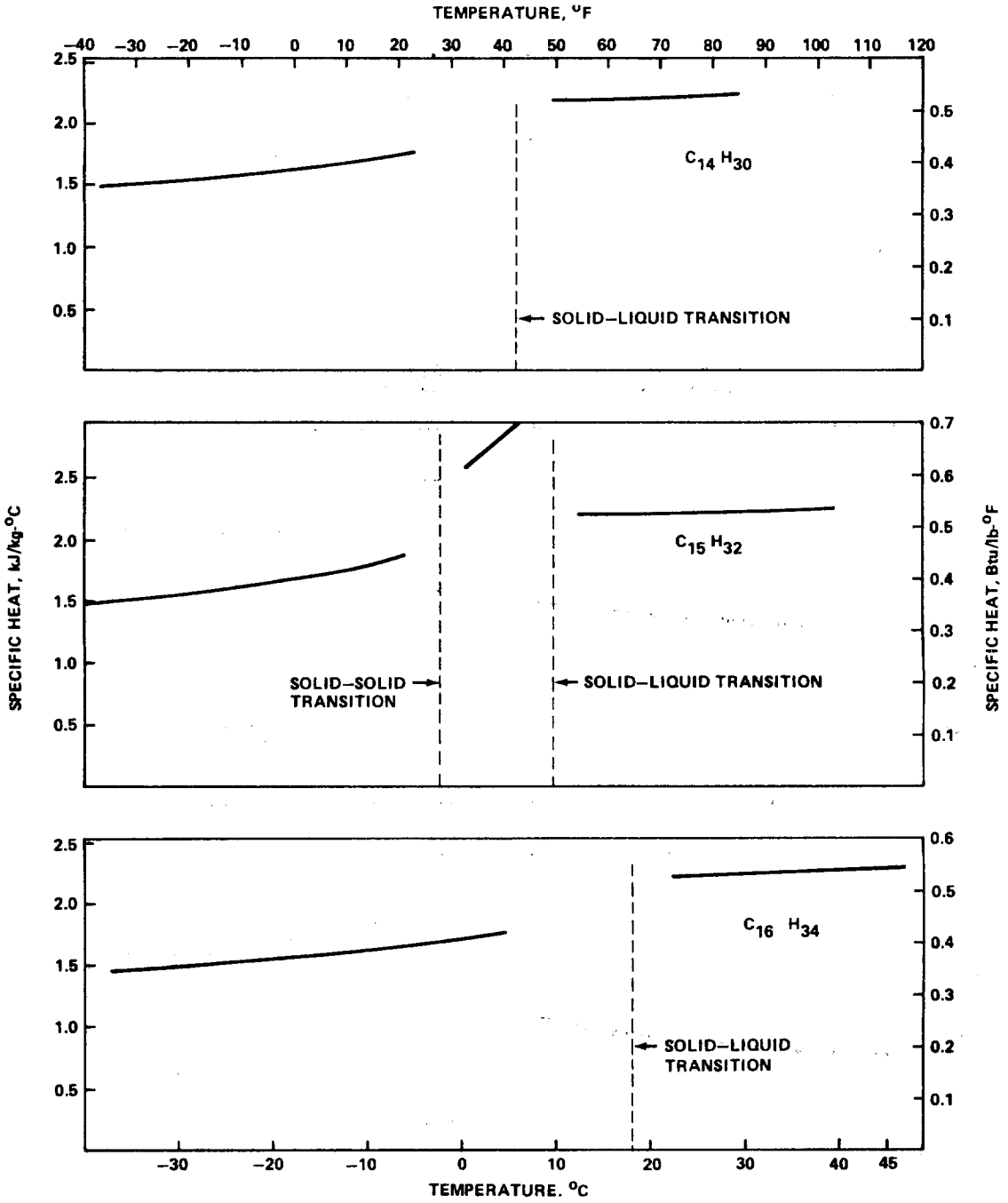

Figure 8. Specific heat versus temperature for $C_{14}H_{30}$, $C_{15}H_{32}$, and $C_{16}H_{34}$ (based on data given in Reference 8).

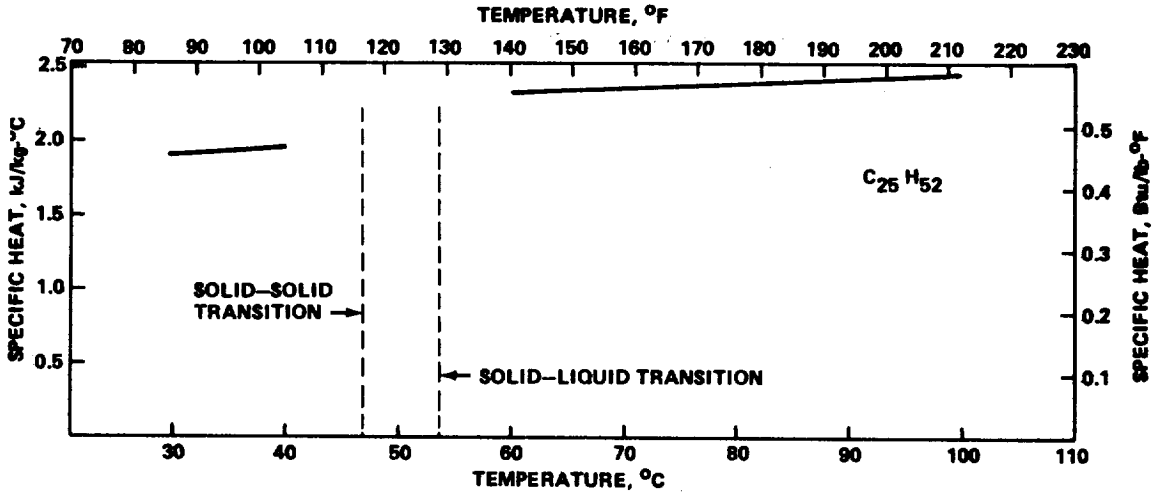

Figure 9. Specific heat versus temperature for $C_{25}H_{52}$ (based on data given in Reference 8).

Measurements of specific heat for several paraffins using samples from two manufacturers are reported by Reference 6. These are tabulated in Table 9 together with values for the same materials from API.

Comparative examination of data shown in Figures 7 through 13 and listed in Table 9 indicates that the specific heat of paraffins is sensitive to impurities.

E. Density

The density of the liquid phase decreases with temperature and data for most of the considered paraffins are shown in Figure 14. The values agree with those reported in Reference 6. For $C_{14}H_{30}$, $C_{16}H_{34}$, $C_{18}H_{38}$, and $C_{20}H_{42}$, density data are also plotted in Figures 15 through 18, respectively, which are from Reference 9 and which include some solid phase density measurements. For these paraffins, density changes across the solid-liquid phase transition ranged from 5 to 8 percent.

F. Thermal Conductivity

There is a limited amount of thermal conductivity data available for paraffins. Most reported values are only for the liquid phase. For selected paraffins Table 10 lists a limited amount of liquid thermal conductivity data, which were reported in Reference 6

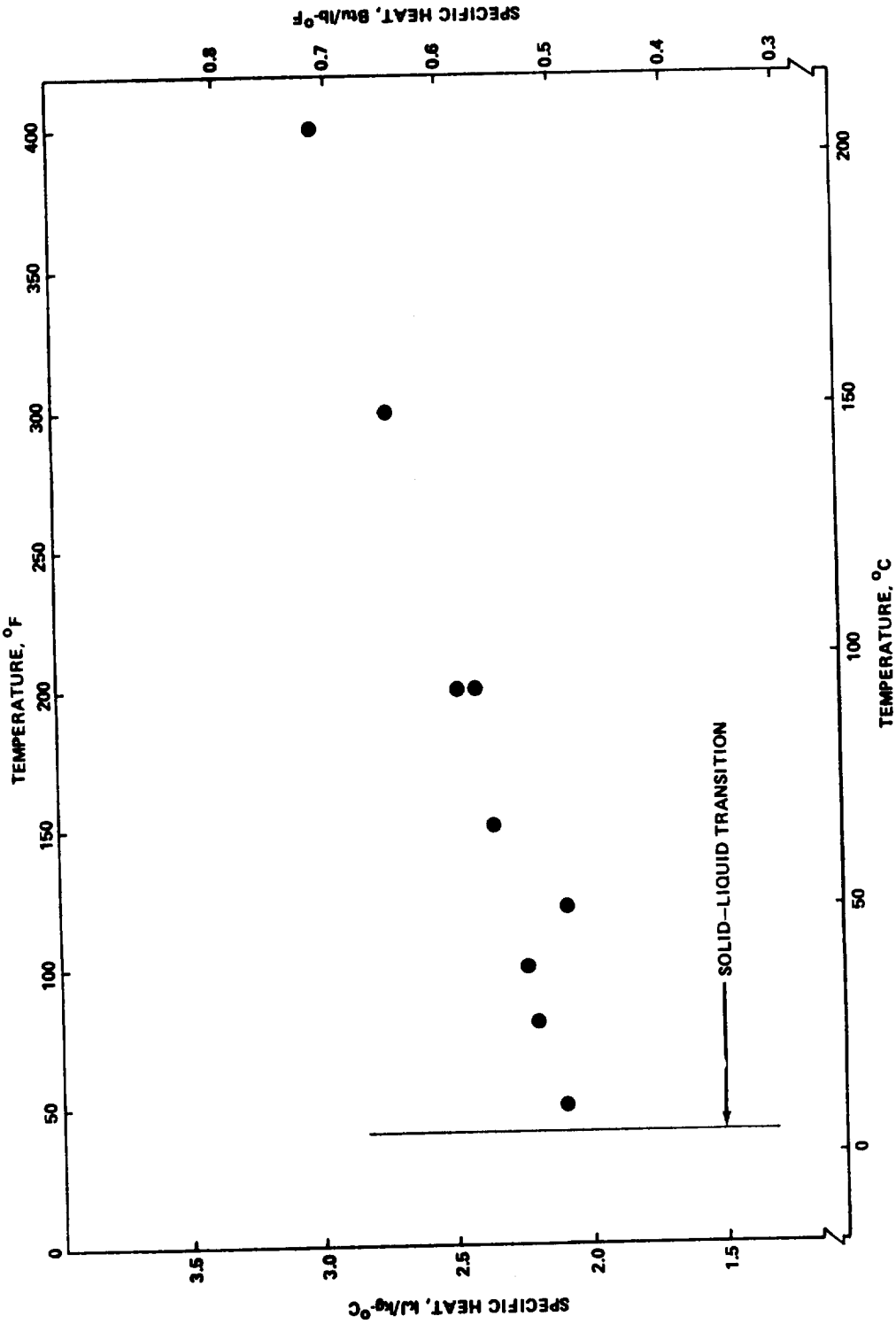

Figure 10. Specific heat of tetradecane ($C_{14}H_{30}$) (from Fig. 8 of Reference 9).

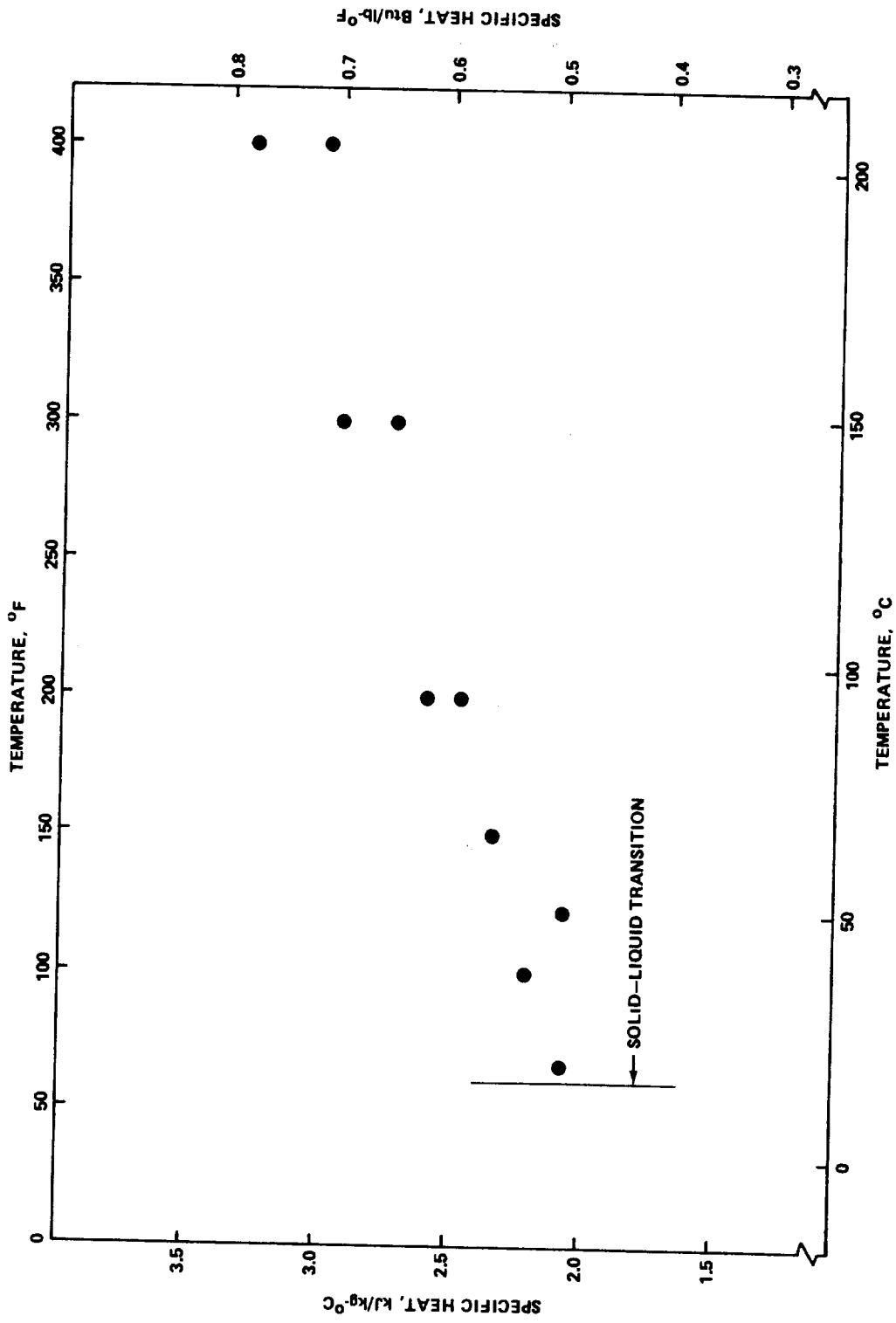

Figure 11. Specific heat of hexadecane ($C_{16}H_{34}$) (from Fig. 9 of Reference 9).

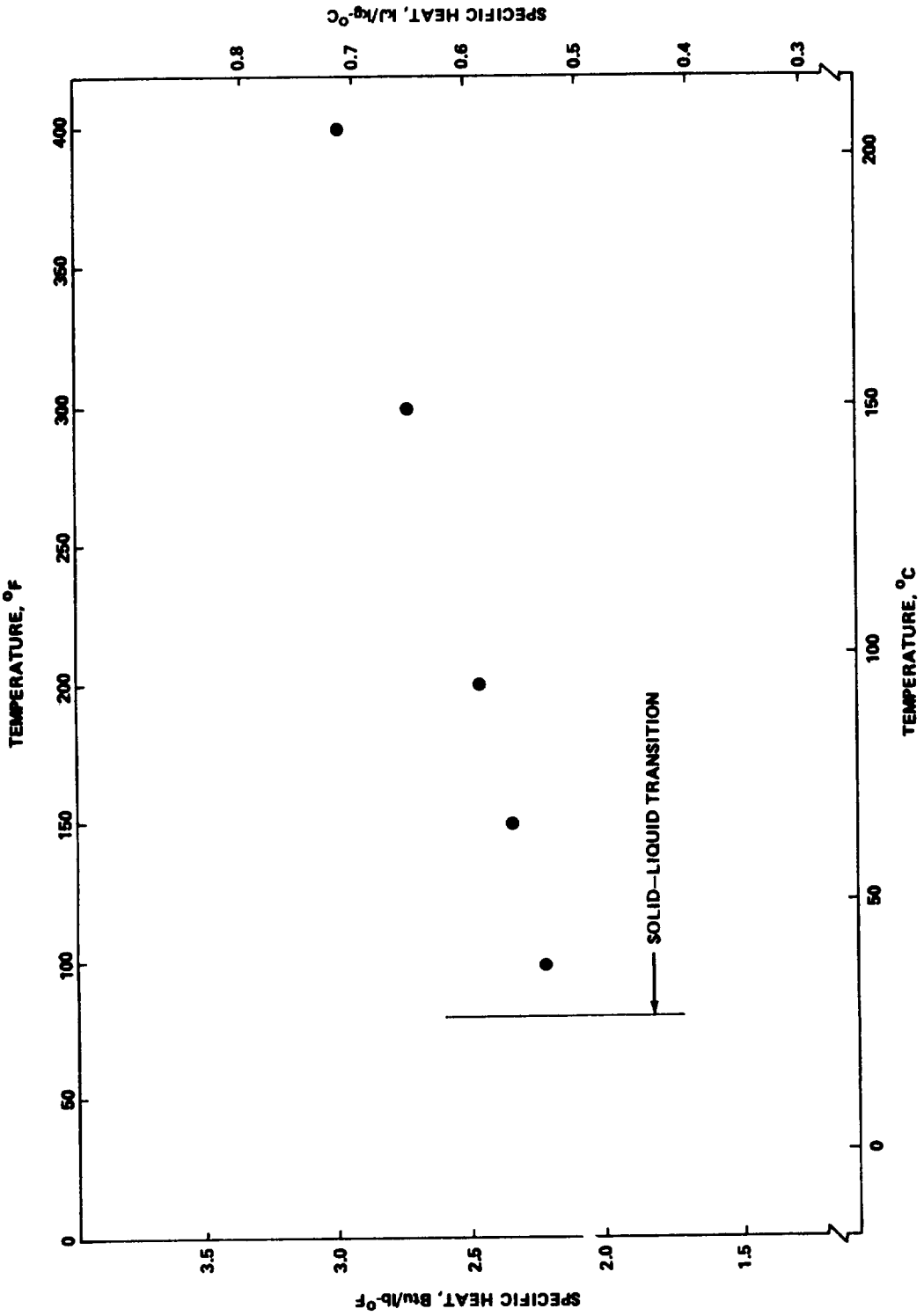

Figure 12. Specific heat of octadecane ($C_{18}H_{38}$) (from Fig. 10 of Reference 9).

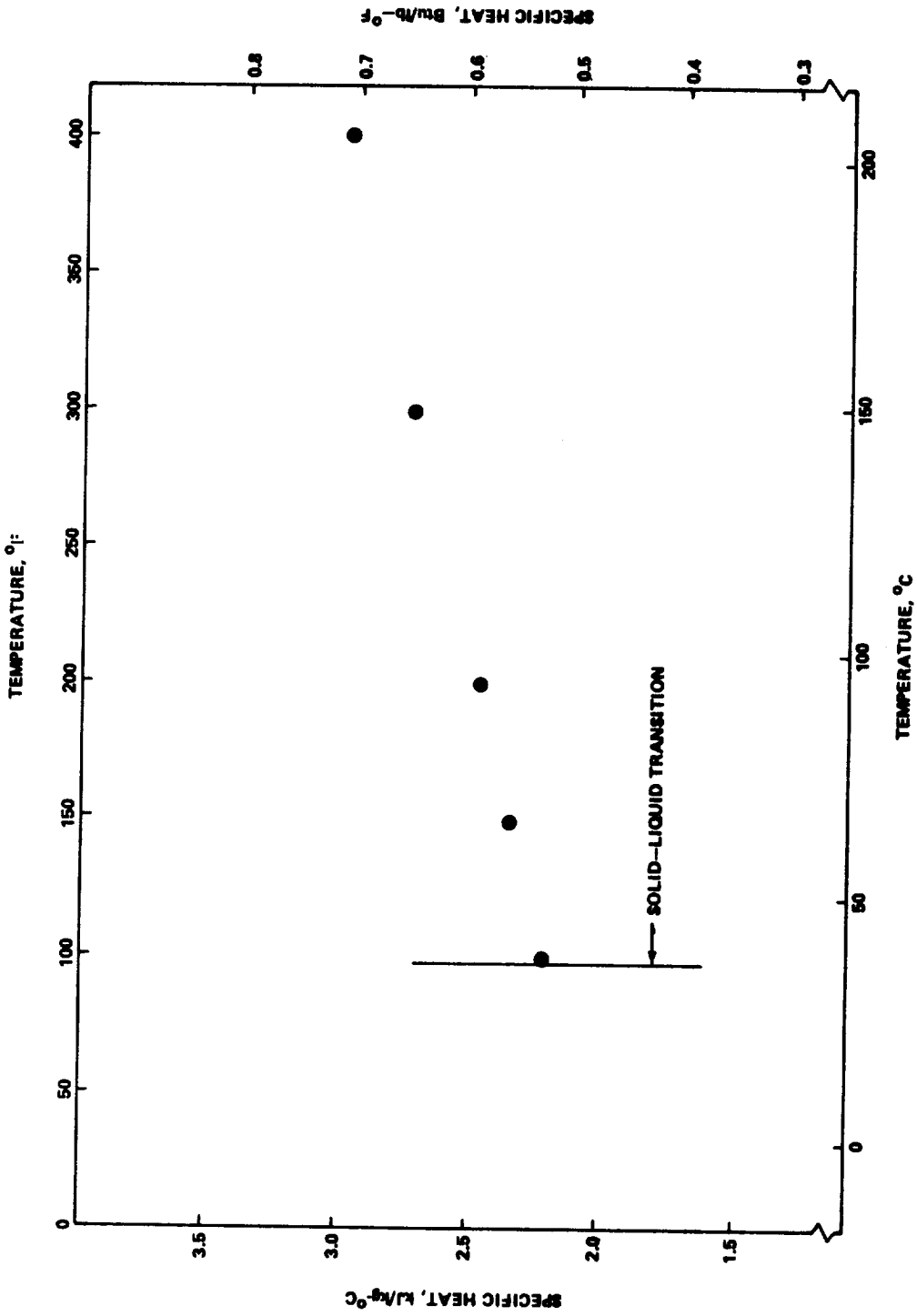

Figure 13. Specific heat of eicosane ($C_{20}H_{42}$) (from Fig. 11 of Reference 9).

TABLE 9. SPECIFIC HEAT DATA FOR CERTAIN PARAFFINS[a]

Material	Formula	Purity (Mole %)	Liquid Specific Heat		Solid Specific Heat	
			Units kJ/kg-°C (Btu/lb-°F)	Temperature °C (°F)	Units kJ/kg-°C (Btu/lb-°F)	Temperature °C (°F)
n-Undecane	$C_{11}H_{24}$	99.96 ± 0.03	1.53 (0.366)	0 (32)	—	—
n-Dodecane	$C_{12}H_{26}$	99.969 ± 0.025	1.53 (0.366)	0 (32)	1.45 (0.347)	-18 (0)
n-Tridecane	$C_{13}H_{28}$	99.91 ± 0.06	1.53 (0.366)	0 (32)	1.45 (0.346)	-18 (0)
n-Hexadecane	$C_{16}H_{34}$	99.90 ± 0.06	1.70 (0.406)	38 (100)	1.45 (0.346)	-18 (0)
n-Octadecane	$C_{18}H_{38}$	99.90 ± 0.08	1.70 (0.406)	38 (100)	1.45 (0.346)	-18 (0)
n-Nonadecane	$C_{19}H_{40}$	99.90 ± 0.08	1.69 (0.405)	38 (100)	1.45 (0.346)	-18 (0)
n-Eicosane	$C_{20}H_{42}$	99.90 ± 0.08	1.94 (0.464)	93 (200)	1.44 (0.345)	-18 (0)
n-Undecane	$C_{11}H_{24}$	99	1.89 (0.451)	–3 (26.6)	1.34 (0.320)	-53 (-63.5)
n-Dodecane	$C_{12}H_{26}$	99	2.15 (0.513)	17 (62.6)	1.69 (0.405)	-23 (-9.4)
n-Tridecane	$C_{13}H_{28}$	99	2.16 (0.516)	27 (80.2)	1.59 (0.380)	-33 (-27.5)
n-Hexadecane	$C_{16}H_{34}$	99	2.31 (0.551)	57 (134.5)	1.80 (0.430)	7 (44.6)
n-Octadecane	$C_{18}H_{38}$	99	2.33 (0.556)	57 (134.5)	1.88 (0.450)	7 (44.6)
n-Nonadecane	$C_{19}H_{40}$	99	2.30 (0.549)	67 (153.5)	1.80 (0.430)	- 3 (26.6)
n-Eicosane	$C_{20}H_{42}$	99	2.46 (0.587)	77 (171.0)	1.92 (0.460)	27 (80.6)
n-Undecane	$C_{11}H_{24}$	99.75	2.13 (0.509)	- 3 (26.6)	1.26 (0.301)	-53 (-63.5)
n-Dodecane	$C_{12}H_{26}$	99	2.26 (0.540)	17 (62.6)	1.76 (0.420)	-23 (-9.4)
n-Tridecane	$C_{13}H_{28}$	99	2.20 (0.526)	27 (80.6)	1.59 (0.380)	-33 (-27.5)
n-Hexadecane	$C_{16}H_{34}$	99	2.31 (0.552)	57 (134.5)	1.68 (0.401)	-3 (26.6)
n-Hexadecane	$C_{16}H_{34}$	95	2.42 (0.578)	57 (134.5)	1.68 (0.402)	-3 (26.6)
n-Octadecane	$C_{18}H_{38}$	95	2.24 (0.536)	57 (134.5)	1.97 (0.470)	-7 (44.6)
n-Nonadecane	$C_{19}H_{40}$	95	2.24 (0.536)	67 (153.5)	1.89 (0.452)	-7 (44.6)
n-Eicosane	$C_{20}H_{42}$	95	2.24 (0.536)	67 (153.5)	1.78 (0.426)	17 (62.6)
n-Eicosane	$C_{20}H_{42}$	90	2.34 (0.559)	67 (153.5)	2.38 (0.569)	17 (62.6)

a. Data based on Reference 6. The first segment corresponds to API. The last two segments correspond to samples acquired from two different companies.

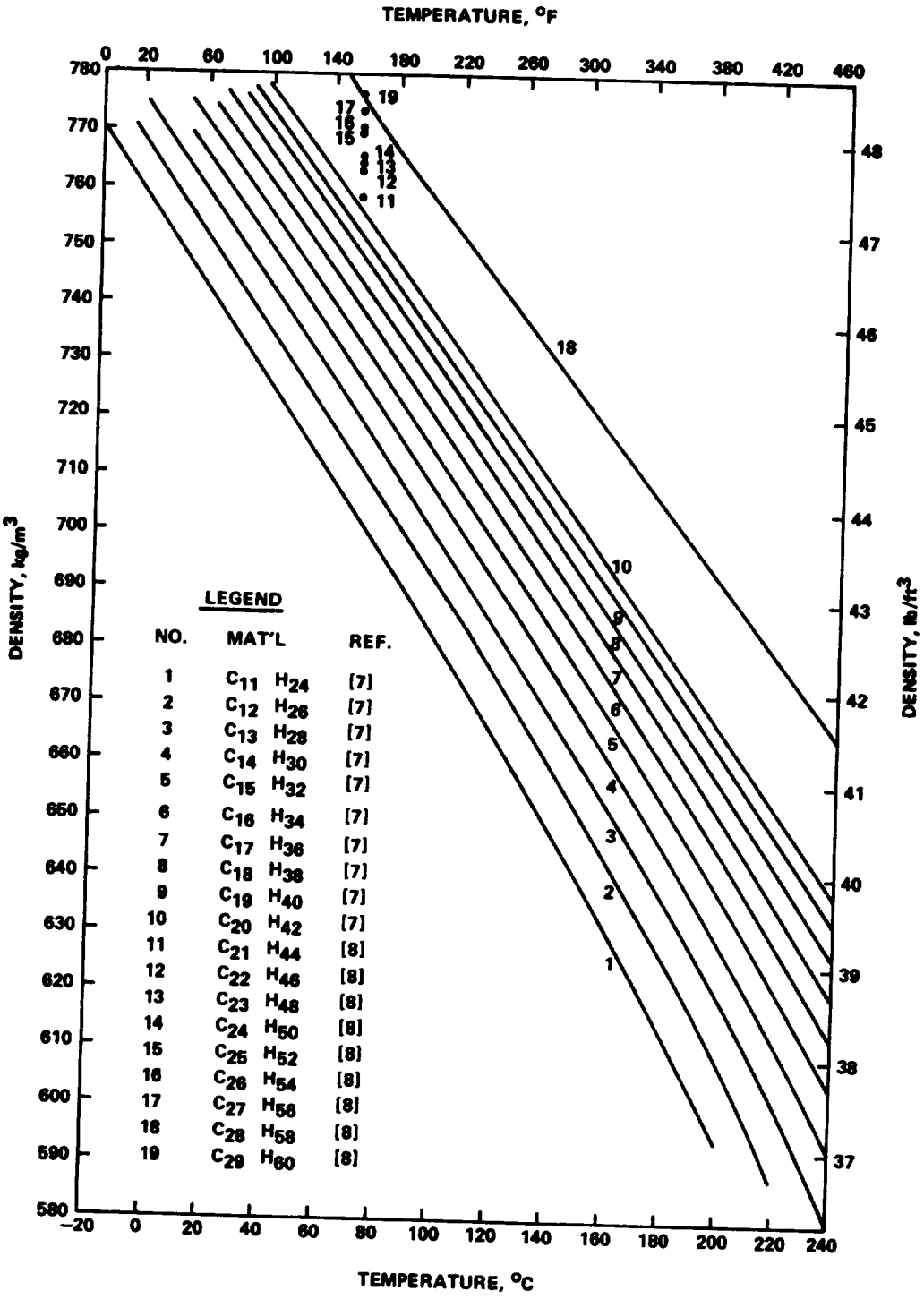

Figure 14. Liquid phase density of several paraffins.

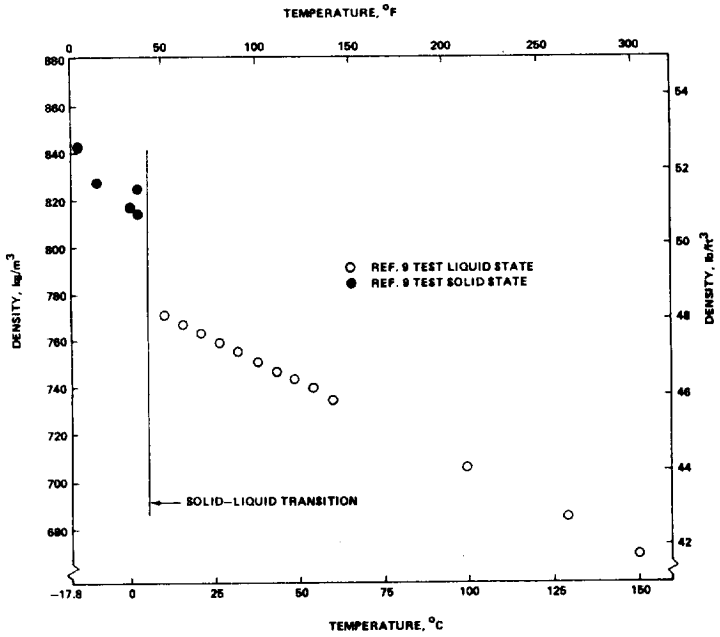

Figure 15. Density of tetradecane ($C_{14}H_{30}$) (from Fig. 4 of Reference 9).

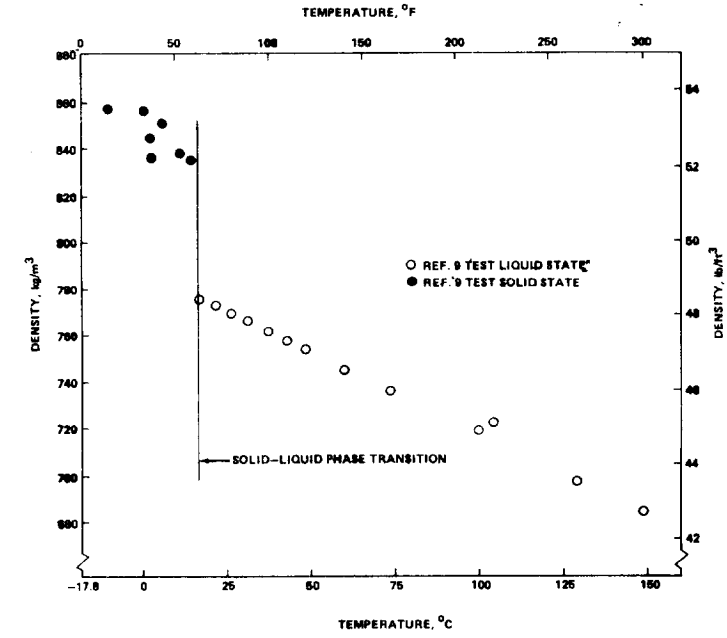

Figure 16. Density of hexadecane ($C_{16}H_{34}$) (from Fig. 5 of Reference 9).

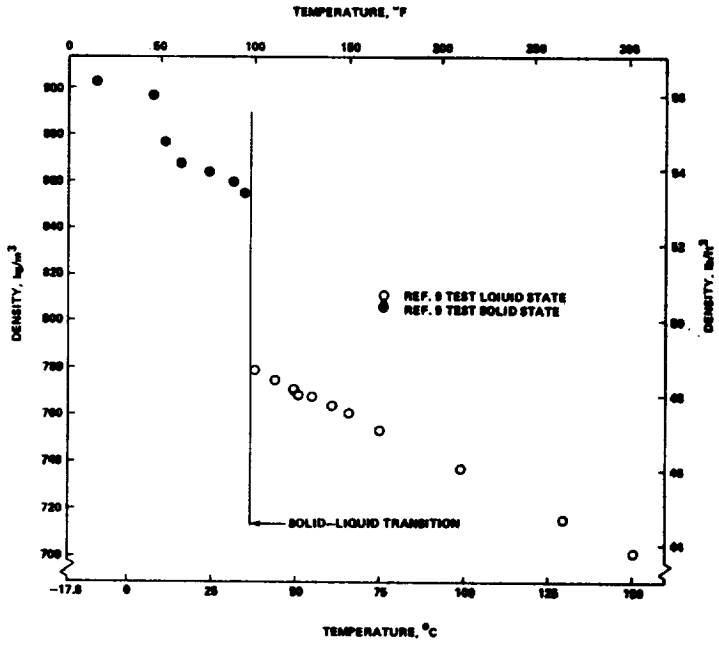

Figure 17. Density of octadecane ($C_{18}H_{38}$) (from Fig. 6 of Reference 9).

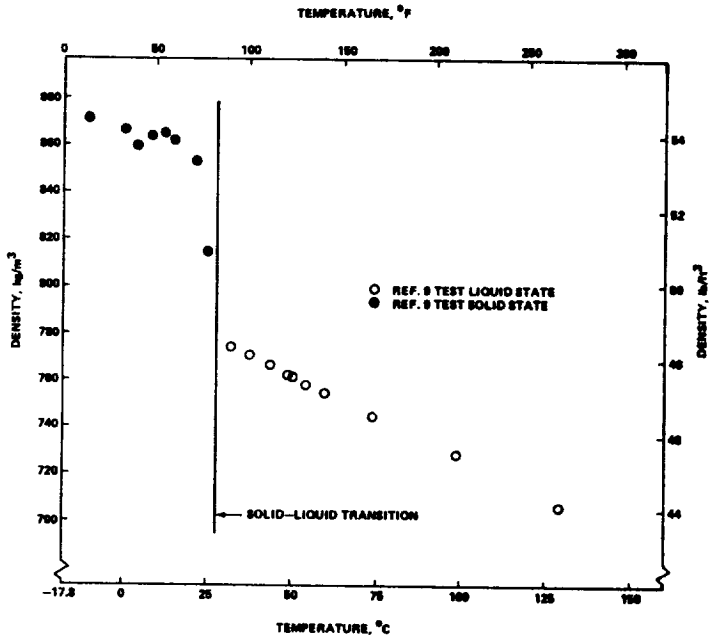

Figure 18. Density of eicosane ($C_{20}H_{42}$) (from Fig. 7 of Reference 9).

TABLE 10. THERMAL CONDUCTIVITY OF SELECTED PARAFFINS (EVALUATED AT PHASE CHANGE TEMPERATURE)[a]

Material	W/m-°C	Btu/h-ft-°F
n-Undecane	0.1496	0.0865
n-Dodecane	0.1488	0.0860
n-Tridecane	0.1496	0.0865
n-Hexadecane	0.1505	0.0870
n-Octadecane	0.1505	0.0870
n-Nonadecane	–	–
n-Eicosane	0.1505	0.0870

a. From Table 8 of Reference 6.

as being available from the API. Thermal conductivity data which are presented in Reference 9 for the liquid phase of $C_{14}H_{30}$, $C_{16}H_{34}$, $C_{18}H_{38}$, and $C_{20}H_{42}$, are shown in Figures 19 through 23. Figure 23 shows a correlation which was extrapolated to obtain thermal conductivities for $C_{20}H_{42}$.

The lack of thermal conductivity data for the solid phase poses some analytical uncertainties when attempting to analyze the phase change process. This concern and related considerations are treated in more detail in Section V.

G. Viscosity

Absolute viscosity data for liquid paraffins $C_{11}H_{24}$ through $C_{20}H_{42}$, which are given in Reference 7, are shown plotted as a function of temperature in Figure 24.

H. Surface Tension

Values of the surface tension for liquid paraffins $C_{11}H_{24}$ through $C_{20}H_{42}$, which are tabulated in Reference 7, are plotted versus temperature in Figure 25. The data varies linearly with temperature with an increase of temperature resulting in a decrease of surface tension.

I. Coefficient of Expansion

Single values of the coefficient of expansion for four of the considered paraffins are shown in Table 11 which were reported in Reference 6 as being from API.

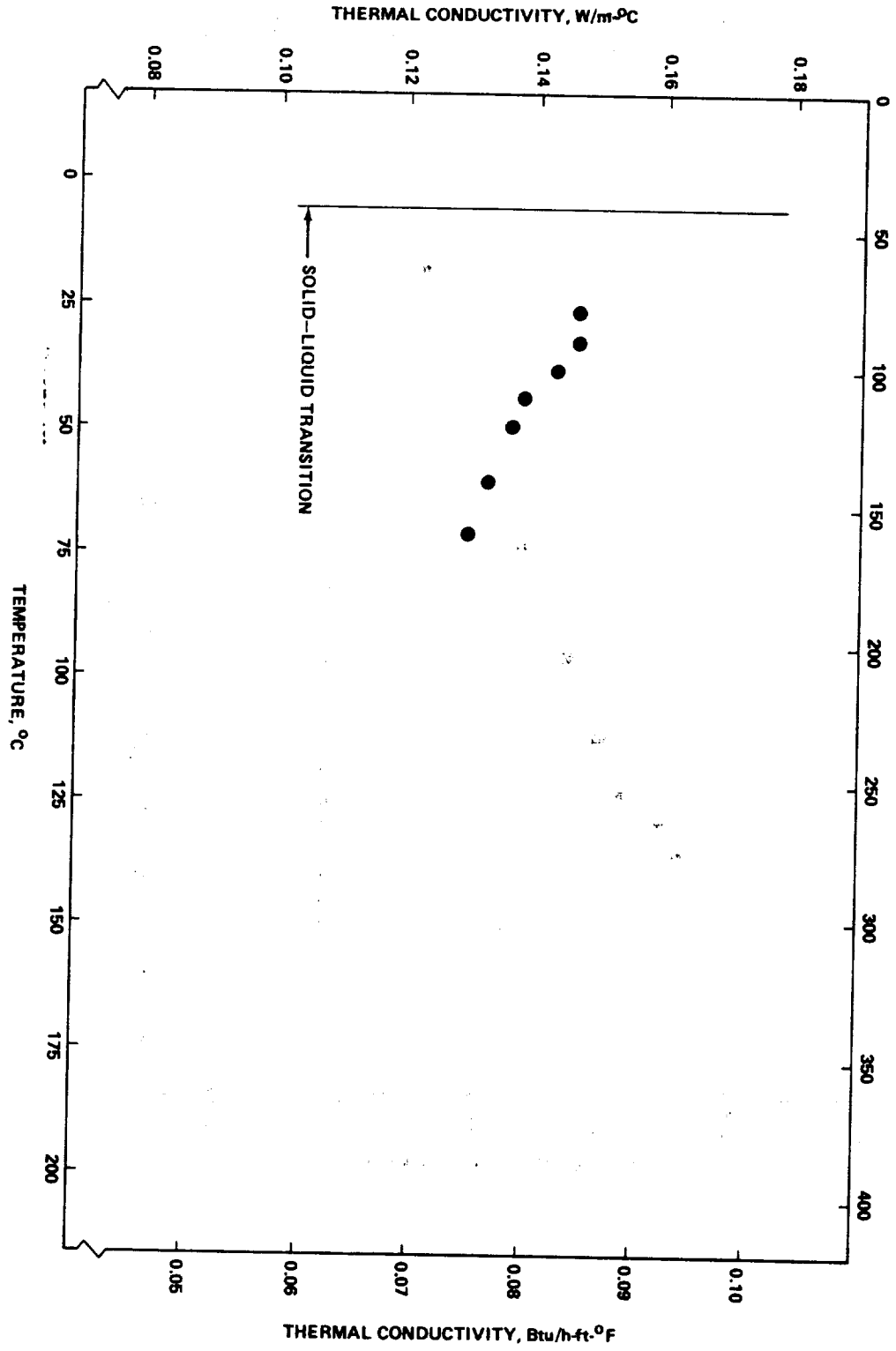

Figure 19. Thermal conductivity of tetradecane ($C_{14}H_{30}$) (from Fig. 12 of Reference 9).

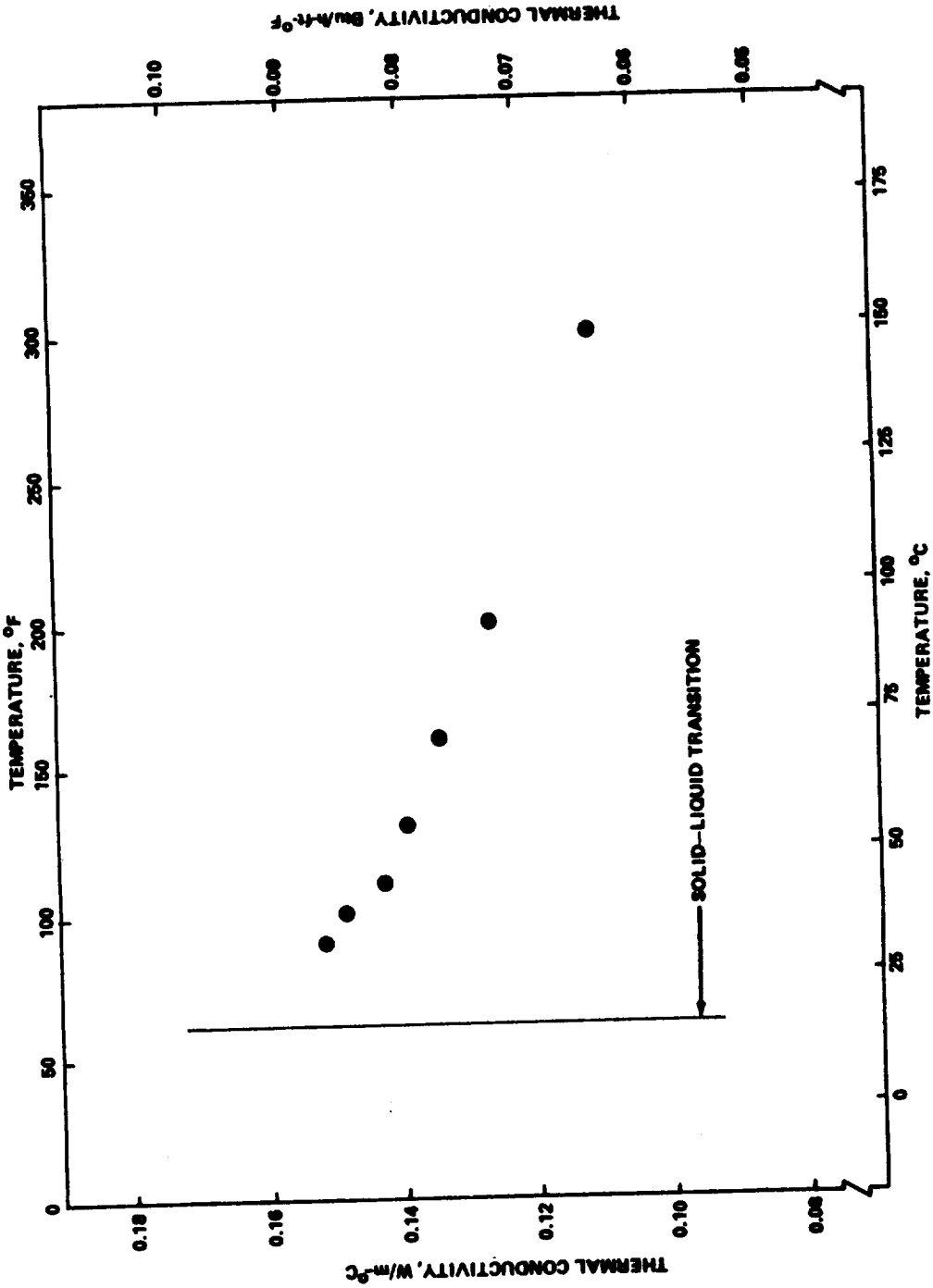

Figure 20. Thermal conductivity of hexadecane ($C_{16}H_{34}$) (from Fig. 13 of Reference 9).

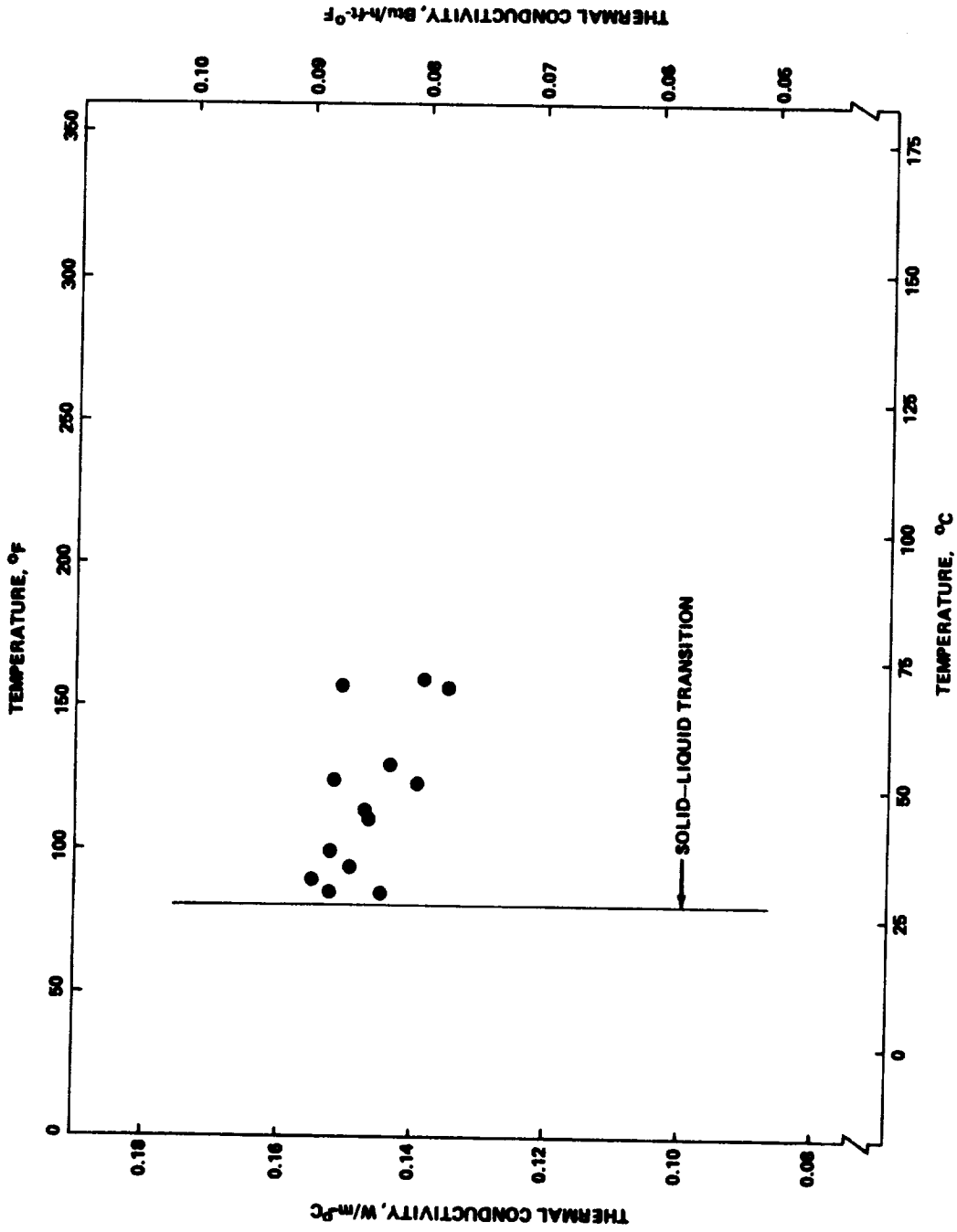

Figure 21. Thermal conductivity of octadecane ($C_{18}H_{38}$) (from Fig. 14 of Reference 9).

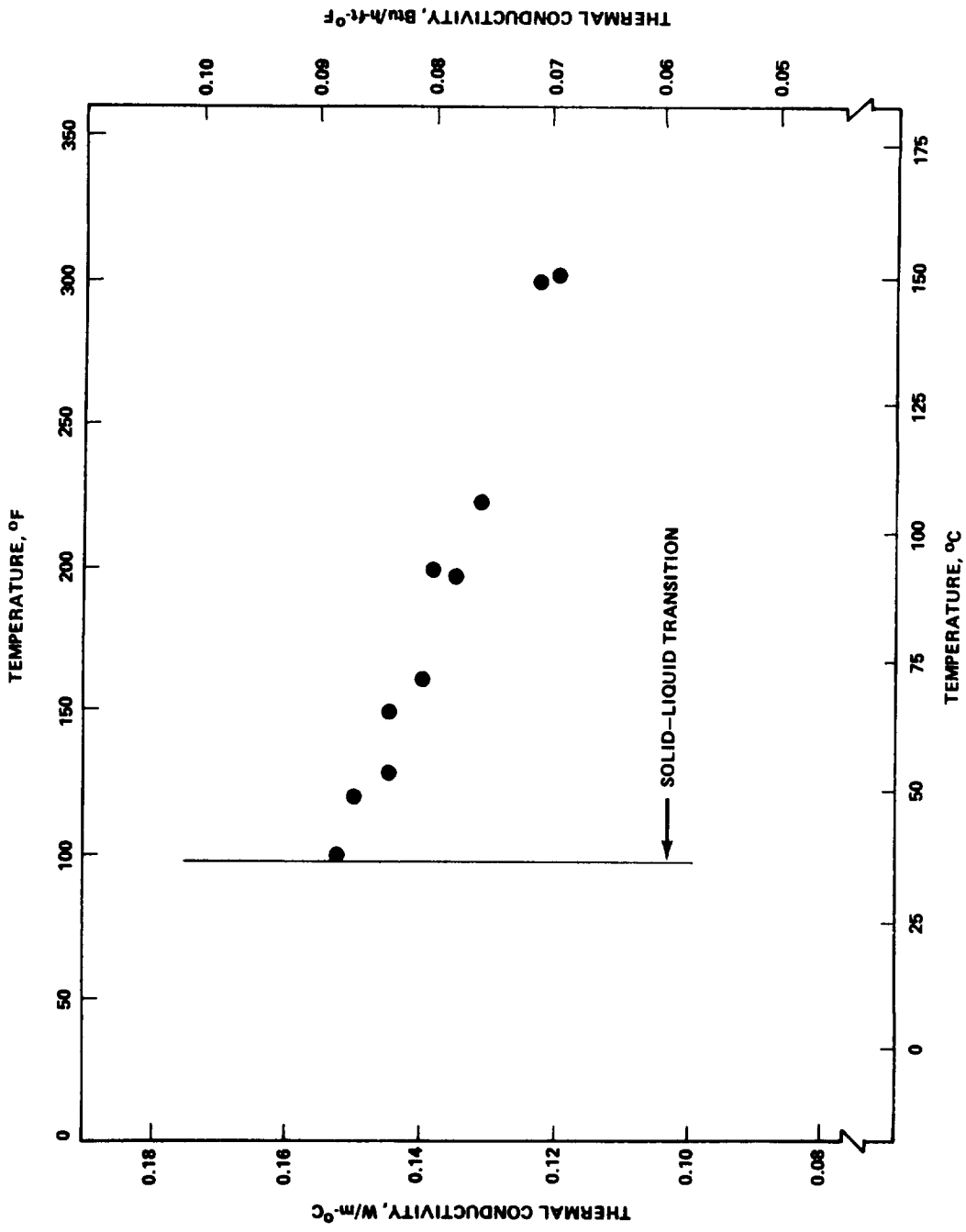

Figure 22. Thermal conductivity of eicosane ($C_{20}H_{42}$) extrapolated from data for lower carbon number paraffins (from Fig. 15 of Reference 9).

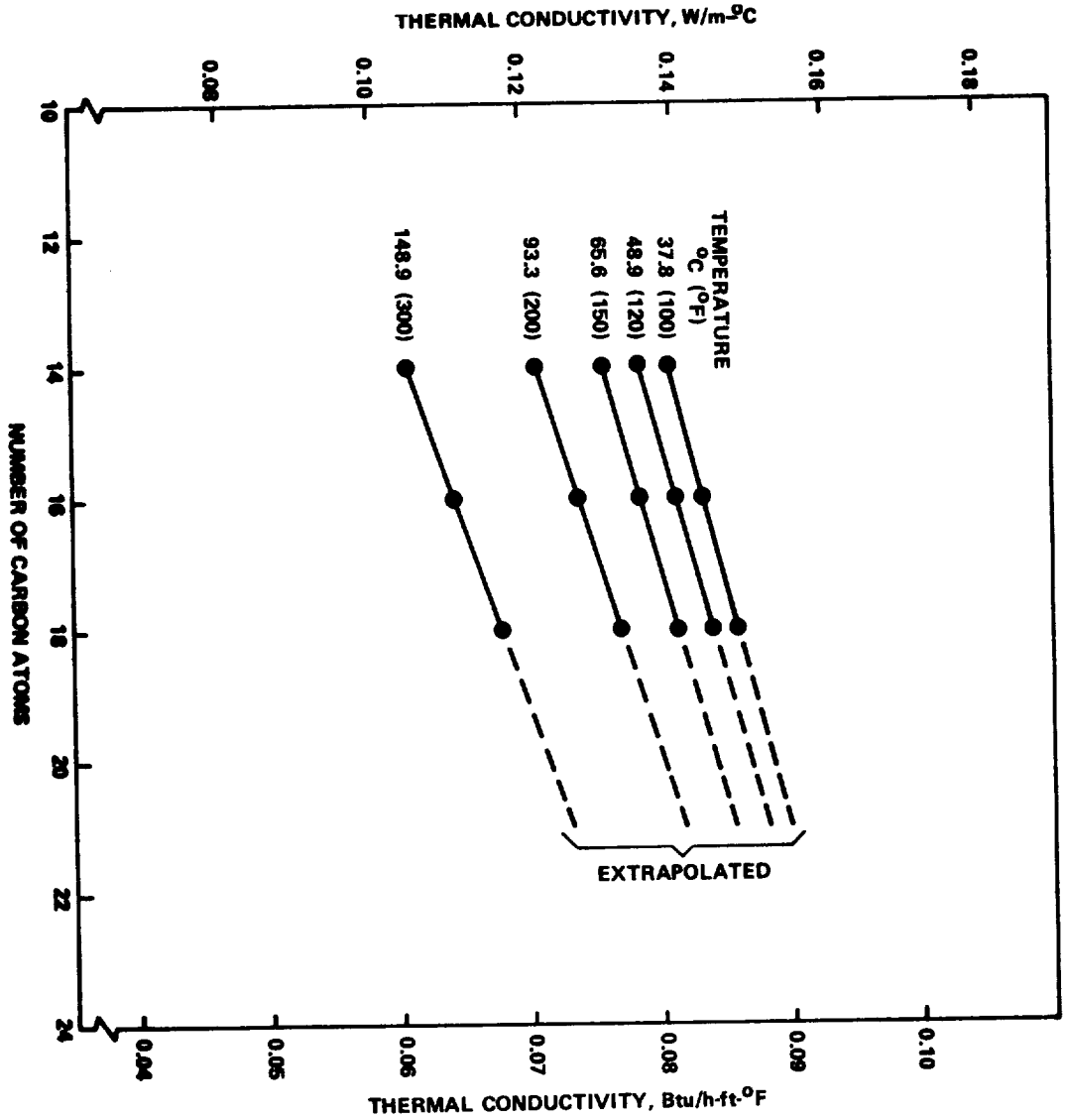

Figure 23. Correlation of thermal conductivity data for normal paraffins (C_nH_{2n+2}) (from Fig. 16 of Reference 9).

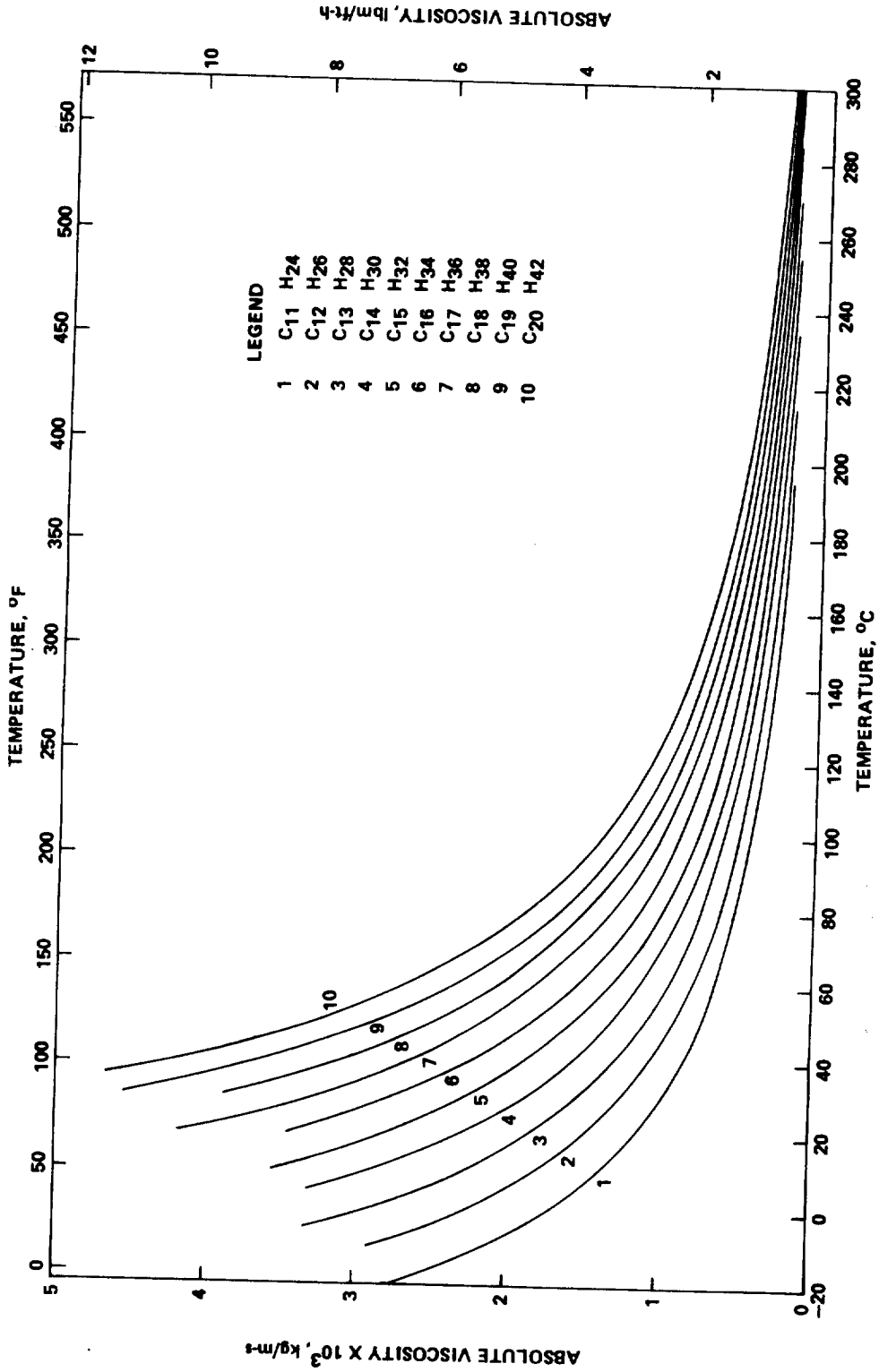

Figure 24. Absolute viscosity of paraffins $C_{11}H_{24}$ through $C_{20}H_{42}$ versus temperature (based on data given in Reference 7).

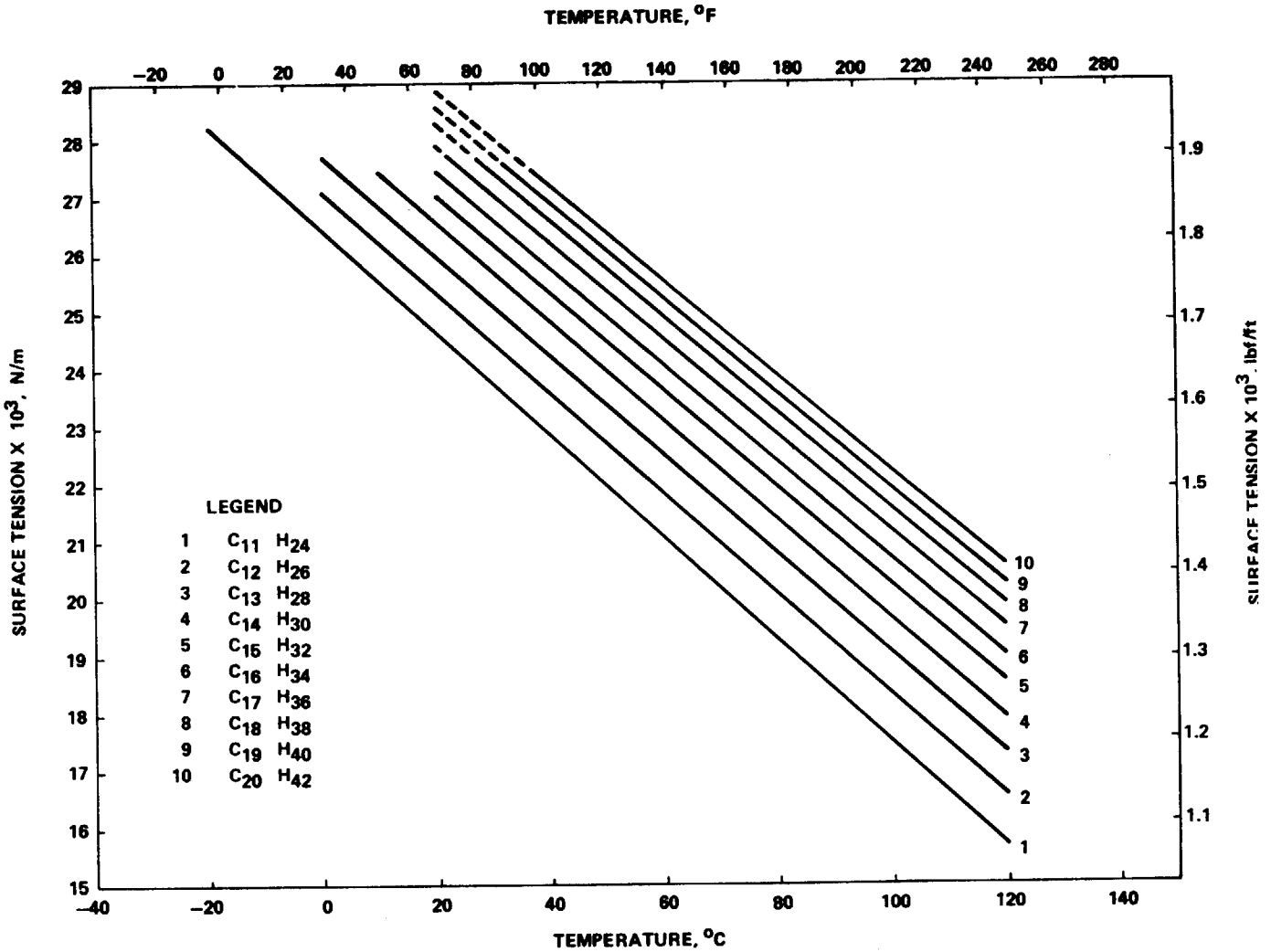

Figure 25. Surface tension for $C_{11}H_{24}$ through $C_{20}H_{42}$ (based on data given in Reference 7).

TABLE 11. VOLUMETRIC COEFFICIENT OF EXPANSION (60°F/15.6°C)[a]

Material	1/K	1/°F
n-Undecane	10.1×10^{-4}	5.6×10^{-4}
n-Dodecane	9.9×10^{-4}	5.5×10^{-4}
n-Tridecane	9.4×10^{-4}	5.2×10^{-4}
n-Eicosane	8.5×10^{-4}	4.7×10^{-4}

a. From Table 18 of Reference 6 .

III. TWO-DIMENSIONAL ANALYSIS OF A PHASE CHANGE DEVICE

A. Introduction

The analysis of two-dimensional conductive heat transfer within a phase change device is outlined in this section. Since convection may be present in certain applications, the design of a phase change device based solely on conduction will in most cases be conservative (i.e., heat transfer rate to and from material will be lower than in a case where convection is present). Additional attention is given in Section V to the effect of convection and how it can be included in the analysis.

The two-dimensional transient heat conduction equation for an isotropic, homogeneous medium in the absence of sources, sinks, or phase change is

$$\alpha\left(\frac{\partial^2 T}{\partial x^2} + \frac{\partial^2 T}{\partial y^2}\right) = \frac{\partial T}{\partial t} \tag{1}$$

In general, solutions of equation (1) for typical applications can best be obtained via numerical techniques, other techniques were outlined by Muehlbauer and Sunderland [10]. For numerical solutions of equation (1), the partial derivatives are approximated by finite difference analogs. A forward difference analog for the time derivatives can be used. With regard to the latter, there are two possibilities for a transient problem [11]. If all temperatures appearing in the spatial analogs are evaluated at the old time level, the formulation is explicit, and the resulting equation for a node involves only one unknown at the new time level. The solution for a system of nodes by this method is fairly simple

and straightforward. If all temperatures appearing in the spatial analogs are evaluated at the new time level, the formulation is implicit. The resulting equation for a node involves five unknown temperatures at the new time level. Solution for a system of nodes involves solving a set of simultaneous equations equal to the number of nodes.

Figure 26 represents a general node (I, J), its surrounding nodes, and the notational scheme for interconnecting thermal conductances.

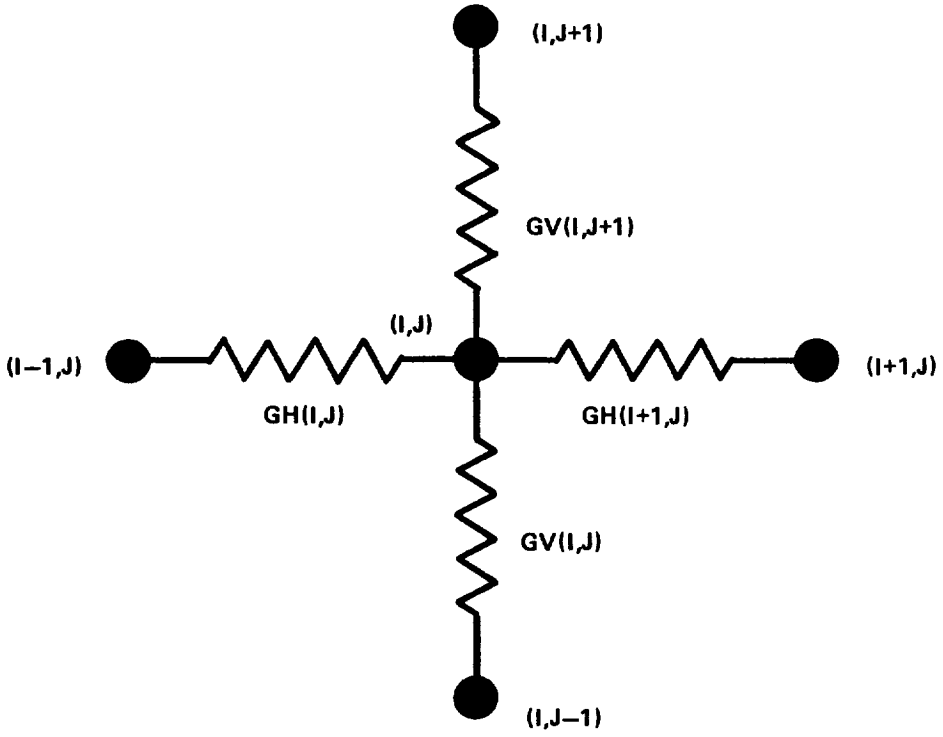

Figure 26. General designations for nodes and connecting conductances.

Physical arguments can be used to formulate the difference analogs previously discussed. The summation of heat transfer to node (I, J) from all surrounding nodes should equal the product of the nodal capacitance and the difference in its old and new temperature. With reference to Figure 26, the explicit formulation based on this physical approach is

$$GH(I,J)[T(I-1,J) - T(I,J)] + GH(I+1,J)[T(I+1,J) - T(I,J)] + GV(I,J)[T(I,J-1) - T(I,J)] + GV(I,J+1)[T(I,J+1) - T(I,J)] = \frac{C(I,J)[\tilde{T}(I,J) - T(I,J)]}{\Delta t} \qquad (2)$$

The implicit formulation is

$$GH(I,J)\ [\tilde{T}(I-1,J) - \tilde{T}(I,J)] + GH(I+1,J)[\tilde{T}(I+1,J) - \tilde{T}(I,J)] + GV(I,J)\ [\tilde{T}(I,J-1) - \tilde{T}(I,J)] + GV(I,J+1)[\tilde{T}(I,J+1) - \tilde{T}(I,J)] = \frac{C(I,J)[\tilde{T}(I,J) - T(I,J)]}{\Delta t} \quad (3)$$

The tildes denote temperatures at the new time level.

Numerical solution of the explicit formulation given by equation (2) is subject to a restriction on the allowable time step given by

$$\Delta t \leqslant \frac{C(I,J)}{GH(I,J) + GH(I+1,J) + GV(I,J) + GV(I,J+1)} \quad (4)$$

For a nodal arrangement, the node having the smallest time step given by equation (4) governs the entire solution.

The implicit formulation given by equation (3) is not restricted by a stability requirement, but the solution is not as simple as one using the explicit formula. In general, it requires a matrix inversion routine and may be impractical for a large number of nodes.

A technique for handling the phase change when using the explicit formulation involves keeping a record of the stored energy at each PCM node. The stored energy at any time is compared to that associated with the initiation and termination of the phase change. When the accumulated energy at a node lies between these two values, the temperature prediction is overridden and the temperature is forced to be equal to the phase change temperature.

The technique for handling the phase change when using the implicit formulation involves comparison of the predicted temperature with the phase change temperature. When the predicted temperature first exceeds the latter value, the predicted value is overridden and the nodal temperature is specified to be the phase change temperature. The energy associated with the excess of the predicted value over the phase change temperature is calculated and allowed to accumulate. Once this accumulated energy reaches a value sufficient to accomplish the phase change, the predicted temperature is allowed to rise in accordance with the governing conduction equations.

B. Physical Model

The physical model selected for study corresponds to a phase change device application which is depicted in Figure 27. Basically, the phase change device consists of a metallic housing in the shape of a parallelepiped which is filled with PCM and straight metallic fins which are included to improve the heat transfer mechanism between the housing and the PCM.

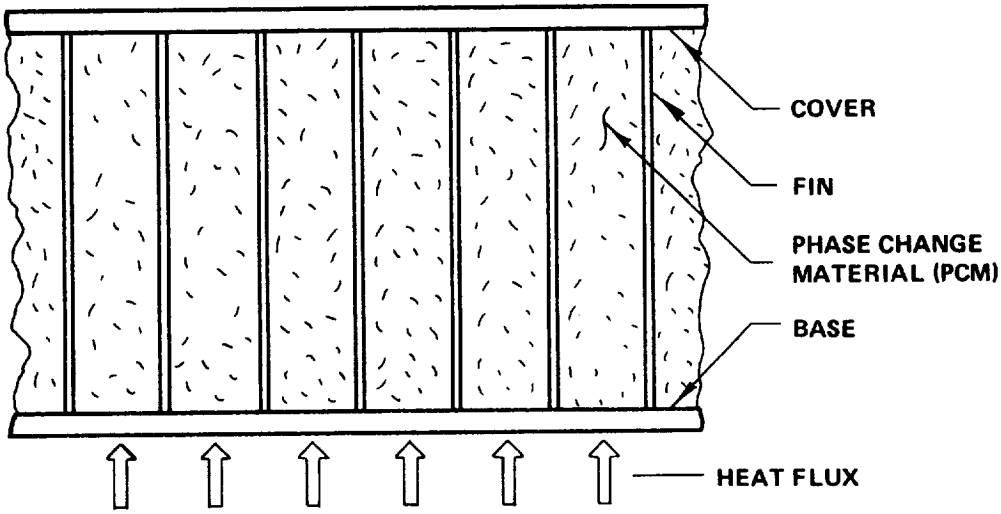

Figure 27. Phase change device application selected for study.

When the phase change device is operating as an energy sink (i.e., it is storing energy), either a hot fluid or a hot surface is considered to be in contact with one surface of the housing resulting in heat transfer into the unit. Hereafter, this surface which is in contact with the hot medium is referred to as the base. The PCM is used to absorb the energy primarily via the phase change process. The stored energy may be later rejected by means of exposing the base or the cover or both to a cooler medium, which in some applications may be the same medium from which the energy was absorbed earlier.

A typical single cell of the device is shown in Figure 28. It is assumed that planes parallel to the fins and passing through their centers represent planes of symmetry as do planes parallel to the fins and located midway between two adjacent fins. Consequently, the analysis is reduced to that of a half-cell represented by the schematic given in Figure 29.

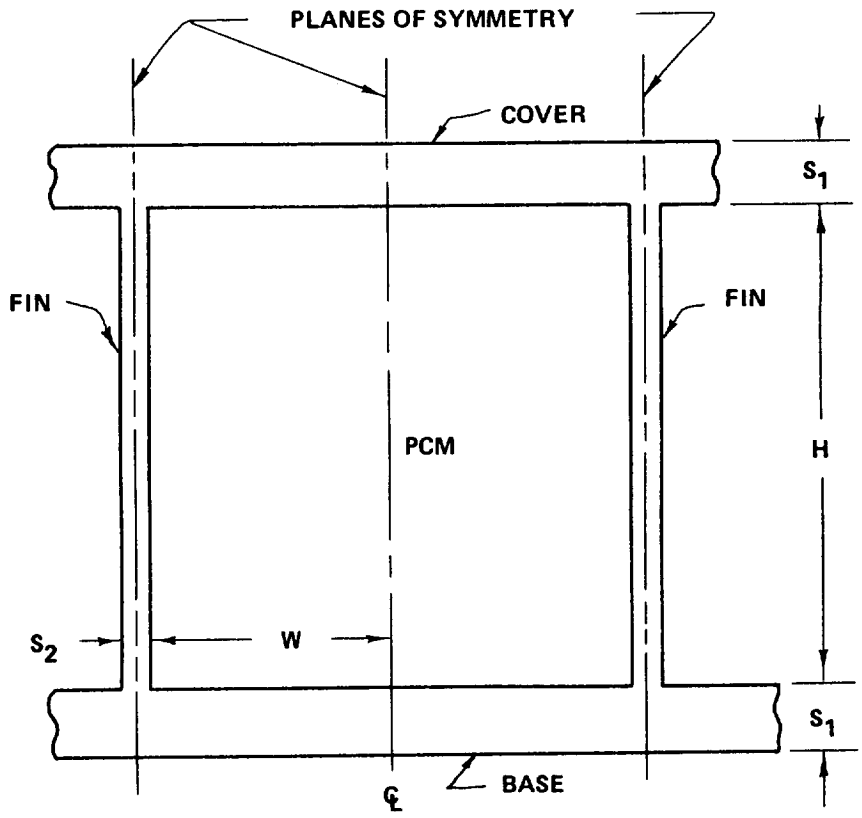

Figure 28. Typical single cell of phase change device.

The following thermal analysis pertains to the symmetrical half-cell shown in Figure 29 with the base exposed to a constant heat flux density. The resulting computer program is also modified for the case of a constant base temperature.

The limitations of the analysis are given by the following assumptions:

- Conduction is the only heat transfer mechanism within the two-dimensional half-cell; the overall phase change device is considered to be composed of many such cells. (The effects of convection are discussed in Section V).

- The problem is two-dimensional; the cell, therefore, is sufficiently long that end effects are small.

- The cover is perfectly insulated.

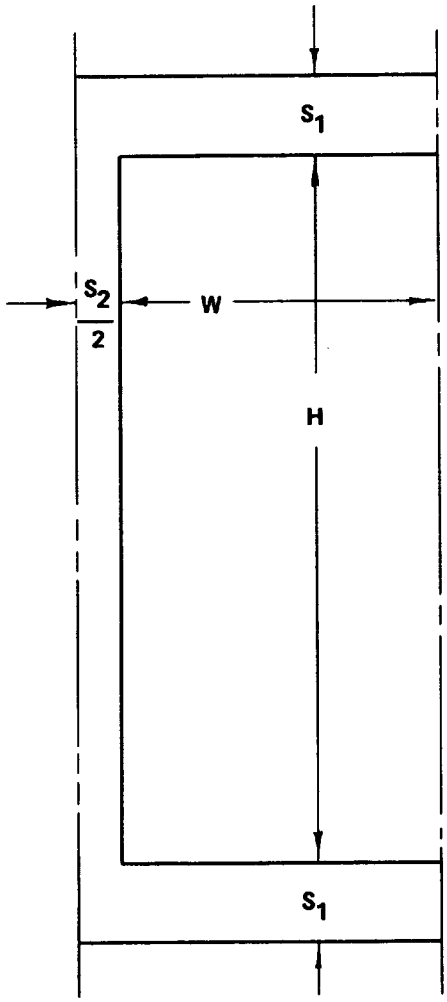

Figure 29. Symmetrical half-cell used in analysis.

- The physical properties, density, specific heat, and thermal conductivity of the metallic fin, cell base, and cell cover are considered to be identical and to have constant values. Likewise, the density, specific heat, and thermal conductivity of the solid and liquid phases of the PCM are considered to be identical and to have constant values. (The model may be easily modified to input temperature variant properties.)

To cast the problem in a nondimensional formulation, appropriate dimensionless parameters are sought. As a means of obtaining the pertinent dimensionless parameters, differential equations for the temperature in the PCM, the fin, the base, and the cover are presented and nondimensionalized. The differential analysis is followed by a numerical analysis which is used for the solutions, the results of which are presented in Section IV.

C. Differential Formulation

Since the principal objective of the differential formulation is to find the appropriate dimensionless parameters for the physical model previously described, the reader interested only in using the results can go directly to the next section on the numerical analysis.

The differential equations pertinent to each region of the model are presented below.

1. PCM Region. The energy differential equation is the usual two-dimensional conduction equation

$$\frac{\partial^2 T}{\partial x^2} + \frac{\partial^2 T}{\partial y^2} = \frac{1}{\alpha}\frac{\partial T}{\partial t} \tag{5}$$

and the two-dimensional interfacial boundary condition according to Rathjen and Jiji [12] is

$$k\left[\left(\frac{\partial T}{\partial y}\right)_s - \left(\frac{\partial T}{\partial y}\right)_\ell\right]\left[1 + \left(\frac{\partial \delta(x,t)}{\partial x}\right)^2\right] = \rho\, h_f \frac{\partial \delta}{\partial t}\bigg|_{y=\delta} \tag{6}$$

where $\delta(x,t)$ is the interfacial location or fusion front. Choosing the width W of the PCM region shown in the symmetrical half-cell in Figure 29 as the characteristic x-dimension, the PCM height H as the characteristic y-dimension, the PCM fusion temperature T_f as the characteristic temperature, and denoting a characteristic time by t_c result in the following dimensionless quantities:

$$x' \equiv x/W \tag{7}$$

$$y' \equiv y/H \tag{8}$$

$$\theta \equiv T/T_f \tag{9}$$

$$t' \equiv t/t_c \tag{10}$$

In terms of these, equation (5) can be written as

$$\left(\frac{H}{W}\right)^2 \frac{\partial^2\theta}{\partial x'^2} + \frac{\partial^2\theta}{\partial y'^2} = \frac{H^2}{\alpha\, t_c}\frac{\partial\theta}{\partial t'} \tag{11}$$

and equation (6) becomes

$$\left[\left(\frac{\partial\theta}{\partial y'}\right)_s - \left(\frac{\partial\theta}{\partial y'}\right)_\ell\right]\left[1+\left(\frac{H}{W}\right)^2\left(\frac{\partial\delta'}{\partial x'}\right)^2\right] = \frac{h_f H^2}{\alpha\, c_p T_f t_c}\left(\frac{\partial\delta'}{\partial t'}\right) \tag{12}$$

2. Fin. Treating the temperature distribution in the fin as one-dimensional, i.e., $T_m = T_m(y,t)$, with conductive heat transfer from the fin to the PCM, which is analogous to the treatment of convective heat transfer in the conventional one-dimensional fin problem, results in

$$\frac{\partial^2 T_m}{\partial y^2} + 2\frac{k}{k_m}\left(\frac{1}{S_2}\right)\left(\frac{\partial T}{\partial x}\right)_{0,y} = \frac{\rho_m c_{p_m}}{k_m}\frac{\partial T_m}{\partial t} \tag{13}$$

where the coordinate system is given in Figure 30. The second term on the left in equation (13) results from considering conduction in the PCM. The temperature in the fin at x = 0, however, is the same as that in the PCM at x = 0.

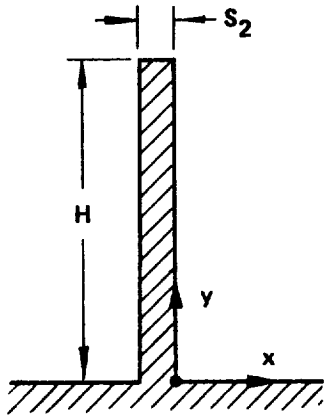

Figure 30. Coordinate system and dimensions for fin.

Nondimensionalization of equation (13) using equations (7) through (10) results in

$$\frac{\partial^2 \theta_m}{\partial y'^2} + 2\,\frac{k}{k_m}\left(\frac{H^2}{S_2 W}\right)\left(\frac{\partial \theta}{\partial x'}\right)_{0,y} = \left(\frac{H^2}{\alpha\, t_c}\right)\left(\frac{\alpha}{\alpha_m}\right)\frac{\partial \theta_m}{\partial t'} \tag{14}$$

3. Cell Base. Treating the cell base as a lumped system, i.e., $T_b = T_b(t)$, and assuming the base and fin properties to be the same result in the following energy equation:

$$\dot{q}''\left(W + \frac{S_2}{2}\right) + k_m \frac{S_2}{2}\left(\frac{\partial T_m}{\partial y}\right)_{0,0} + kW\left(\overline{\frac{\partial T}{\partial y}}\right)_{x,0} = \rho_m c_{p_m} S_1 \left(W + \frac{S_2}{2}\right)\frac{dT_b}{dt} \tag{15}$$

where it has been assumed that the base is exposed to a constant heat flux density, $\dot{q}''$. The coordinate system and physical dimensions for the cell base are given in Figure 31. The subscripts x,0 on the third term on the left side of equation (15) denote evaluation at $0.5\ S_2 \leqslant x \leqslant W$ and $y = 0$. In terms of the previously defined dimensionless variables, equation (15) becomes

$$\frac{\dot{q}''H}{kT_f}\left(1 + \frac{S_2}{2W}\right) + \frac{k_m}{k}\,\frac{S_2}{2W}\left(\frac{\partial \theta_m}{\partial y'}\right)_{0,0} + \left(\overline{\frac{\partial \theta}{\partial y'}}\right)_{x',0} = \frac{S_1}{H}\left(1 + \frac{S_2}{2W}\right)\left(\frac{H^2}{\alpha t_c}\right)\left(\frac{k_m}{k}\right)\left(\frac{\alpha}{\alpha_m}\right)\frac{d\theta_b}{dt'} \tag{16}$$

In equations (15) and (16) the overbar on the third term on the left side denotes a value spatially averaged over the x-length W.

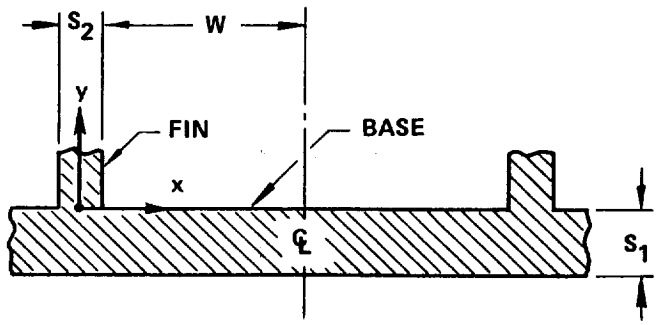

Figure 31. Coordinate system and dimensions for base.

4. Cell Cover. Since the treatment of the cell cover is analogous to that of the cell base except for the assumption that the cover is insulated, no new dimensionless parameters should appear; therefore, the appropriate equation is omitted for brevity.

To this point the dimensionless equations contain a undefined reference time, t_c. By selecting this characteristic time to be given by

$$t_c = \frac{H^2}{\alpha} \tag{17}$$

the ratio $H^2/\alpha t_c$ becomes 1.0 in equations (11), (12), (14), and (16). Examination of the reduced set of equations reveals seven salient dimensionless ratios for this class of problem. Summarizing these ratios by category, with pure constants omitted, yields

Geometric:

$$R_1 = H/W$$

$$R_2 = H/S_1$$

$$R_3 = W/S_2$$

Material Properties:

$$R_4 = \frac{k_m}{k}$$

$$R_5 = \alpha_m/\alpha$$

$$R_6 = \frac{h_f}{c_p T_f}$$

Thermal Loading:

$$R_7 = \frac{\dot{q}'' H}{k T_f}$$

These ratios developed with the differential equation formulation of the problem are also appropriate for the finite difference formulation. Hence, the finite difference equations are cast in dimensionless form with the seven aforementioned dimensionless parameters appearing explicitly and serving as focal points for a parametric numerical study.

D. Finite Difference Formulation

The finite difference formulation begins with a subdivision of the region of interest into a network of nodal points. For the two-dimensional, symmetrical half-cell shown in Figure 29, the nodal network and nodal point designation scheme are shown in Figure 32. The approach provides flexibility for increasing or decreasing the number of PCM nodes in accordance with the dictates of size and shape, there being M by N PCM nodes. Also note that all base nodes correspond to J = 1 and all fin nodes correspond to I = 1. The number of base or fin nodes is, of course, directly related to the PCM subdivision. Figure 26 depicts a general node (I,J), its four surrounding nodes, and the notational scheme for interconnecting thermal conductances.

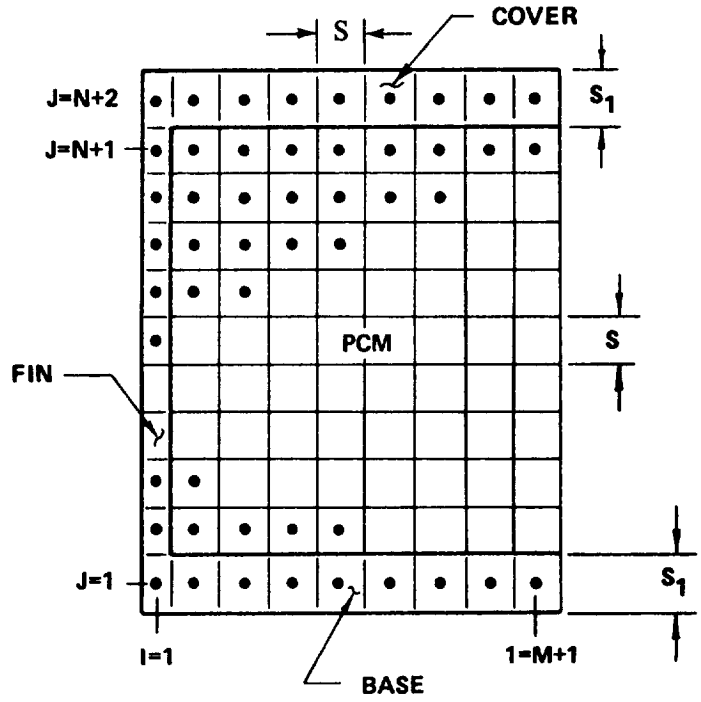

Figure 32. Nodal grid designation.

Physical arguments can be used to formulate the temperature finite difference equations. With reference to Figure 26 the net heat transfer to node (I,J) from its surrounding nodes (during time Δt) should equal the product of the nodal thermal capacitance and the temperature difference occurring during the time increment. The explicit formulation based on this approach in nondimensional form is

$$GH'(I,J)\,[\theta(I-1,J)-\theta(I,J)] + GH'(I+1,J)\,[\theta(I+1,J)-\theta(I,J)] + GV'(I,J)\,[\theta(I,J-1)$$

$$-\theta(I,J)] + GV'(I,J+1)\,[\theta(I,J+1)-\theta(I,J)] = \frac{C'(I,J)\,[\tilde{\theta}(I,J)-\theta(I,J)]}{R_1^2\,M^2\,\Delta t'} \qquad (18)$$

The implicit formulation is

$$GH'(I,J)\,[\tilde{\theta}(I-1,J)-\tilde{\theta}(I,J)] + GH'(I+1,J)\,[\tilde{\theta}(I+1,J)-\tilde{\theta}(I,J)] + GV'(I,J)\,[\tilde{\theta}(I,J-1)$$

$$-\tilde{\theta}(I,J)] + GV'(I,J+1)\,[\tilde{\theta}(I,J+1)-\tilde{\theta}(I,J)] = \frac{C'(I,J)\,[\tilde{\theta}(I,J)-\theta(I,J)]}{R_1^2\,M^2\,\Delta t'} \qquad (19)$$

In the nondimensionalization of all thermal conductances, the nondimensional value is obtained by dividing the respective conductance by kB which is the conductance between two general PCM nodes. Similarly, nondimensional thermal capacitance values are obtained by dividing the respective dimensional value by $\rho S^2 Bc_p$ which is the thermal capacitance of a general PCM node. It should be noted that the nondimensional conductances and capacitances that are entirely within the PCM have the numerical value of 1.0. All other dimensionless conductances and capacitances have values other than unity. As an example, the dimensionless horizontal conductance between the fin and the lower left hand corner PCM node is

$$GH'(2,2) = \frac{2}{1+\dfrac{M}{2\,R_3 R_4}} \qquad (20)$$

A dimensionless base nodal capacitance, for example, is

$$C'(2,1) = \frac{M\,R_1 R_4}{R_2 R_5} \qquad (21)$$

1. Computer Programs. Numerical solutions of the problem described herein via computers can be affected by use of either the explicit formulation given by equation (18) or the implicit formulation given by equation (19). The two general approaches together with the inherent advantages and disadvantages related to each are discussed in

the general heat transfer literature; see, for example, Chapman [11] or Özisik [13]. It is well established that solution of the explicitly formulated set of equations is subject to a stability restriction which dictates the maximum allowable time increment. This restriction is given by equation (4). For a small grid size, this requirement leads to excessive computer time. While solutions of the implicitly formulated set of equations is not restricted by a stability requirement, the method involves the solution of a set of simultaneous equations equal in number to the number of nodes. For a small grid size, large computer storage is needed.

The problem under consideration involves thin metallic fins; most attention, consequently, has been given to the implicit approach. The stability restriction dictated by a node located in the fin resulted in extremely small time increments for the explicit approach.

A computer program based on the implicit approach, equation (19), for the problem described in this section is given in Table 12. A modification of the program to accommodate a sudden change in the base temperature rather than imposition of a constant heat flux density is given in Table 13. In both programs, a band algorithm technique given by Funderlic [14] is used to solve the equations. A dimensional computer program based on the explicit approach is presented and briefly discussed in Appendix D.

2. Instructions for Using Computer Programs. To use the programs, the following steps are suggested:

a. Establish the grid size (see Fig. 32) by specifying M and N. M represents the number of vertical columns and N represents the number of horizontal rows within the PCM. The ratio of N to M must equal R_1. The accuracy of the transient results may be affected by the choice of M and N, particularly in the early part of the transient. The user should conduct a sensitivity study by altering M and N along with DT (Step f) in a systematic manner until the results appear to be unaltered to within an acceptable level by further changes. The influence of the choice of M and N is discussed and illustrated in Section IV along with discussion of the parametric study.

b. Determine appropriate values for the dimensionless ratios R_1 through R_7 as defined in the analysis. Note that R_7 is denoted as R_8 in the program. Also, for the constant temperature case R_7 is not needed, but a temperature difference (DELT) is needed. This difference is defined by

$$\text{DELT} = \frac{T_B}{T_F} - 1$$

c. The dimension card must be set correctly. The dimensions depend on M and N as indicated below.

```
A(LL,L1)
T1(M1,N2)
```

T2(LL)
GH(M2,N2)
GV(M1,N2)
C(M1,N2)
F(LL)
TEXC(LL)
D(LL)
MELT(LL)

where

$LL = (N2) \times (M1)$

$L1 = (2) \times (M1 + 1)$

$M1 = M + 1$

$M2 = M + 2$

$N2 = N + 2$

d. Input required parameters in accordance with Formats 998 and 999. The required inputs are shown by the Read statements. NR is reserved for a reference run number.

e. The program is written with the initial PCM temperature at T_f. If it is desired to run for other values of initial temperature, set TIN by

$$TIN = T_{initial}/T_f$$

f. Select a nondimensional time set by specifying DT. It is suggested that the magnitude of this time increment be explored for its influence on the accuracy of the results. Note the discussion given in Step a also.

g. Set ITT. This quantity controls the printout of results. The program is written to yield output at the end of the first time increment and then on intervals given by

$$(ITT - 1) \times (DT)$$

The output includes

TIME – Nondimensional time measured from start of melting

TRISE – $(T_{Base} - T_f)/T_f$ (use absolute temperatures)

UCOEF – Nondimensional overall heat transfer coefficient defined by

$$UCOEF = \frac{R_7}{T_{Base} - T_f}$$

FMELT – Fraction of PCM melted at given time (or solidified for freeze case)

SQF – Energy stored in fin

SQB – Energy stored in base

SQT – Energy stored in top

SQS – Energy stored in solid

SQL – Energy stored in liquid

QLAT – Energy used to change phase

QTOT – Summation of SQF, SQB, SQT, SQS, SQL and QLAT

EIN – Total energy transferred into base which is dependent on q'' and time

RATIO – QTOT/EIN – check on energy balance.

All the energy values which were listed are nondimensional and evaluated with respect to initial values of zero. The energy value used in the nondimensionalization is the latent energy for a single PCM node.

The programs given in Tables 12 and 13 can be altered slightly to accommodate freezing for the case of a constant heat flux density withdrawal at the base and a step reduction in the base temperature, respectively. The changes needed to accomplish this are:

a. In the parameters at the beginning, replace QLATM by -QLATM.

b. In the third, second, and first lines above statement 150, change the statements to

TABLE 12. COMPUTER PROGRAM FOR BASE EXPOSED TO A CONSTANT HEAT FLUX DENSITY

```
C *** CONSTANT HEAT RATE PROGRAM
      DIMENSION A(126,7), T1(3,42), T2(126), GH(4,42), GV(3
     1,42),C(3,42), F(126), TEXC(126), D(126), MELT(126)
      IMPLICIT REAL*8(A-H,O-Z)
C *** R1 = H/W ; R2 = 4/S1 ; R3 = W/S2 ; R4 = K/KW ; *******
C     ************
C *** R5 = (K/DEN*CP)/(KW/DENW*CPW) ; R6 = HMELT/CPW*TMELT *
C     ************
C *** R7 = HMELT/HTR ; R8 = Q*H/KW*TMELT ********************
C     ************
      READ(5,998) R1,R2,R3,R4,R5,R6,R8
      READ(5,999) NR,M,N
C *** COMPUTATIONAL PARAMETERS ***
      TIN=1.0
      DT=0.0005
      ITT=41
      CW = 1.0
      TMELT = 1.0
      ITTT = 1
      TPHASE = R6
      AN = N
      AM = M
      QLATM = AM*AN
      AM1 = AM + 1.0
      M1 =  M + 1
      M2 = M1 + 1
      N1 = N + 1
      N2=N+2
      LL=N2*M1
      L1 = 2*M1 + 1
      L = M2
      CD = (R1**2)*(AM**2)
C *** INITIAL VALUES
      SQS = 0.0
      SQF = 0.0
      SQB = 0.0
      SQT=0.0
      SQL = 0.0
      QLAT = 0.0
      EBOT=0.0
      TTCB=0.0
      MM = 0
      TBOT = 0.0
      TIME = 0.0
      DO 10 I = 1,LL
      F(I) = 1.0
      MELT(I)=0
   10 TEXC(I) = 0.0
      DO 20 J=1,N2
      DO 20 I = 1,M1
   20 T1(I,J) = TIN
```

TABLE 12. (Continued)

```
C  ***** HORIZONTAL CONDUCTANCES,VERTICAL CONDUCTANCES
C     ,CAPACITANCES **
C ****  ARE CALCULATED  *******
      GV(1,1) = 0.0
      DO 30 J=2,N1
      D0 30 I=2,M1
      GH(I,J) = 1.0
      C(I,J) = 1.0
   30 GV(I,J) = 1.0
      DO 40 J = 2,N1
      C(1,J) = (R4*AM)/(2.0*R5*R3)
      GV(1,J) = (AM*R4)/(2.0*R3)
      GH(2,J) = 2.0/(1.0 + AM/(2.0*R3*R4))
      GH(M2,J)=0.0
   40 GH(1,J) = 0.0
      DO 50 I = 2,M1
      C(I,1) = (AM*R1*R4)/(R2*R5)
      C(I,N2)=C(I,1)
      GV(I,2) = 2.0/(1.0 + (R1*AM/(R2*R4)))
      GV(I,N2)=GV(I,2)
      GV(I,1) = 0.0
      GH(I,1) = R4*AM*R1/R2
   50 GH(I,N2)=GH(I,1)
      GH(1,1) = 0.0
      GH(1,N2)=0.0
      GH(M2,1)=0.0
      GH(M2,N2)=0.0
      GH(2,1) = 2.0*R4/((R2/R1)*(1.0/(2.0*R3) + 1.0/AM))
      GH(2,N2)=GH(2,1)
      GV(1,2) = R4/(R3*(1.0/AM + R1/R2))
      GV(1,N2)=GV(1,2)
      C(1,1) = (R1*R4*(AM**2))/(2.0*R2*R3*R5)
      C(1,N2)=C(1,1)
      DO 55 I=1,M1
   55 TTCB=TTCB+C(I,1)
C    **** TEMPERATURES AT EACH NODE CALCULATED ***
      WRITE(6,7500) R1, R2, R3, R4, R5, R6, R8, M, N, NR
   60 TIME = TIME + DT
      DO 70 I = 1,LL
      DO 70 J = 1,L1
   70 A(I,J) =0.0
      DO 80 J=2,N1
      DO 80 I = 1,M1
      K = (J-1)*M1 + I
      A(K,L-M1) = GV(I,J)
      A(K,L+M1) = GV(I,J+1)
      A(K,L) = -GH(I+1,J) - GV(I,J) - GV(I,J+1)-(C(I,J)/(DT
     1*CD))-GH(I,J)
      A(K,L-1) = GH(I,J)
      A(K,L+1) = GH(I+1,J)
   80 D(K) = -C(I,J)*T1(I,J)/(CD*DT)
```

TABLE 12. (Continued)

```
      DO 90 I=1,M1
      K=N1*M1+I
      A(I,L) = -GH(I+1,1) - GH(I,1) - GV(I,2)    - C(I,1)/(DT
     1*CD)
      A(I,L+1) = GH(I+1,1)
      A(I,L-1) = GH(I,1)
      A(I,L+M1) = GV(I,2)
      A(K,L) = -GH(I,N2) - GH(I+1,N2) - GV(I,N2) - C(I,N2)/
     1(DT*CD)
      A(K,L-1) = GH(I,N2)
      A(K,L+1) = GH(I+1,N2)
   90 A(K,L-M1) = GV(I,N2)
      DO 110 I=1,M1
      K=N1*M1+I
      D(I) = -C(I,1)*T1(I,1)/(DT*CD) - R8/(R1*A4)
  110 D(K) = -C(I,N2)*T1(I,N2)/(DT*CD)
      D(1) = -C(1,1)*T1(1,1)/(CD*DT) - R8/(2.0*R3*R1)
      CALL BANSOL(A,LL,L1,D,LL)
      DO 120 I = 1,LL
  120 T2(I) = D(I)
C   *** QUALITY CALCULATED ***
      DO 150 J=2,N1
      DO 150 I=2,M1
      K=(J-1)*M1 + I
      IF(MELT(K).EQ.1) GO TO 150
      IF(T2(K).GT.TMELT)TEXC(K) = TEXC(K) + (T2(K) - TMELT)
      IF(T2(K).GT.TMELT)F(K) = 1.0 - TEXC(K)/(R6*TMELT)/ T2
     1(K)=TMELT
      IF(TEXC(K).GE.TPHASE)T2(K)=TMELT+TEXC(K)-TPHASE)/F
     1(K)=0.0;MELT(K)=1
  150 CONTINUE
      DO 160 J = 1,N2
      DO 160 I = 1,M1
      K = (J-1)*M1 + I
  160 T1(I,J) = T2(K)
      QLAT = 0.0
      DO 170 J= 2,N1
      DO 170 I = 2,M1
      K = (J-1)*M1 + I
  170 QLAT = QLAT + ( 1.0 - F(K))
      IF(ABS(QLATM - QLAT).LT.0.0001) GO TO 180
      IF(TIME.EQ.DT)ITTT = ITTT + 1
      IF(TIME.EQ.DT)GO TO 180
      IF(ITT.NE.ITTT)ITTT = ITTT + 1
      IF(ITT.NE.ITTT)GO TO 240
        ITTT = 1
  180 DO 175 I=1,M1
  175 EBOT=EBOT+(C(I,1)*(T1(I,1)-TIN))
      TBOT=TIN+(EBOT/TTCB)
      EBOT=0.0
      TRISE = TBOT - TMELT
```

TABLE 12. (Continued)

```
      UCOEF = R8/(TBOT - TMELT)
      WRITE(6,8000)TIME,TRISE,UCOEF
C    *** ENERGY BALANCE) ***
      DO 200 J = 2,N1
  200 SQF = SQF + (C(1,J)*(T1(1,J) - TIN)/R6)
      DO 210 I = 1,M1
      SQT=SQT+(C(I,N2)*(T1(I,N2)-TIN)/R6)
  210 SQB = SQB + (C(I,1)*(T1(I,1) - TIN)/R6)
      DO 220 J = 2,N1
      DO 220 I = 2,M1
      K = (J-1)*M1 + I
      SQS=SQS+(CW*(T2(K)-TIN)*F(K)/R6)
  220 SQL=SQL+(CW*(T2(K)-TIN)*(1.0-F(K))/R6)
      QTOT = SQF + SQB + SQS + SQL + QLAT +SQT
      EIN = (AM**2*R1*R8/R6)*(1.0 + (1.0/(2.0*R3)))*TIME
      RATIO = QTOT/EIN
      FMELT=QLAT/QLATM
      WRITE(6,1500)SQF,SQB,SQT,SQS,SQL,QLAT,QTOT,EIN,RATIO,
     1 FMELT
      SQF = 0.0
      SQB = 0.0
      SQT=0.0
      SQS = 0.0
      SQL = 0.0
      TBOT = 0.0
  240 IF(ABS(QLATM - QLAT).GT.0.0001) GO TO 60
  998 FORMAT(7F10.5)
  999 FORMAT(3I3)
 1000 FORMAT(1H ,I3,1X,NF10.5)
 1500 FORMAT(1H ,'SQF =',F10.5,5X,'SQB =',F10.5,5X,'SQT ='
     1,F10.5,5X, 'SQS =',F10.5,5X,'SQL=',F10.5,/,'QLAT ='
     2,F10.5,5X,'QTOT =',F10.5,5X,'EIN =',F10.5,5X,'RATIO ='
     3,F10.5,5X,'FMELT=', F10.5)
 2000 FORMAT(1H1)
 3000 FORMAT(1H , I3,NF10.5)
 4000 FORMAT(1H ,T35,'HORIZONTAL CONDUCTANCE')
 5000 FORMAT(1H ,T35,'VERTICAL CONDUCTANCE')
 6000 FORMAT(1H ,T35,'THERMAL CAPACITANCE')
 7000 FORMAT(1H )
 7500 FORMAT(1H1,'R1=',F7.3,3X,'R2=',F6.1,3X,'R3=',F5.1,3X
     1,'R4=',F7.1,3X,'R5=',F5.1,3X,'R6=',F5.3,3X,'R8=',F6.3
     2,3X,'M=',I2,3X,'N=',I3,3X,'RUN NO. =',I4)
 8000 FORMAT(1H0,'TIME =',F7.5,5X,'TRISE =',F7.5,5X,'UCOEF
     1 =',F10.5)
      CALL EXIT
      END
       SUBROUTINE BANSOL(C,N,M,V,ID)
      DIMENSION C(ID,M),V(ID)
      IMPLICIT REAL*8(A-H,O-Z)
      L = (M+1)/2
      L1 = L - 1
```

TABLE 12. (Concluded)

```
      DO 2 IR = 1,L1
      LR = L = IR
      DO 2 I = 1,LR
      DO 1  J = 2,M
    1 C(IR,J-1) = C(IR,J)
      NP1 = N + 1 = IR
      MP1 = M + 1 = I
      C(NP1,MP1) = 0.0
    2 C(IR,M) = C(NP1,MP1)
      N1 = N = 1
      DO 9 I = 1,N1
      IPIV = I
      IRE = I + 1
      DO 3 IR = IRE ,L
      IF(ABS(C(IR,1))-.E-ABS(C(IPIV,1))) GO TO 3
      IPIV = IR
    3 CONTINUE
      IF(IPIV.EQ.I) GO TO 5
      T = V(I)
      V(I) = V(IPIV)
      V(IPIV) = T
      DO 4 J = 1,M
      T = C(I,J)
      C(I,J) = C(IPIV,J)
    4 C(IPIV,J) = T
    5 V(I) = V(I)/C(I,1)
      DO 6 J = 2,M
    6 C(I,J) = C(I,J)/C(I,1)
      DO 8 IR = IRE,L
      T = C(IR,1)
      V(IR) = V(IR) - T*V(I)
      DO 7 J = 2,M
    7 C(IR,J-1) = C(IR,J) - T*C(I,J)
    8 C(IR,M) = 0.0
      IF(L.EQ.N) GO TO 9
      L = L + 1
    9 CONTINUE
      V(N) = V(N)/C(N,1)
      JM = 2
      DO 11 ICE = 1,N1
      IR = N = ICE
      DO 10 J = 2,JM
      IRM1 = IR = 1 + J
   10 V(IR) = V(IR) - C(IR,J)*V(IRM1)
      IF(JM.EQ.M) GO TO 11
      JM = JM + 1
   11 CONTINUE
      RETURN
      END
```

TABLE 13. COMPUTER PROGRAM FOR BASE EXPOSED TO A STEP INCREASE IN TEMPERATURE

```
C *** CONSTANT BASE TEMPERATURE PROGRAM
      DIMENSION A(243,7), T1(3,82), T2(243), GH(4,82), GV(3
     1,82), C(3,82), F(243), TEXC(243), D(243), MELT(243)
      IMPLICIT REAL*8(A-H,O-Z)
C *** R1 = H/W ; R2 = H/S1 ; R3 = W/S2 ; R4 = K/KW ; *******
C     ************
C *** R5 = (K/DEN*CP)/(KW/DENW*CPW) ; R6 = HMELT/CPW*TMELT *
C     ************
C *** R7 = HMELT/HTR ; R8 = Q*H/KW*TMELT ********************
C     ************
      READ(5,998) R1,R2,R3,R4,R5,R6,DELT
      READ(5,999) NR,M,N
C *** COMPUTATIONAL PARAMETERS ***
      TIN=1.0
      DT = 0.00050
      ITT=6
      CW = 1.0
      TMELT = 1.0
      ITTT = 1
      TPHASE = R6
      AN = N
      AM = M
      QLATM = AM*AN
      M1 =  M + 1
      M2 = M1 + 1
      N1 = N + 1
      N2=N+2
      LL=N1*M1
      L1 = 2*M1 + 1
      L = M2
      CD = (R1**2)*(AM**2)
C *** INITIAL VALUES
      SQS = 0.0
      SQF = 0.0
      SQB = 0.0
      SQT=0.0
      SQL = 0.0
      QLAT = 0.0
      EBOT=0.0
      TTCB=0.0
      TBOT = 0.0
      TIME = 0.0
      QTOT1 = 0.0
      DO 10 I = 1,LL
      F(I) = 1.0
      MELT(I)=0
   10 TEXC(I) = 0.0
      DO 20 I=1,M1
      T1(I,1)=TIN+DELT
      DO 20 J=2,N2
   20 T1(I,J) = TIN
```

TABLE 13. (Continued)

```
C  ***** HORIZONTAL CONDUCTANCES, VERTICAL CONDUCTANCES
C     ,CAPACITANCES **
C ****  ARE CALCULATED  *******
      GV(1,1) = 0.0
      DO 30 J=2,N1
      DO 30 I=2,M1
      GH(I,J) = 1.0
      C(I,J) = 1.0
   30 GV(I,J) = 1.0
      DO 40 J = 2,N1
      C(1,J) = (R4*AM)/(2.0*R5*R3)
      GV(1,J) = (AM*R4)/(2.0*R3)
      GH(2,J) = 2.0/(1.0 + AM/(2.0*R3*R4))
      GH(M2,J)=0.0
   40 GH(1,J) = 0.0
      DO 50 I = 2,M1
      C(I,1) = (AM*R1*R4)/(R2*R5)
      C(I,N2)=C(I,1)
      GV(I,2) = 2.0/(1.0 + (R1*AM/(R2*R4)))
      GV(I,N2)=GV(I,2)
      GV(I,1) = 0.0
      GH(I,1) = R4*AM*R1/R2
   50 GH(I,N2)=GH(I,1)
      GH(1,1) = 0.0
      GH(1,N2)=0.0
      GH(M2,1)=0.0
      GH(M2,N2)=0.0
      GH(2,1) = 2.0*R4/((R2/R1)*(1.0/(2.0*R3) + 1.0/AM))
      GH(2,N2)=GH(2,1)
      GV(1,2) = R4/(R3*(1.0/AM + R1/R2))
      GV(1,N2)=GV(1,2)
      C(1,1) = (R1*R4*(AM**2))/(2.0*R2*R3*R5)
      C(1,N2)=C(1,1)
      DO 55 I=1,M1
   55 TTCB=TTCB+C(I,1)
C    **** TEMPERATURES AT EACH NODE CALCULATED ***
      WRITE (6,7250) NR
      WRITE(6,7500) R1, R2, R3, R4, R5, R6, DELT, M, N
   60 TIME = TIME + DT
      DO 70 I = 1,LL
      DO 70 J = 1,L1
   70 A(I,J) =0.0
      DO 80 J=2,N1
      DO 80 I = 1,M1
      K = (J-2)*M1 + I
      IF (J.NE.2)  GO TO 75
      D(K) = -C(I,J)*T1(I,J)/(CD*DT)-GV(I,J)*T1(I,J-1)
      GO TO 79
   75 D(K)= -C(I,J) * T1(I,J)/(CD*DT)
      A(K,L-M1) = GV(I,J)
   79 A(K,L+M1) = GV(I,J+1)
```

TABLE 13. (Continued)

```
      A(K,L) = -GH(I+1,J) - GV(I,J) - GV(I,J+1)-(C(I,J)/(DT
     1*CD))-GH(I,J)
      A(K,L-1) = GH(I,J)
   80 A(K,L+1) = GH(I+1,J)
      DO 90 I=1,M1
      K= N*M1+I
      A(K,L) = -GH(I,N2) - GH(I+1,N2) - GV(I,N2) - C(I,N2)/
     1(DT*CD)
      A(K,L-1) = GH(I,N2)
      A(K,L+1) = GH(I+1,N2)
   90 A(K,L-M1) = GV(I,N2)
      DO 110 I=1,M1
      K= N*M1+I
  110 D(K) = -C(I,N2)*T1(I,N2)/(DT*CD)
      CALL BANSOL (A,LL,L1,D,LL)
      DO 120 I = 1,LL
  120 T2(I) = D(I)
C   *** QUALITY CALCULATED ***
      DO 150 J=2,N1
      DO 150 I=2,M1
      K=(J-2)*M1 + I
      IF(MELT(K).EQ.1) GO TO 150
      IF(T2(K).GT.TMELT)TEXC(K) = TEXC(K) + (T2(K) - TMELT)
      IF(T2(K).GT.TMELT)F(K) = 1.0 - TEXC(K)/(R6*TMELT)/ T2
     1(K)=TMELT
      IF(TEXC(K).GE.TPHASE)T2(K)=TMELT+TEXC(K)-TPHASE/F
     1(K)=0.0;MELT(K)=1
  150 CONTINUE
      DO 160 J = 2,N2
      DO 160 I = 1,M1
      K = (J-2)*M1 + I
  160 T1(I,J) = T2(K)
      QLAT = 0.0
      DO 170 J= 2,N1
      DO 170 I = 2,M1
      K = (J-2)*M1 + I
  170 QLAT = QLAT + ( 1.0 - F(K))
      TBOT = 0.0
      DO 175 I=1,M1
  175 EBOT=EBOT+(C(I,1)*(T1(I,1)-TIN))
      TBOT=TIN+(EBOT/TTCB)
      EBOT=0.0
      TRISE = TBOT - TMELT
C    *** ENERGY BALANCE) ***
      SQF = 0.0
      SQB = 0.0
      SQT = 0.0
      SQS = 0.0
      SQL = 0.0
      DO 200 J = 2,N1
  200 SQF = SQF + (C(1,J)*(T1(1,J) - TIN)/R6)
```

TABLE 13. (Continued)

```
      DO 210 I = 1,M1
      SQT=SQT+(C(I,N2)*(T1(I,N2)-TIN)/R6)
  210 SQB = SQB + (C(I,1)*(T1(I,1) - TIN)/R6)
      DO 220 J = 2,N1
      DO 220 I = 2,M1
      K = (J-2)*M1 + I
      SQS=SQS+(CW*(T2(K)-TIN)*F(K)/R6)
  220 SQL=SQL+(CW*(T2(K)-TIN)*(1.0-F(K))/R6)
      QTOT2 = SQF + SQB + SQS + SQL + QLAT +SQT
      QRATE = (QTOT2-QTOT1)/DT
      UCOEF = (QRATE*R6)/((TBOT-TMELT)*(M**2)*R1*    (1+2*R3)
     1/(2*R3))
      QTOT1=QTOT2
      FMELT = QLAT/(AM*AN)
      IF (ABS(QLATM - QLAT).LT.0.0001) GO TO 180
      IF (TIME.EQ.DT)  ITTT = ITTT + 1
      IF (TIME.EQ.DT)  GO TO 180
      IF (ITT.NE.ITTT)  ITTT = ITTT + 1
      IF (ITT.NE.ITTT)  GO TO 240
      ITTT = 1
  180 WRITE (6,8000)  TIME,TRISE,UCOEF
      WRITE (6,1500) SQF,SQB,SQT,SQS,SQL,QLAT,QTOT2,FMELT
  240 IF(ABS(QLATM - QLAT).GT.0.0001) GO TO 60
 1500 FORMAT(1H ,10X,'SQF =',F10.5,5X,'SQB =',F10.5,5X,'SQT
     1 =',F10.5,5X, /,11X,'SQS =',F10.5,5X,'SQL =',F10.5,4X
     2,'QLAT =',F10.5,/, 10X, 'QTOT =',F10.5,4X,'FMELT ='
     3,F10.5)
  998 FORMAT(7F10.5)
  999 FORMAT(3I3)
 2000 FORMAT(1H1)
 7250 FORMAT (1H1,4X,'RUN NO. ', I4)
 7500 FORMAT(1HO,9X,'R1 =',F7.3,3X,'R2 =',F6.1,3X,'R3 ='
     1,F5.1,3X,'R4 =',F7.1,/,10X,'R5 =',F5.1,5X,'R6 =',F5.3
     2,4X,'DELT =',F6.4,3X,'M = ', I2,5X,'N =',I4)
 8000 FORMAT(1HO,9X,'TIME =',F7.5,5X,'TRISE =',F7.5,3X
     1,'UCOEF =',F10.5)
      WRITE (6,2000)
      CALL EXIT
      END
      SUBROUTINE BANSOL(C,NNEW,MNEW,V,ID)
      IMPLICIT REAL*8(A-H,O-Z)
      DIMENSION C(ID,M),V(ID)
      L = (MNEW+1)/2
      L1 = L - 1
      DO 2 IR = 1,L1
      LR = L - IR
      DO 2 I = 1,LR
      DO 1  J = 2,MNEW
    1 C(IR,J-1) = C(IR,J)
      NP1 = NNEW + 1 - IR
      MP1 = MNEW + 1 - I
```

TABLE 13. (Concluded)

```
      C(NP1,MP1) = 0.0
    2 C(IR,MNEW) = C(NP1,MP1)
      N1 = NNEW = 1
      DO 9 I = 1,N1
      IPIV = I
      IRE = I + 1
      DO 3 IR = IRE ,L
      IF(ABS(C(IR,1)).LE.ABS(C(IPIV,1))) GO TO 3
      IPIV = IR
    3 CONTINUE
      IF(IPIV.EQ.I) GO TO 5
      T = V(I)
      V(I) = V(IPIV)
      V(IPIV) = T
      DO 4 J = 1,MNEW
      T = C(I,J)
      C(I,J) = C(IPIV,J)
    4 C(IPIV,J) = T
    5 V(I) = V(I)/C(I,1)
      DO 6 J = 2,MNEW
    6 C(I,J) = C(I,J)/C(I,1)
      DO 8 IR = IRE,L
      T = C(IR,1)
      V(IR) = V(IR) - T*V(I)
      DO 7 J = 2,MNEW
    7 C(IR,J-1) = C(IR,J) - T*C(I,J)
    8 C(IR,MNEW) = 0.0
      IF(L.EQ.NNEW) GO TO 9
      L = L + 1
    9 CONTINUE
      V(NNEW) = V(NNEW)/C(NNEW,1)
      JM = 2
      DO 11 ICE = 1,N1
      IR = NNEW - ICE
      DO 10 J = 2,JM
      IRM1 = IR - 1 + J
   10 V(IR) = V(IR) - C(IR,J)*V(IRM1)
      IF(JM.EQ.MNEW) GO TO 11
      JM = JM + 1
   11 CONTINUE
      RETURN
      END
```

IF(T2(K).LT.TMELT)TEXC(K)=TEXC(K)-(T2(K)-TMELT)

IF(T2(K).LT.TMELT)F(K)=1.0-TEXC(K)/(R6*TMELT); T2(K)=TMELT

IF(TEXC(K).GE.TPHASE)T2(K)=TMELT-TEXC(K)+TPHASE;F(K)=0.0;MELT(K)=1.0.

c. In statement 170, change sign to give QLAT = QLAT - (1.0 - F(K)).

d. In the line above statement 220 and statement 220, make changes to give

SQS=SQS+(CW*(T2(K)-TIN)*(1.0-F(K)/R6)

220 SQL=SQL+(CW*(T2(K)-TIN)*F(K)/R6)

An extensive parametric study for the case of melting with the initial PCM temperature at the fusion temperature was conducted using the computer program given in Table 12. This parametric study is discussed in more detail and the results are presented in Section IV.

IV. GENERAL PARAMETRIC STUDY

A. Introduction

Presented in this section are some details and typical results of a parametric study for a particular phase change device application. Since there are many phase change device applications, each having its own unique constraints, it would be unrealistic to propose that the results obtained for a particular set of conditions and constraints could be quantitatively extrapolated to other conditions and constraints. However, results obtained for a particular case such as those presented herein may afford valuable insight, qualitatively, into such considerations as trends and acceptable operating ranges.

The parametric study consisted of a thermal analysis of the symmetrical half-cell shown in Figure 29 with the base exposed to a constant heat flux density. The model and assumptions are described in Section III.

B. Scope and Definitions

Numerical results have been obtained using the implicit formulation described in Section III.

A band algorithm [14] was used to reduce the required computer storage in comparison to that which would have been required using a general matrix inversion routine.

Of the seven dimensionless variables previously given, some of the physical parameters were considered to be fixed for the computations. Independent variation of all seven parameters would render the problem untractable.

By selection of a particular PCM and metal for the housing and fins, the three dimensionless parameters denoted by R_4, R_5, and R_6 are all fixed. Since aluminum was typically used in most of the previous phase change device applications and paraffin was commonly used as the PCM, properties corresponding to these materials were used in the computations. For the results presented herein, the representative properties used in the computations for these materials are given in Table 14. With the property values given in Table 14, the values for the fixed dimensionless ratios are

$$R_4 = 1069 \quad ,$$

$$R_5 = 753$$

and

$$R_6 = 0.381 \quad .$$

Values of the geometrical variables and the heat flux density chosen for the numerical predictions are based on a survey of past applications. The values are listed in Table 15. For the range of variables outlined in Table 15, there are 300 possible combinations which indicates the need for an equal number of computer runs to obtain results encompassing these conditions. Because of the large number of computer runs involved, it was not practical to conduct a sensitivity study for each run on the choice of M and N and DT, a suggestion outlined in Section III under the instructions for using the computer programs. The choice of M and N was made such that the node size S for the range of geometric variables given in Table 15 never exceeded an approximate value of 0.254 cm (0.1 in.). This value, for some cases, was not sufficiently small to avoid there being an effect on the character of the transient results. This is discussed later in this section.

Specifically, for the results shown hereafter in this section, the parametric computations were performed for the case of melting only. The entire cell was considered to be initially at the fusion temperature of the PCM and in the solid phase.

If one assumes that the phase change is reversible, the results can also be applied to freezing. There is evidence, however, that the rate of freezing is typically underpredicted by the model. However, in most designs, these data will indicate conservatively slower freeze rates than actually occur. Additional discussion of the freezing case is presented in Section V.

TABLE 14. PCM AND METAL PROPERTIES USED IN COMPUTATIONS

Material	Density		Specific Heat		Thermal Conductivity		Heat of Fusion		Melt Temperature	
	$\frac{kg}{m^3}$	$\left(\frac{lbm}{ft^3}\right)$	$\frac{kJ}{kg\text{-}°C}$	$\left(\frac{Btu}{lbm\text{-}°F}\right)$	$\frac{J}{sec\text{-}m\text{-}°C}$	$\left(\frac{Btu}{hr\text{-}ft\text{-}°F}\right)$	$\frac{kJ}{kg}$	$\left(\frac{Btu}{lbm}\right)$	K	(R)
Metal	2707	(169)	0.88	(0.21)	160.9	(93)	–	–	–	–
PCM	80	(50)	2.09	(0.50)	0.15	(0.087)	232.4	(100)	291.7	(525)

TABLE 15. VALUES OF GEOMETRIC VARIABLES AND HEAT FLUX DENSITY CHOSEN FOR THE NUMERICAL STUDY

Cell Height, H	cm (in.)	1.27 (0.5)	2.54 (1.0)	5.08 (2.0)	10.16 (4.0)	20.32 (8.0)
One Half-Fin Spacing, W	cm (in.)	0.127 (0.05)	0.254 (0.1)	0.508 (0.2)	1.016 (0.4)	2.032 (0.8)
Fin Thickness, S_2	cm (in.)	0.0127 (0.005)	0.0508 (0.020)	0.127 (0.050)		
Base Plate Thickness, S_1	cm (in.)	0.0635 (0.025)				
Heat Flux Density, $\dot{q}''$	$\frac{J}{s\text{-}m^2}$	1076.4	2152.8	4305.6	6458.3	
	$\frac{Btu}{h\text{-}ft^2}$	(341.4)	(682.9)	(1365.7)	(2048.6)	

The problem is transient in character. The computer program provides a printout of a number of computed quantities at time intervals which can be chosen as any multiple of the time increment used in the numerical expressions. The quantities computed at each time included the temperature difference between the base and the melt temperature (ΔT_b), an overall heat transfer coefficient (U), the latent energy which represents the amount of PCM which has melted (QLAT), and the sensible energy stored in the fin (SQS), the base (SQB), the cover (SQT), the solid PCM (SQS), and the liquid PCM (SQL). Computations automatically terminate when all the PCM has melted.

For the geometry considered here, the latent energy associated with the PCM per unit area of the base is expressed by

$$E_{\ell}'' = \frac{2\,\rho\,h_f\,H}{2 + S_2/W} \qquad (22)$$

This parameter is defined because it is useful in expressing the latent energy storage capability of the device. In using equation (22) to determine the latent energy storage capability, the appropriate area to use with this equation is the inside plan area of the device. This leads to a negligible error since equation (22) is based on a symmetrical cell and the two outermost end cells of the device are unsymmetrical. The latent energy is linearly related to H for fixed values of S_2 and W.

C. Results

For the range of H, W, S_2, and the physical properties considered in this study, equation (22) is represented graphically in Figures 33 through 35. Also shown is the case for infinite W which corresponds to the case for which the entire housing is filled with PCM without fins. The effect of increasing fin thickness is readily apparent by comparing the curves shown in Figures 33 through 35.

An important consideration, especially in temperature control design, is the temperature rise of the base. Ratios of the base temperature rise at the termination of melting to the absolute fusion temperature of the PCM for the range of conditions considered herein are shown plotted versus W in Figures 36 through 50. Over the examined range, the base temperature rise increases with an increase in W. For a specified set of parameters, the data indicate that the temperature rise approaches an asymptotic value which corresponds to expected behavior since the problem should reduce to that of a one-dimensional case as W becomes large. It is also expected that the temperature rise would increase at very small values of W as the problem approaches that for the heating of a metal slab. Computations were not performed for these very low values of W. It should also be noted that some of the values for the base temperature rise which are shown are too large to be of much practical significance; some of these are included, however, to indicate trends and to facilitate approximate interpolation. For some of the larger heat-flux-density cases, the curves are terminated at lower values of W than they are for the lower heat-flux-density cases because the resultant temperature rises are much too large for practical considerations.

In Figures 36 through 50 as well as in all subsequent figures showing results of the parametric study, computed data are represented by solid circles. Curves have been faired through the points; it should be recognized, however, that the value for points on the curve between two computed values are only approximate.

The data shown in Figures 36 through 50 are cross plotted versus fin height in Figures 51 through 62. For some geometries within the considered range, the curves indicate the presence of a relative maximum and a relative minimum. This feature is attributable to the two-dimensional character of the problem. This characteristic is discussed in more detail in Appendix B.

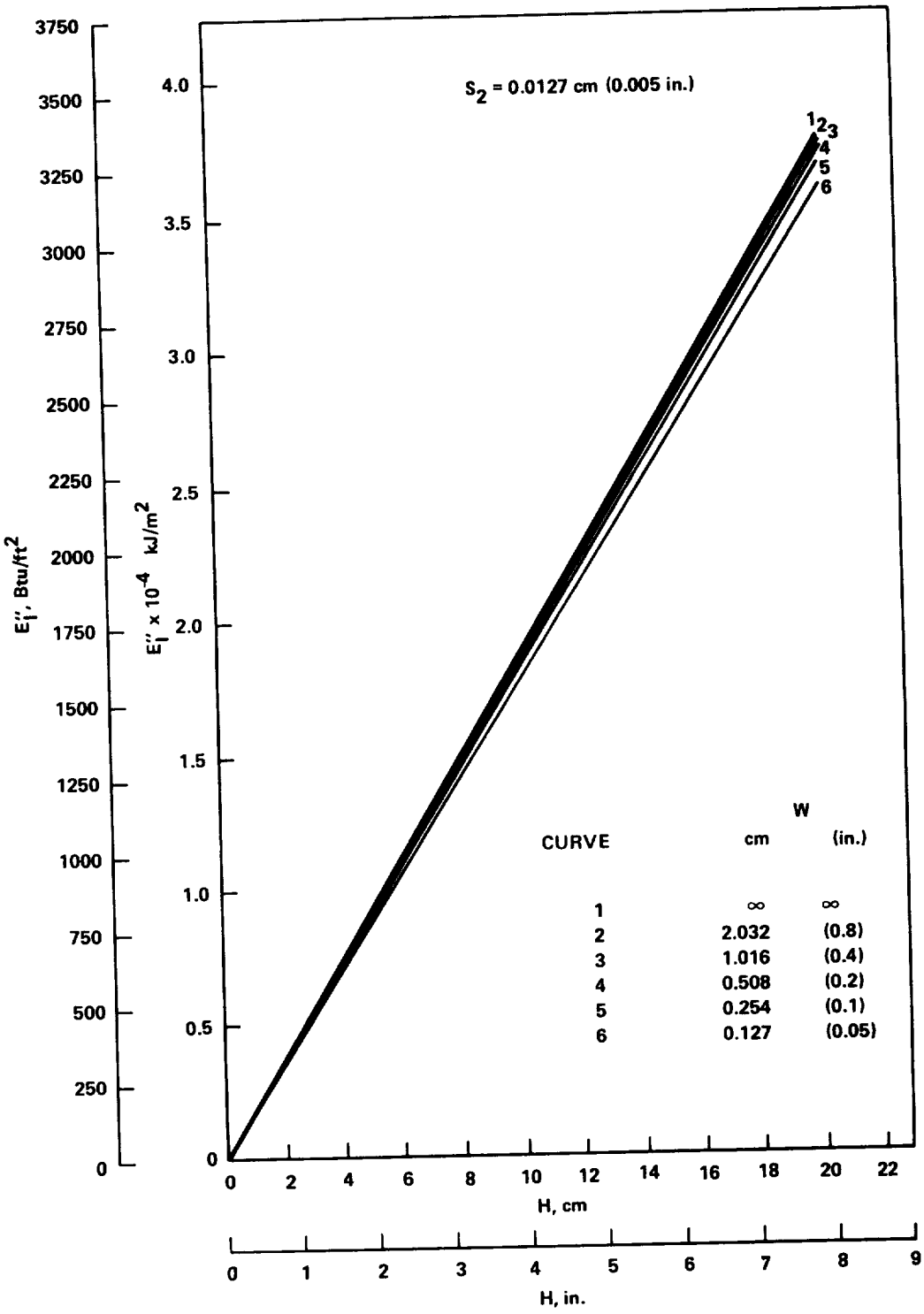

Figure 33. Latent energy storage per unit base area versus fin height for fin thickness of 0.0127 cm (0.005 in.).

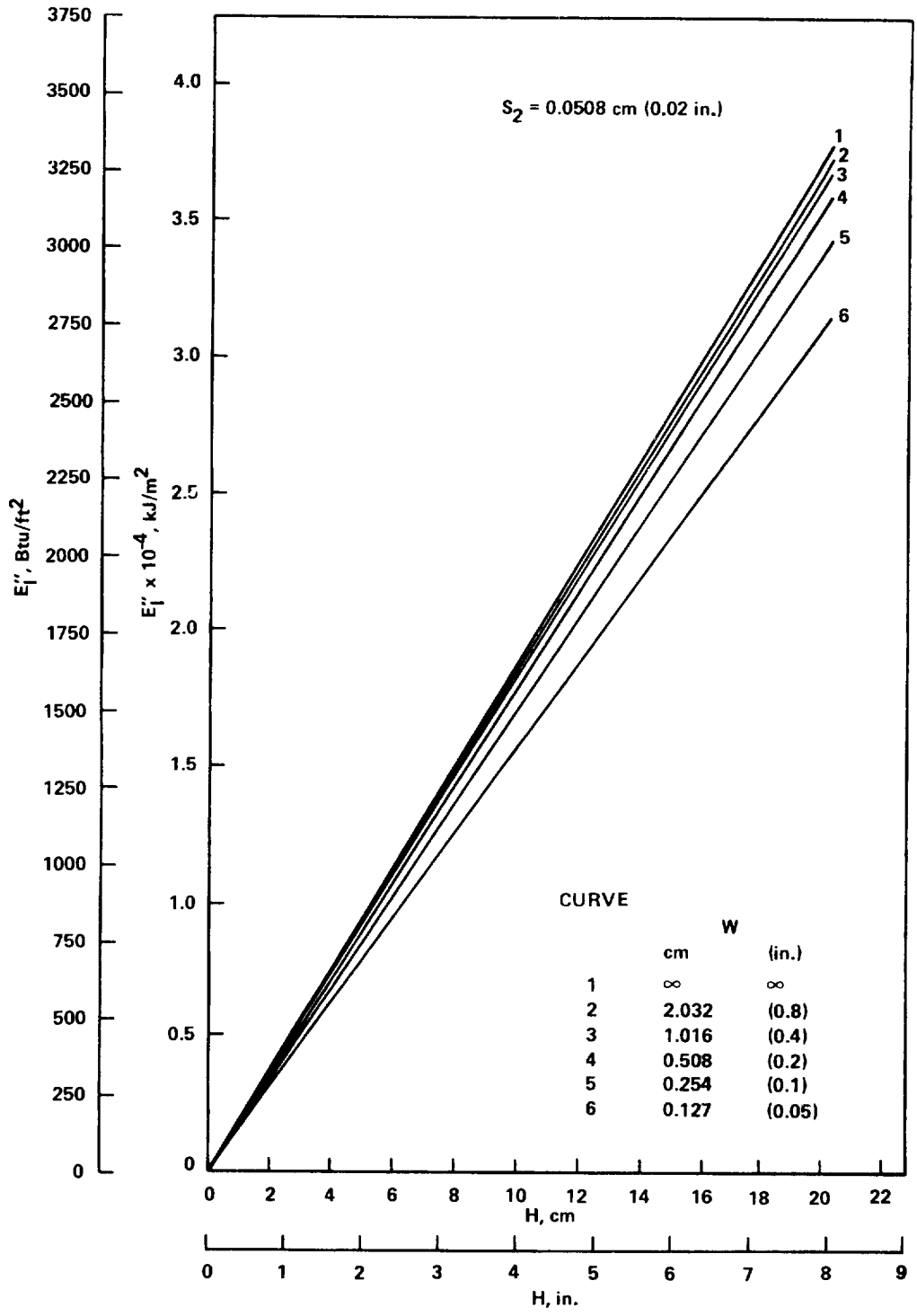

Figure 34. Latent energy storage per unit base area versus fin height for fin thickness of 0.0508 cm (0.02 in.).

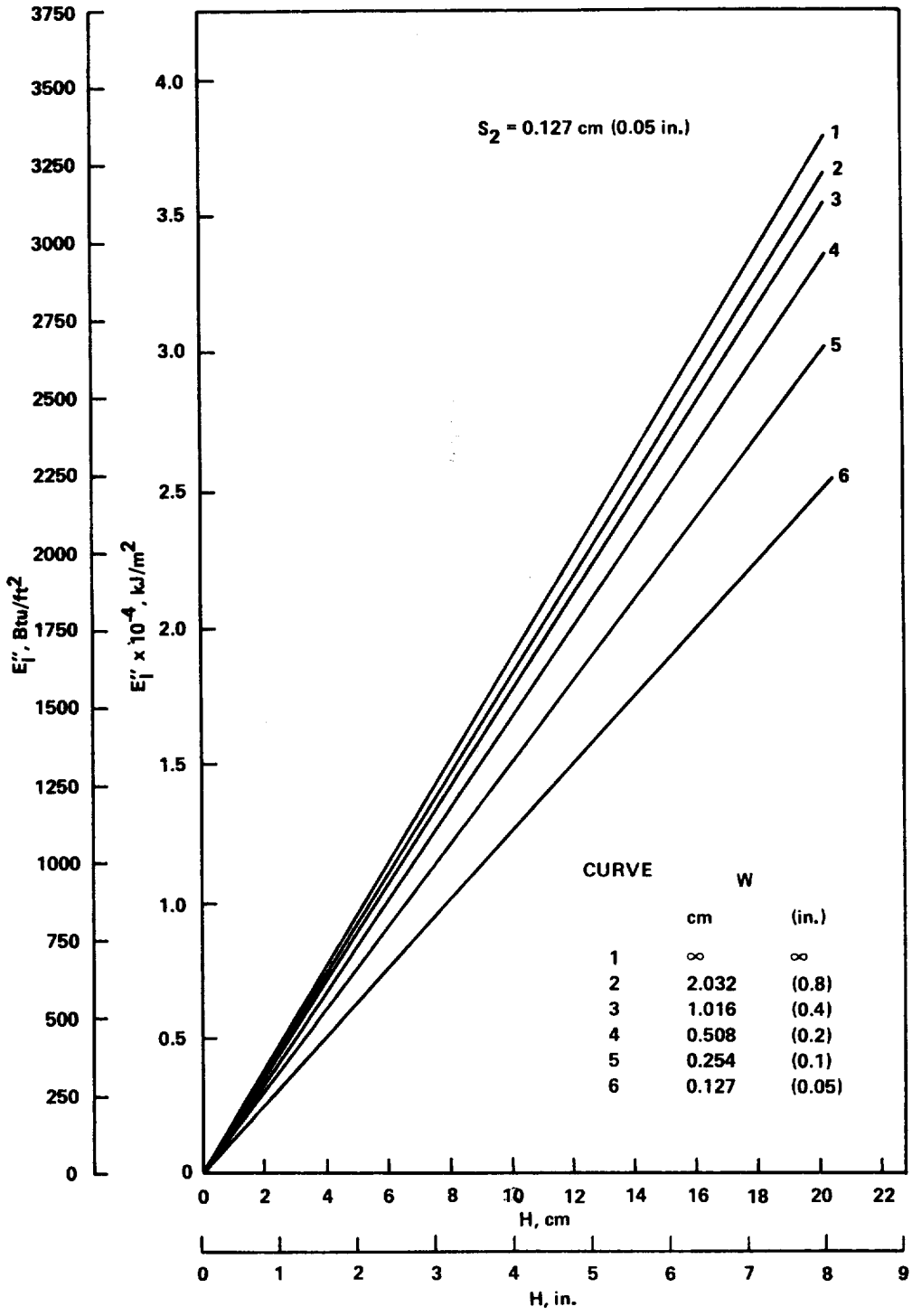

Figure 35. Latent energy storage per unit base area versus fin height for fin thickness of 0.127 cm (0.05 in.).

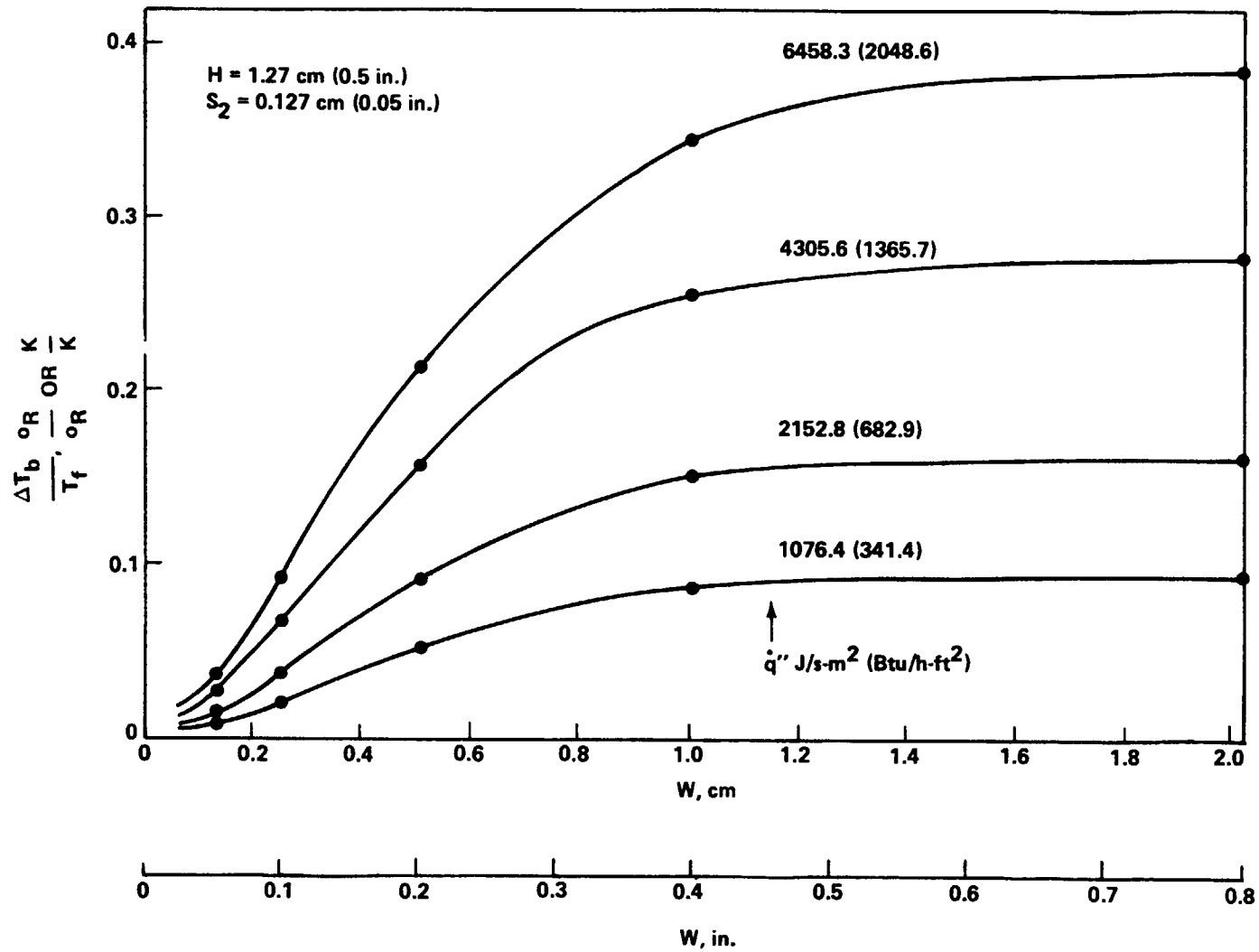

Figure 36. Base temperature rise at the termination of melting versus W for H = 1.27 cm (0.5 in.) and S_2 = 0.127 cm (0.05 in.).

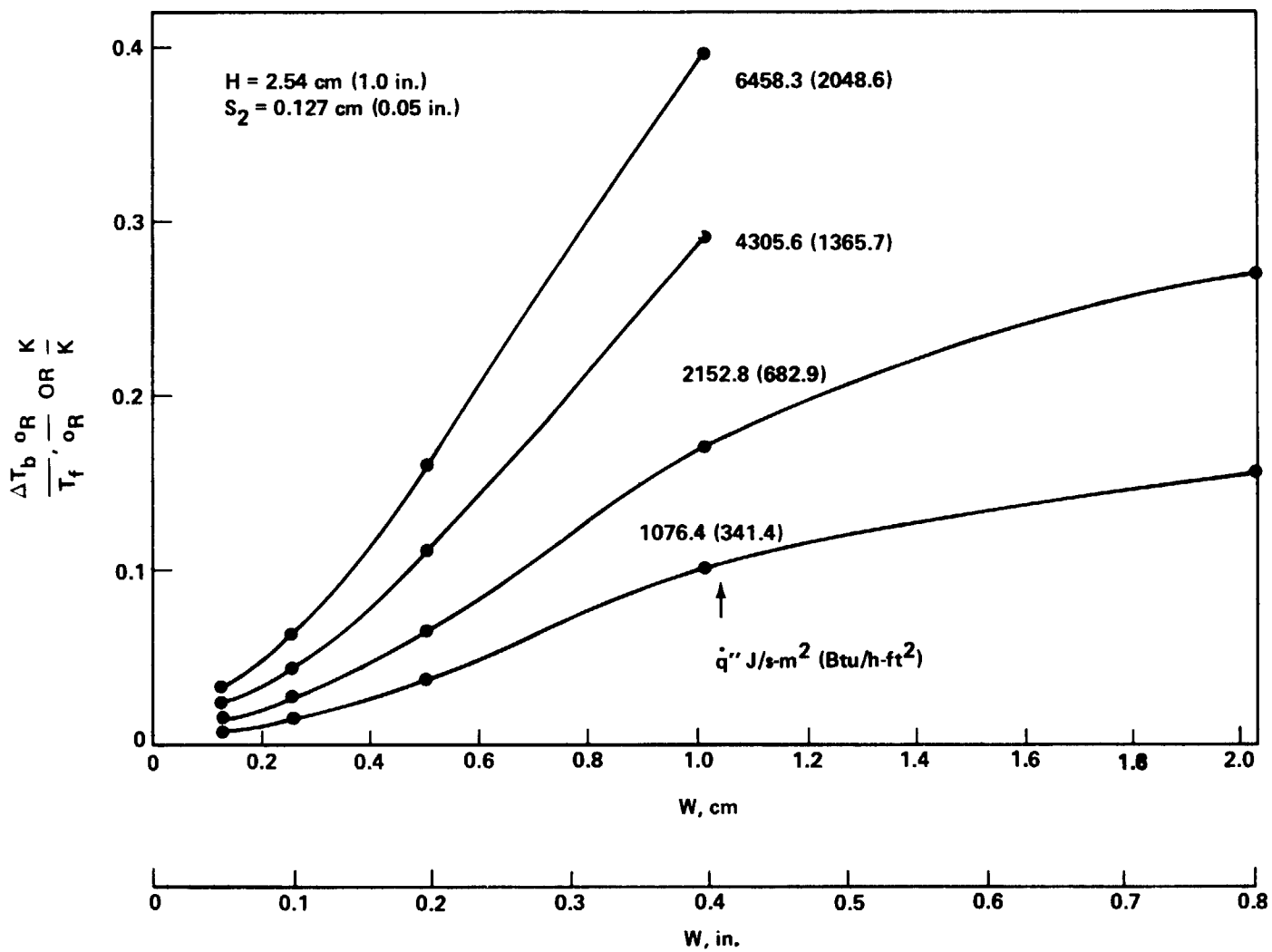

Figure 37. Base temperature rise of the termination at melting versus W for H = 2.54 cm (1.0 in.) and S_2 = 0.127 cm (0.05 in.).

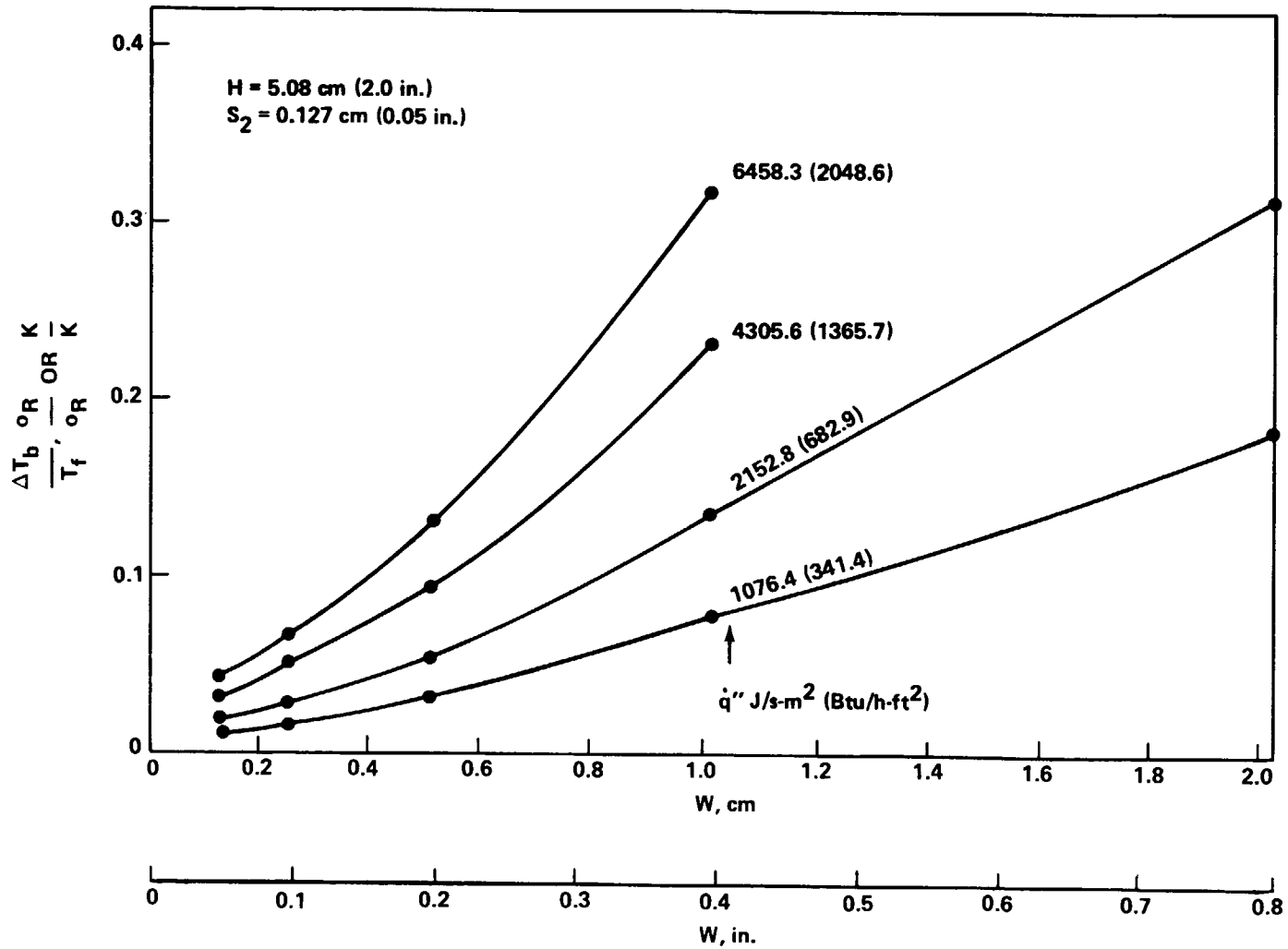

Figure 38. Base temperature rise at the termination of melting versus W for H = 5.08 cm (2.0 in.) and S_2 = 0.127 cm (0.05 in.).

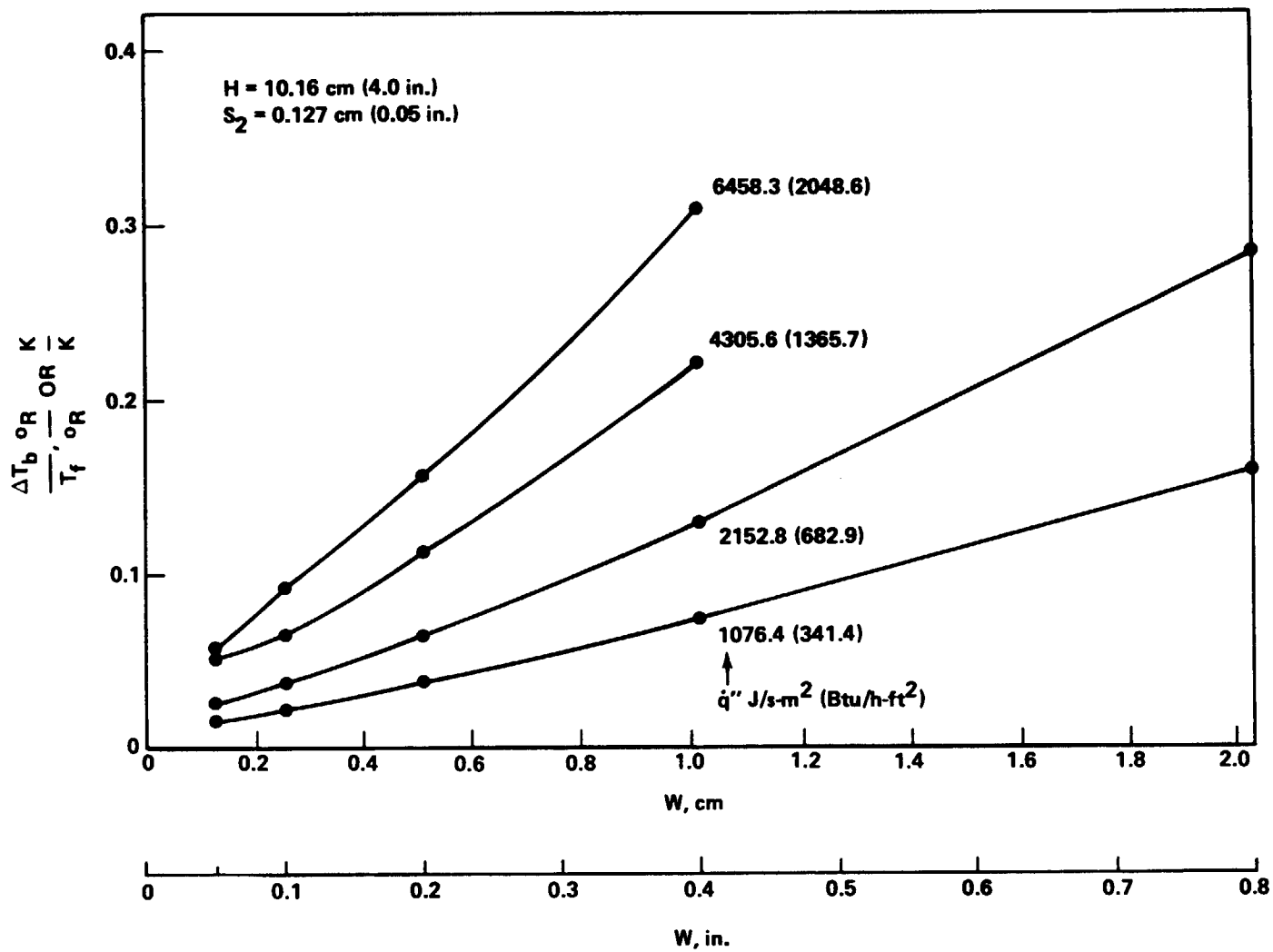

Figure 39. Base temperature rise at the termination of melting versus W for H = 10.16 cm (4.0 in.) and S_2 = 0.127 cm (0.05 in.).

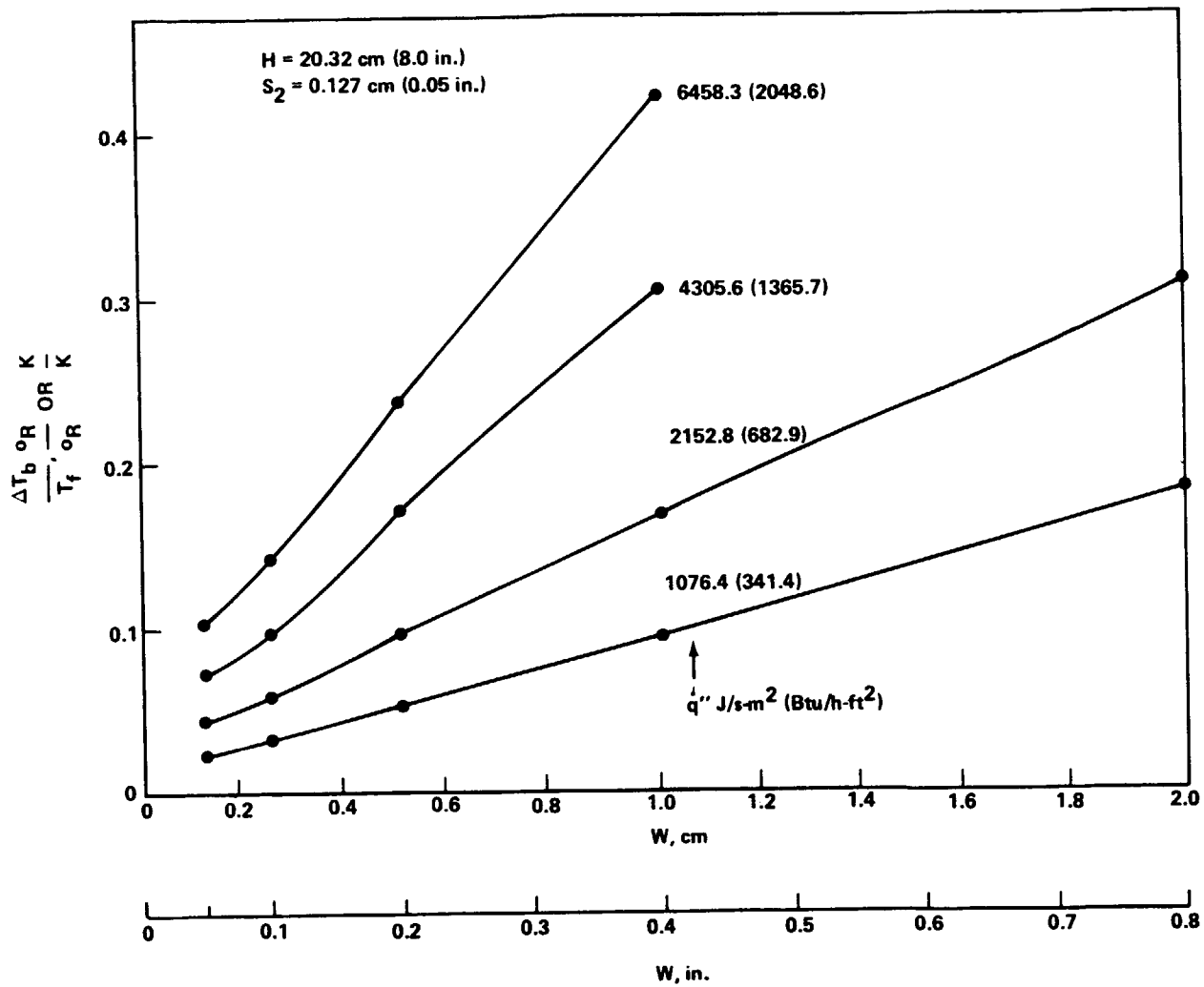

Figure 40. Base temperature rise at the termination of melting versus W for H = 20.32 cm (8.0 in.) and S_2 = 0.127 cm (0.05 in.).

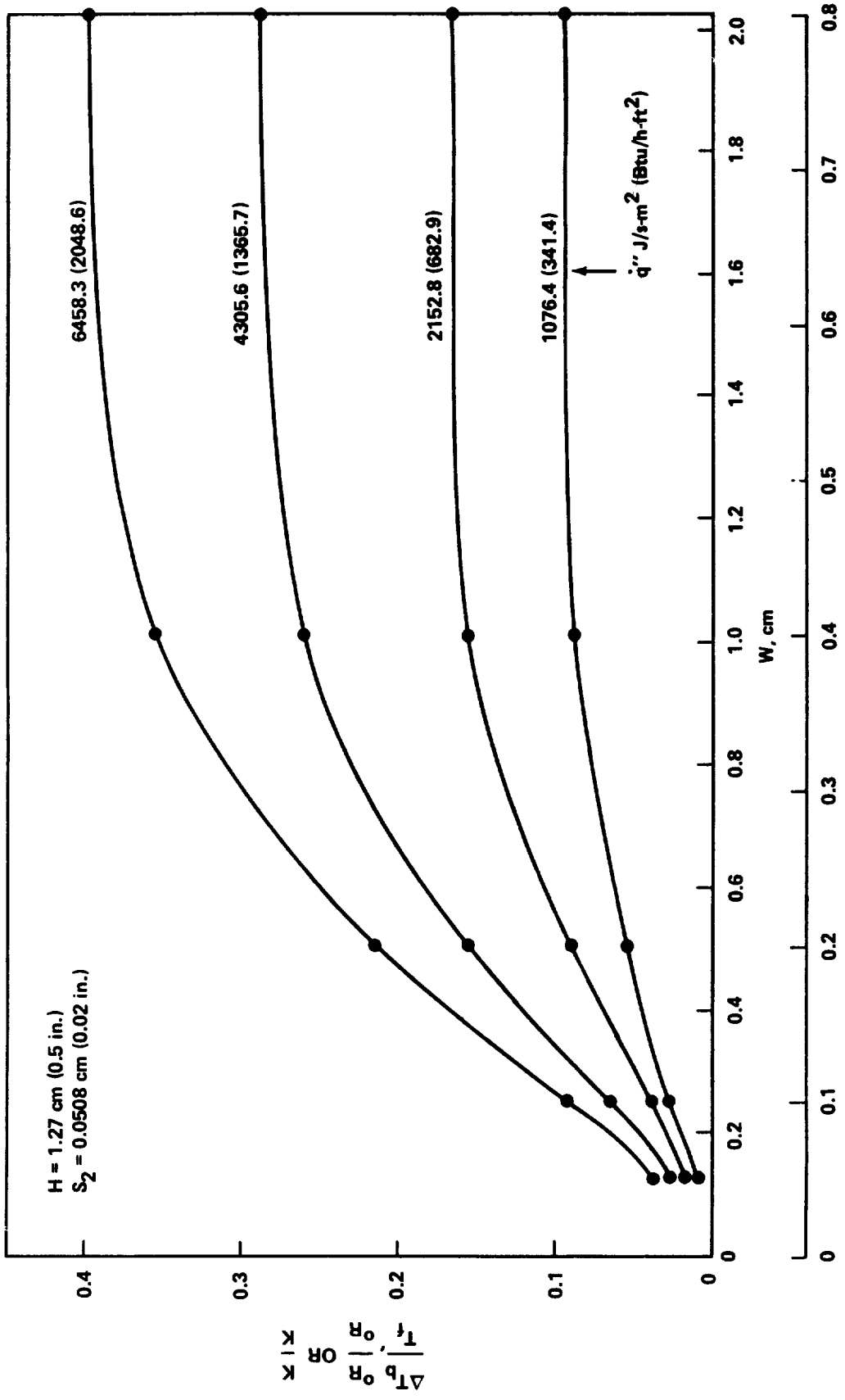

Figure 41. Base temperature rise at the termination of melting versus W for H = 1.27 cm (0.5 in.) and S_2 = 0.0508 cm (0.02 in.).

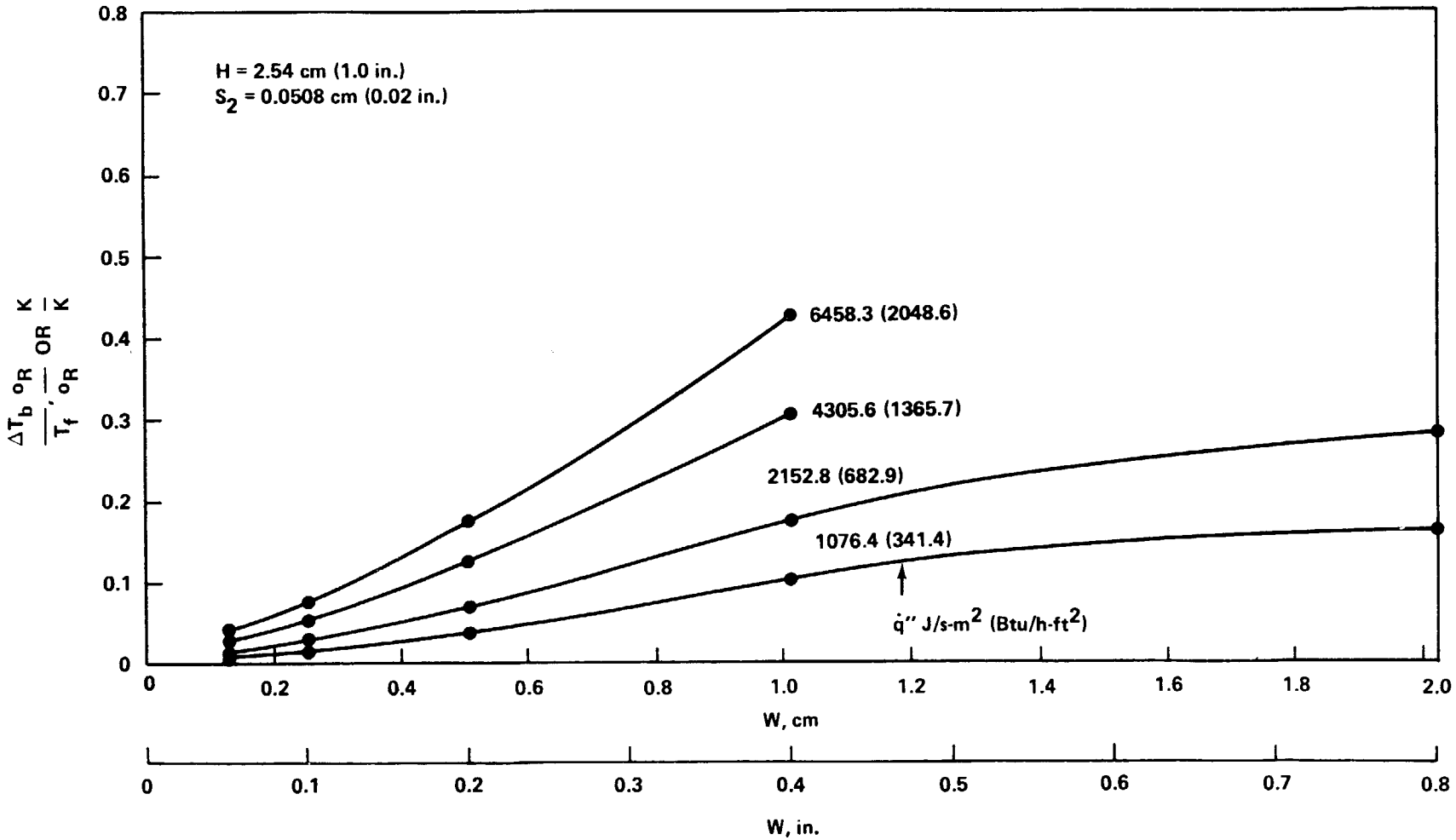

Figure 42. Base temperature rise at termination of melting versus W for H = 2.54 cm (1.0 in.) and S_2 = 0.0508 cm (0.02 in.).

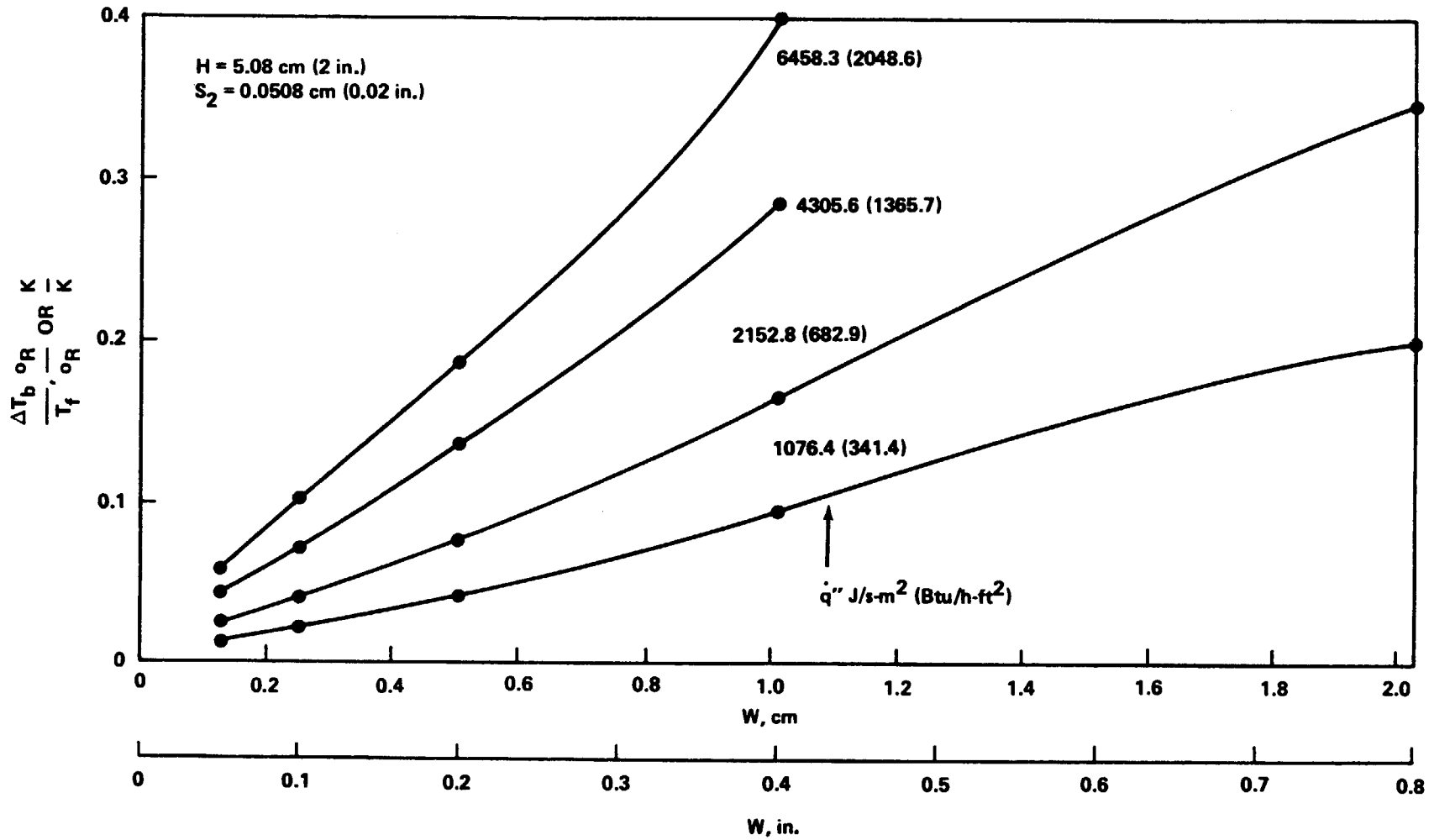

Figure 43. Base temperature rise at termination of melting versus W for H = 5.08 cm (2.0 in.) and S_2 = 0.0508 cm (0.02 in.).

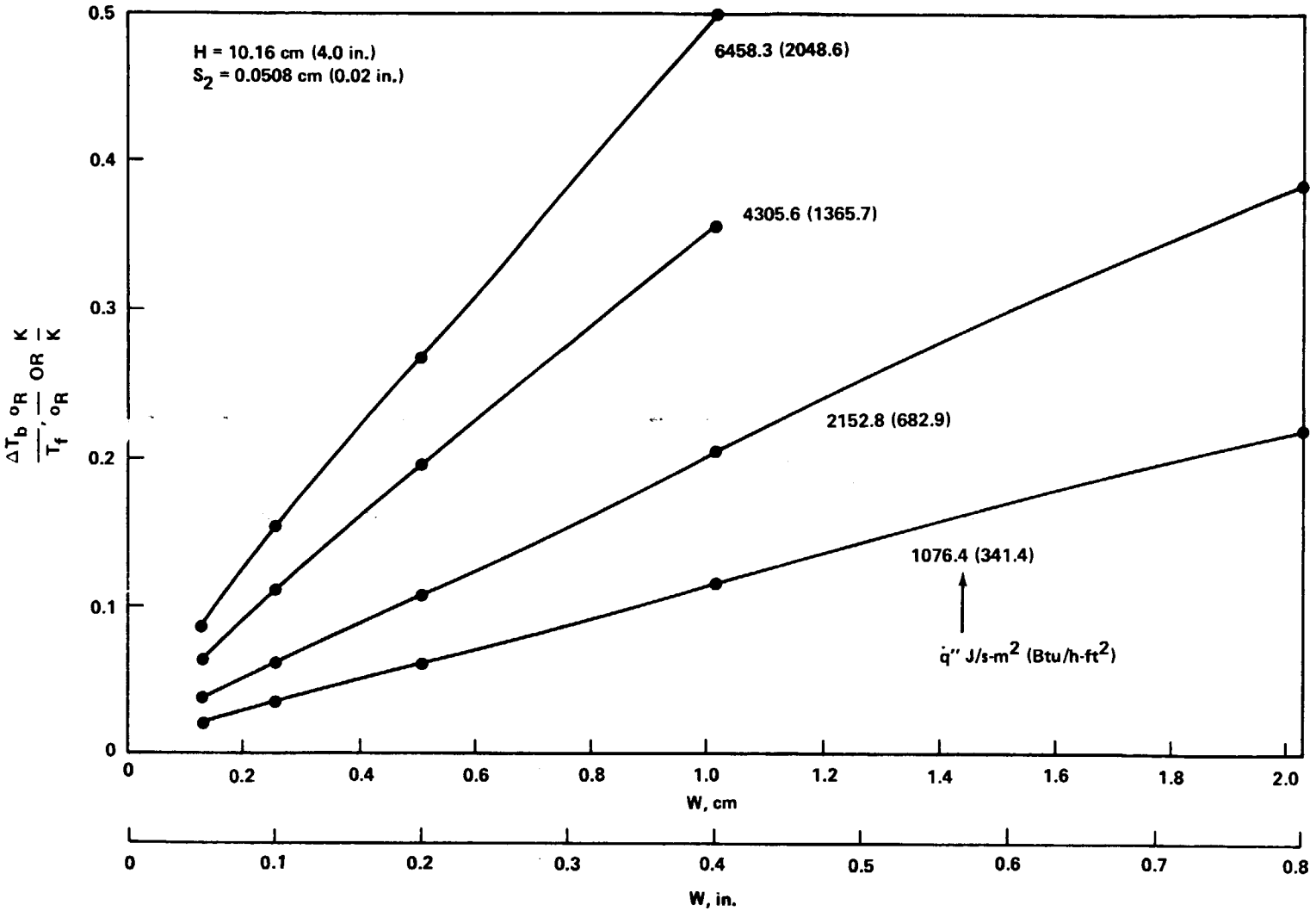

Figure 44. Base temperature rise at termination of melting versus W for H = 10.16 cm (4.0 in.) and S_2 = 0.0508 cm (0.02 in.).

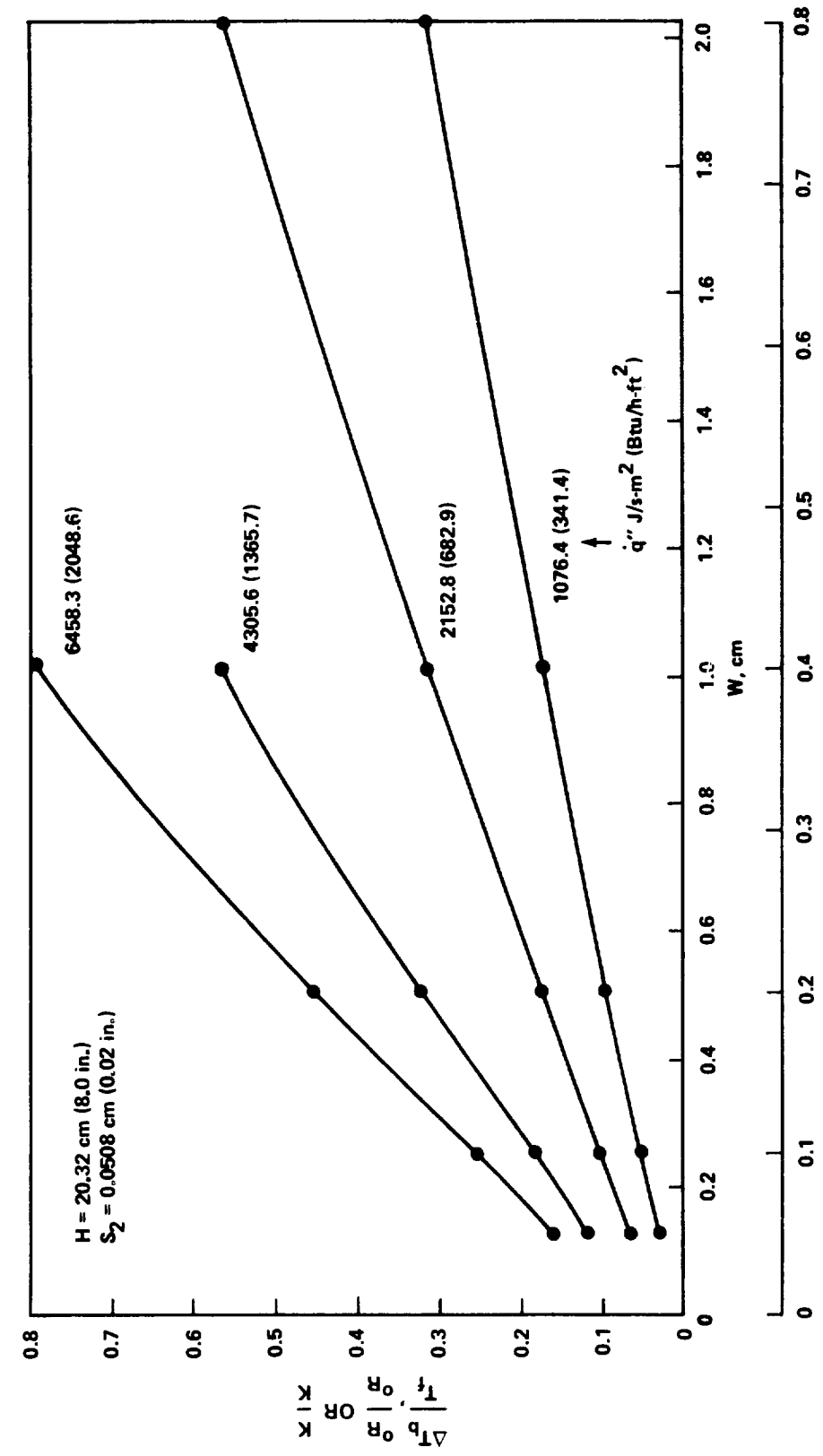

Figure 45. Base temperature rise at termination of melting versus W for H = 20.32 cm (8.0 in.) and S_2 = 0.0508 cm (0.02 in.).

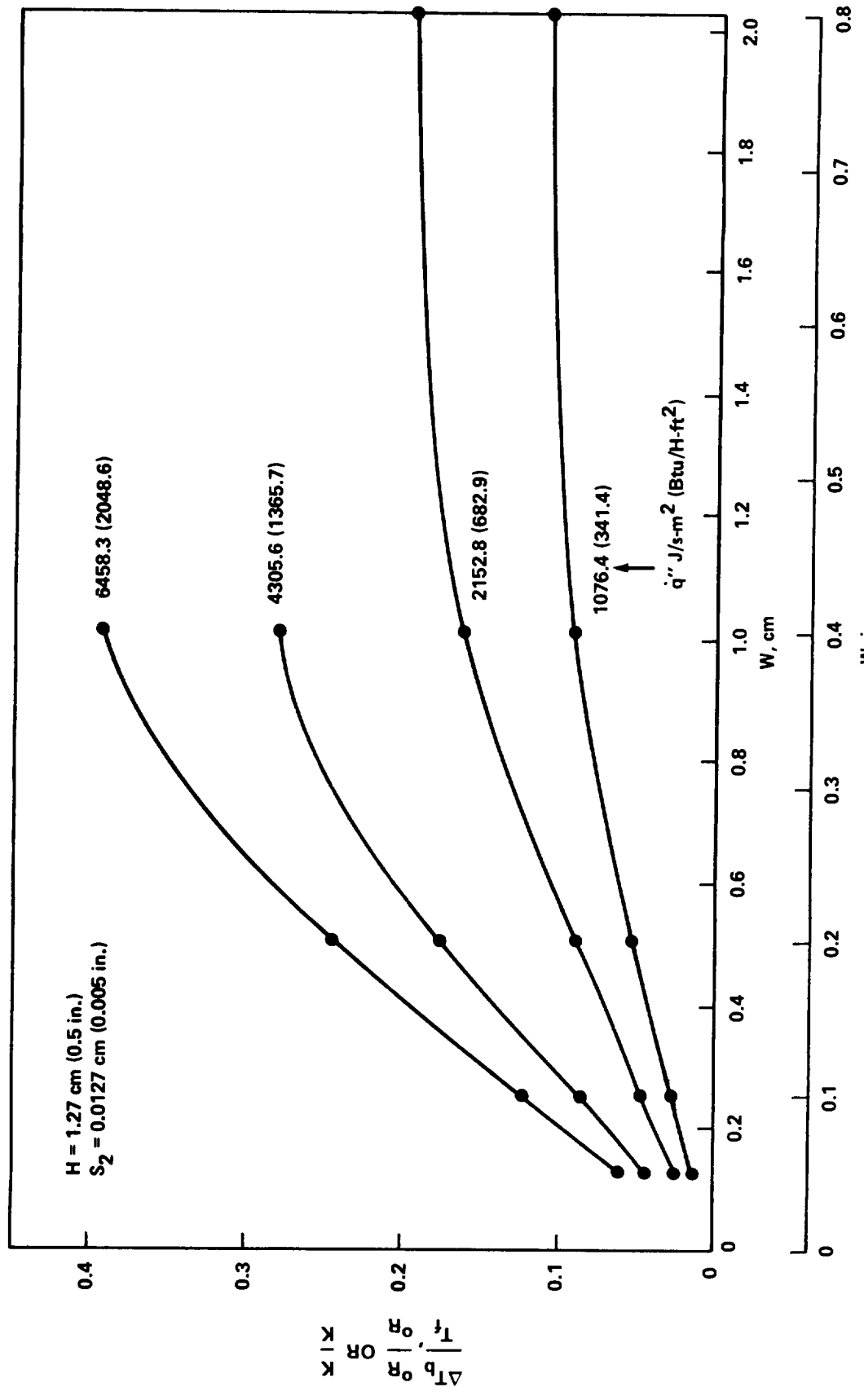

Figure 46. Base temperature rise at termination of melting versus W for H = 1.27 cm (0.5 in.) and S_2 = 0.0127 cm (0.005 in.).

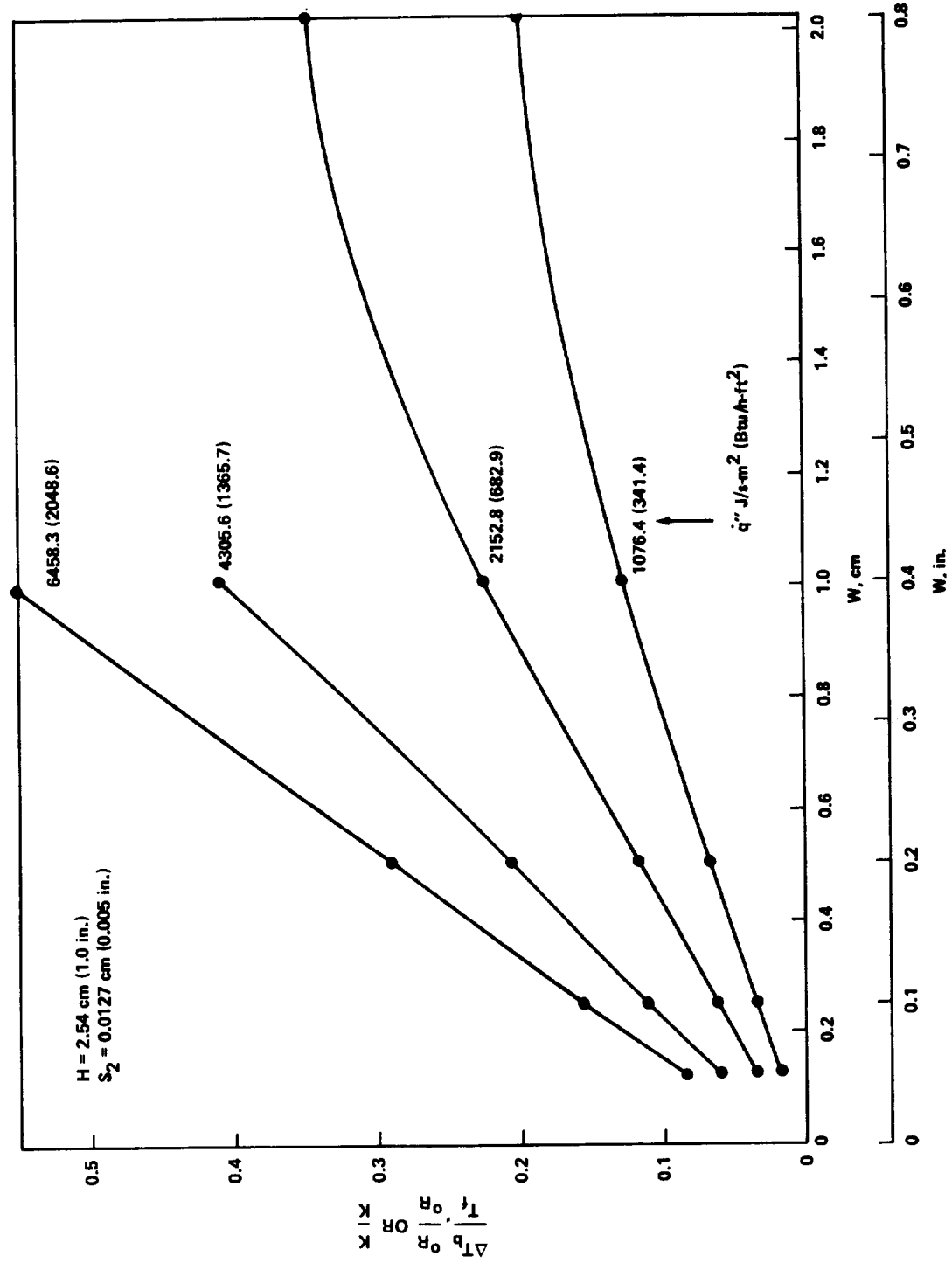

Figure 47. Base temperature rise at termination of melting versus W for H = 2.54 cm (1.0 in.) and S_2 = 0.0127 cm (0.005 in.).

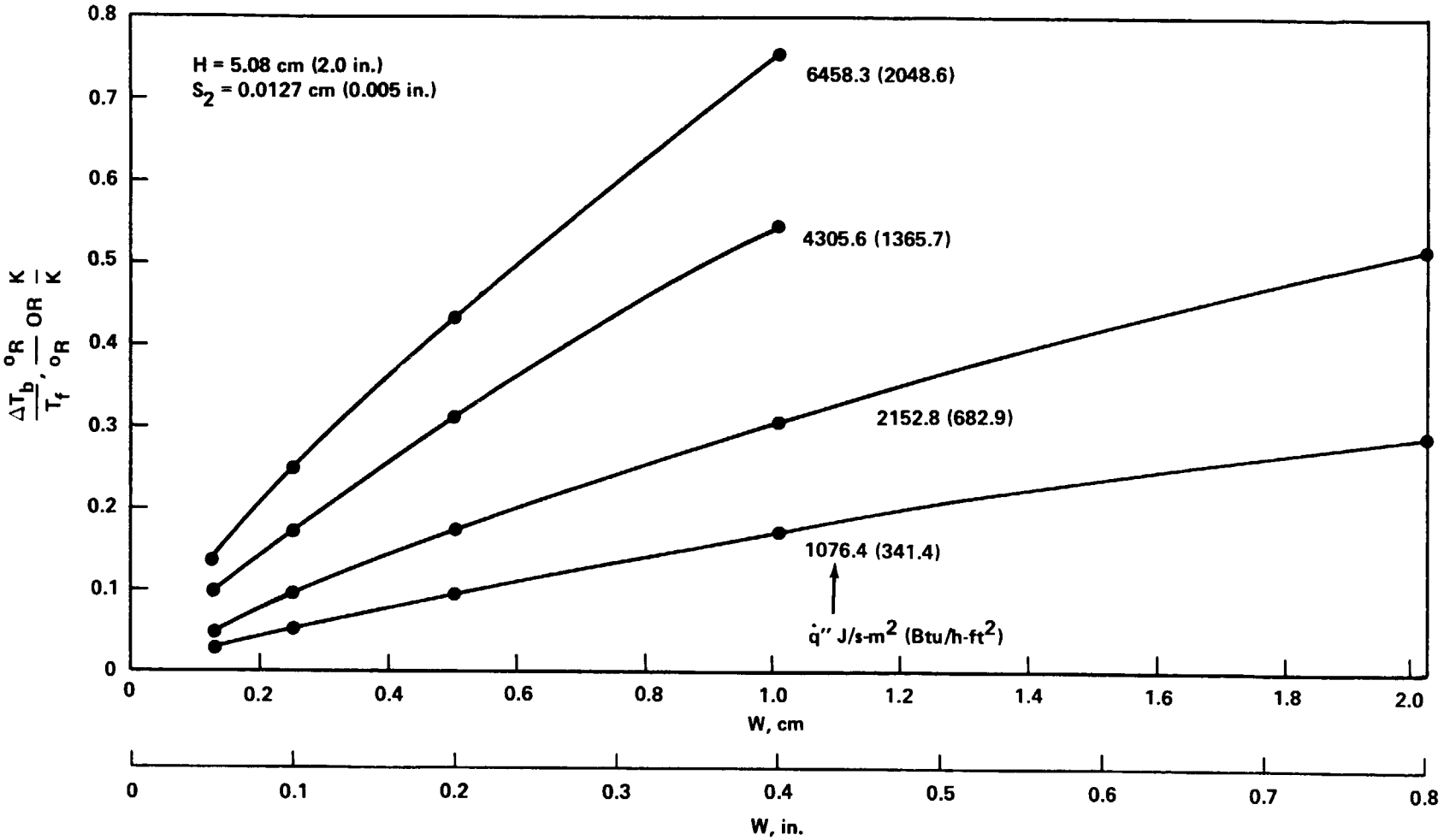

Figure 48. Base temperature rise at termination of melting versus W for H = 5.08 cm (2.0 in.) and S_2 = 0.0127 cm (0.005 in.).

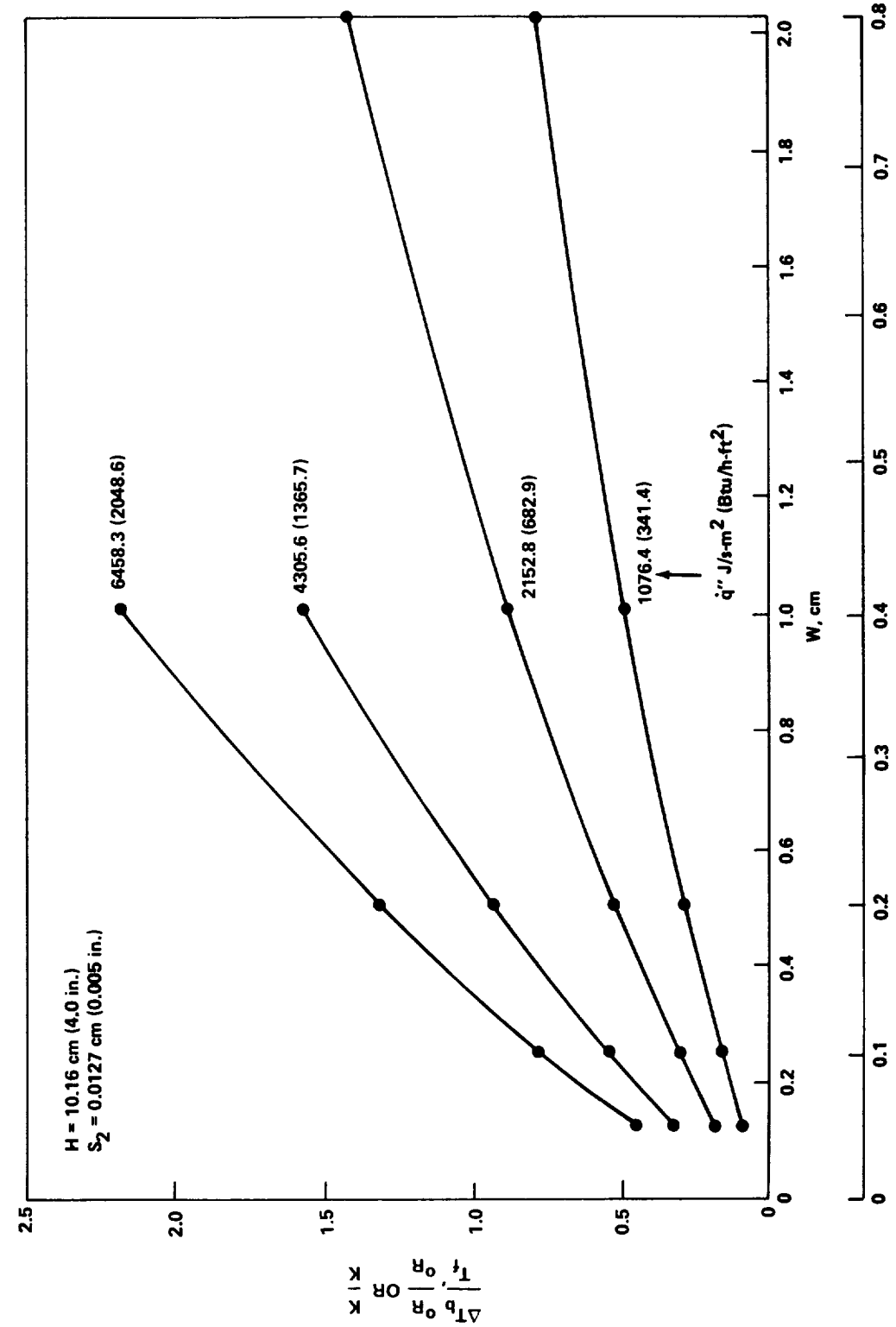

Figure 49. Base temperature rise at termination of melting versus W for H = 10.16 cm (4.0 in.) and S_2 = 0.0127 cm (0.005 in.).

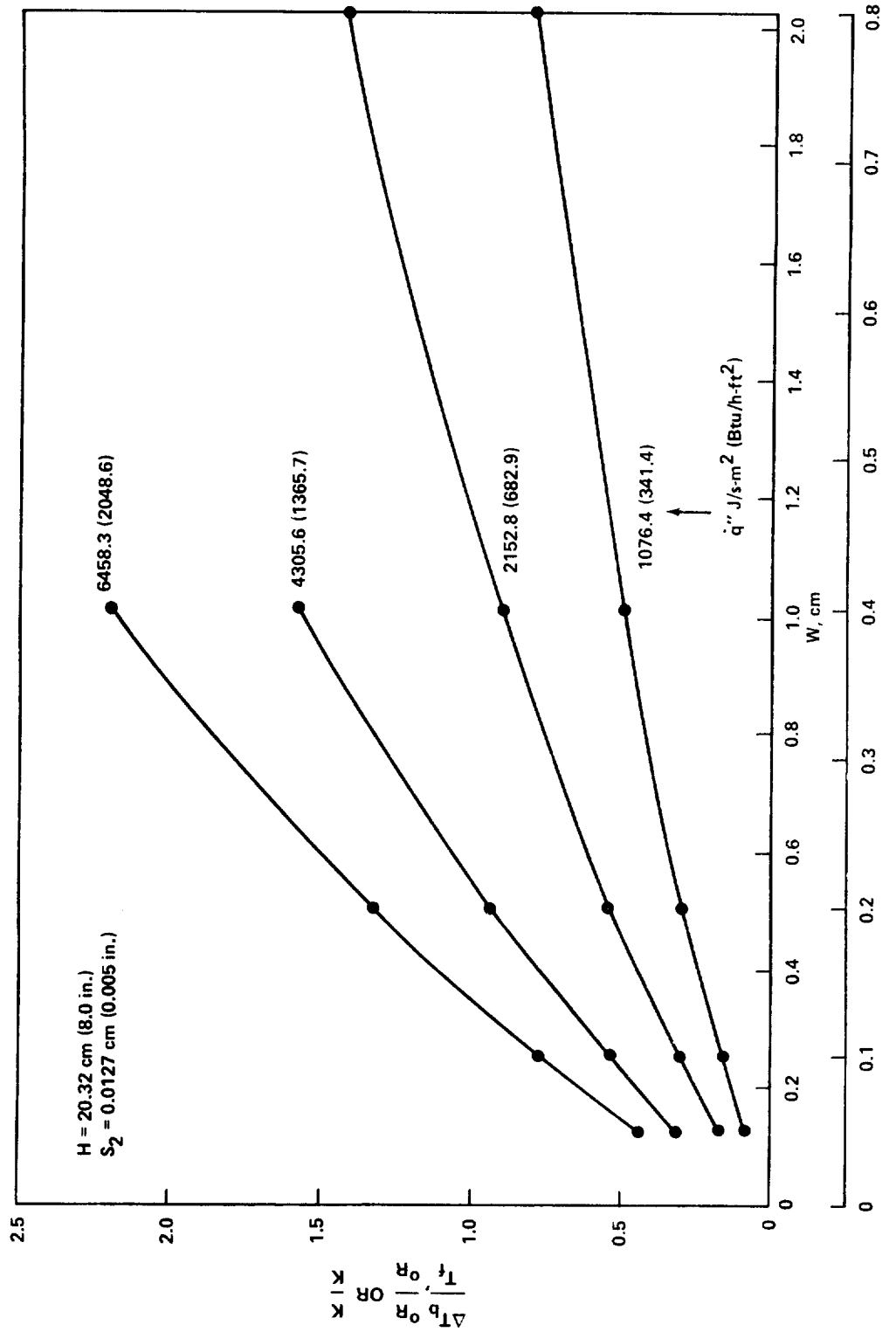

Figure 50. Base temperature rise at termination of melting versus W for H = 20.32 cm (8.0 in.) and S_2 = 0.0127 cm (0.005 in.).

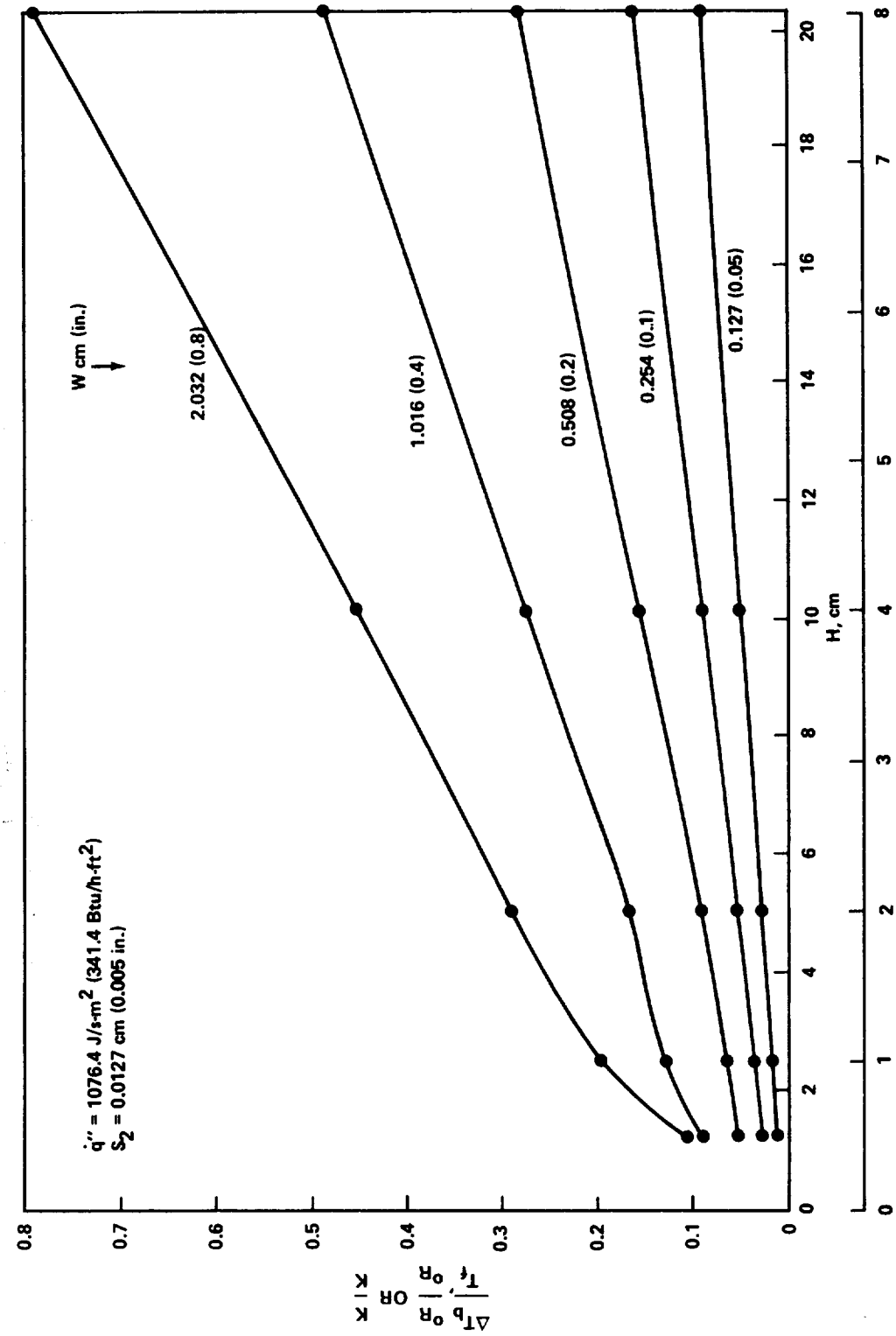

Figure 51. Base temperature rise at the termination of melting versus H for $\dot{q}''$ = 1076.4 J/s-m^2 (341.4 Btu/h-ft^2) and S_2 = 0.0127 cm (0.005 in.).

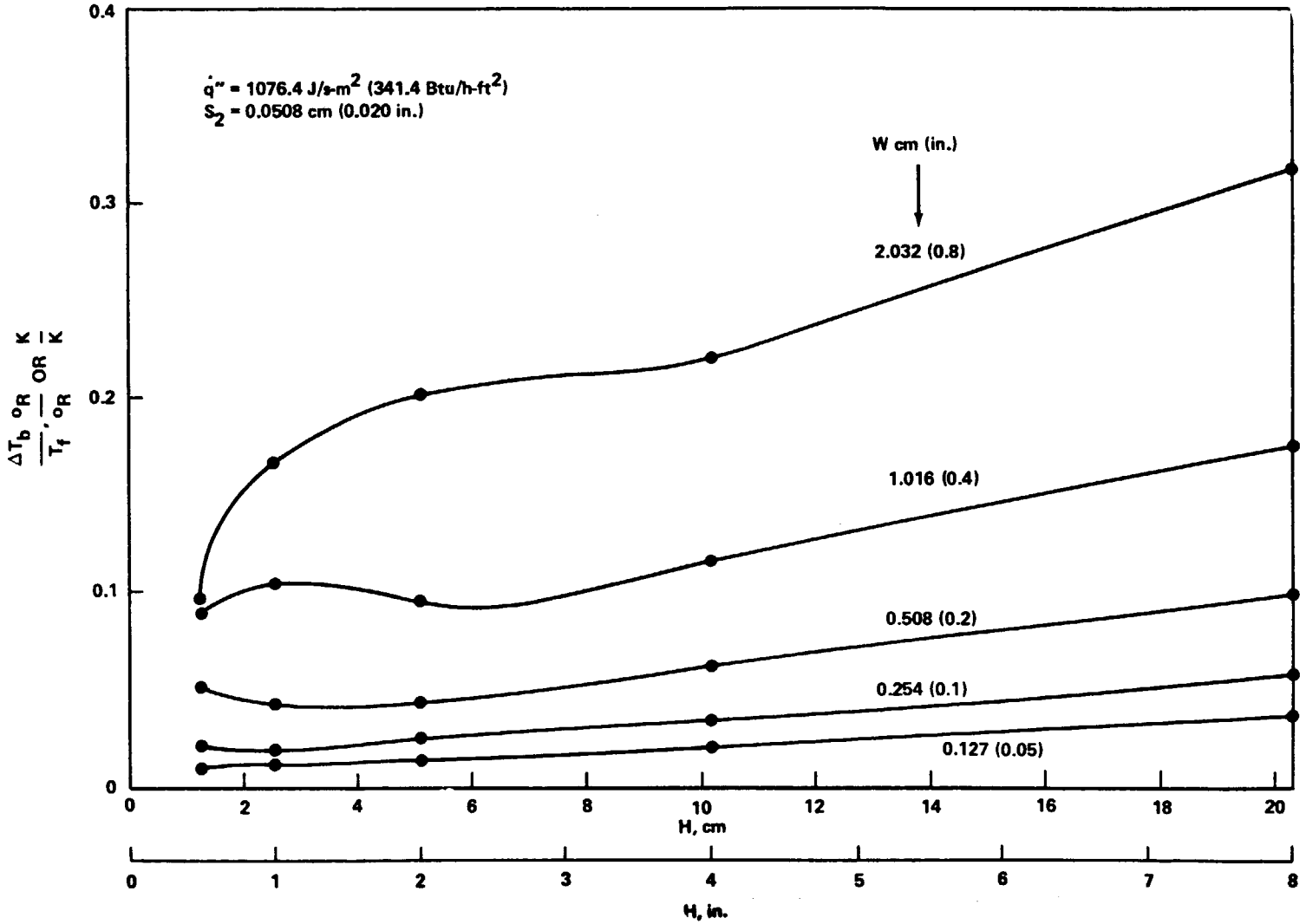

Figure 52. Base temperature rise at the termination of melting versus H for $q'' = 1076.4$ J/s-m^2 (341.4 Btu/h-ft^2) and $S_2 = 0.0508$ cm (0.020 in.).

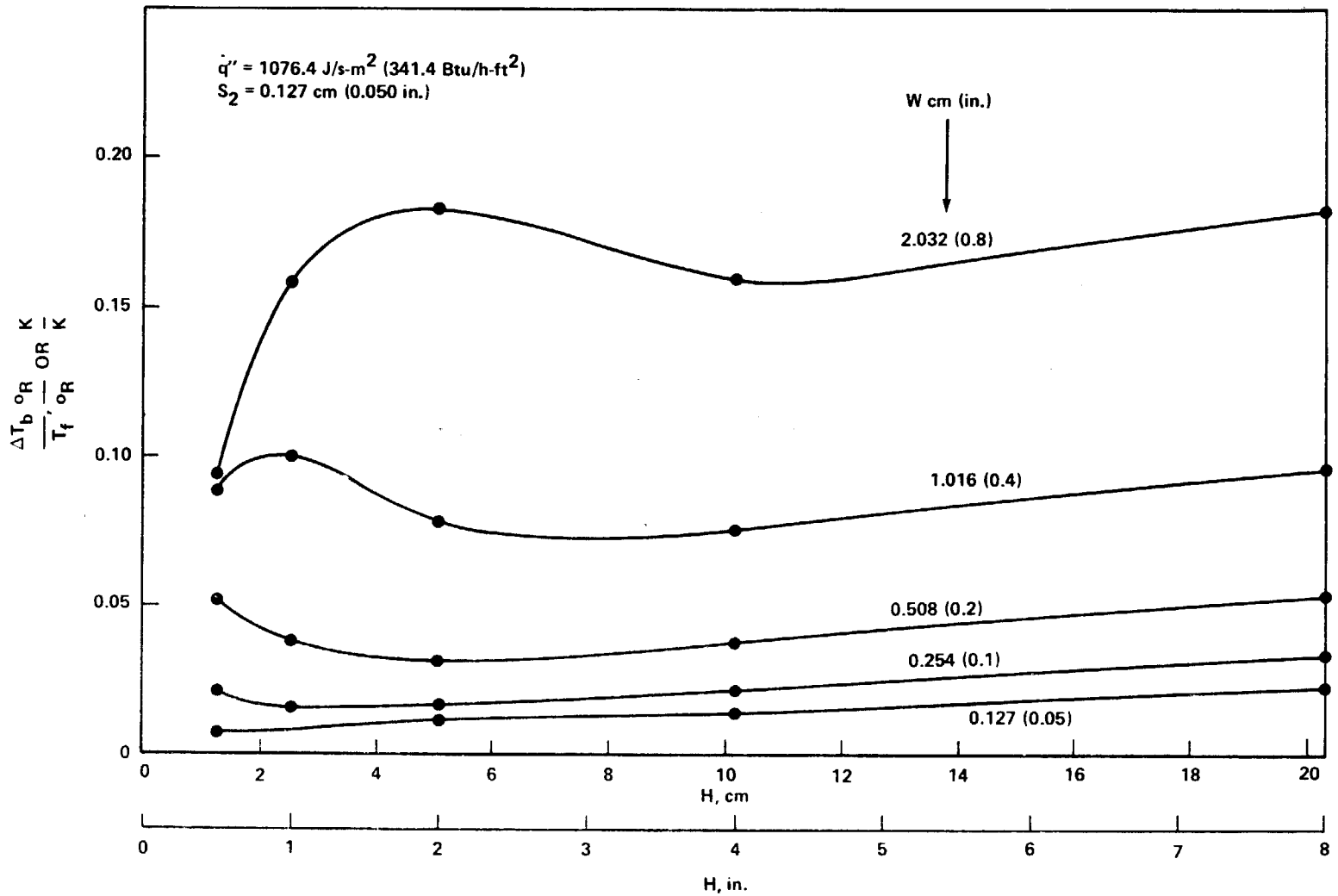

Figure 53. Base temperature rise at the termination of melting versus H for $\dot{q}''$ = 1076.4 J/s-m^2 (341.4 Btu/h-ft^2) and S_2 = 0.127 cm (0.050 in.).

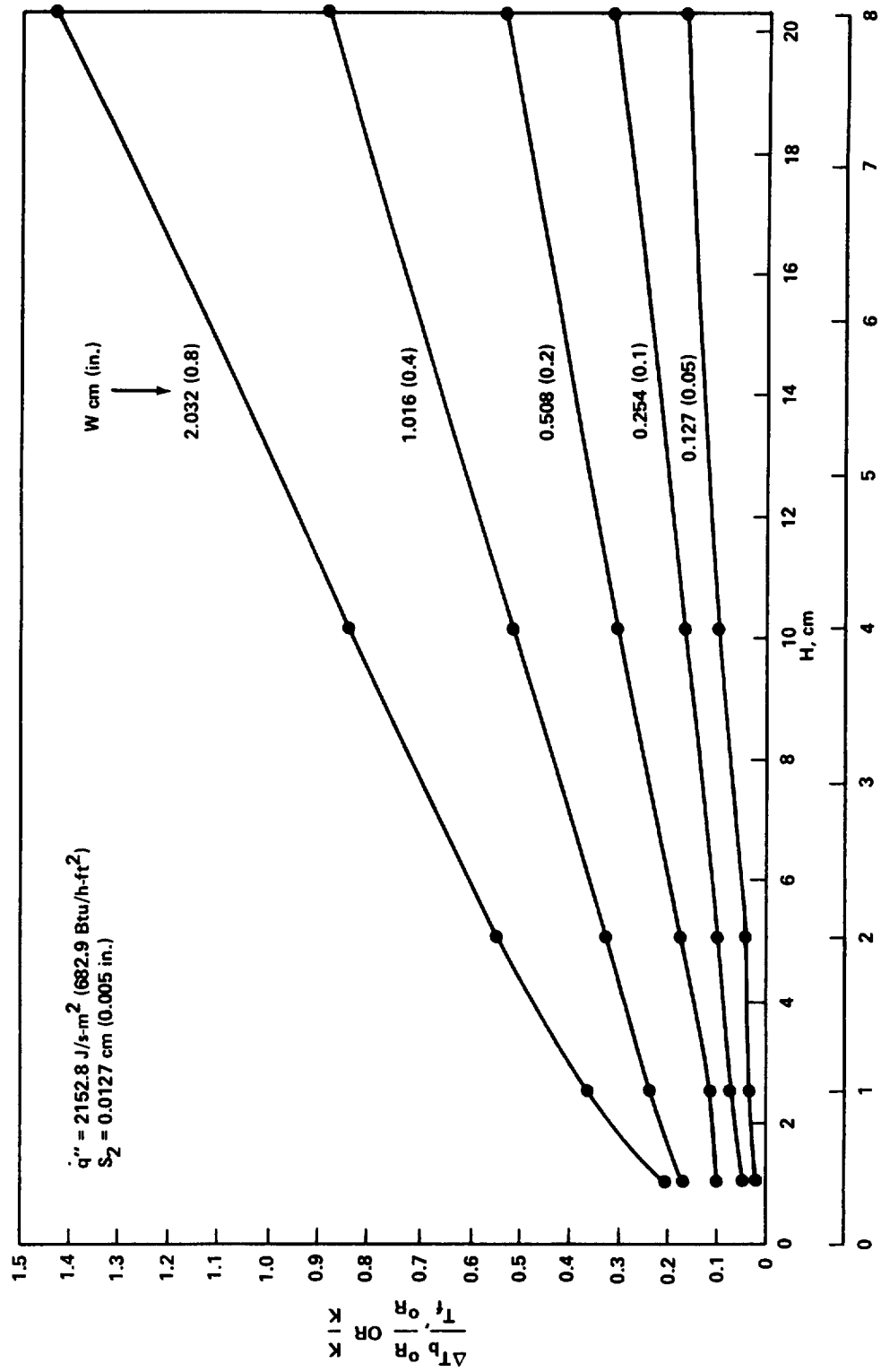

Figure 54. Base temperature rise at the termination of melting versus H for $q'' = 2152.8$ J/s-m^2 (682.9 Btu/h-ft^2) and $S_2 = 0.0127$ cm (0.005 in.).

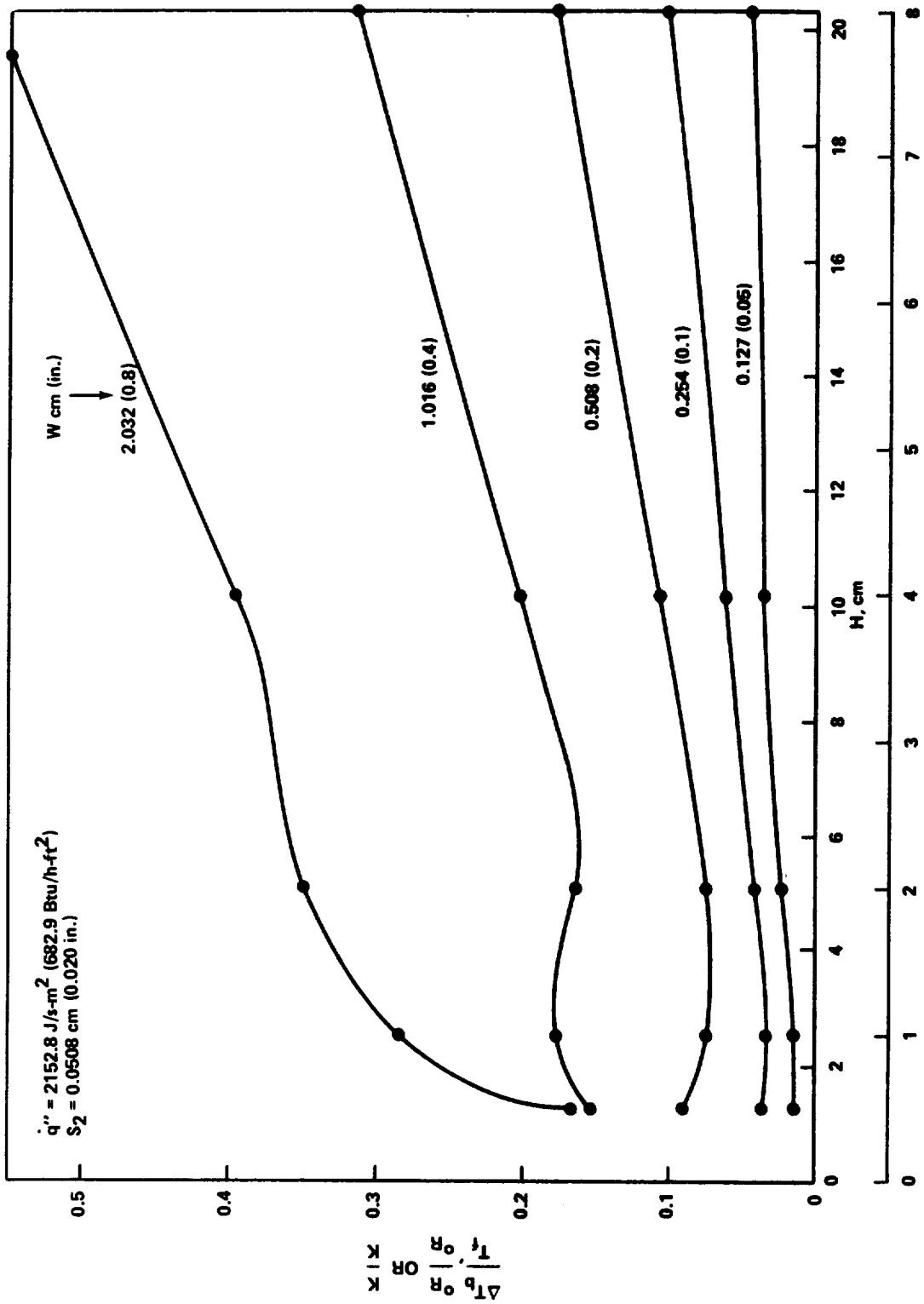

Figure 55. Base temperature rise at the termination of melting versus H for $\dot{q}'' = 2152.8$ J/s-m^2 (682.9 Btu/h-ft^2) and $S_2 = 0.0508$ cm (0.020 in.).

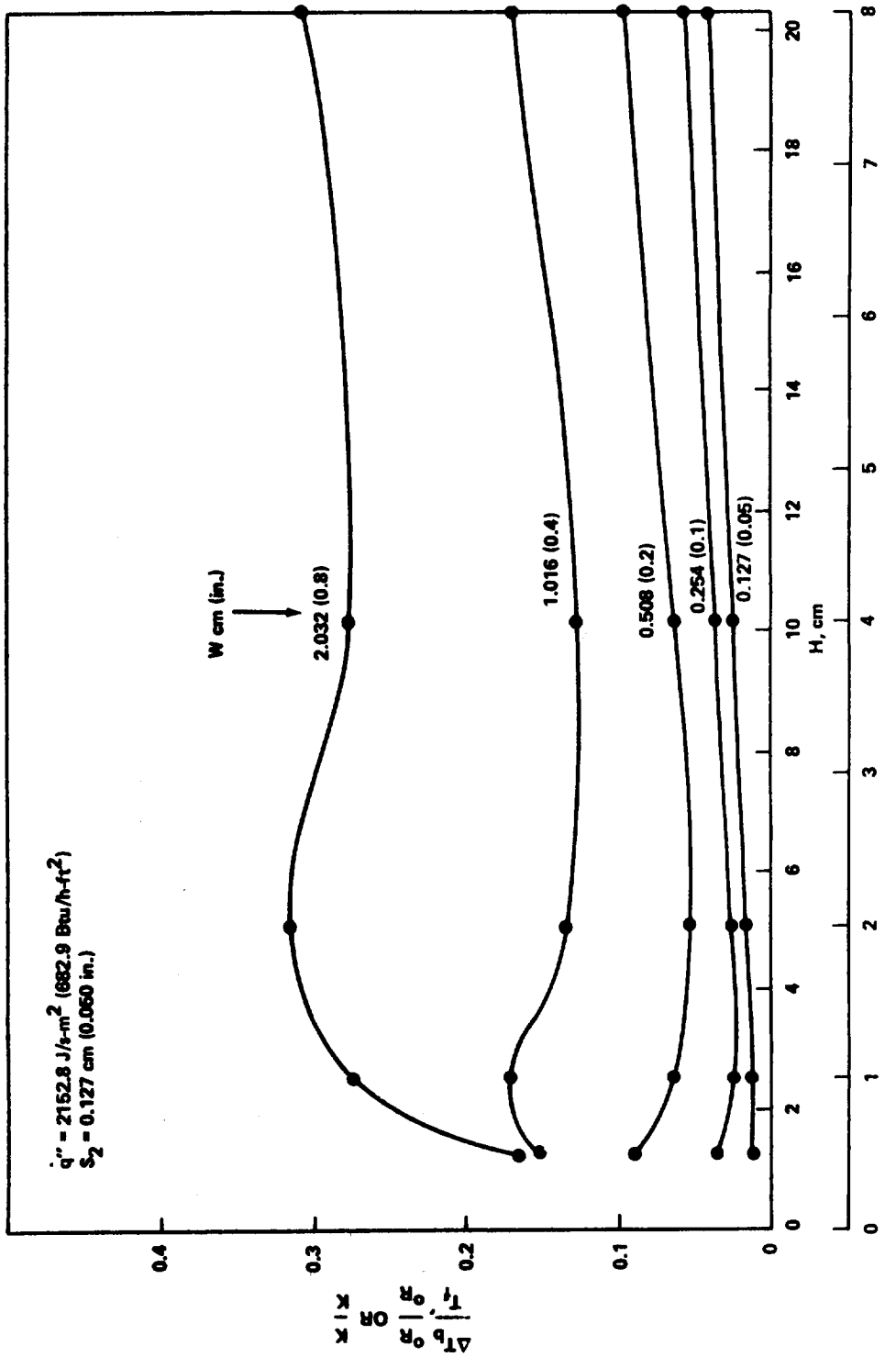

Figure 56. Base temperature rise at the termination of melting versus H for $\dot{q}'' = 2152.8$ J/s-m^2 (682.9 Btu/h-ft^2) and $S_2 = 0.127$ cm (0.05 in.).

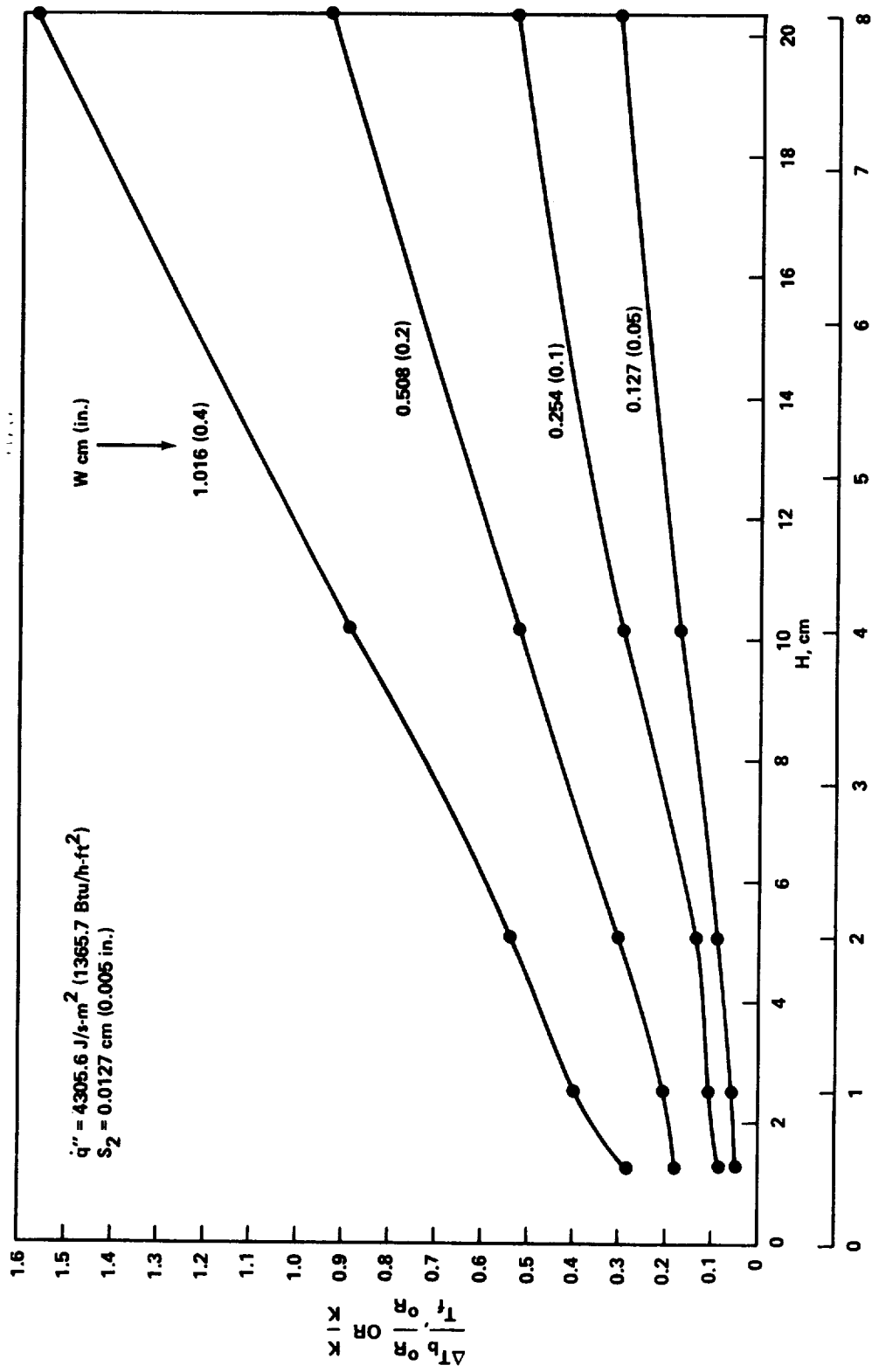

Figure 57. Base temperature rise at the termination of melting versus H for $\dot{q}'' = 4305.6$ J/s-m^2 (1365.7 Btu/h-ft^2) and $S_2 = 0.0127$ cm (0.005 in.).

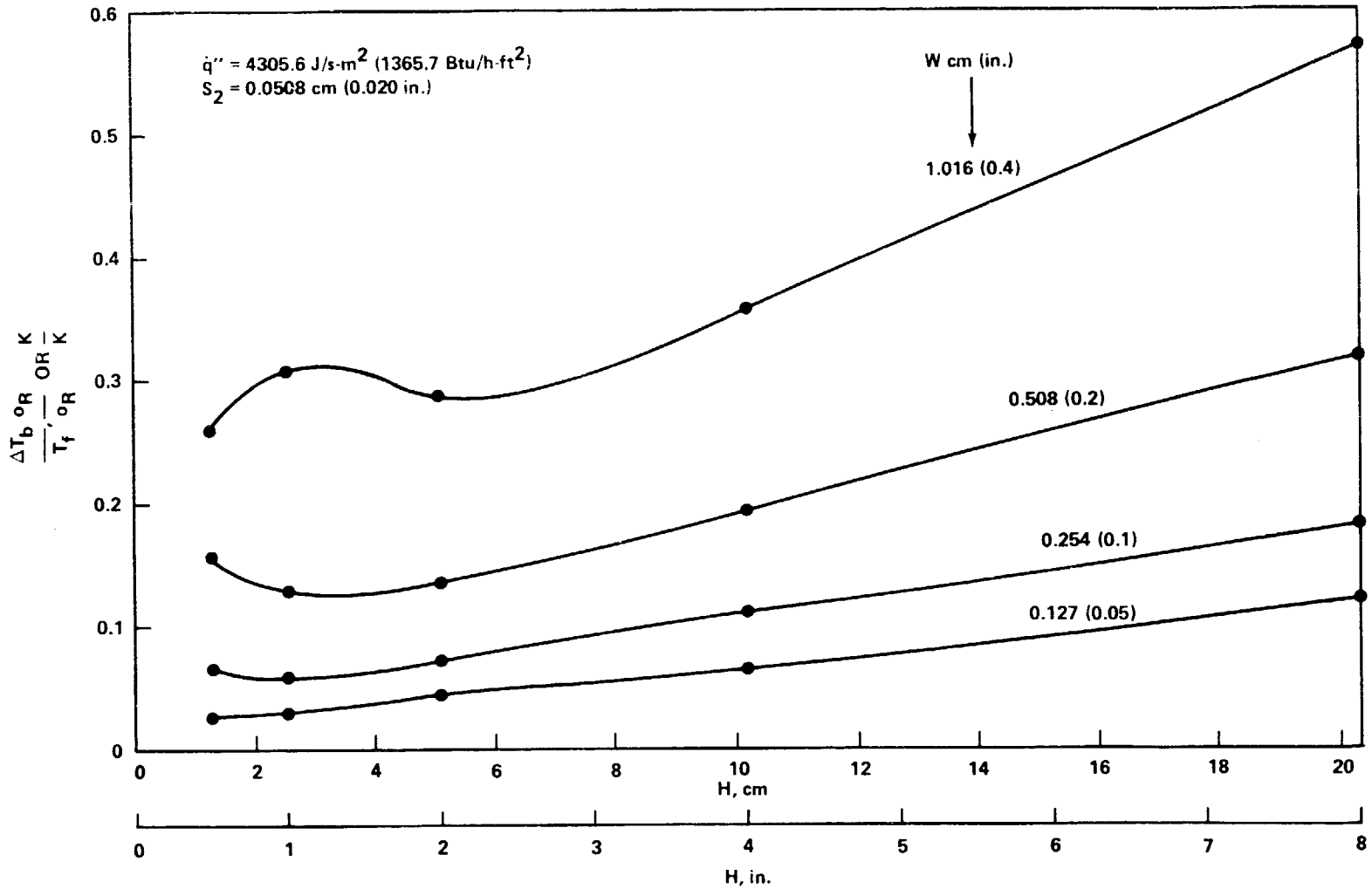

Figure 58. Base temperature rise at the termination of melting versus H for $\dot{q}''$ = 4305.6 J/s-m^2 (1365.7 Btu/h-ft^2) and S_2 = 0.0508 cm (0.020 in.).

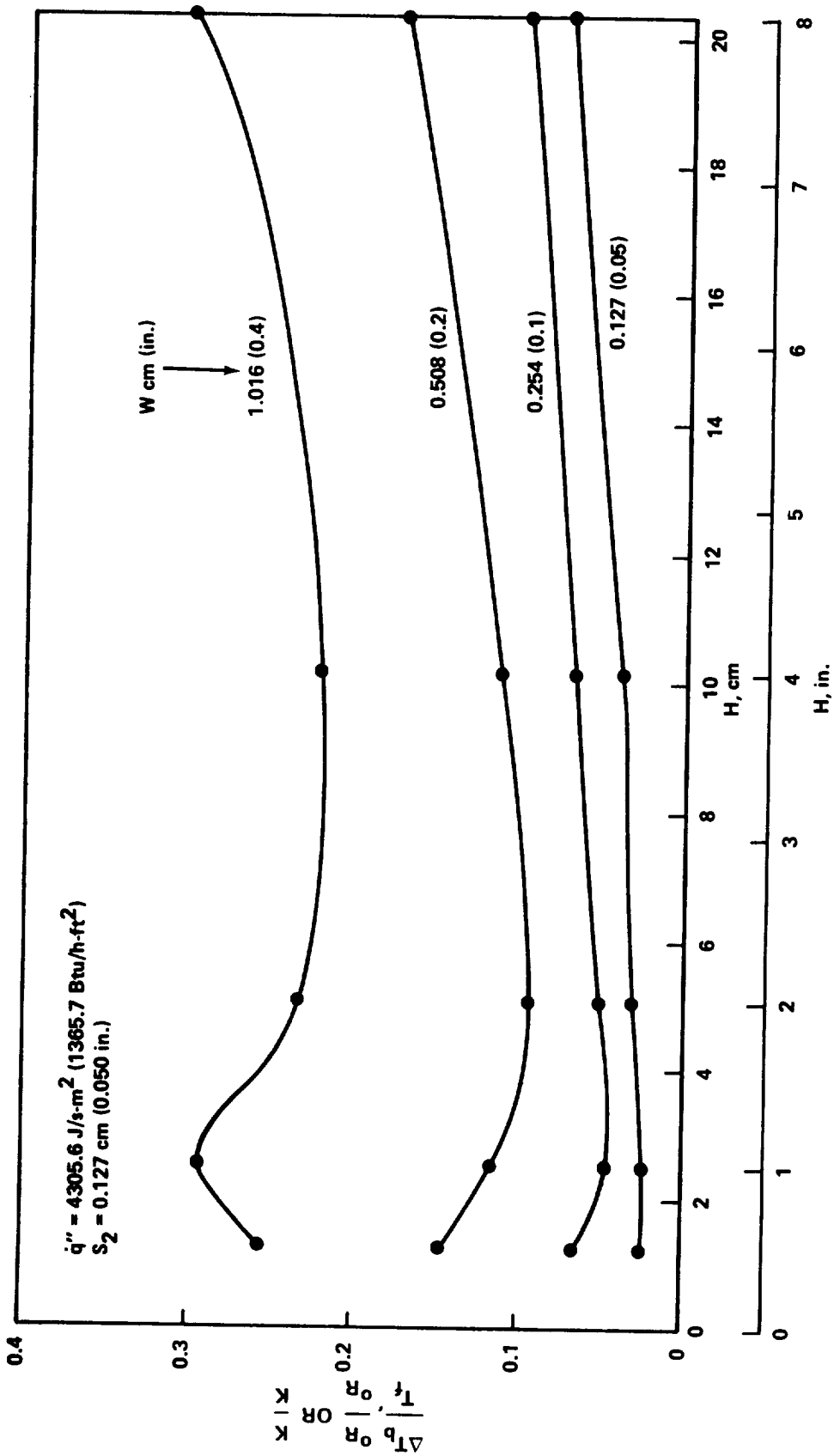

Figure 59. Base temperature rise at the termination of melting versus H for $\dot{q}''$ = 4305.6 J/s-m^2 (1365.7 Btu/h-ft^2) and S_2 = 0.127 cm (0.050 in.).

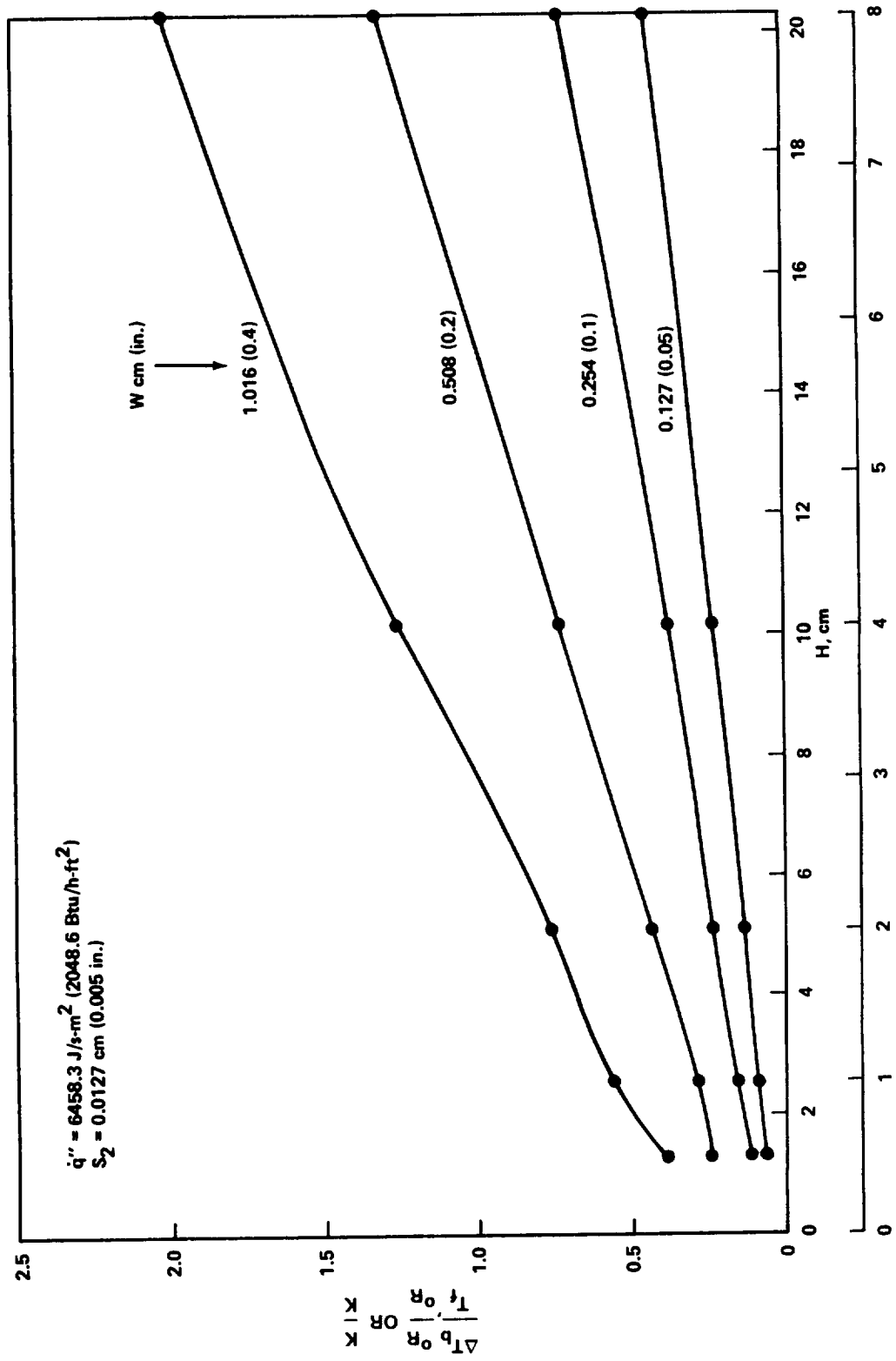

Figure 60. Base temperature rise at the termination of melting versus H for $\dot{q}'' = 6458.3$ J/s-m^2 (2048.6 Btu/h-ft^2) and $S_2 = 0.0127$ cm (0.005 in.).

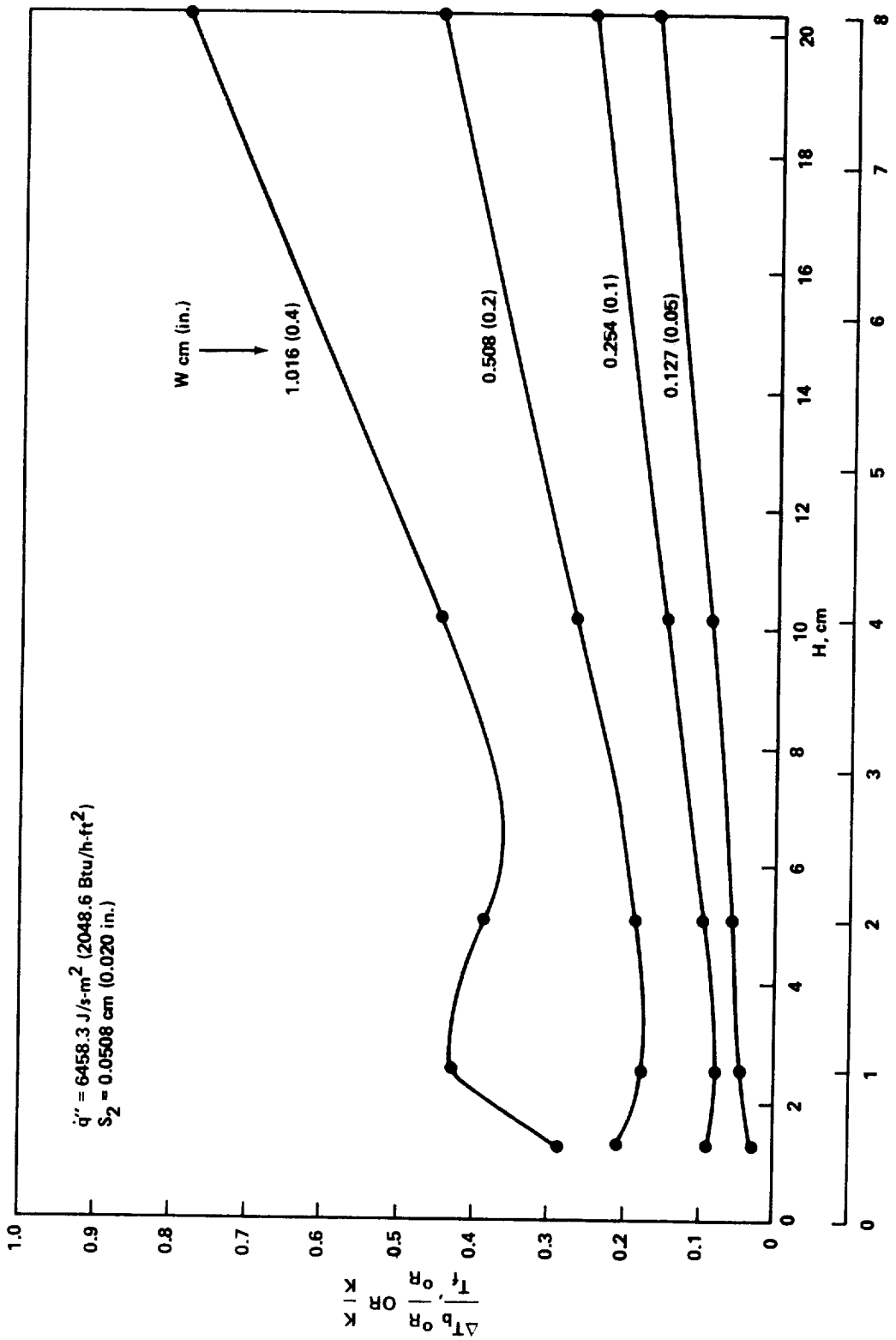

Figure 61. Base temperature rise at the termination of melting versus H for $\dot{q}''$ = 6458.3 J/s-m^2 (2048.6 Btu/h-ft^2) and S_2 = 0.0508 cm (0.020 in.).

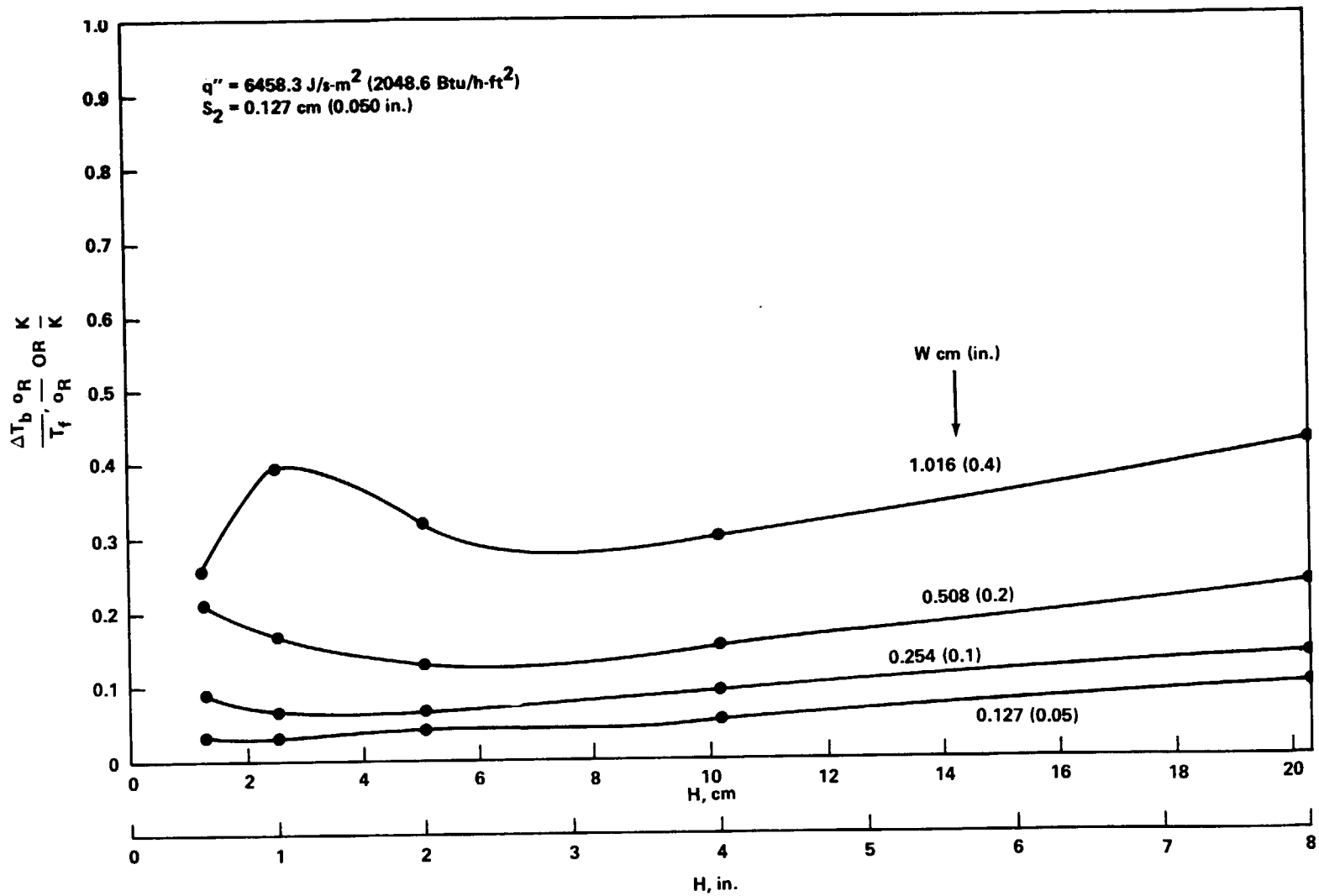

Figure 62. Base temperature rise at the termination of melting versus H for $\dot{q}''$ = 6458.3 J/s-m² (2048.6 Btu/h-ft²) and S_2 = 0.127 cm (0.050 in.).

The base temperature rises shown in Figures 36 through 62 correspond to the termination of melting. If the entire amount of PCM is not melted, the temperature rise of the base may be considerably less than that reflected in Figures 36 through 62. As an indication of the transient behavior of the base temperature, certain transient data are plotted in Figures 63 through 77. For some cases, the base temperature rise remains relatively low over a large percentage of the phase change process and rises rapidly near the end of the process. In other cases, the rise occurs nearly uniformly throughout the phase change process. In either case, designs based on the data shown in Figures 36 through 62 should be conservative, especially if the design does not require complete melting of the PCM. However, as indicated by these data, in cases where base plate temperature control is the object, it may be more desireable to limit phase change in order to avert unreasonable fin spacing and/or heights.

Some of the curves shown in Figures 63 through 77 exhibit fluctuations in the transient base temperature. For those curves where a sharp rise occurs in the computed base temperature (e.g., the upper curve in Figure 63), the accuracy with which the predictions describe the actual physical variation is questionable, particularly during the early part of the transient. The computing model attempts to predict the behavior of a continuous system with use of a limited number of finite size nodes. Since the phase change is handled in the model by forcing an entire node to remain at the phase change temperature until sufficient energy has accumulated to account for the phase change, one would expect some stepping in the results unless the nodes are made very small. This, however, is related to the choice of M and N, which in turn dictates computed requirements. Since the problem examined in the parametric study involved a step input of a constant heat flux at the base, the initial level to which the computer temperature rises is dependent on the node size. The influence of N on the computed results is illustrated in Figure 63 for three runs, in Figure 64 for one run, and in Figure 65 for one run. For these selected runs, computations are shown for N values of 5 and 10. When 5 is used, a horizontal row of nodes represents 20 percent of the PCM. Obviously, the precise detail of the transient variation is affected in each case, but the principal difference is at the beginning; it appears that increasing N results in a smoothing out of the fluctuations and shortens the initial plateau. The general trend of the results remains consistent and there appears to be only a slight effect in the latter stages of a run. For reference purposes the values of N used in the computations are given for the respective curve in Figures 63 through 77.

The time required for the PCM to melt is depicted graphically in Figures 78 through 89. These times exceed those which would be required by purely latent considerations because of the effect of sensible heating.

Since there is a certain amount of sensible energy storage, ratios of the total stored energy at the termination of melting to the latent energy required to change phase of the PCM are shown plotted versus heat flux density at the base in Figures 90 through 104.

A few additional computer runs were made for selected values of the parameters to examine the influence of the fusion temperature on the predicted temperature rise of the base at the termination of melting. The results of these computations are shown in Figures 105 through 107.

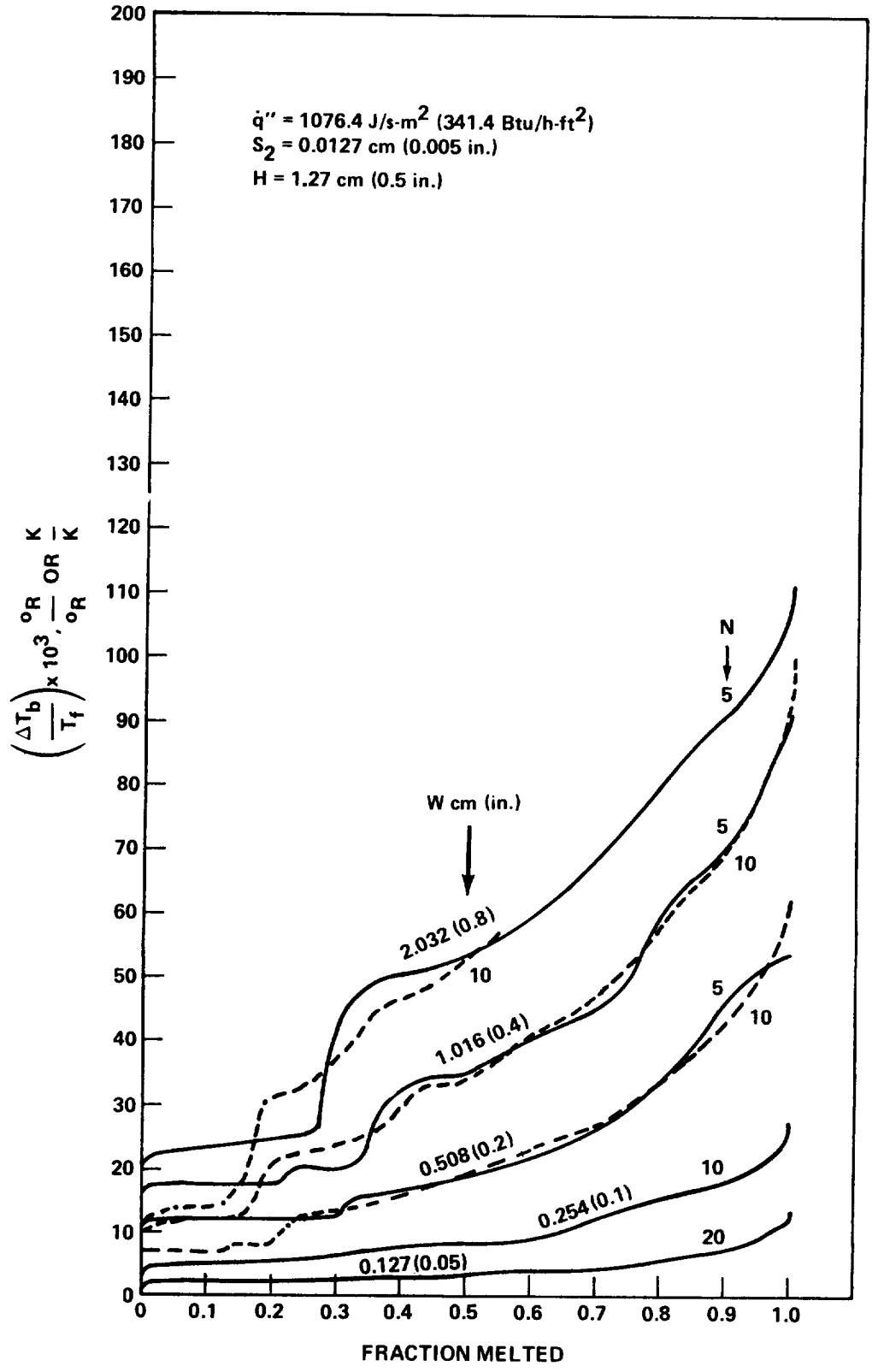

Figure 63. Transient base temperature rise versus fraction of PCM melted for H = 1.27 cm (0.5 in.) and S_2 = 0.0127 cm (0.005 in.).

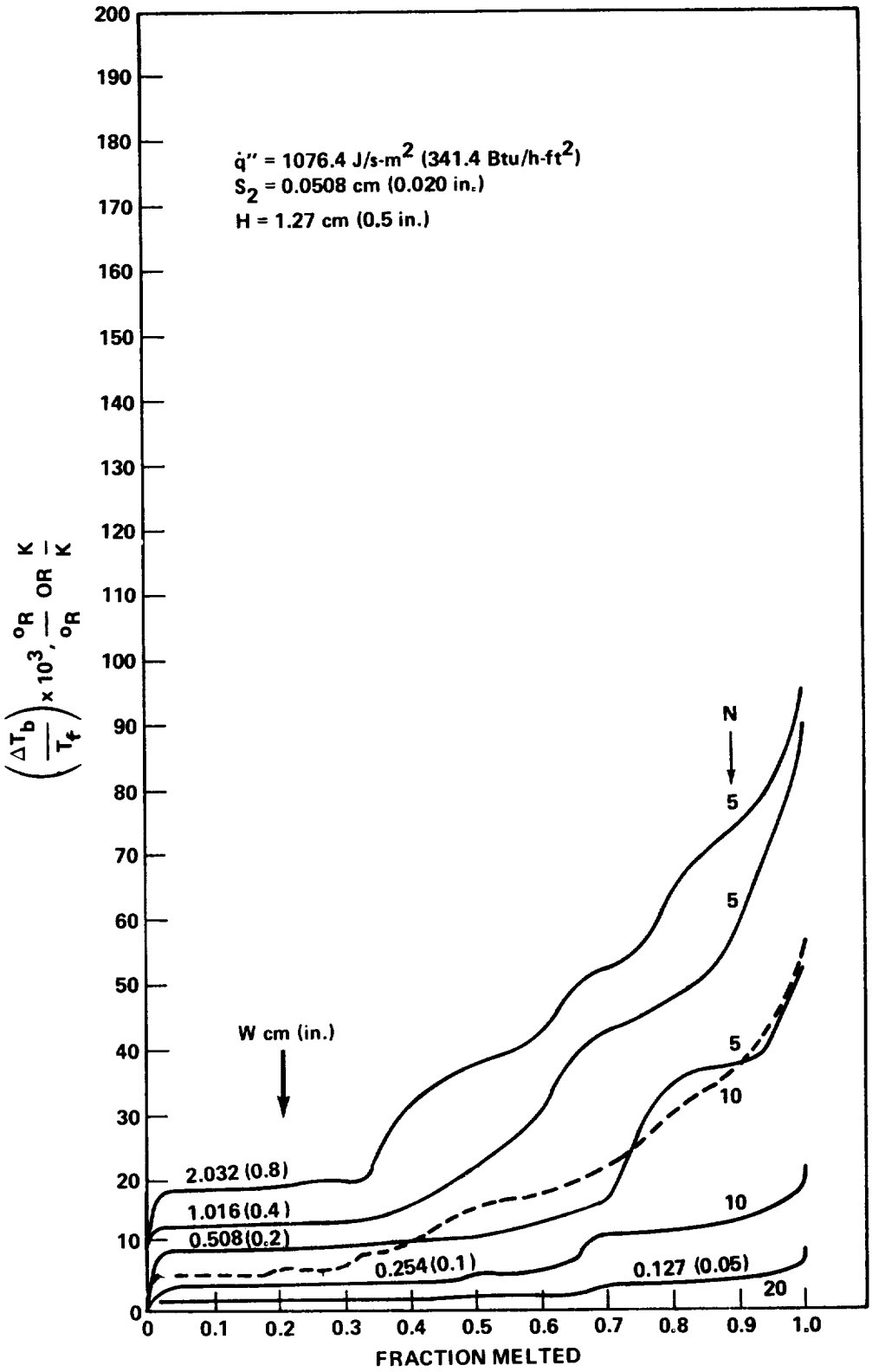

Figure 64. Transient base temperature rise versus fraction of PCM melted for H = 1.27 cm (0.5 in.) and S_2 = 0.0508 cm (0.020 in.).

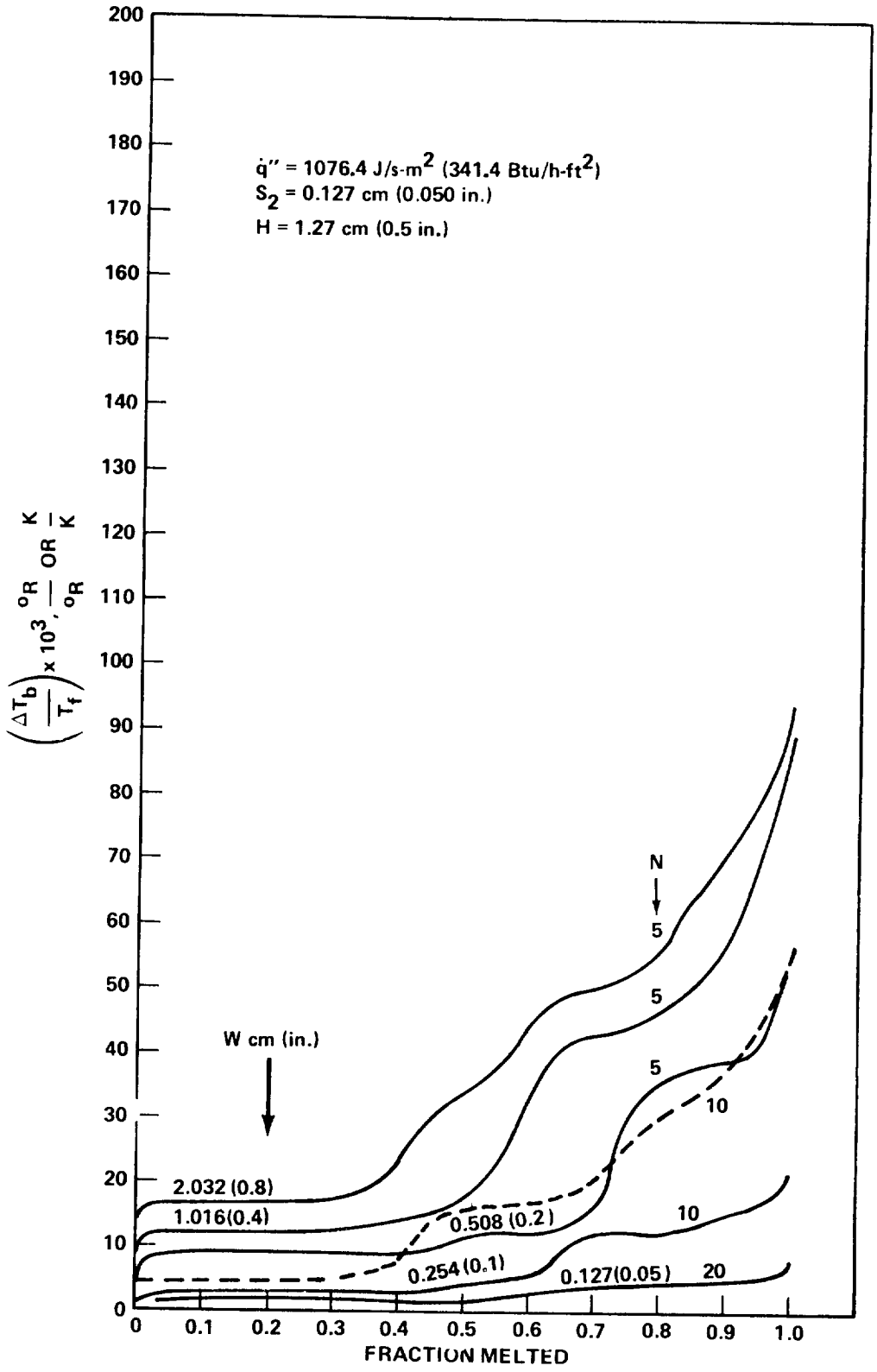

Figure 65. Transient base temperature rise versus fraction of PCM melted for H = 1.27 cm (0.5 in.) and S_2 = 0.127 cm (0.05 in.).

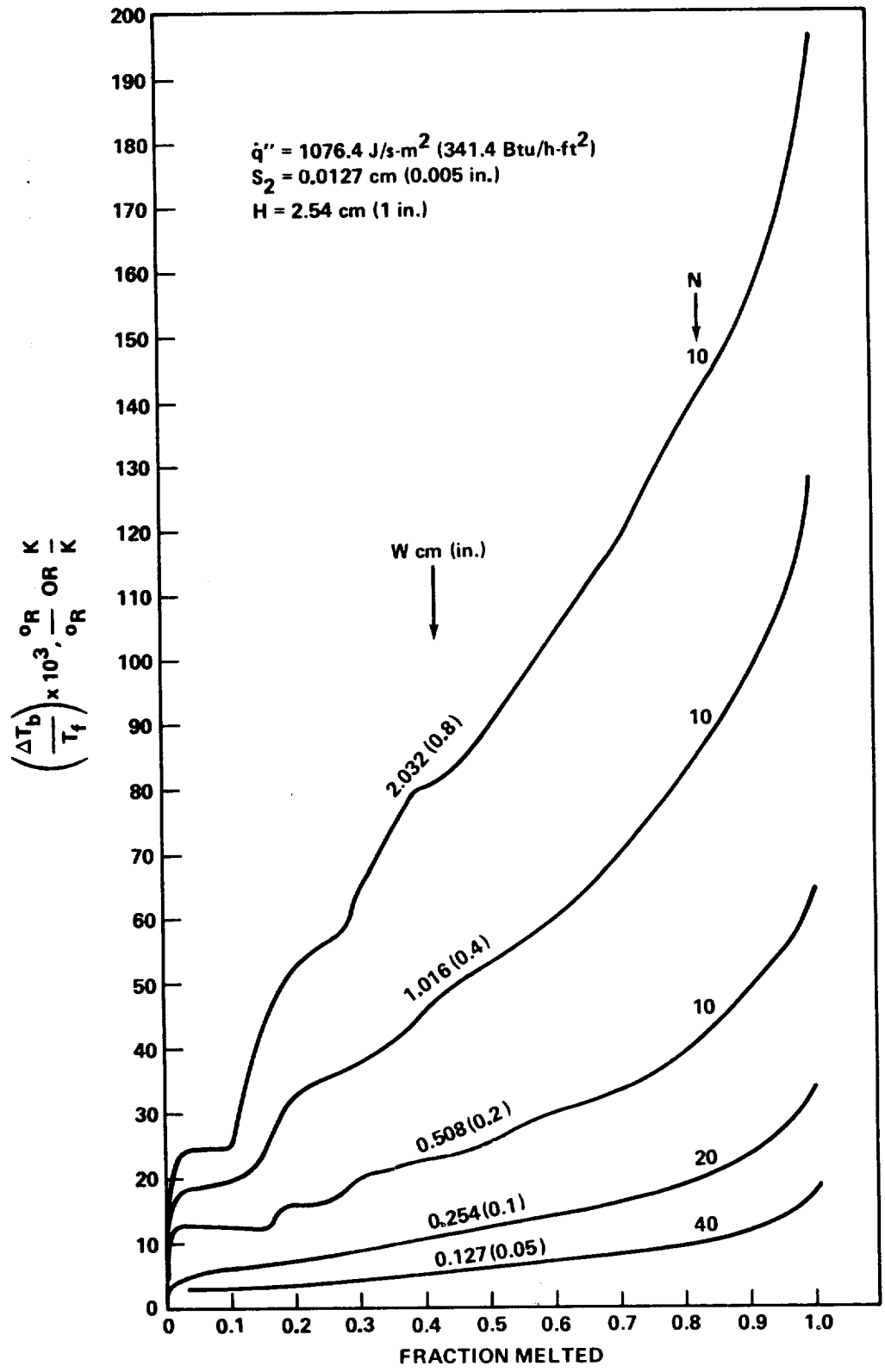

Figure 66. Transient base temperature rise versus fraction of PCM melted for H = 2.54 cm (1 in.) and S_2 = 0.0127 cm (0.005 in.).

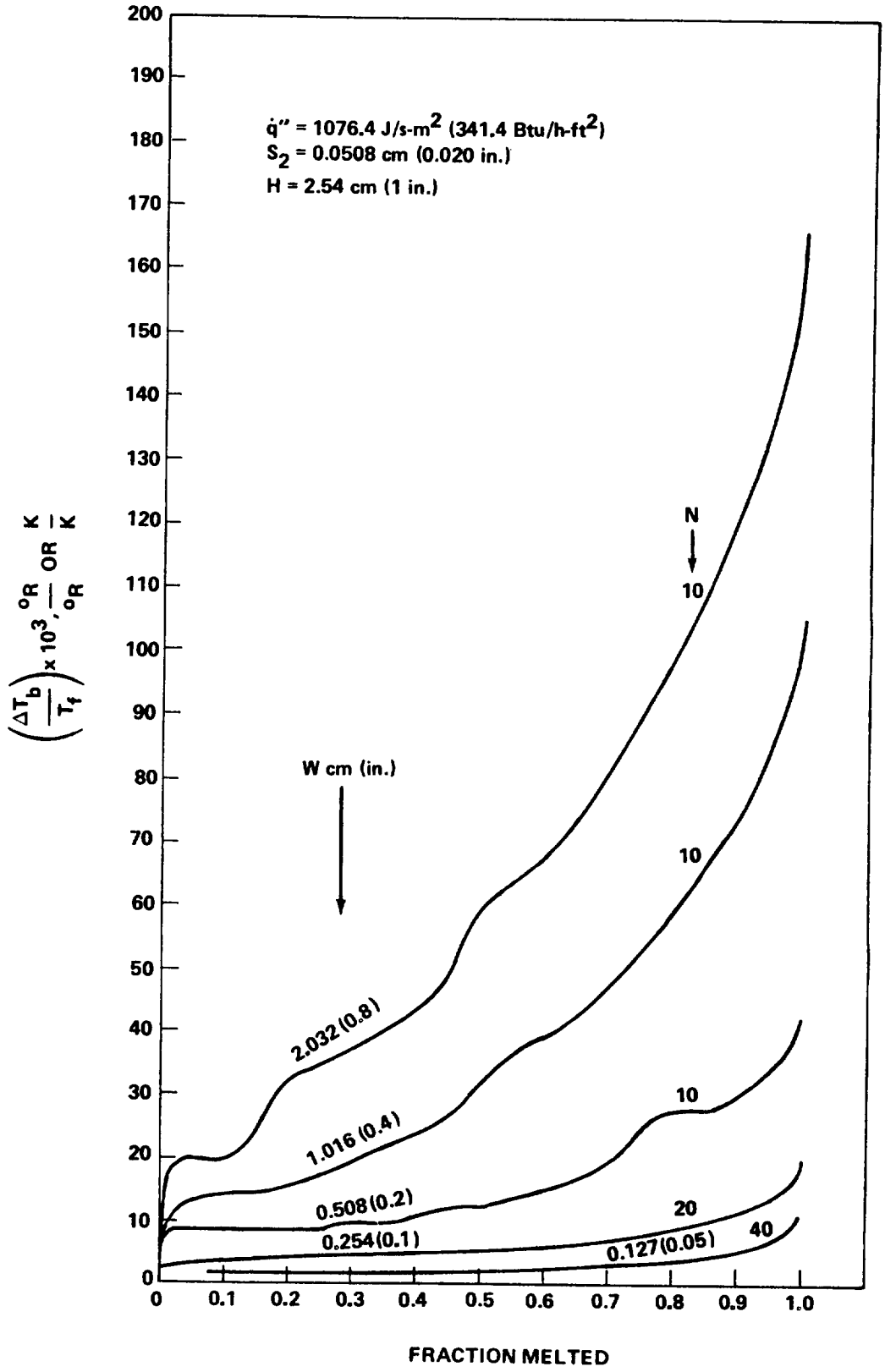

Figure 67. Transient base temperature rise versus fraction of PCM melted for H = 2.54 cm (1 in.) and S_2 = 0.0508 cm (0.020 in.).

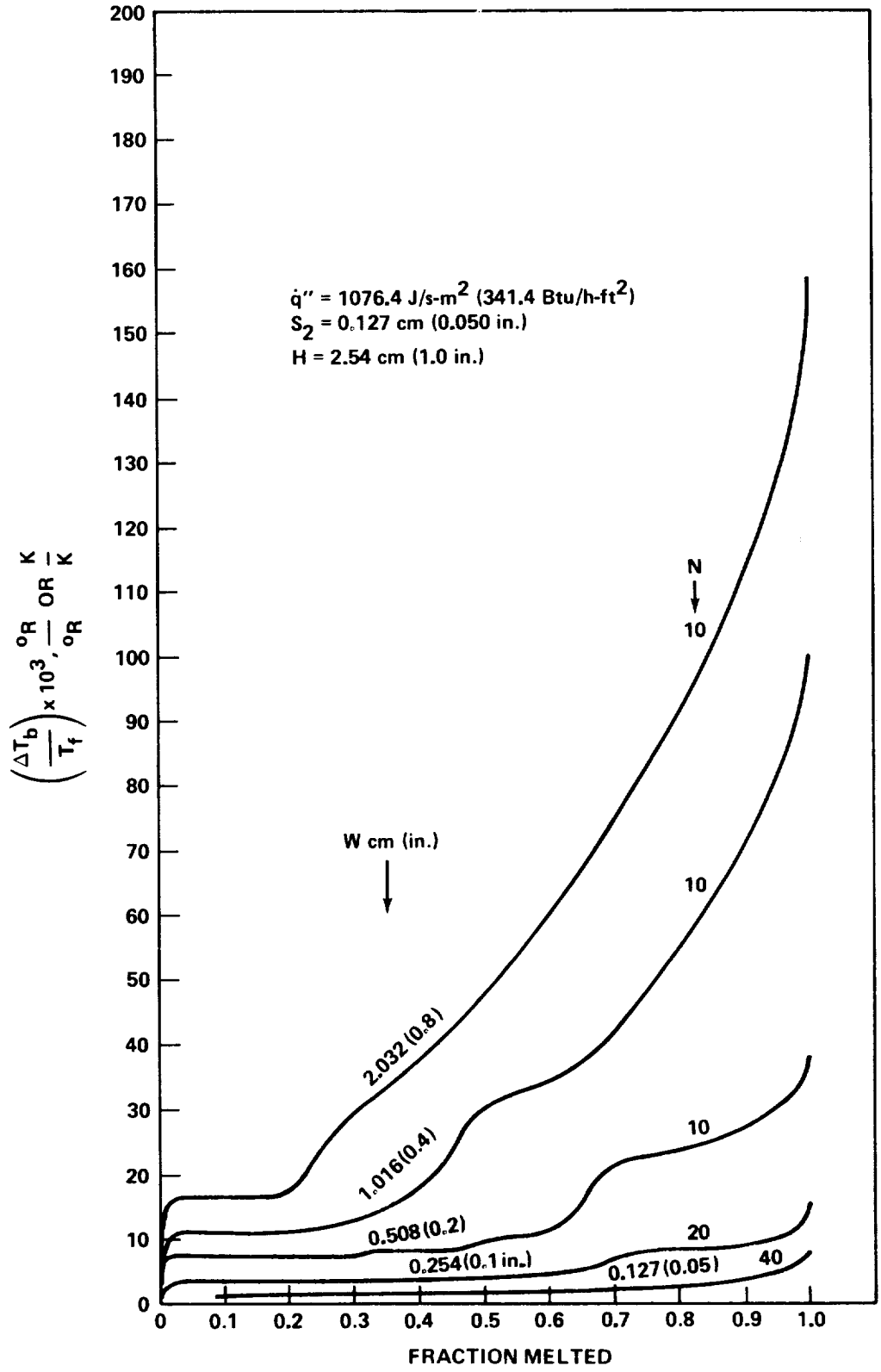

Figure 68. Transient base temperature rise versus fraction of PCM melted for H = 2.54 cm (1 in.) and S_2 = 0.127 cm (0.05 in.).

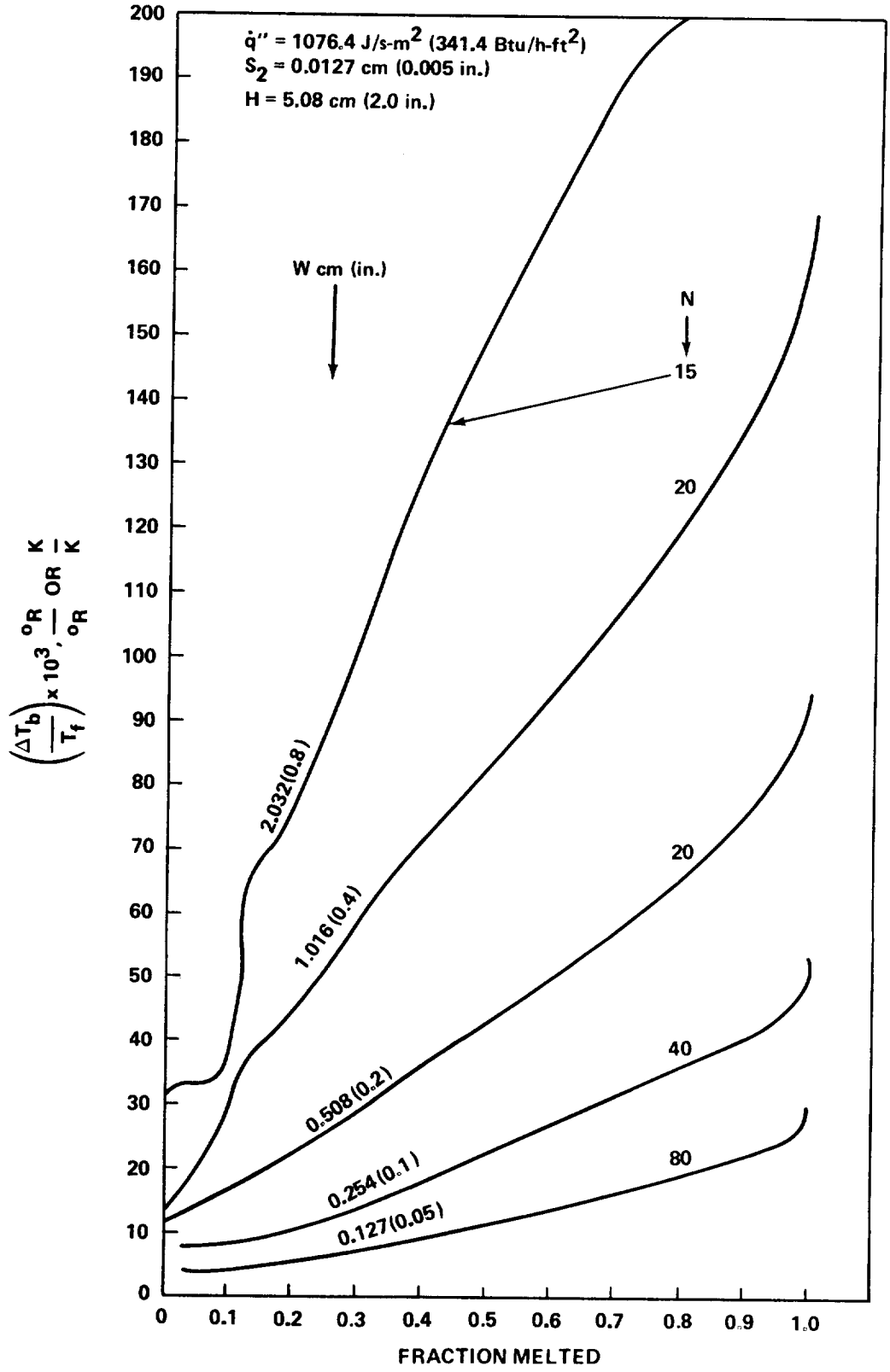

Figure 69. Transient base temperature rise versus fraction of PCM melted for H = 5.08 cm (2 in.) and S_2 = 0.0127 cm (0.005 in.).

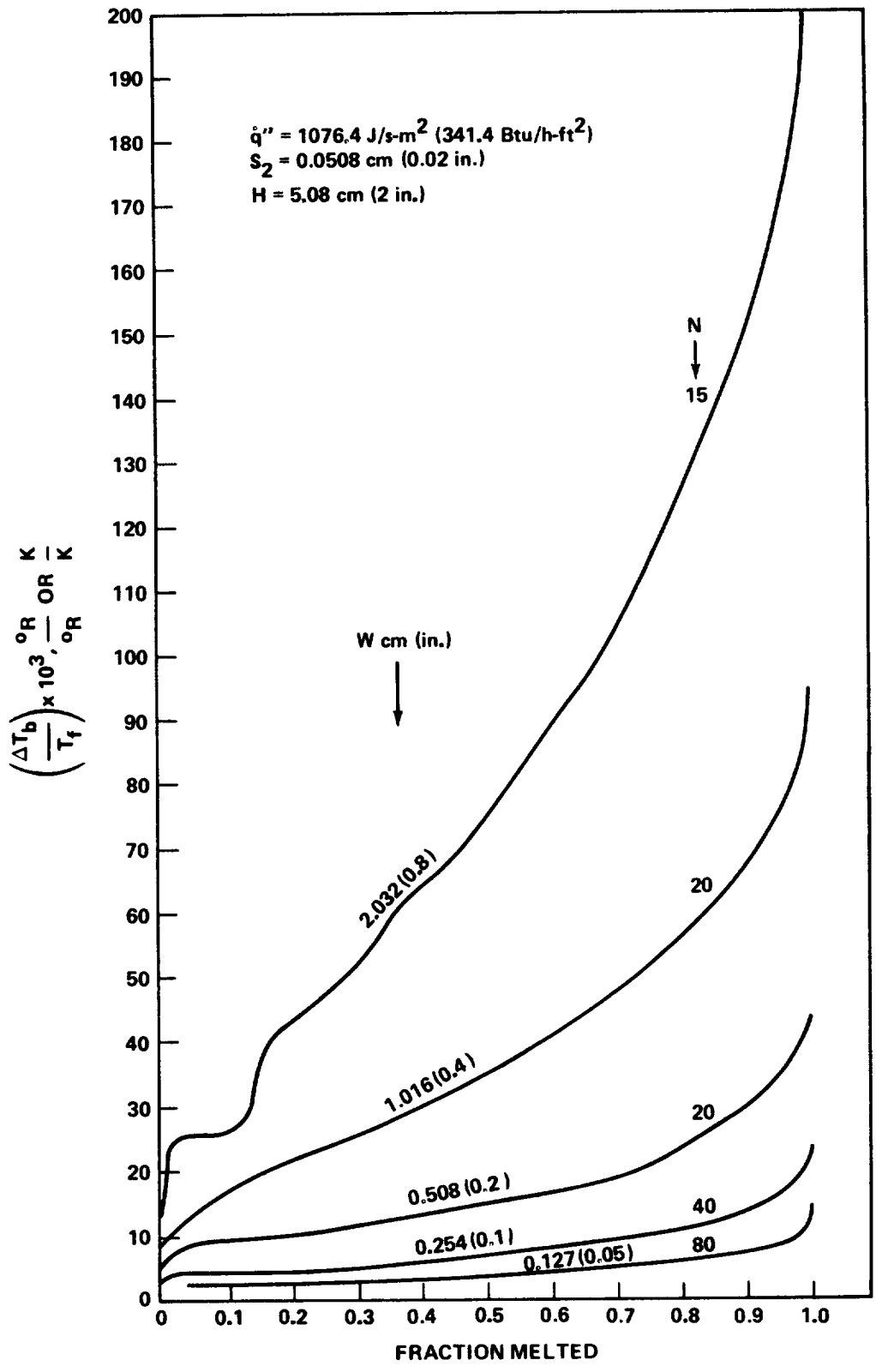

Figure 70. Transient base temperature rise versus fraction of PCM melted for H = 5.08 cm (2 in.) and S_2 = 0.0508 cm (0.02 in.).

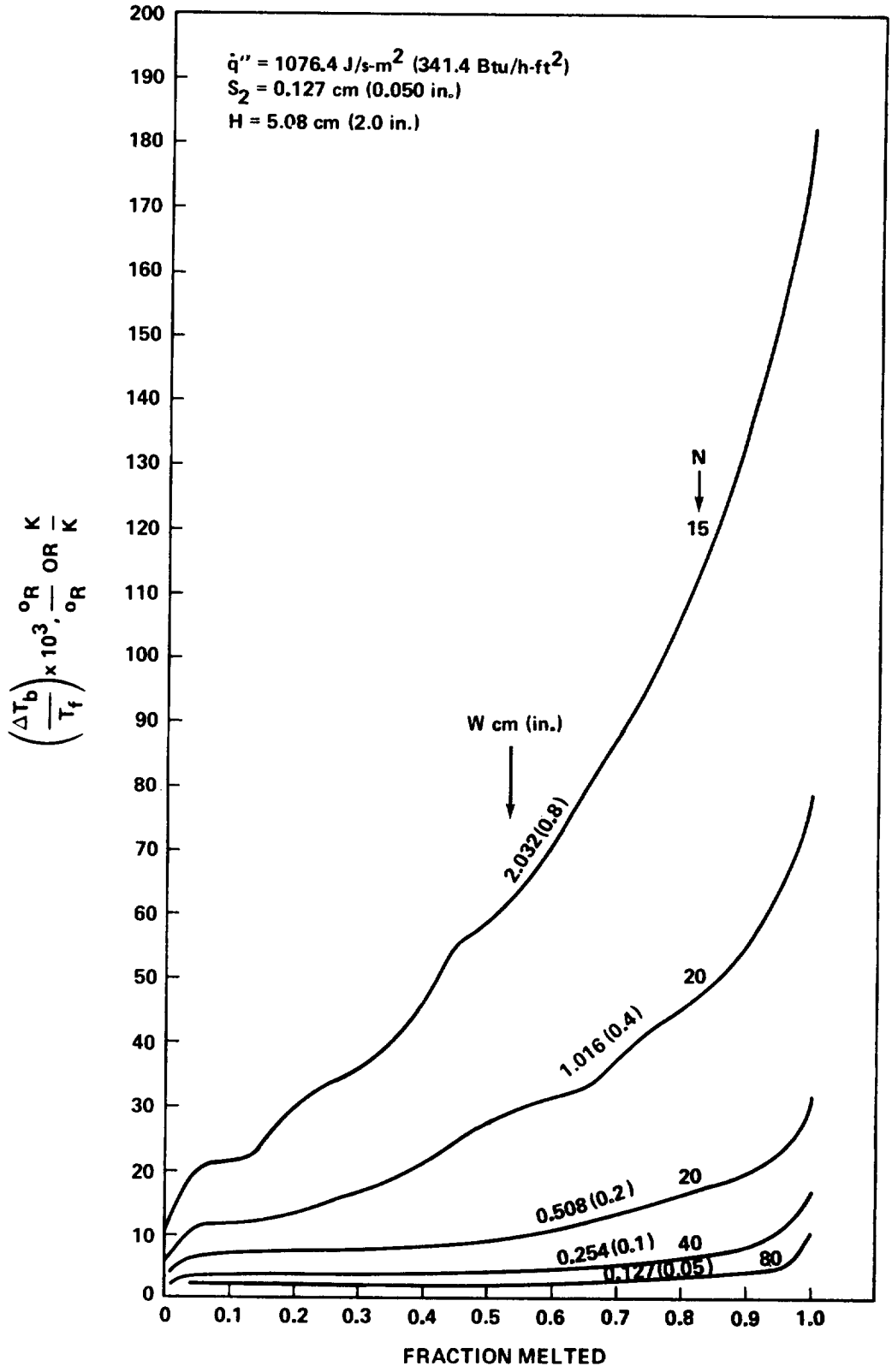

Figure 71. Transient base temperature rise versus fraction of PCM melted for H = 5.08 cm (2 in.) and S_2 = 0.127 cm (0.05 in.).

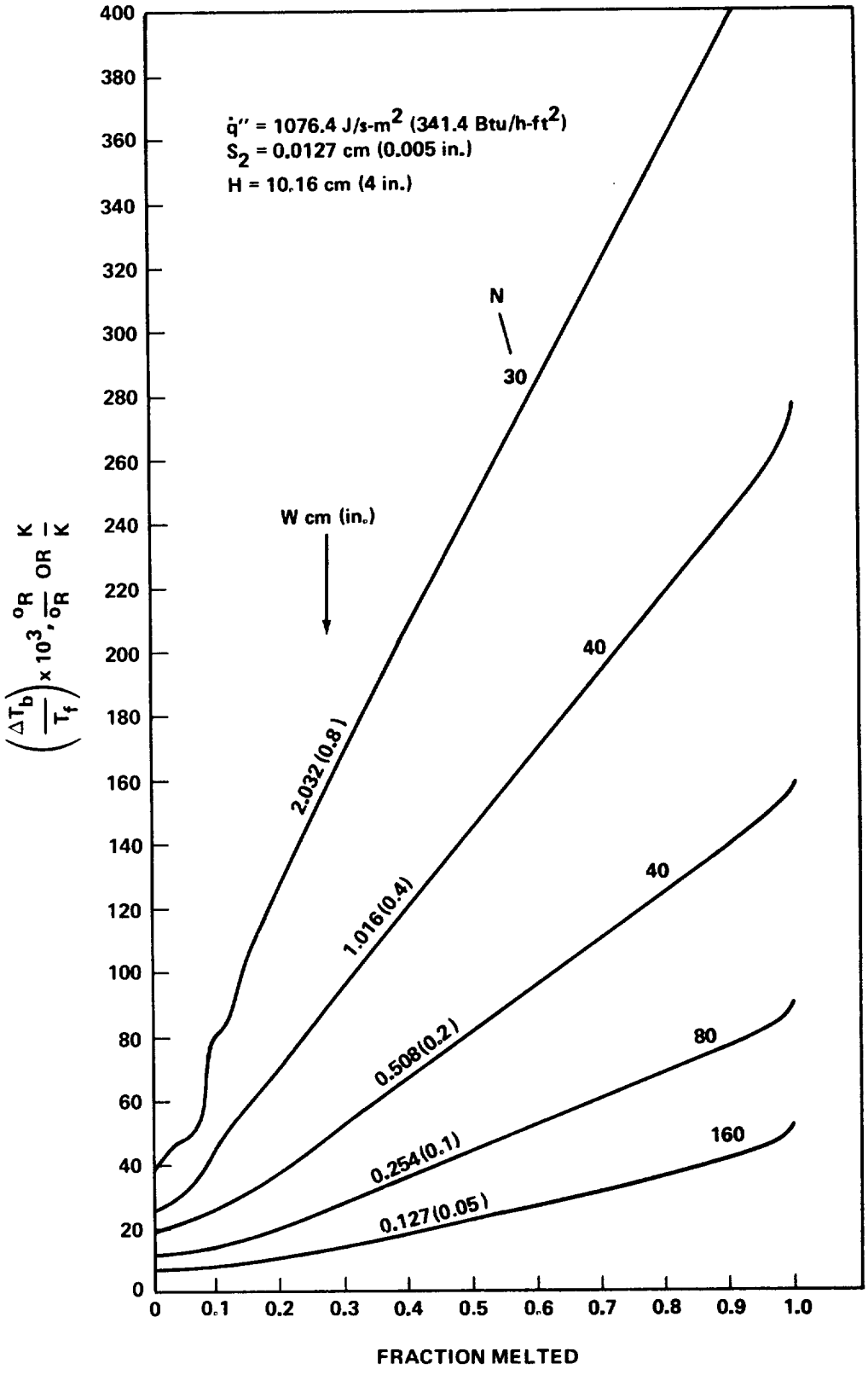

Figure 72. Transient base temperature rise versus fraction of PCM melted for H = 10.16 cm (4 in.) and S_2 = 0.0127 cm (0.005 in.).

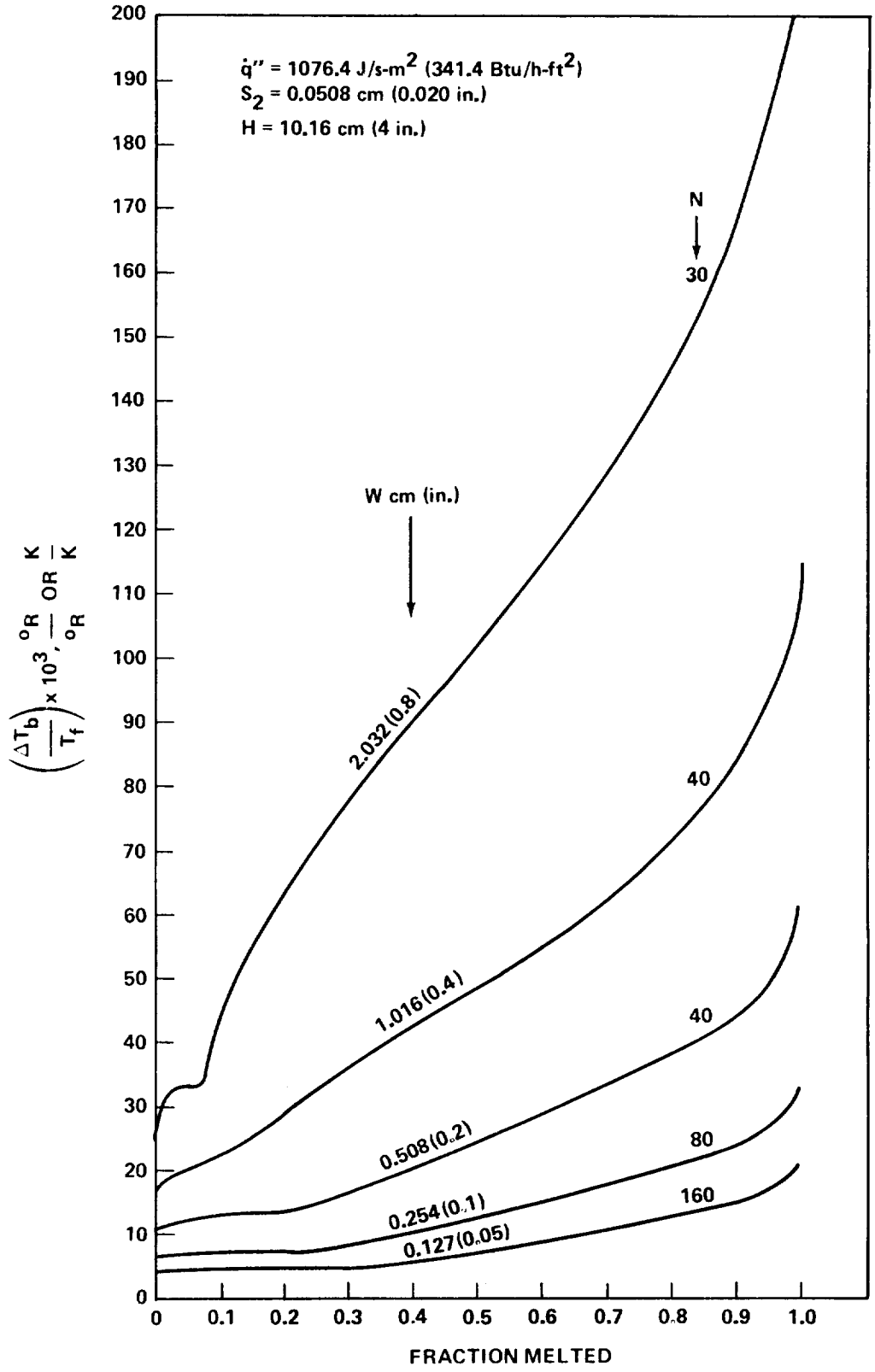

Figure 73. Transient base temperature rise versus fraction of PCM melted for H = 10.16 cm (4 in.) and S_2 = 0.0508 cm (0.02 in.).

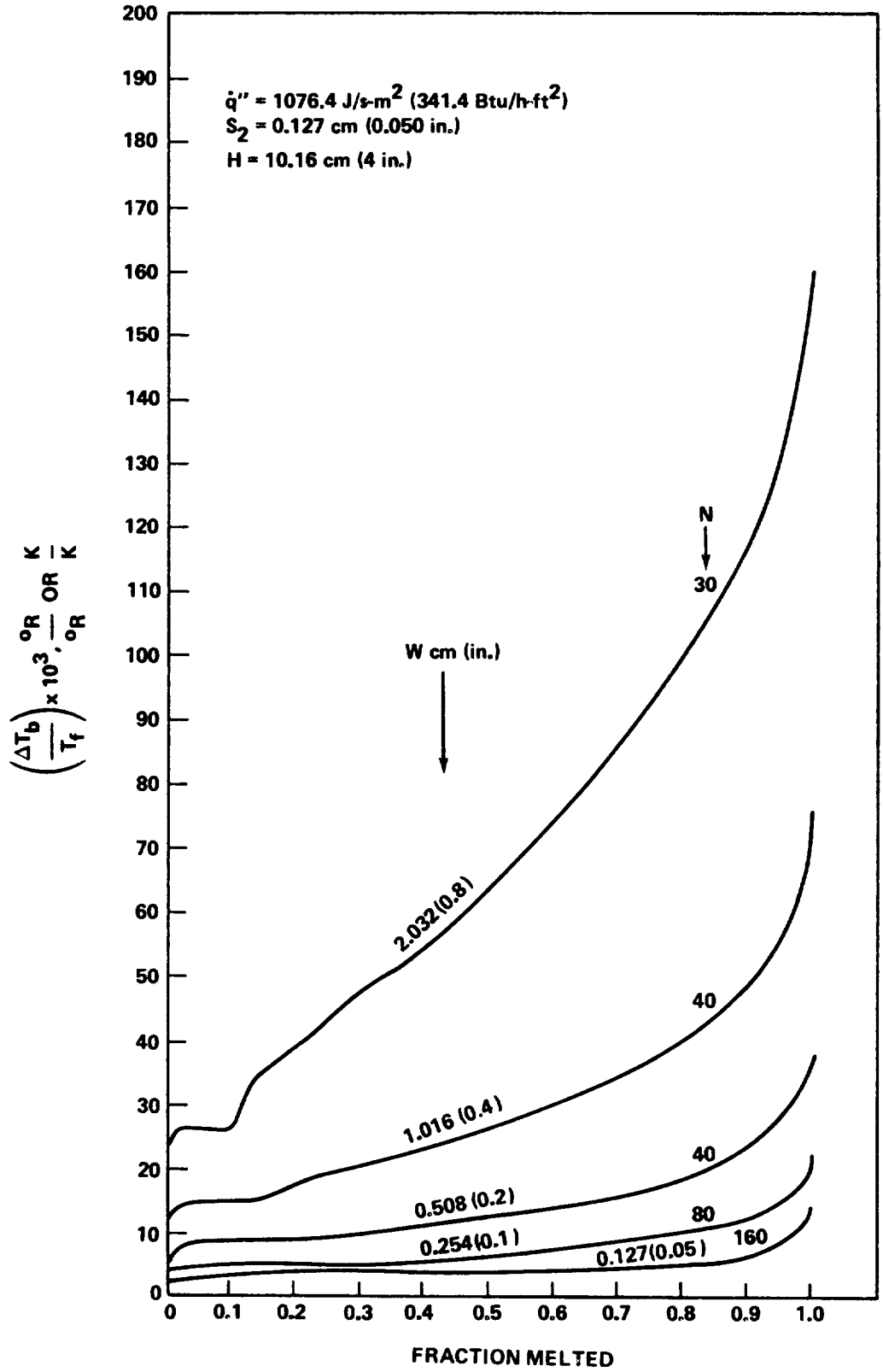

Figure 74. Transient base temperature rise versus fraction of PCM melted for H = 10.16 cm (4 in.) and S_2 = 0.127 cm (0.05 in.)

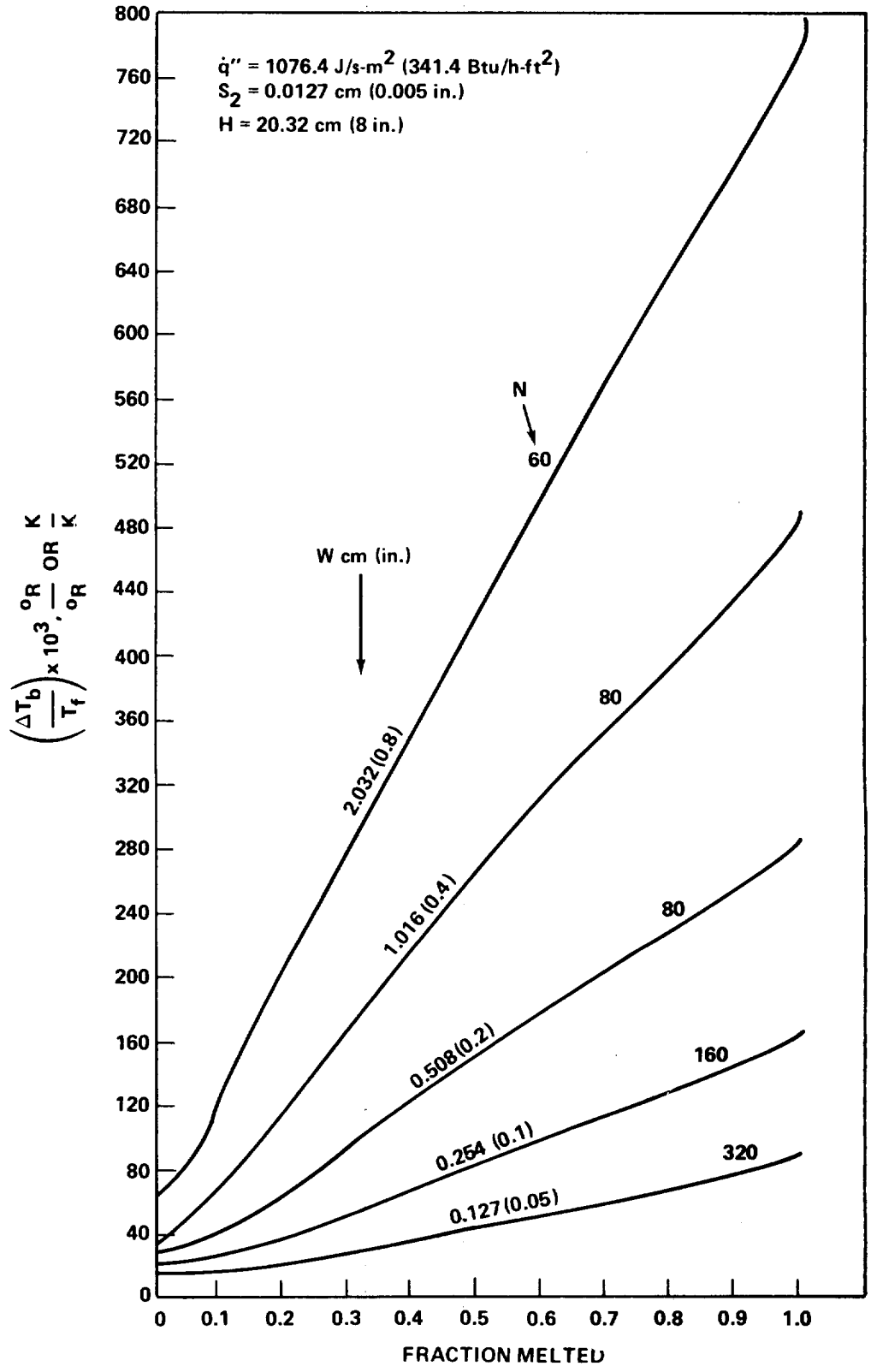

Figure 75. Transient base temperature rise versus fraction of PCM melted for H = 20.32 cm (8 in.) and S_2 = 0.0127 cm (0.005 in.).

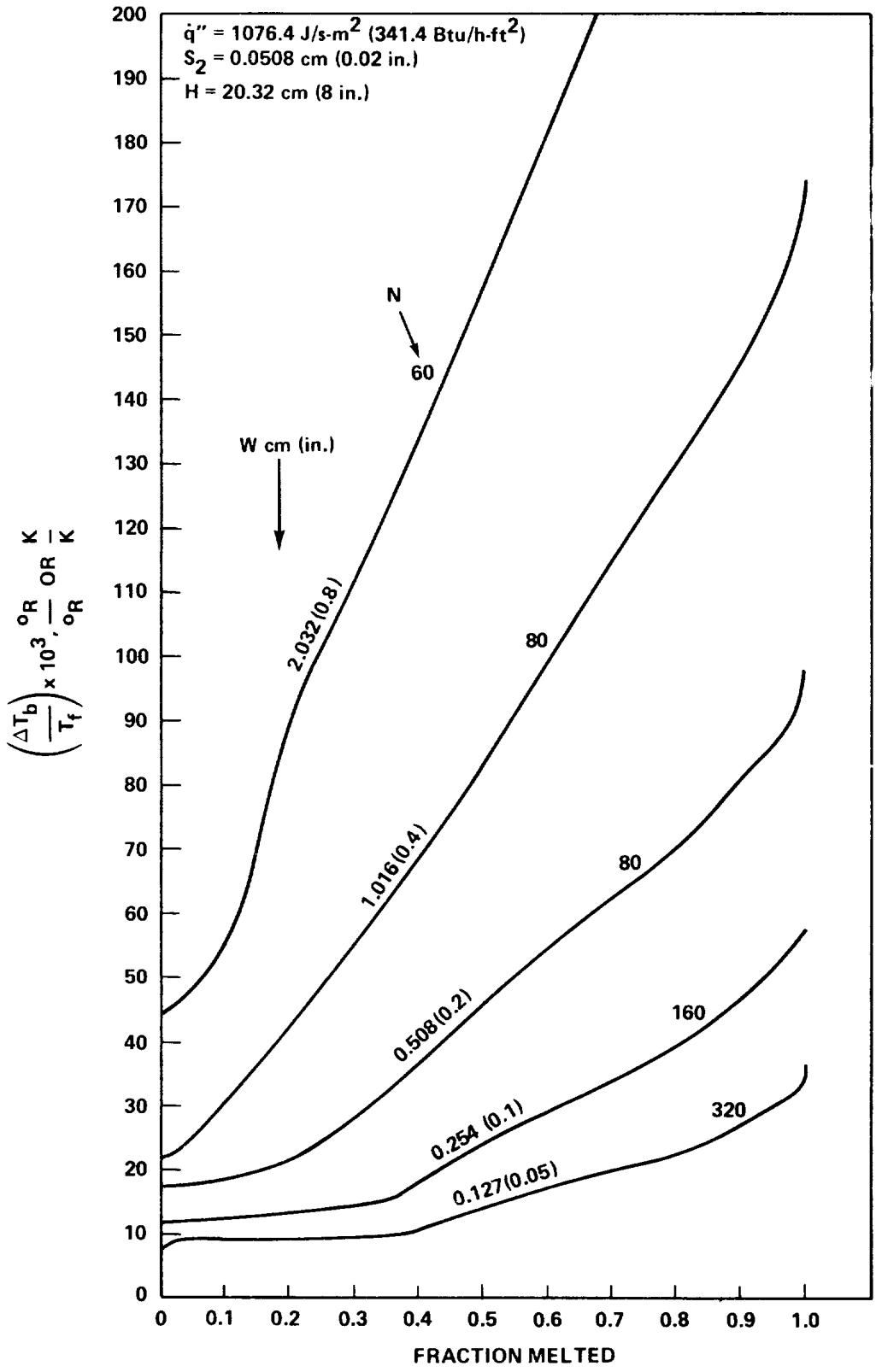

Figure 76. Transient base temperature rise versus fraction of PCM melted for H = 20.32 cm (8 in.) and S_2 = 0.0508 cm (0.02 in.).

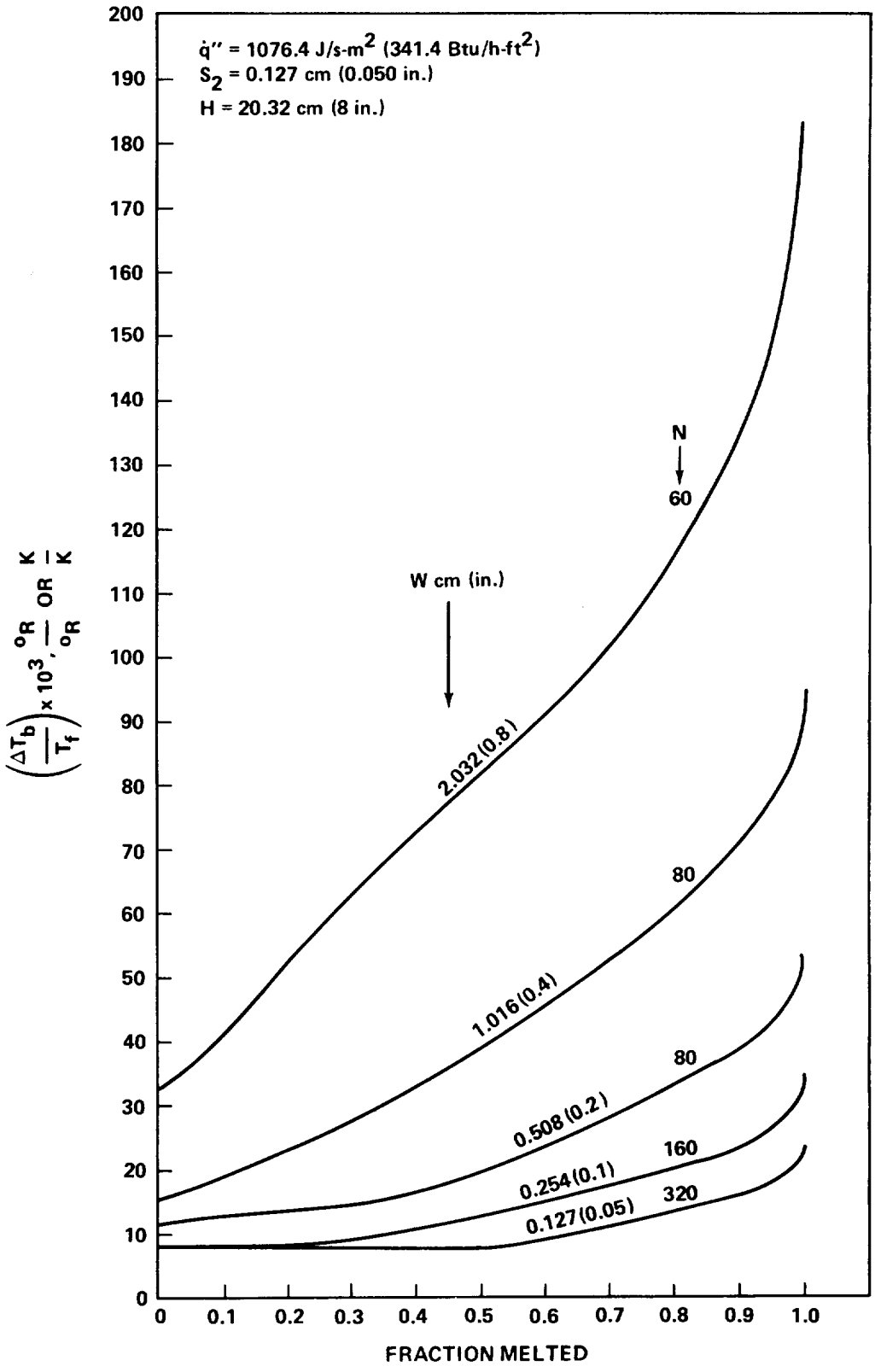

Figure 77. Transient base temperature rise versus fraction of PCM melted for H = 20.32 cm (8 in.) and S_2 = 0.127 cm (0.05 in.).

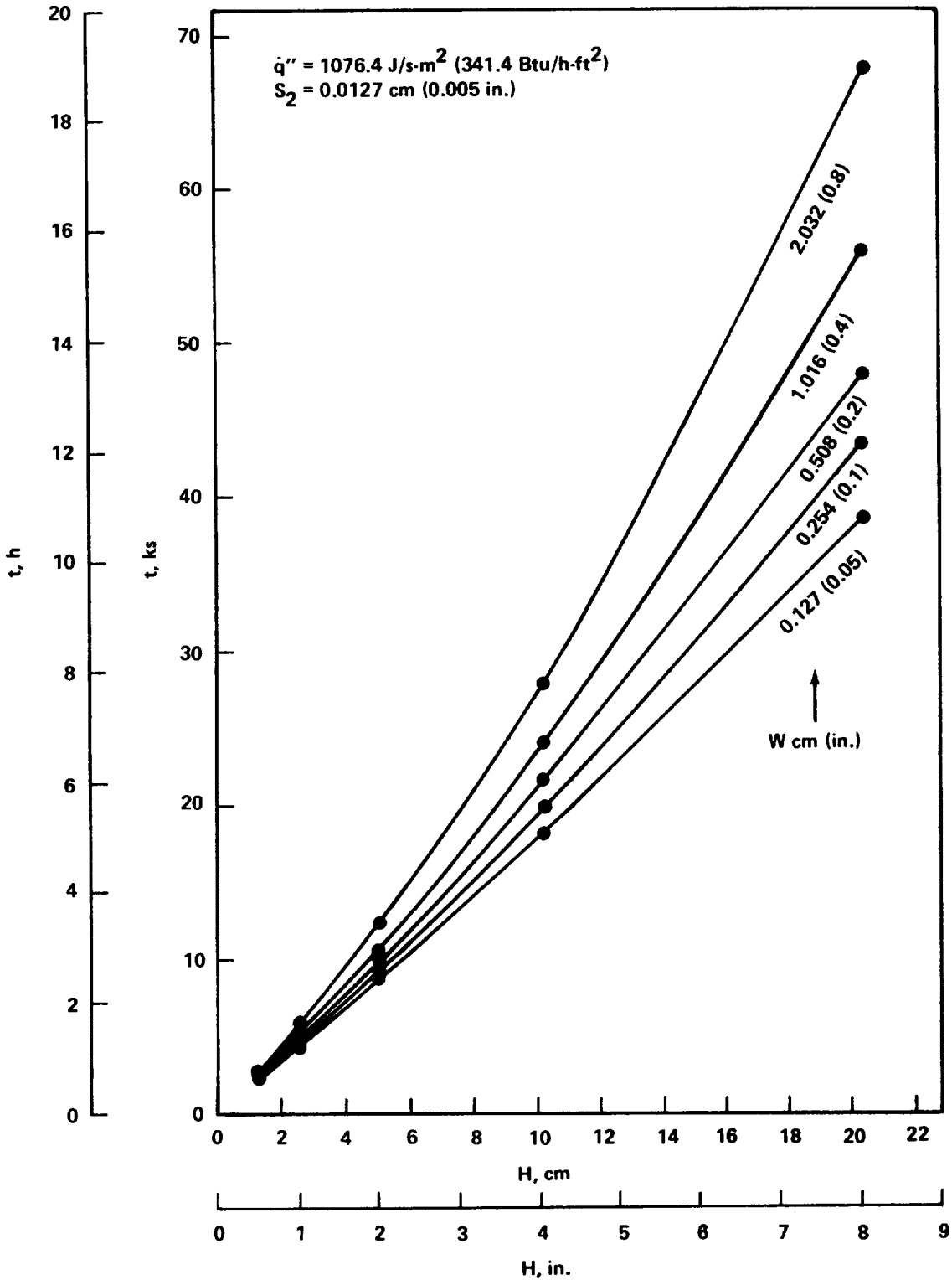

Figure 78. Time required for PCM to melt for $\dot{q}''$ = 1076.4 J/s-m^2 (341.4 Btu/h-ft^2) and S_2 = 0.0127 cm (0.005 in.).

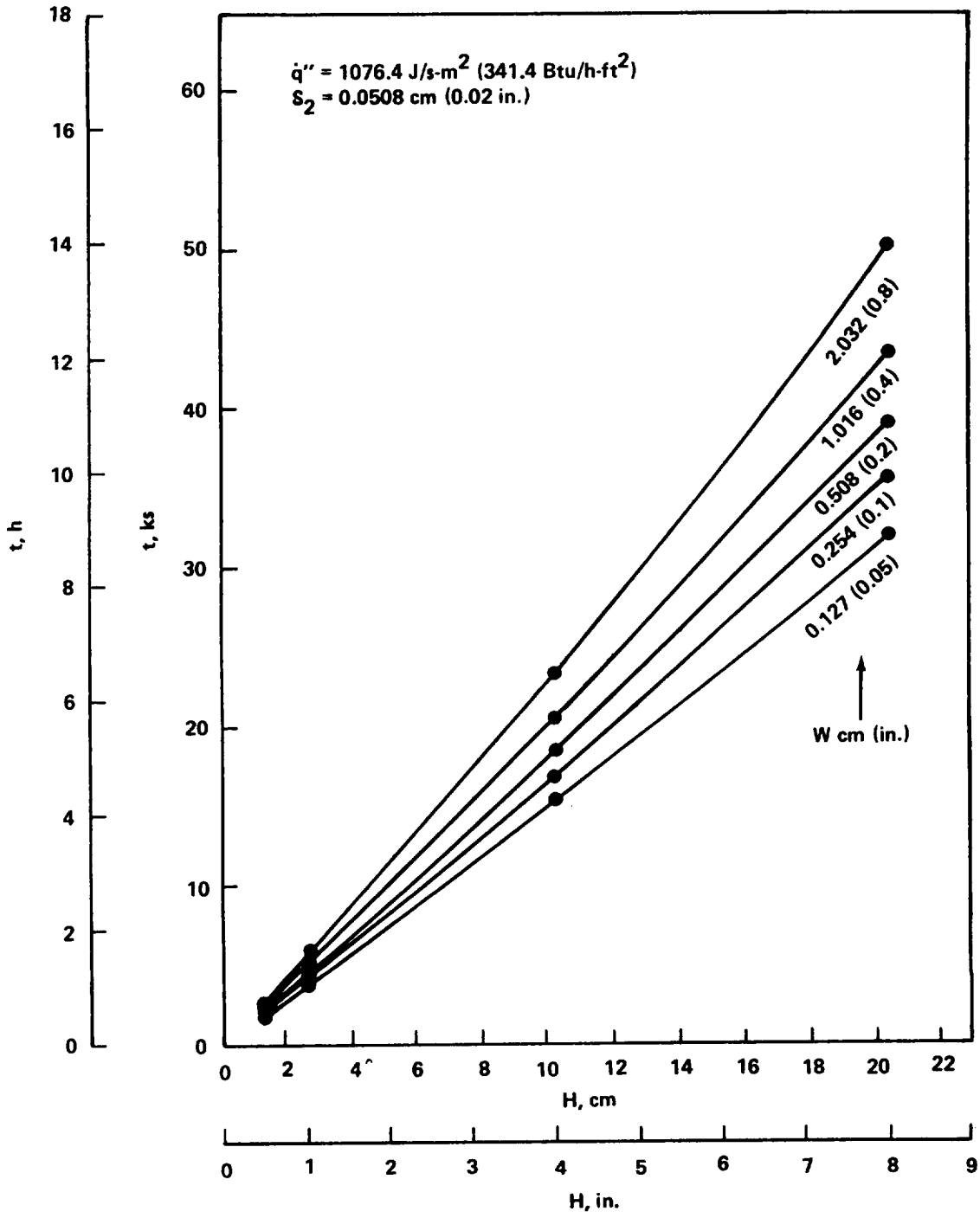

Figure 79. Time required for PCM to melt for $\dot{q}'' = 1076.4$ J/s-m^2 (341.4 Btu/h-ft^2) and $S_2 = 0.0508$ cm (0.02 in.).

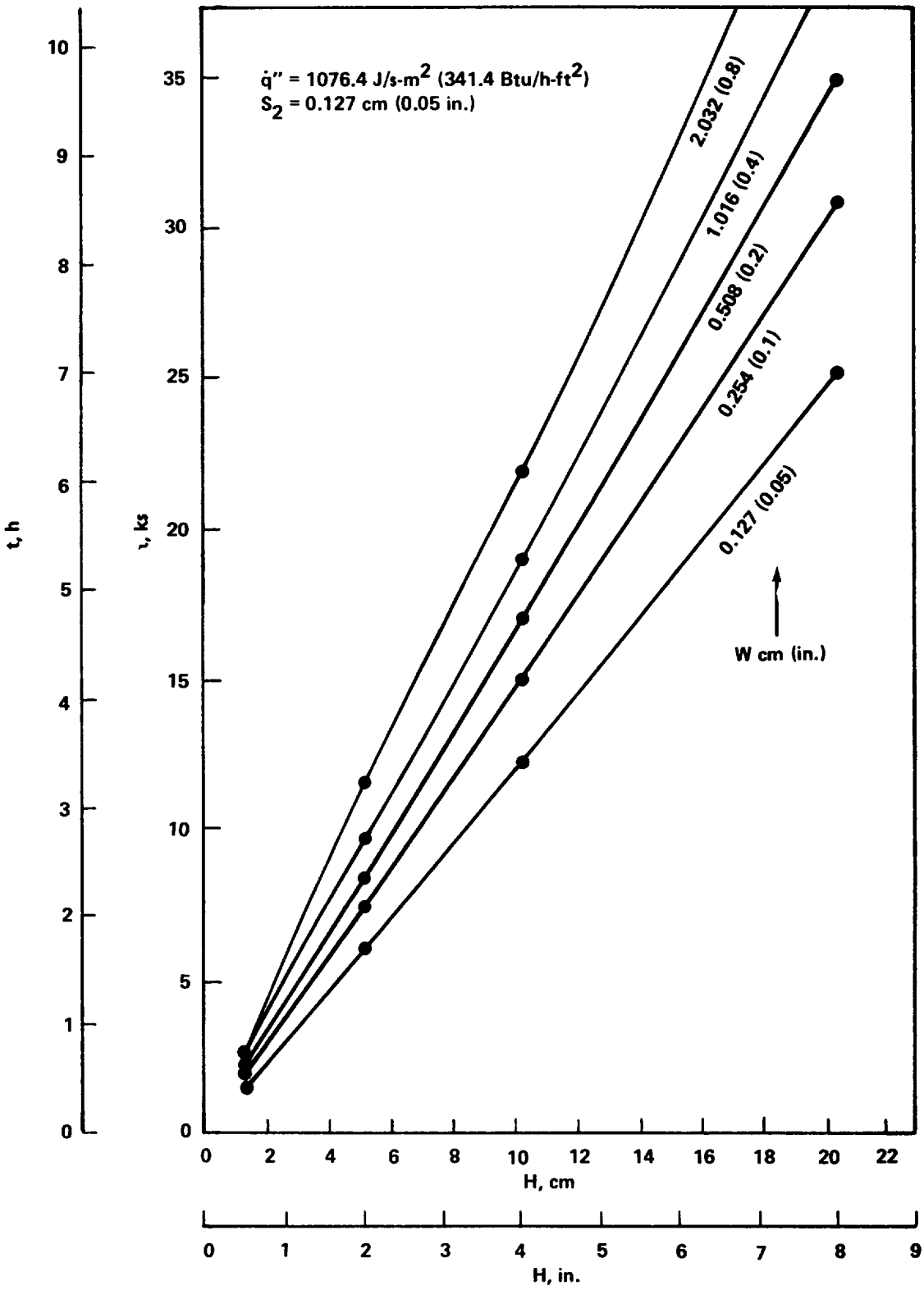

Figure 80. Time required for PCM to melt for $\dot{q}'' = 1076.4$ J/s-m^2 (341.4 Btu/h-ft^2) and $S_2 = 0.127$ cm (0.05 in.).

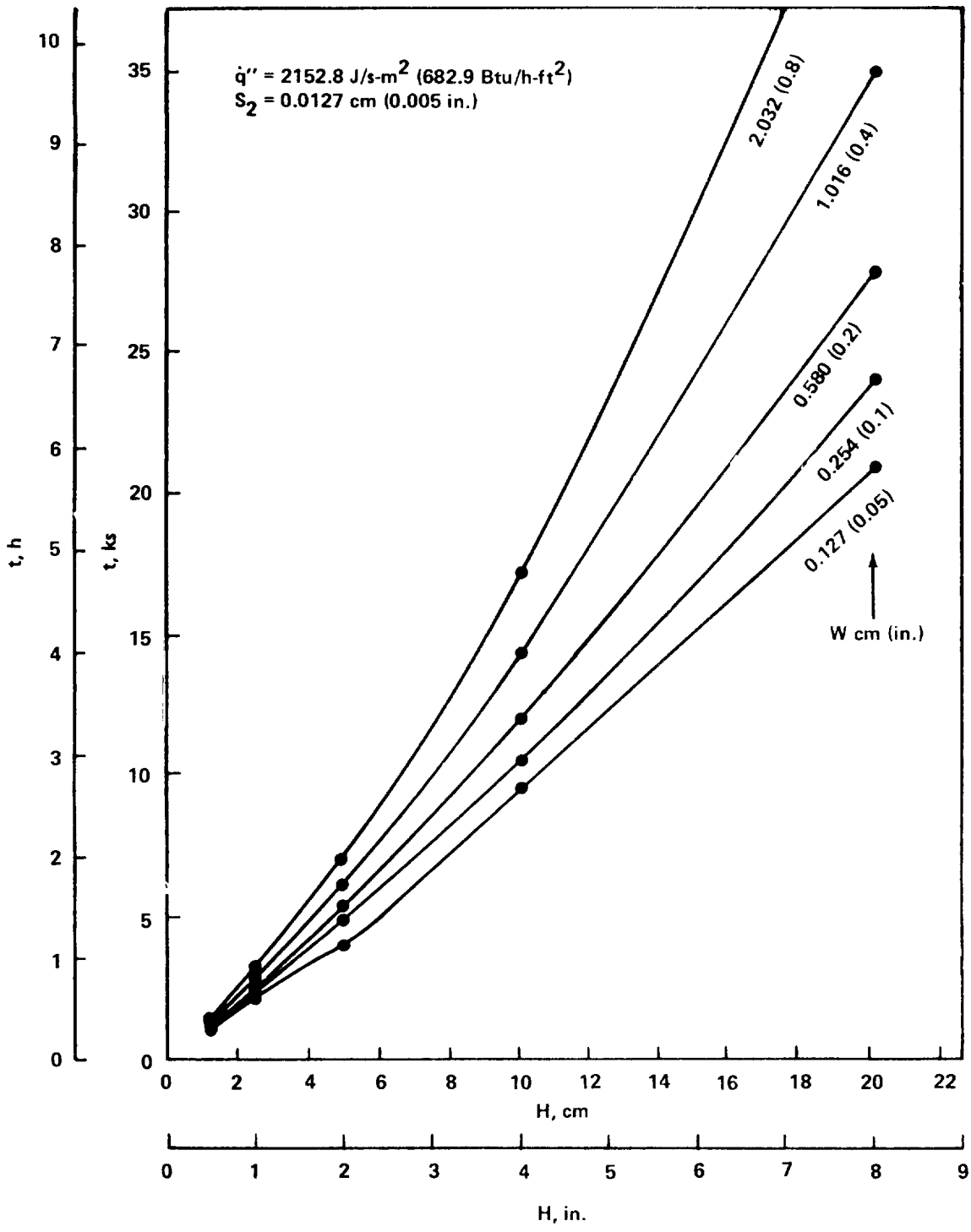

Figure 81. Time required for PCM to melt for $\dot{q}''$ = 2152.8 J/s-m^2 (682.9 Btu/h-ft^2) and S_2 = 0.0127 cm (0.005 in.).

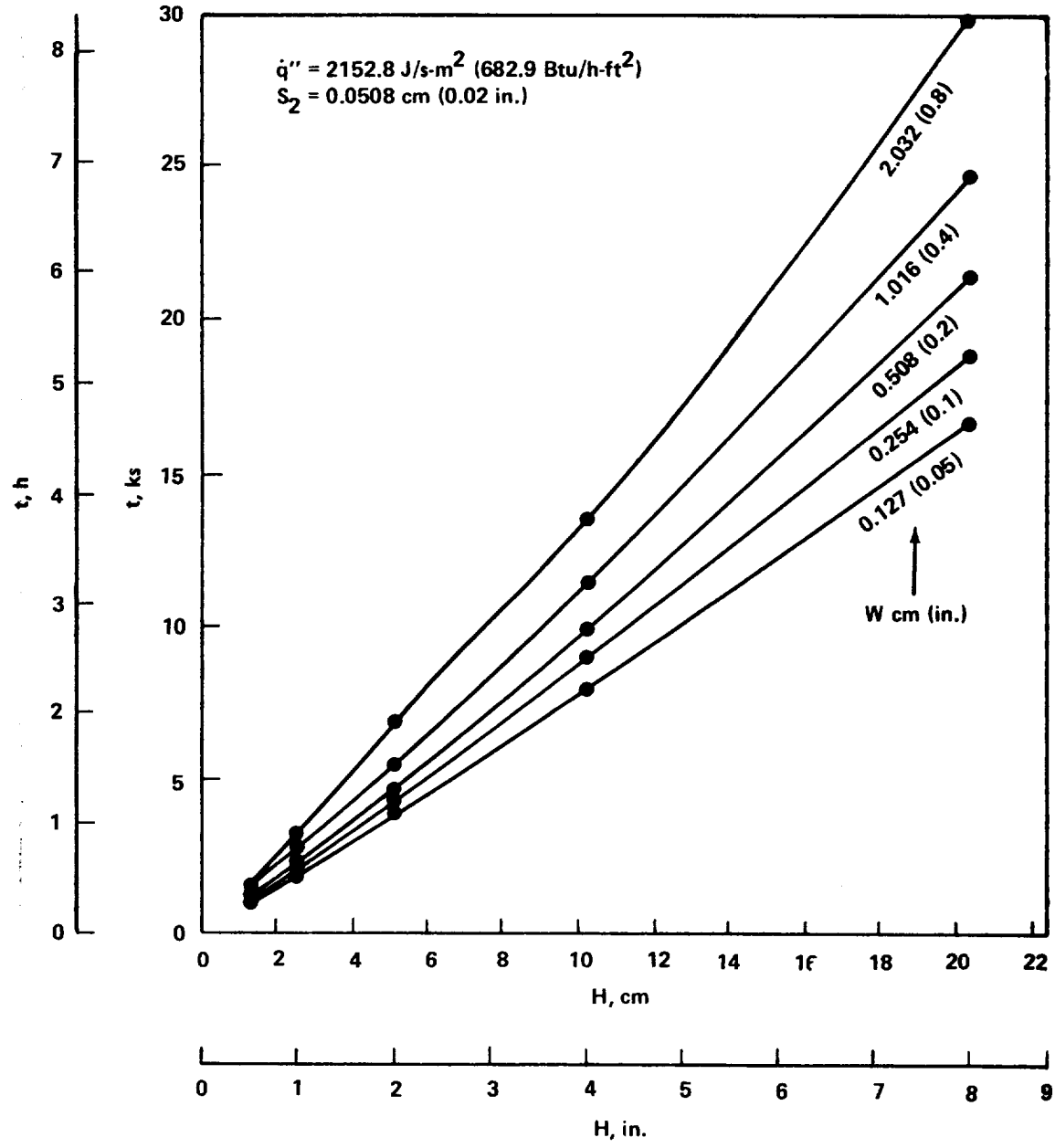

Figure 82. Time required for PCM to melt for $\dot{q}'' = 2152.8$ J/s-m^2 (682.9 Btu/h-ft^2) and $S_2 = 0.0508$ cm (0.02 in.).

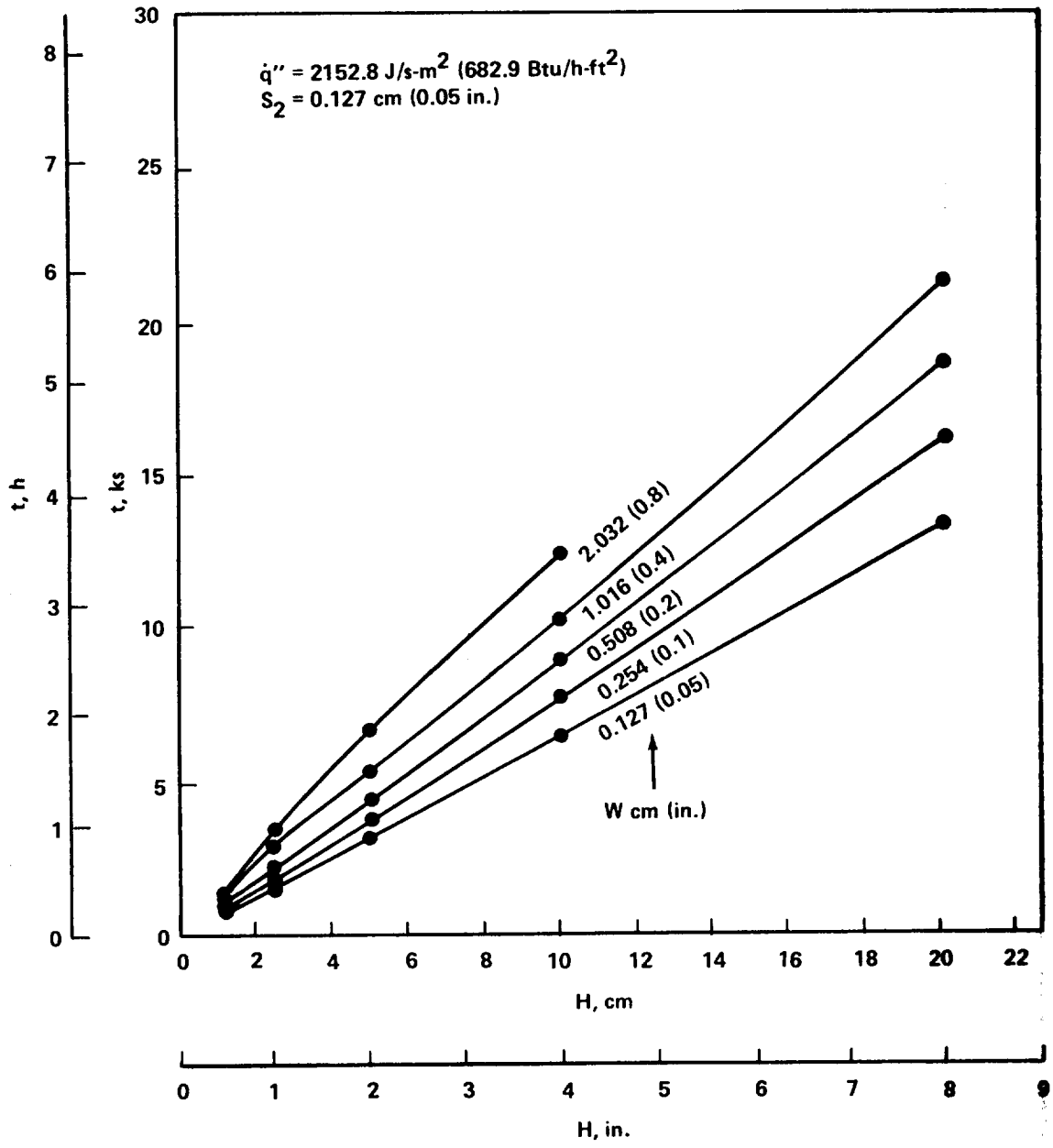

Figure 83. Time required for PCM to melt for $\dot{q}'' = 2152.8$ J/s-m^2 (682.9 Btu/h-ft^2) and $S_2 = 0.127$ cm (0.05 in.).

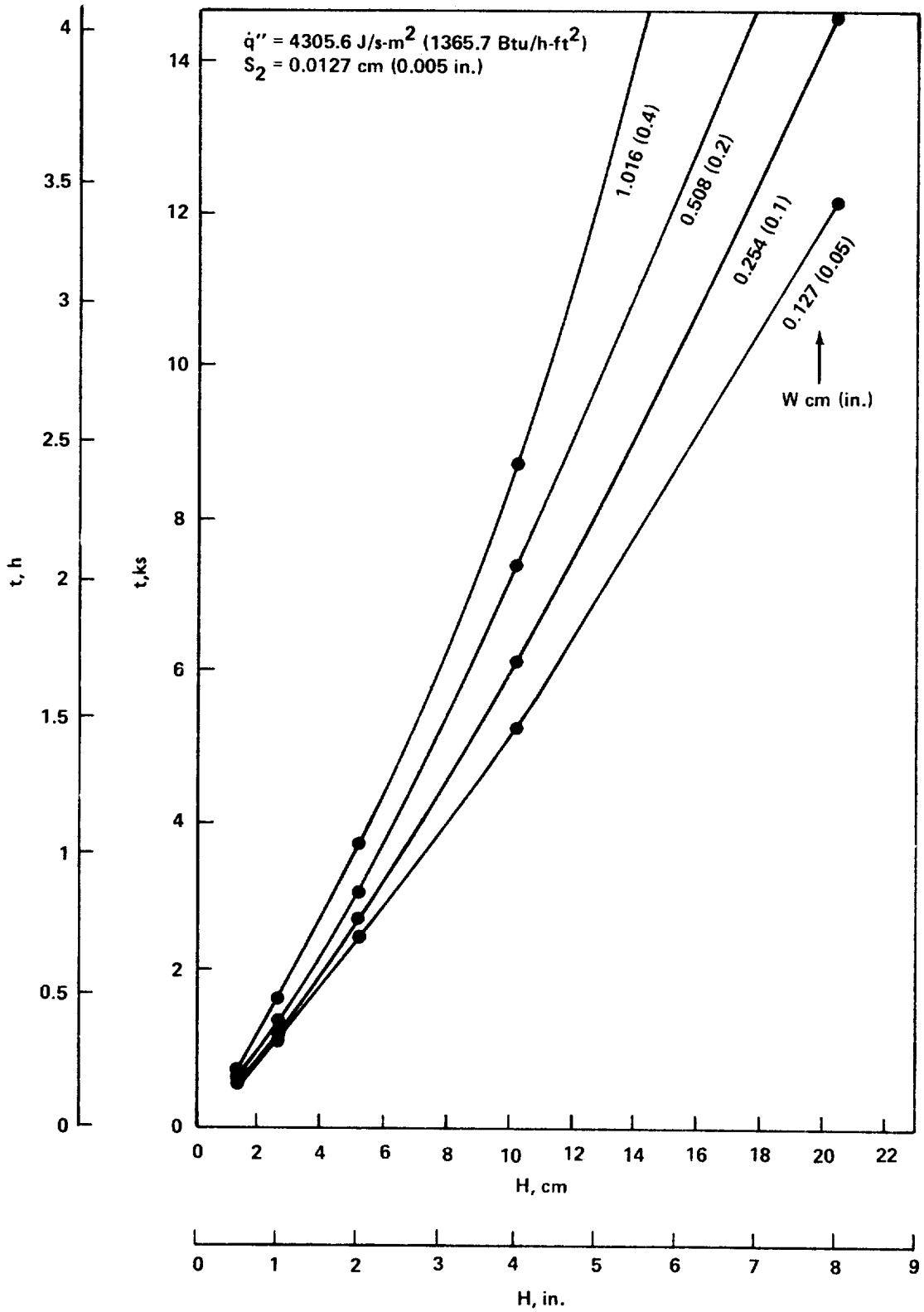

Figure 84. Time required for PCM to melt for $\dot{q}'' = 4305.6$ J/s-m^2 (1365.7 Btu/h-ft^2) and $S_2 = 0.0127$ cm (0.005 in.).

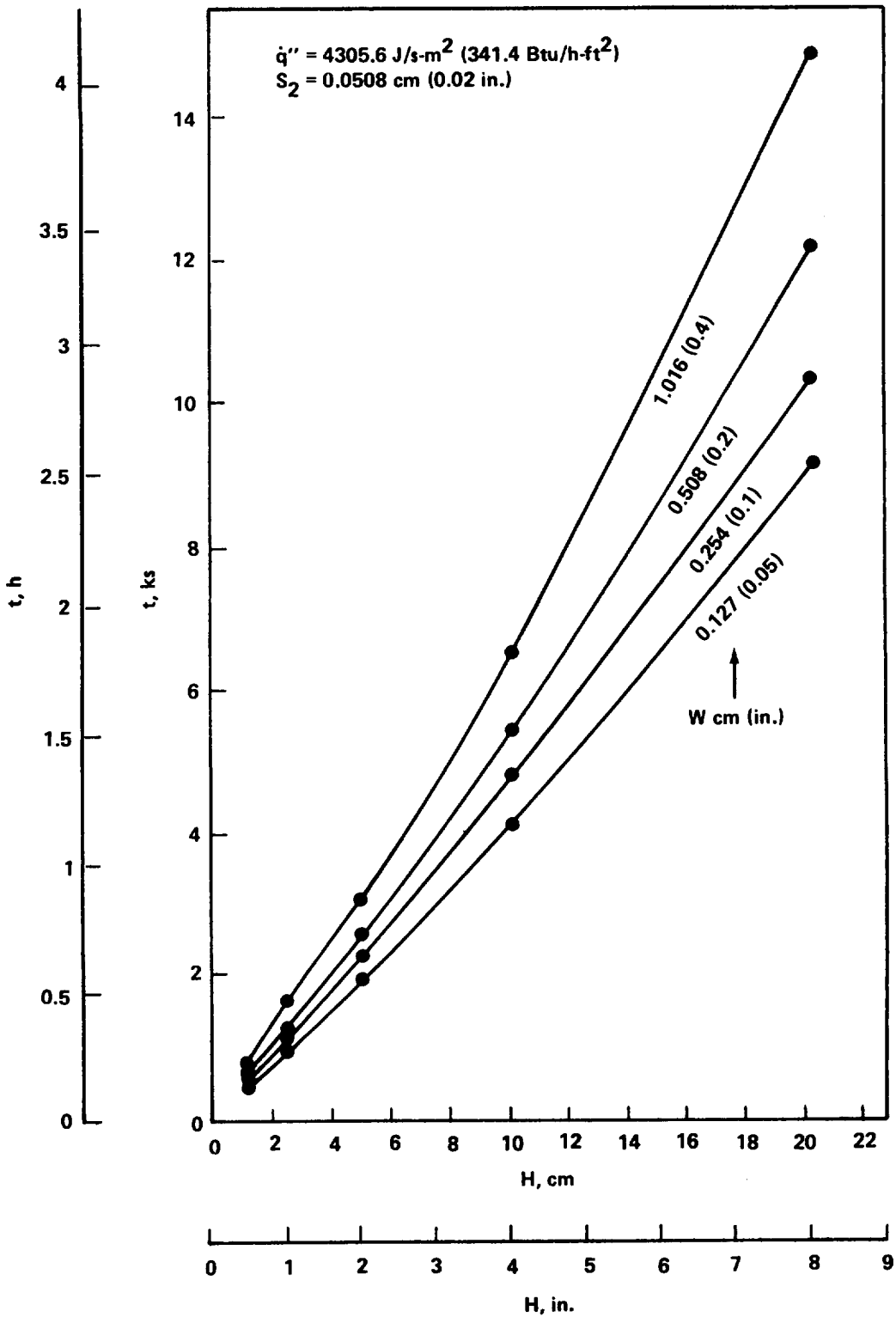

Figure 85. Time required for PCM to melt for $\dot{q}'' = 4305.6$ J/s-m^2 (341.4 Btu/h-ft^2) and $S_2 = 0.0508$ cm (0.02 in.).

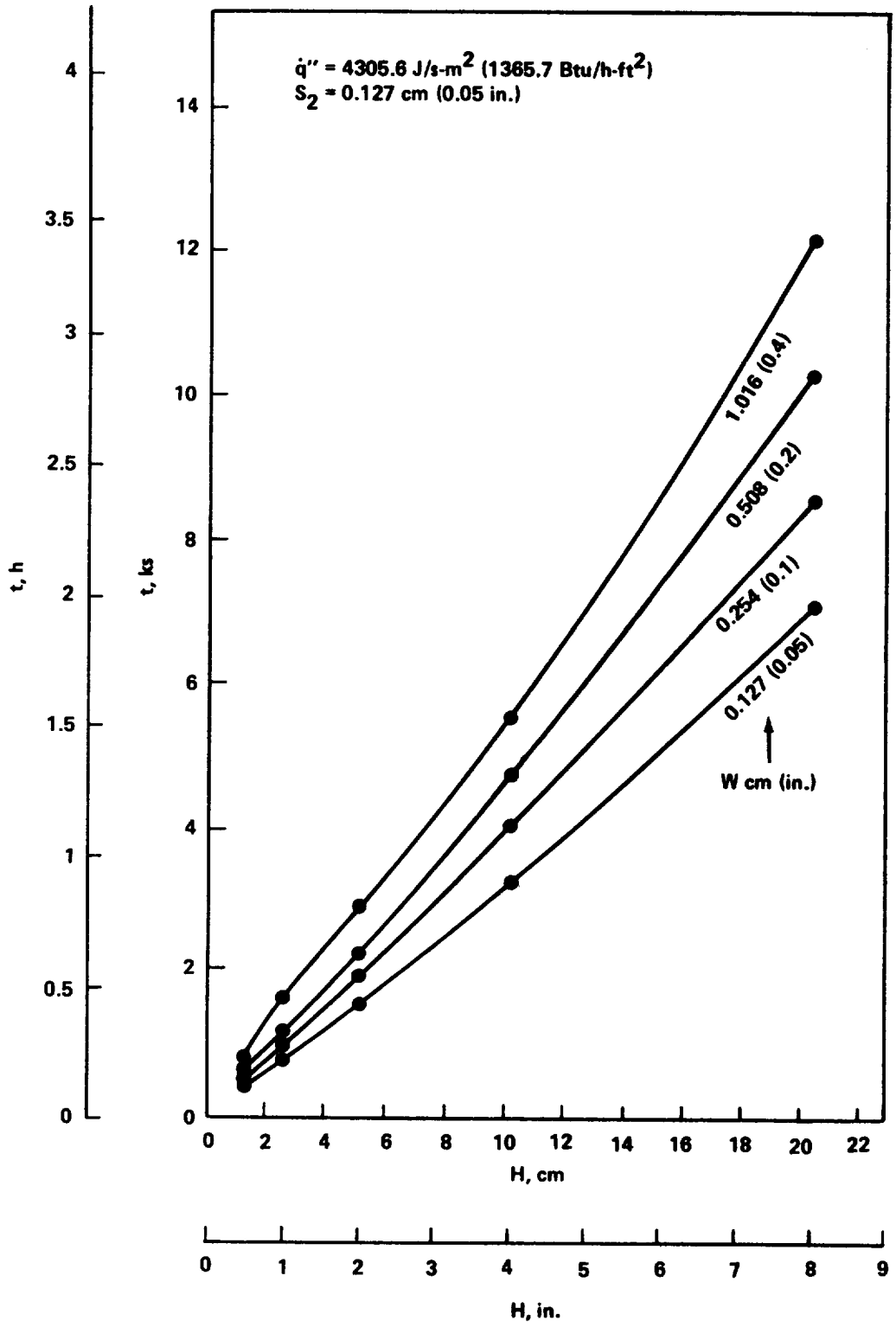

Figure 86. Time required for PCM to melt and $\dot{q}'' = 4305.6$ J/s-m^2 (1365.7 Btu/h-ft^2) and $S_2 = 0.127$ cm (0.05 in.).

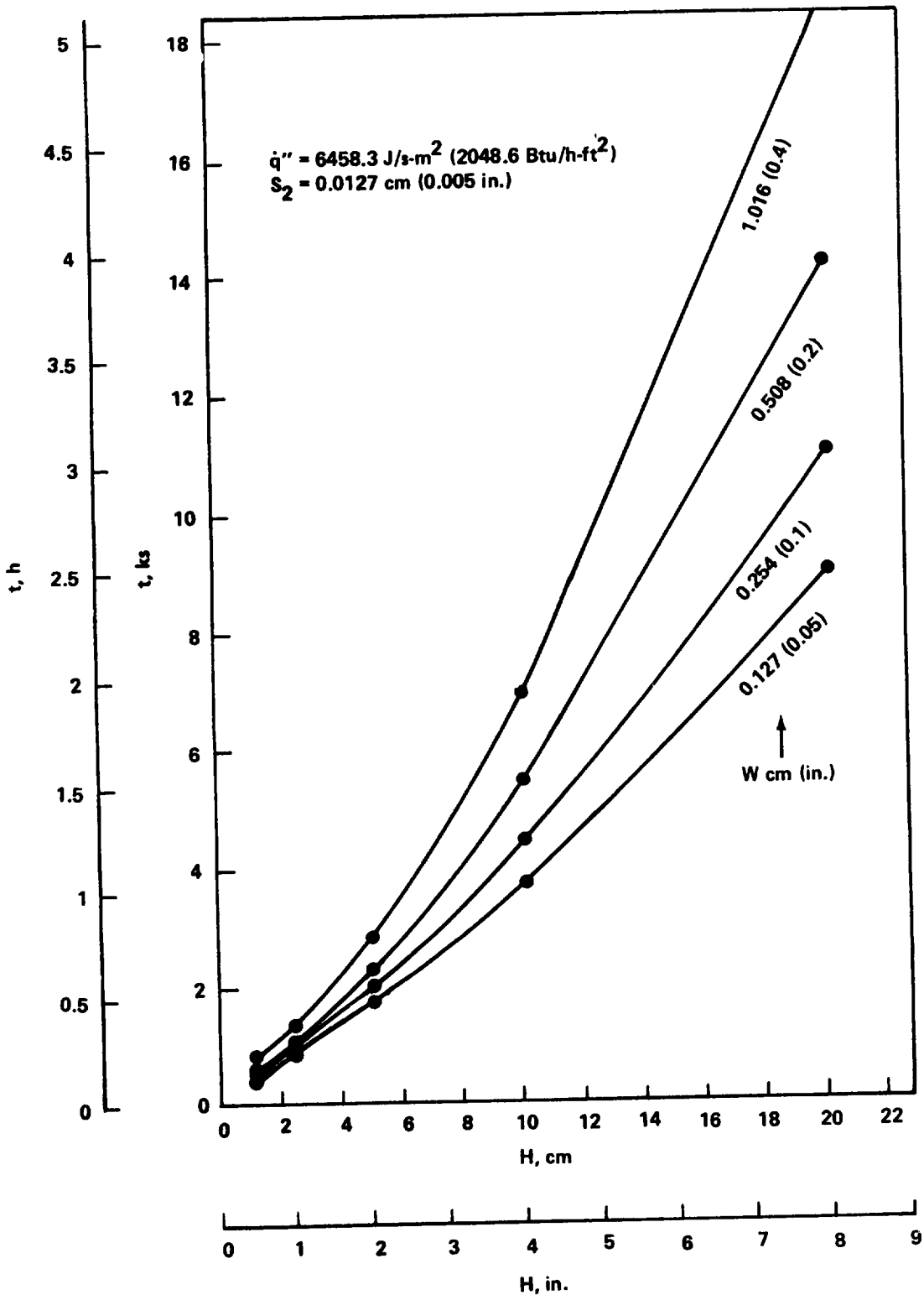

Figure 87. Time required for PCM to melt for $\dot{q}'' = 6458.3$ J/s-m^2 (2048.6 Btu/h-ft^2) and $S_2 = 0.0127$ cm (0.005 in.).

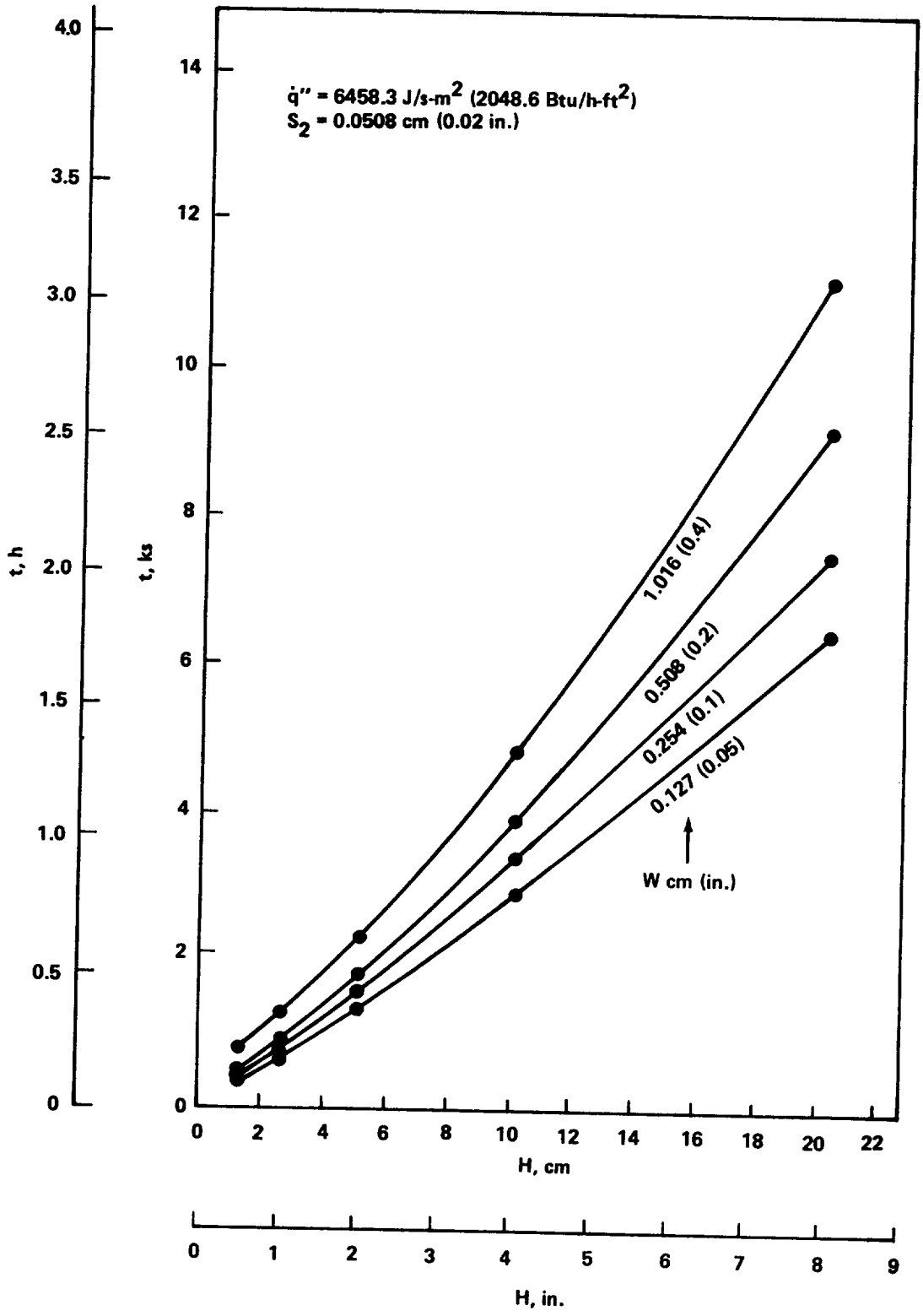

Figure 88. Time required for PCM to melt for $\dot{q}''$ = 6458.3 J/s-m^2 (2048.6 Btu/h-ft^2) and S_2 = 0.0508 cm (0.02 in.).

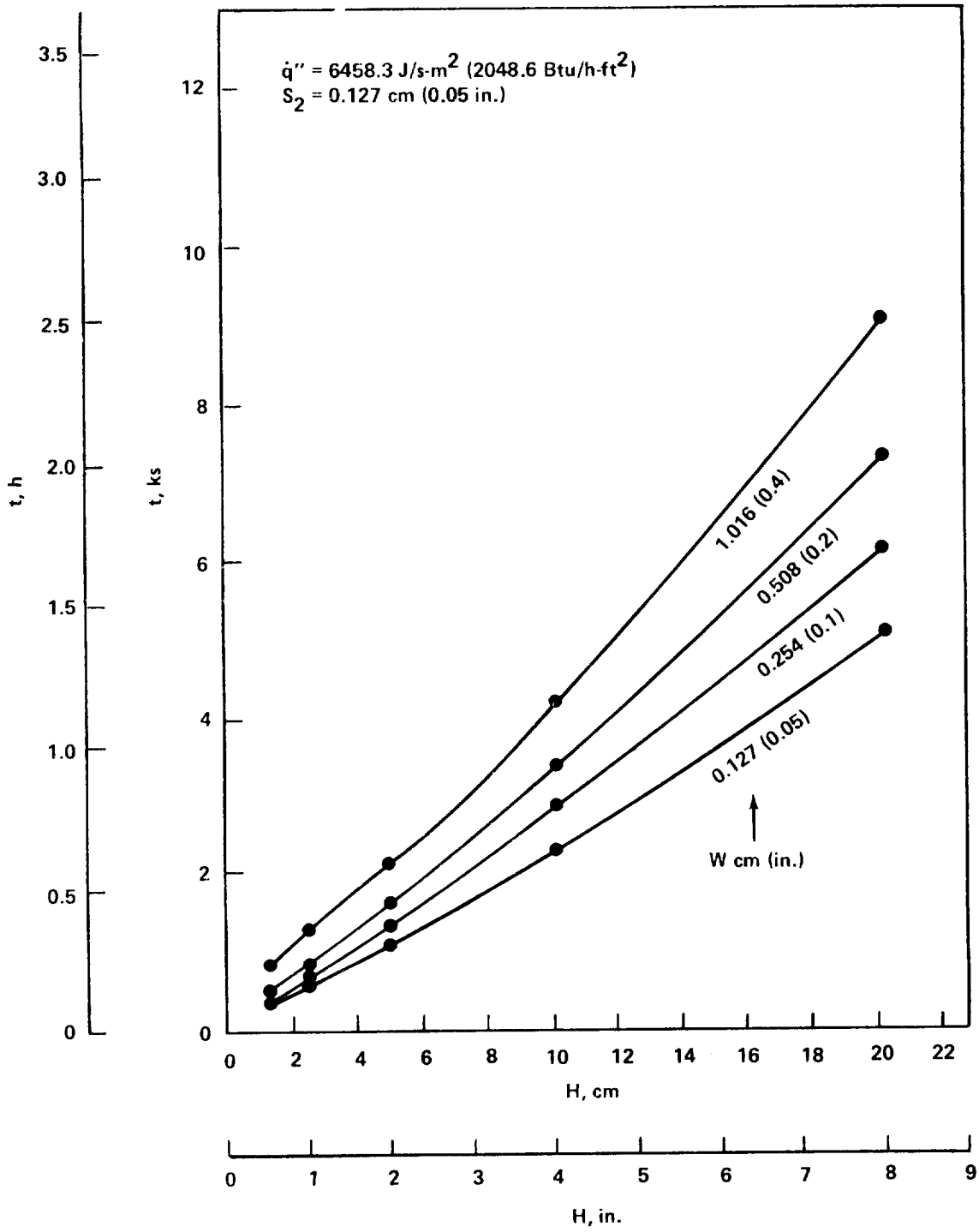

Figure 89. Time required for PCM to melt for $\dot{q}''$ = 6458.3 J/s-m^2 (2048.6 Btu/h-ft^2) and S_2 = 0.127 cm (0.05 in.).

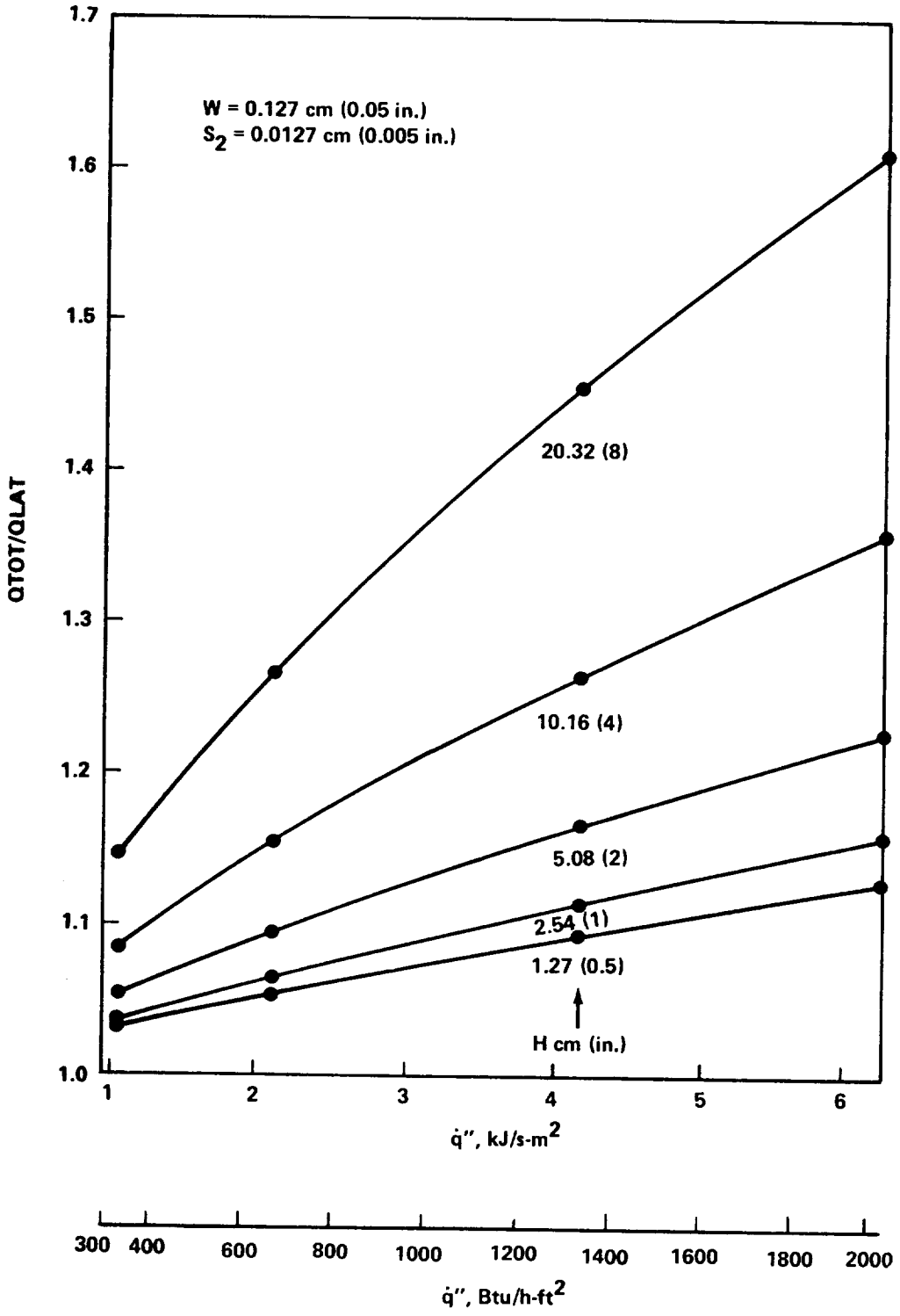

Figure 90. Energy ratio versus heat flux density for W = 0.127 cm (0.05 in.) and S_2 = 0.0127 cm (0.005 in.).

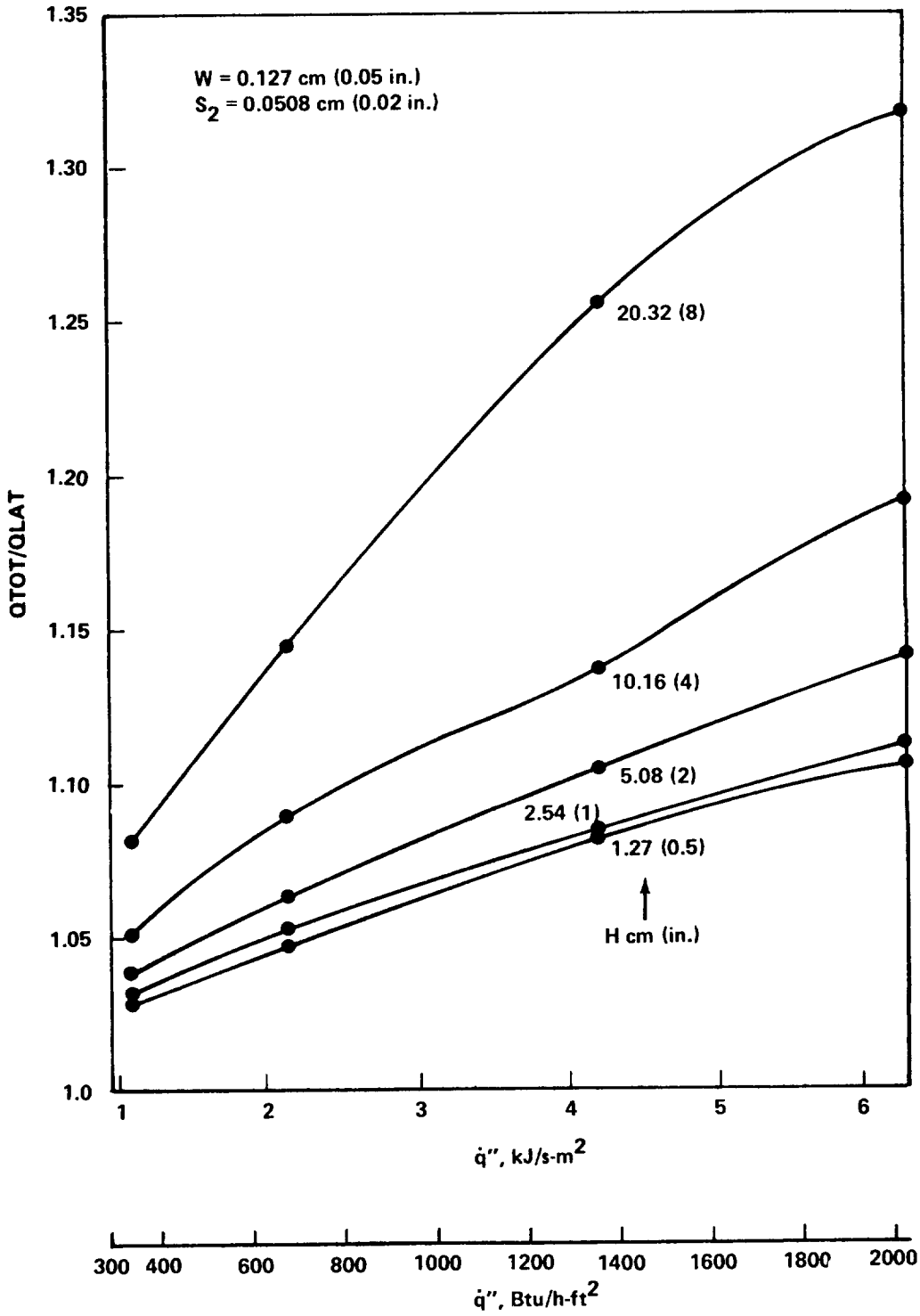

Figure 91. Energy ratio versus heat flux density for W = 0.127 cm (0.05 in.) and S_2 = 0.0508 cm (0.02 in.).

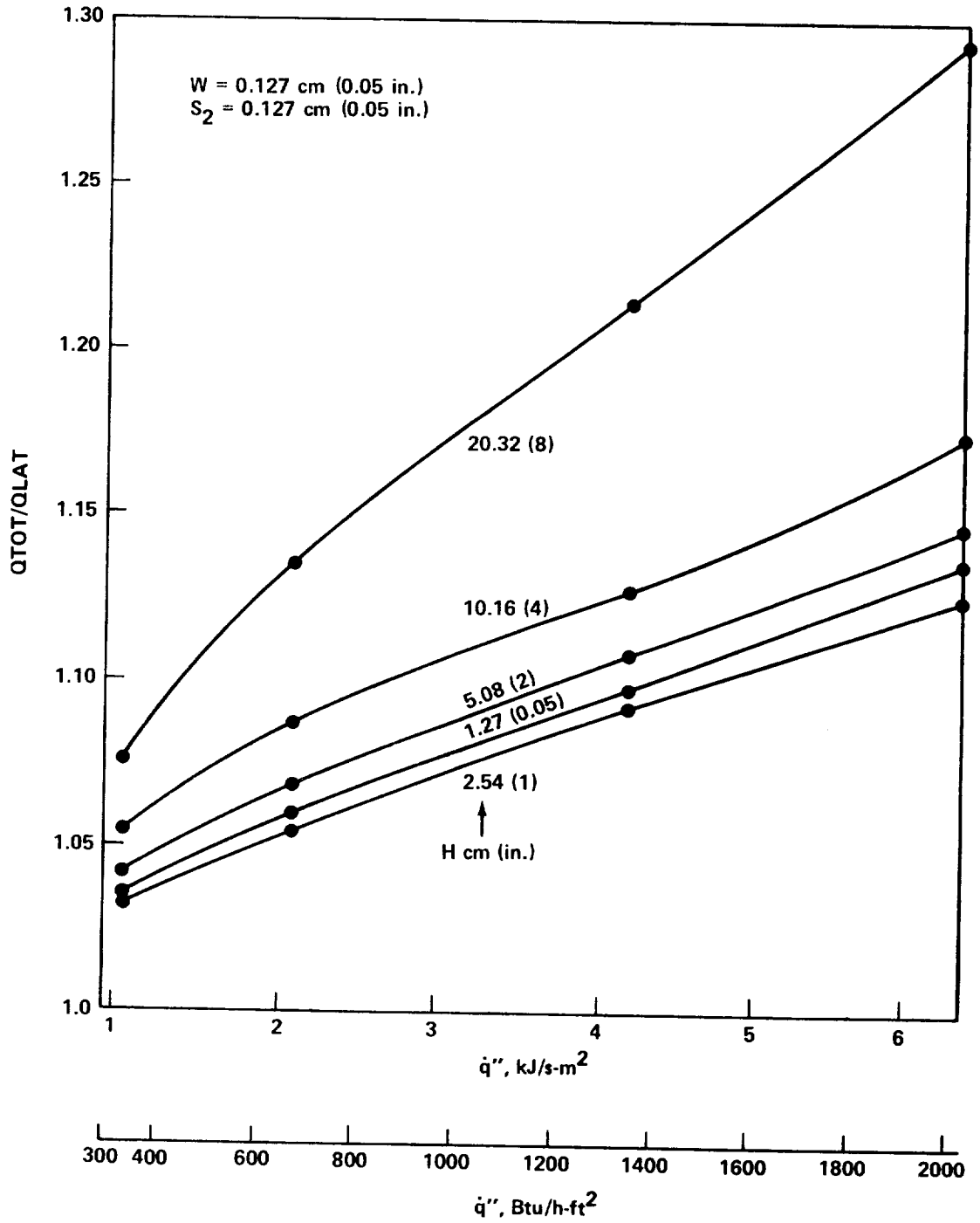

Figure 92. Energy ratio versus heat flux density for W = 0.127 cm (0.05 in.) and S_2 = 0.127 cm (0.05 in.).

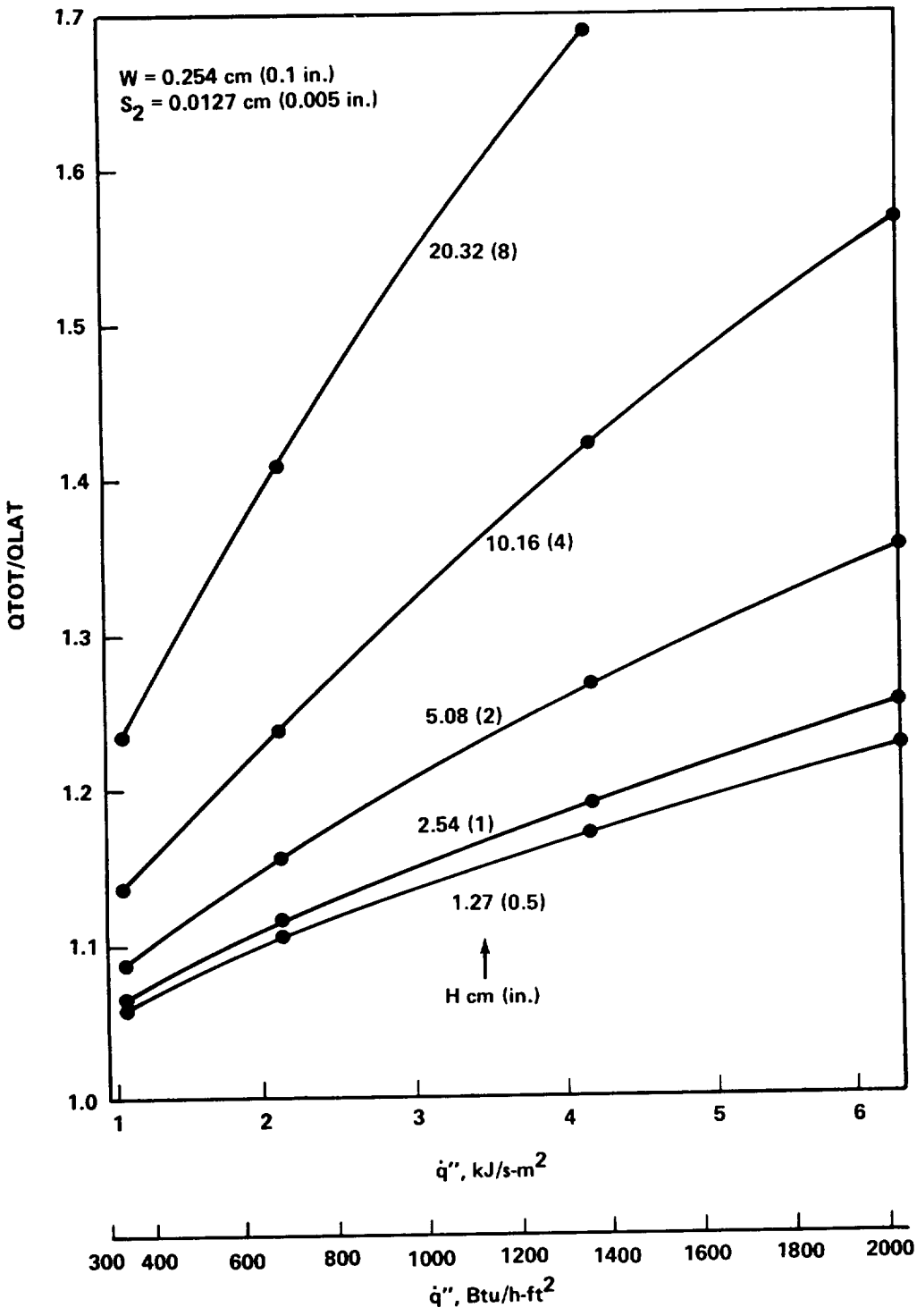

Figure 93. Energy ratio versus heat flux density for W = 0.254 cm (0.1 in.) and S_2 = 0.0127 cm (0.005 in.).

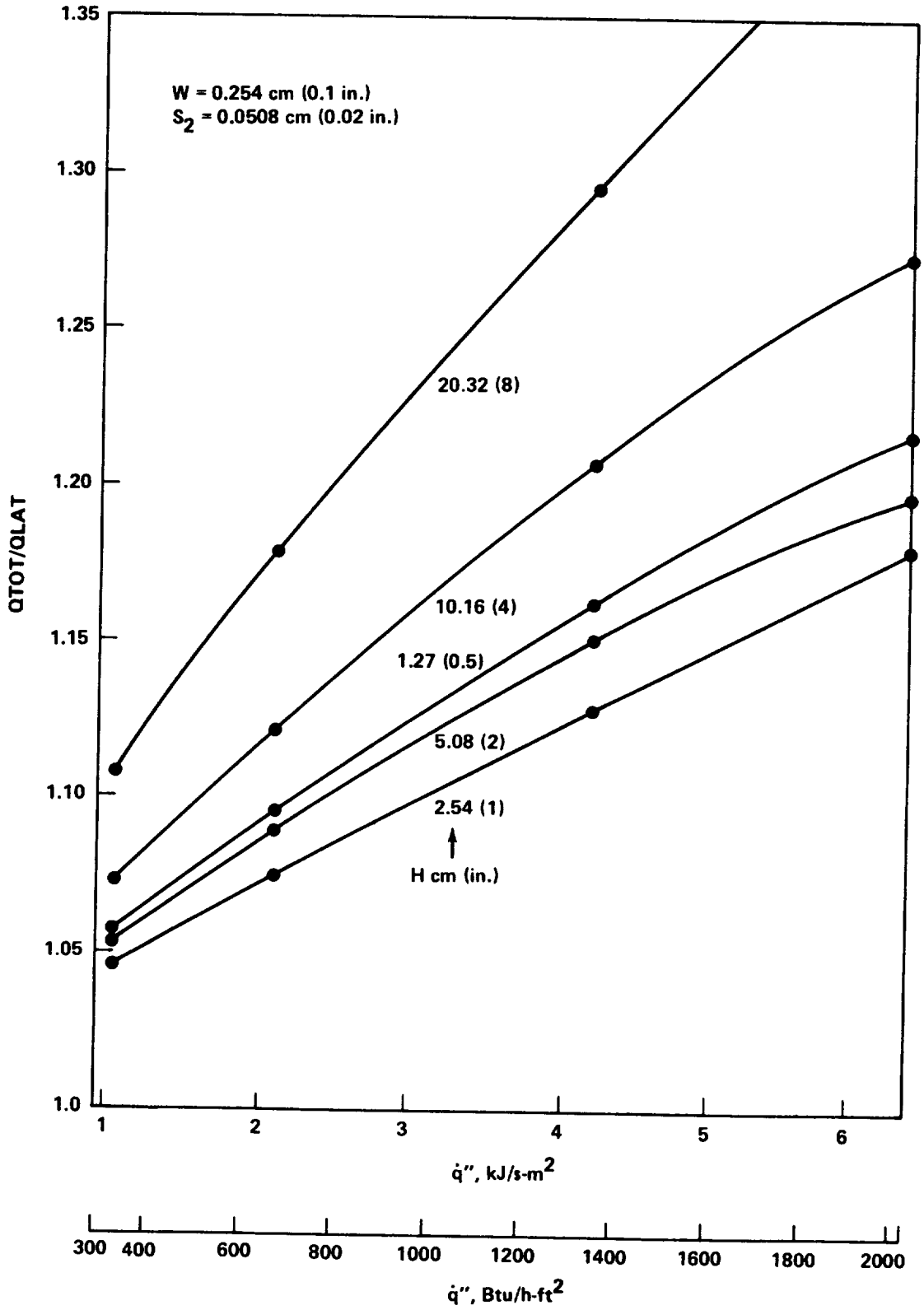

Figure 94. Energy ratio versus heat flux density for W = 0.254 cm (0.1 in.) and S_2 = 0.0508 cm (0.02 in.).

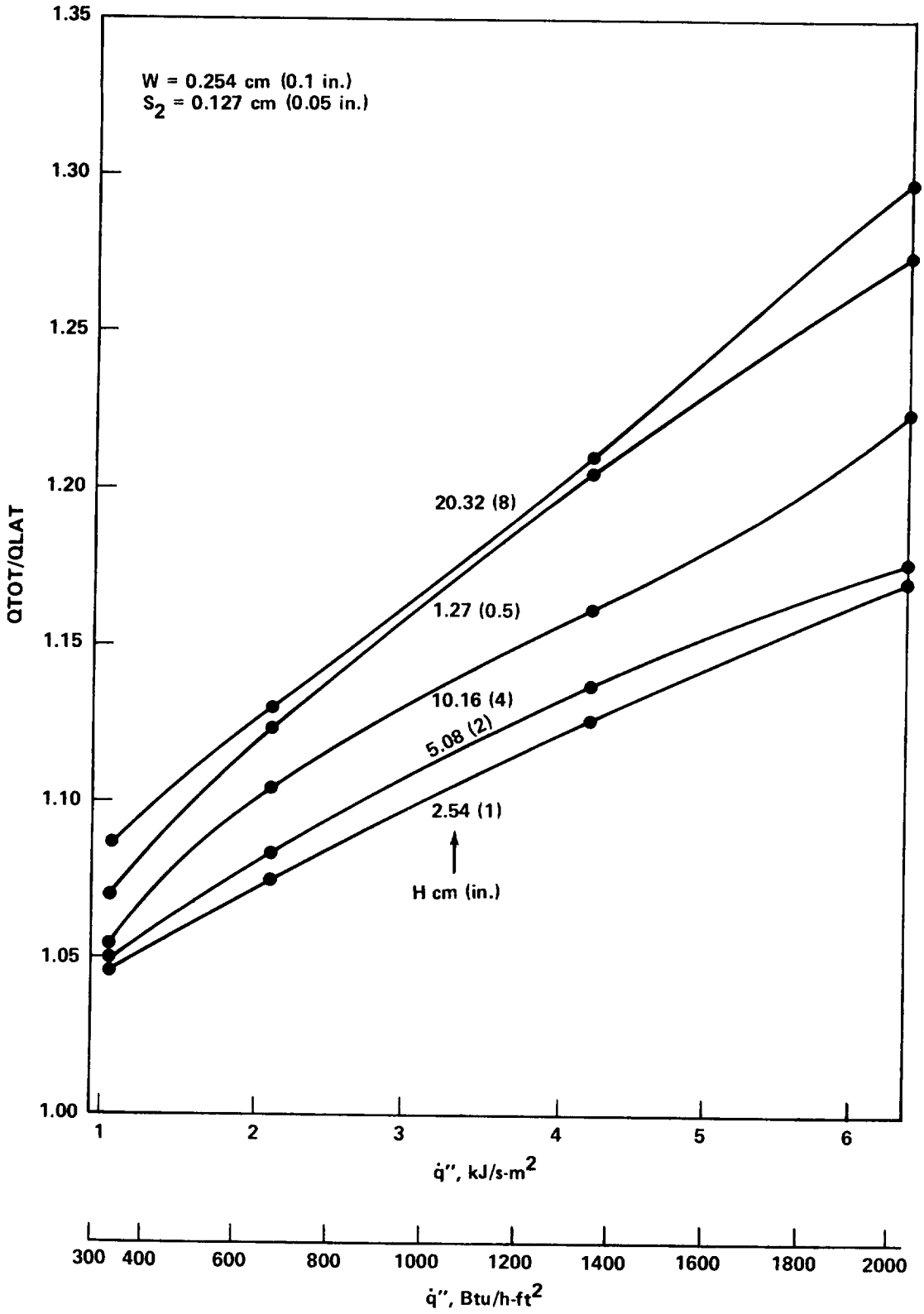

Figure 95. Energy ratio versus heat flux density for W = 0.254 cm (0.1 in.) and S_2 = 0.127 cm (0.05 in.).

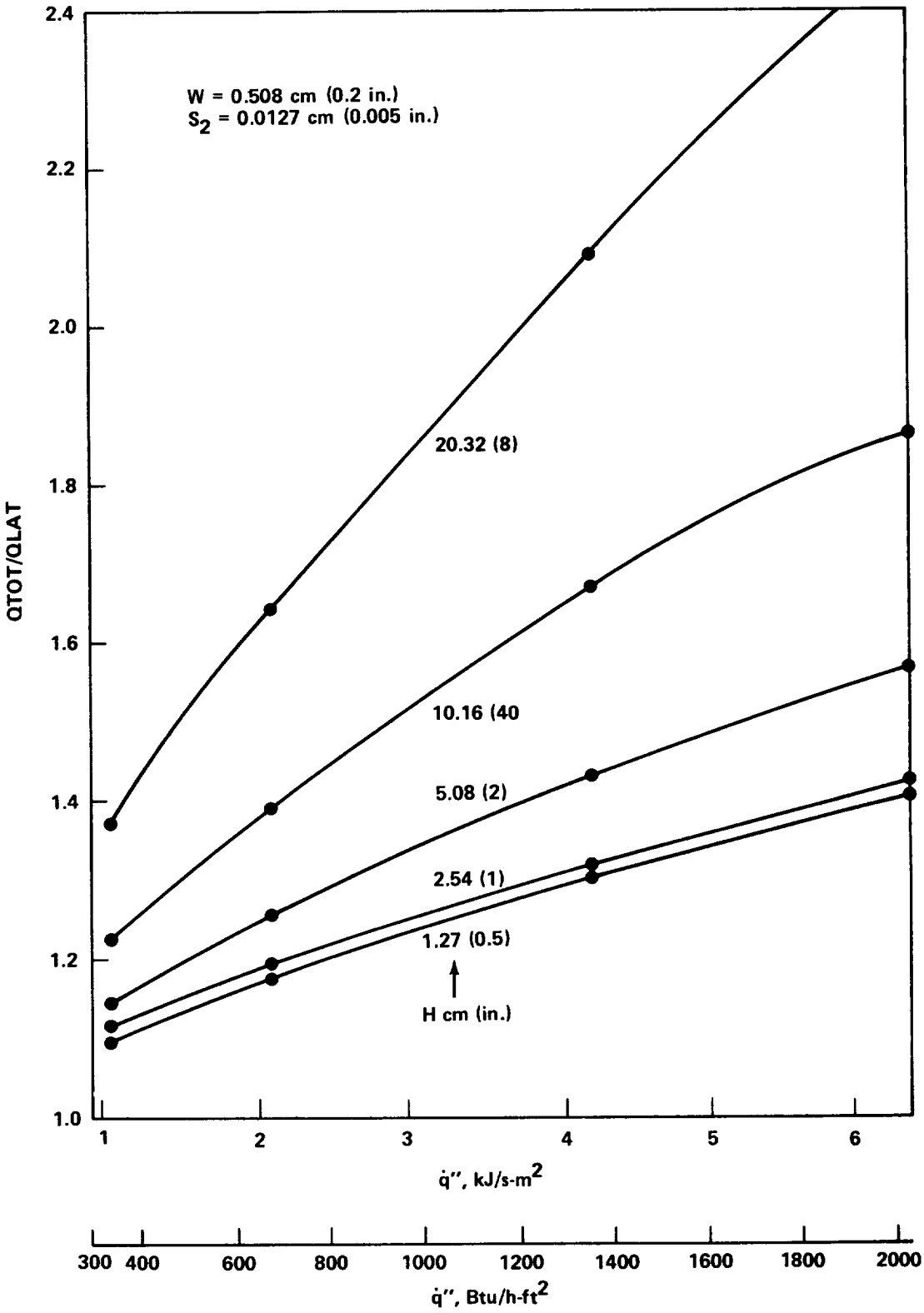

Figure 96. Energy ratio versus heat flux density for W = 0.508 cm (0.2 in.) and S_2 = 0.0127 cm (0.005 in.).

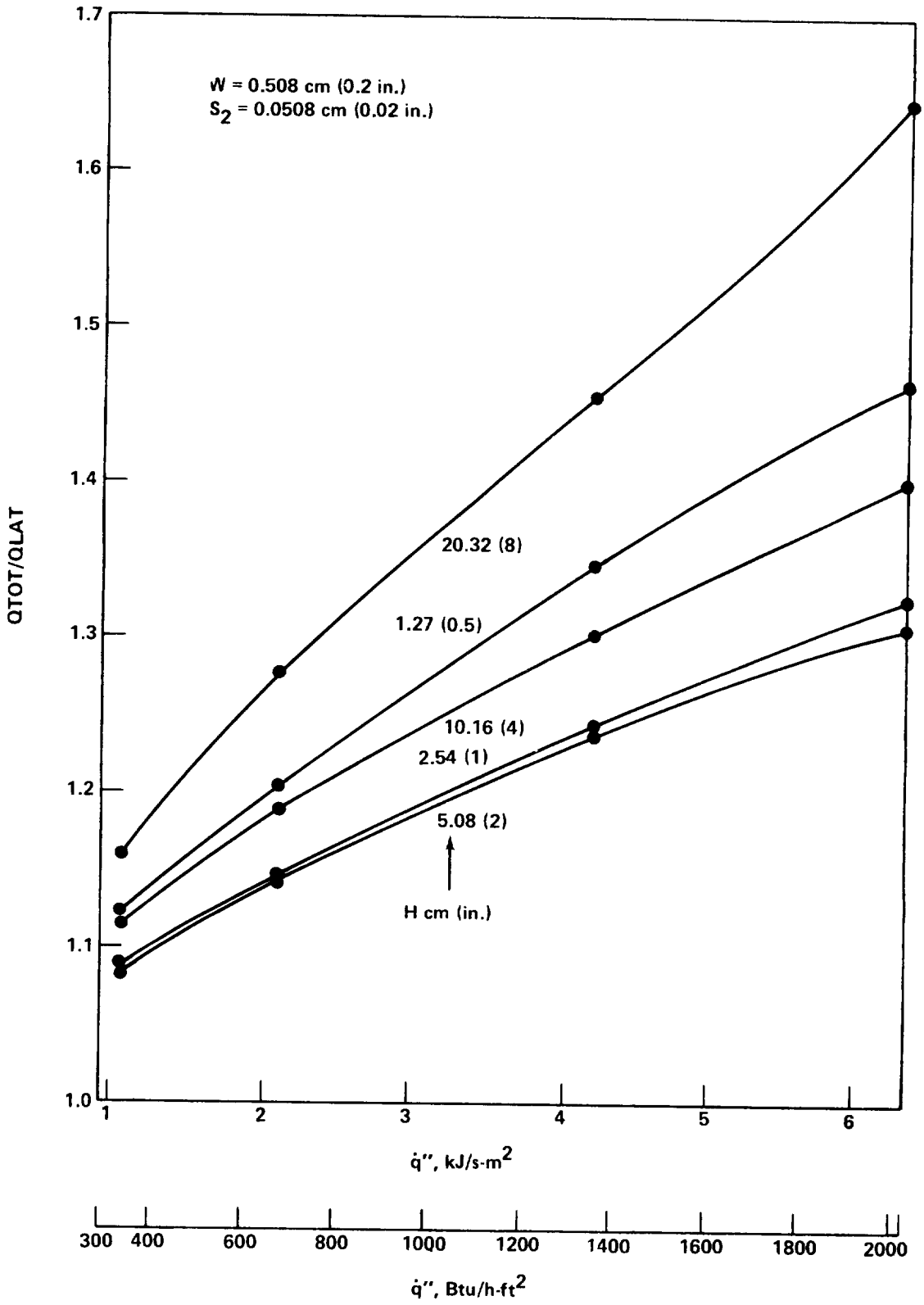

Figure 97. Energy ratio versus heat flux density for W = 0.508 cm (0.2 in.) and S_2 = 0.0508 cm (0.02 in.).

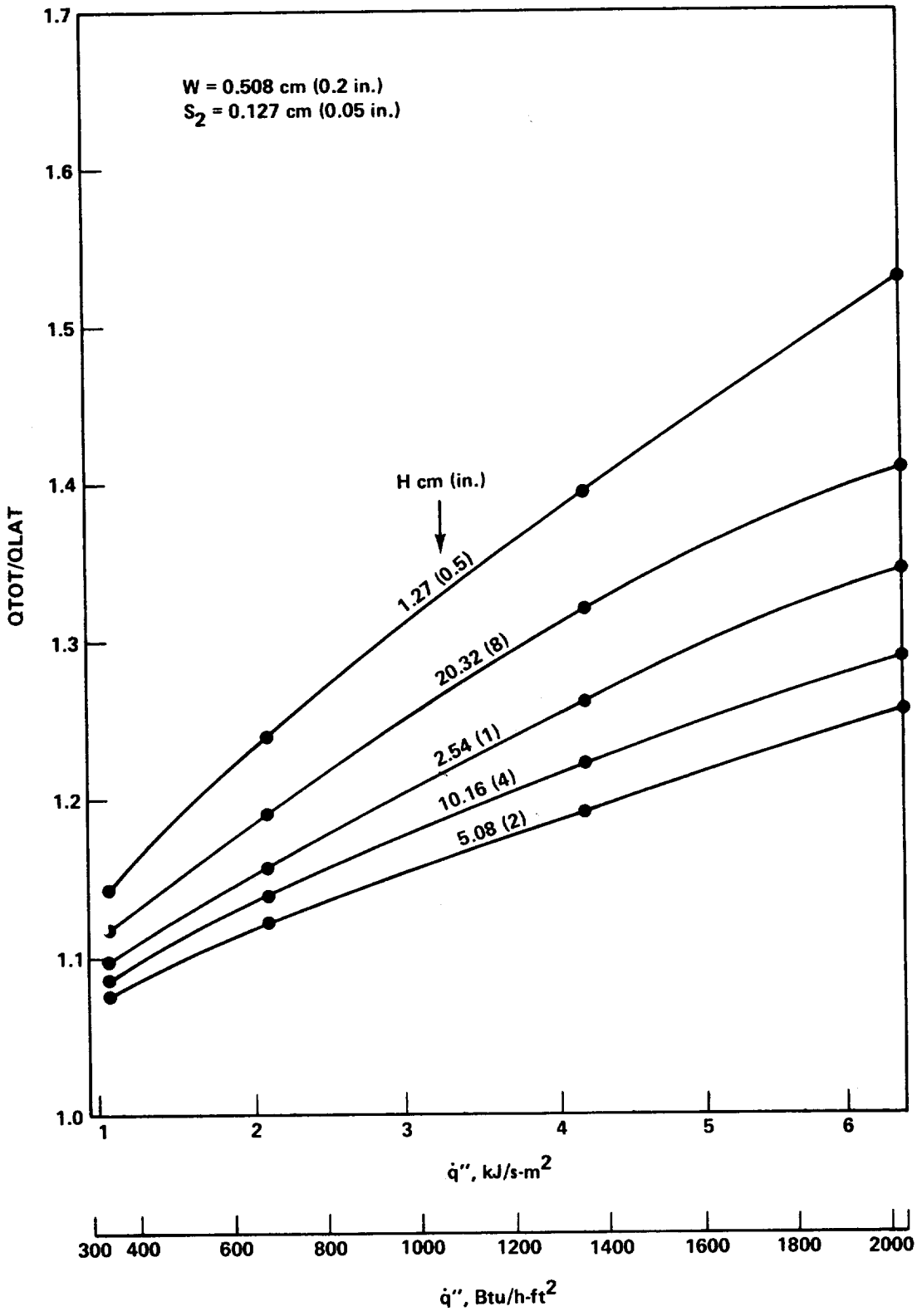

Figure 98. Energy ratio versus heat flux density for W = 0.508 cm (0.2 in.) and S_2 = 0.127 cm (0.05 in.).

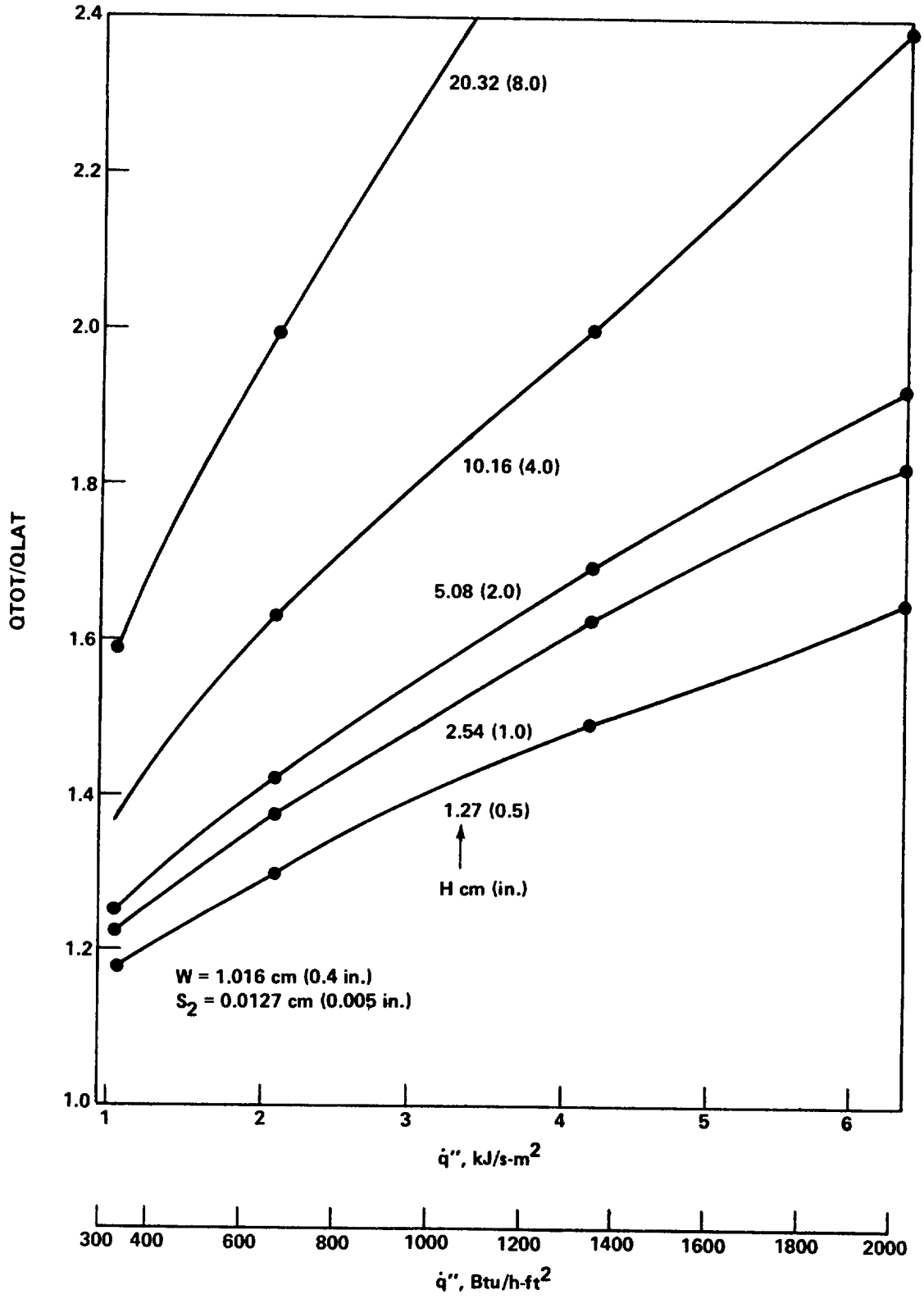

Figure 99. Energy ratio versus heat flux density for W = 1.016 cm (0.4 in.) and S_2 = 0.0127 cm (0.005 in.).

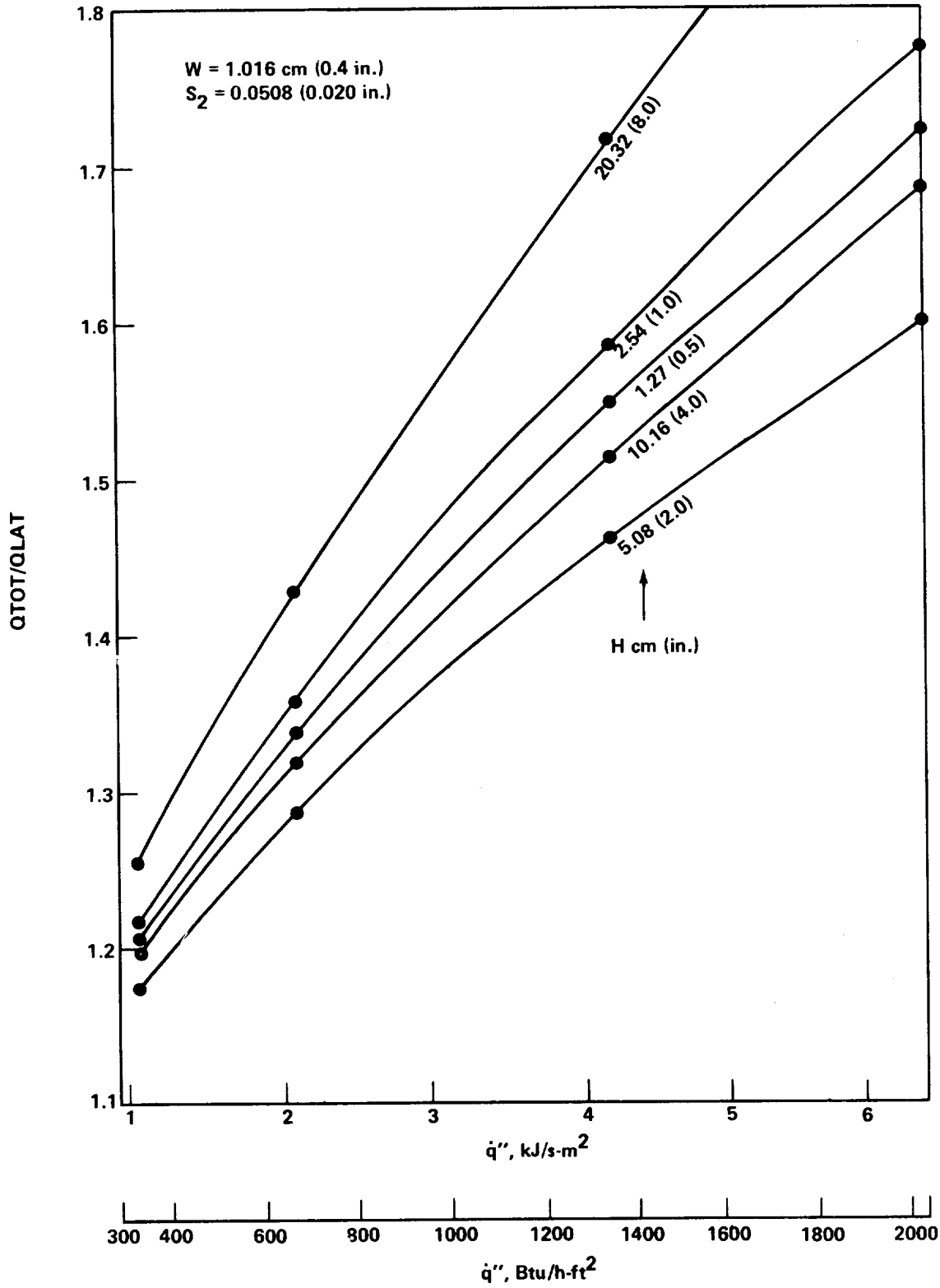

Figure 100. Energy ratio versus heat flux density for W = 1.016 cm (0.4 in.) and S_2 = 0.0508 cm (0.02 in.).

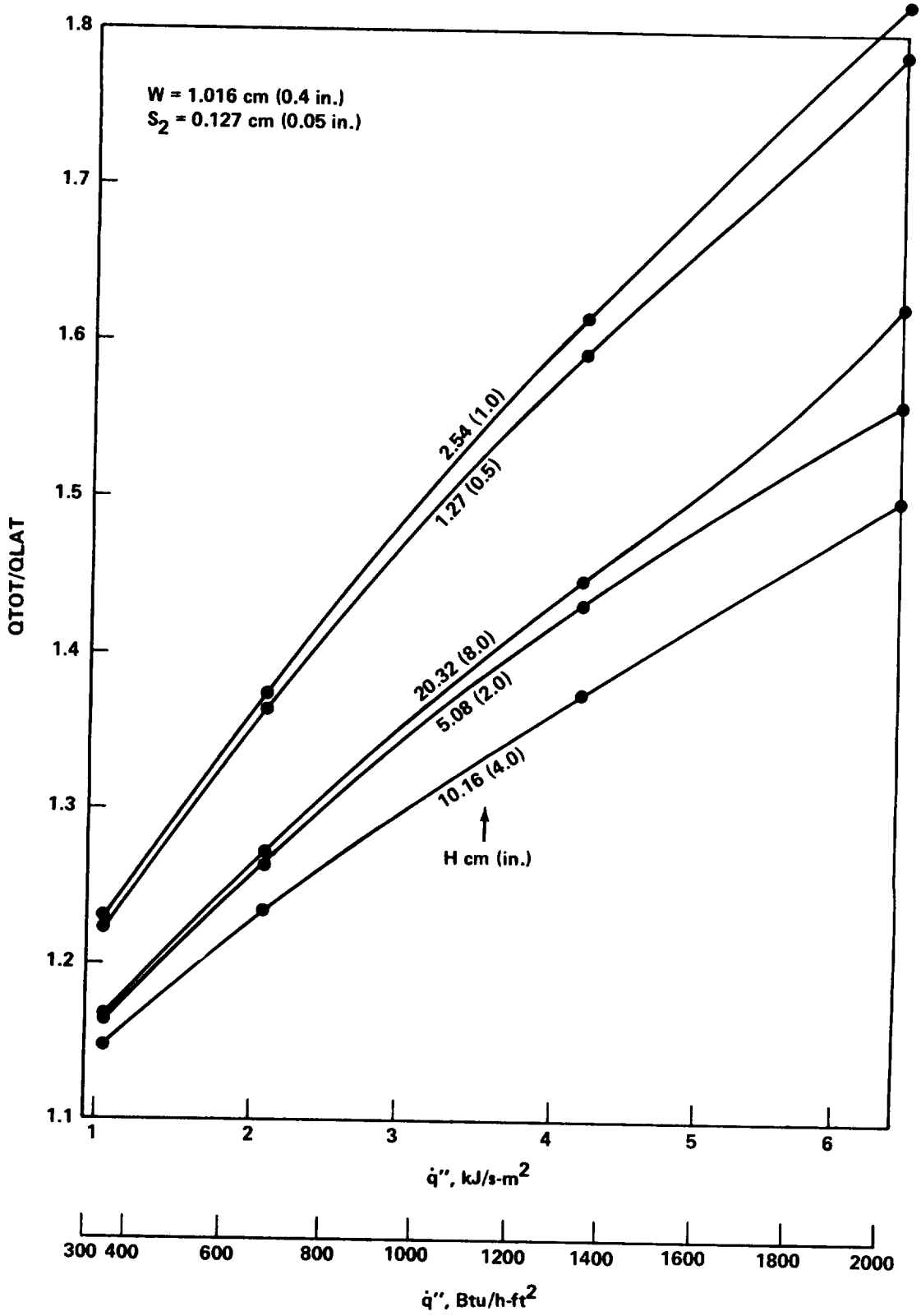

Figure 101. Energy ratio versus heat flux density for W = 1.016 cm (0.4 in.) and S_2 = 0.127 cm (0.05 in.).

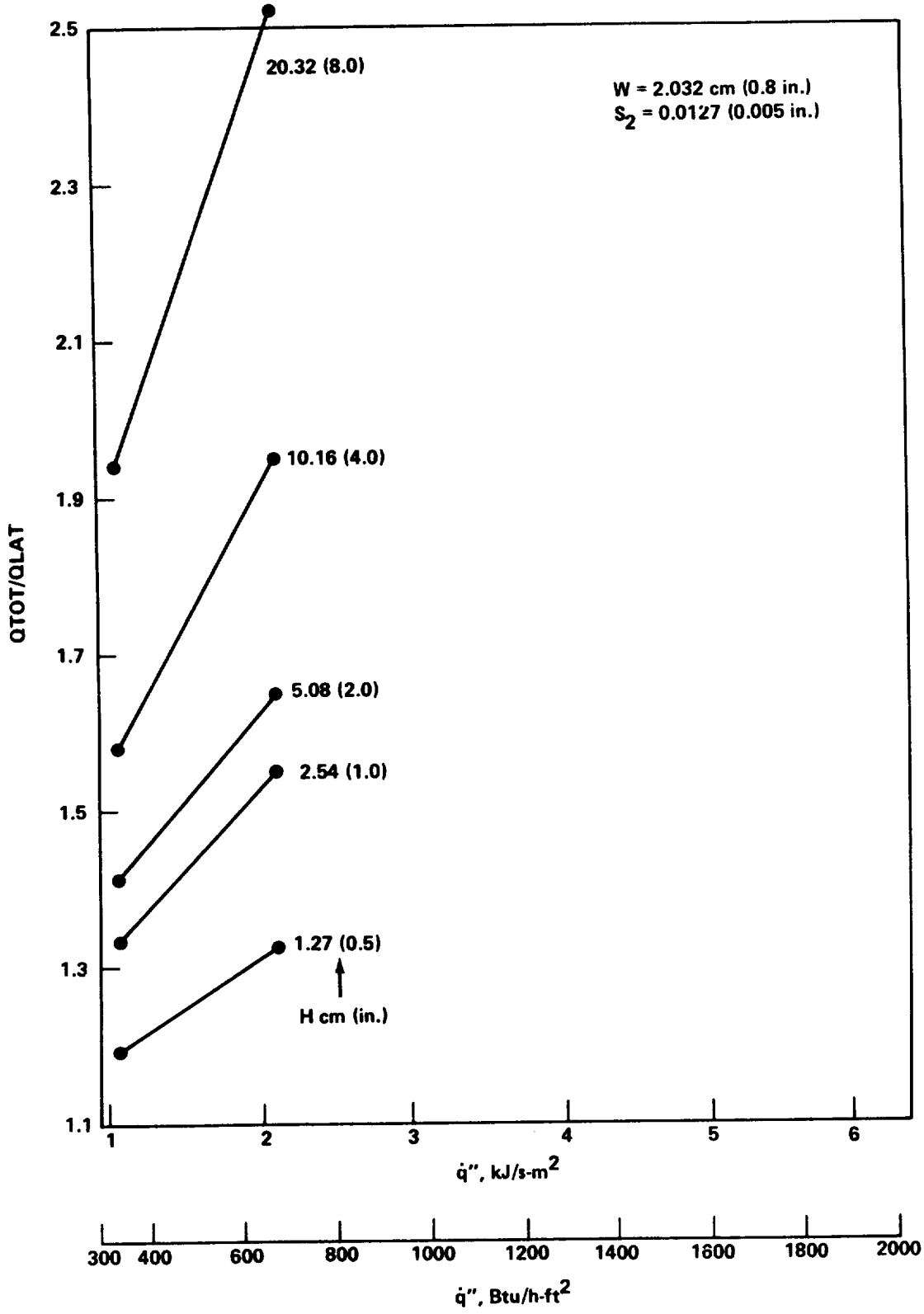

Figure 102. Energy ratio versus heat flux density for W = 2.032 cm (0.8 in.) and S_2 = 0.0127 cm (0.005 in.).

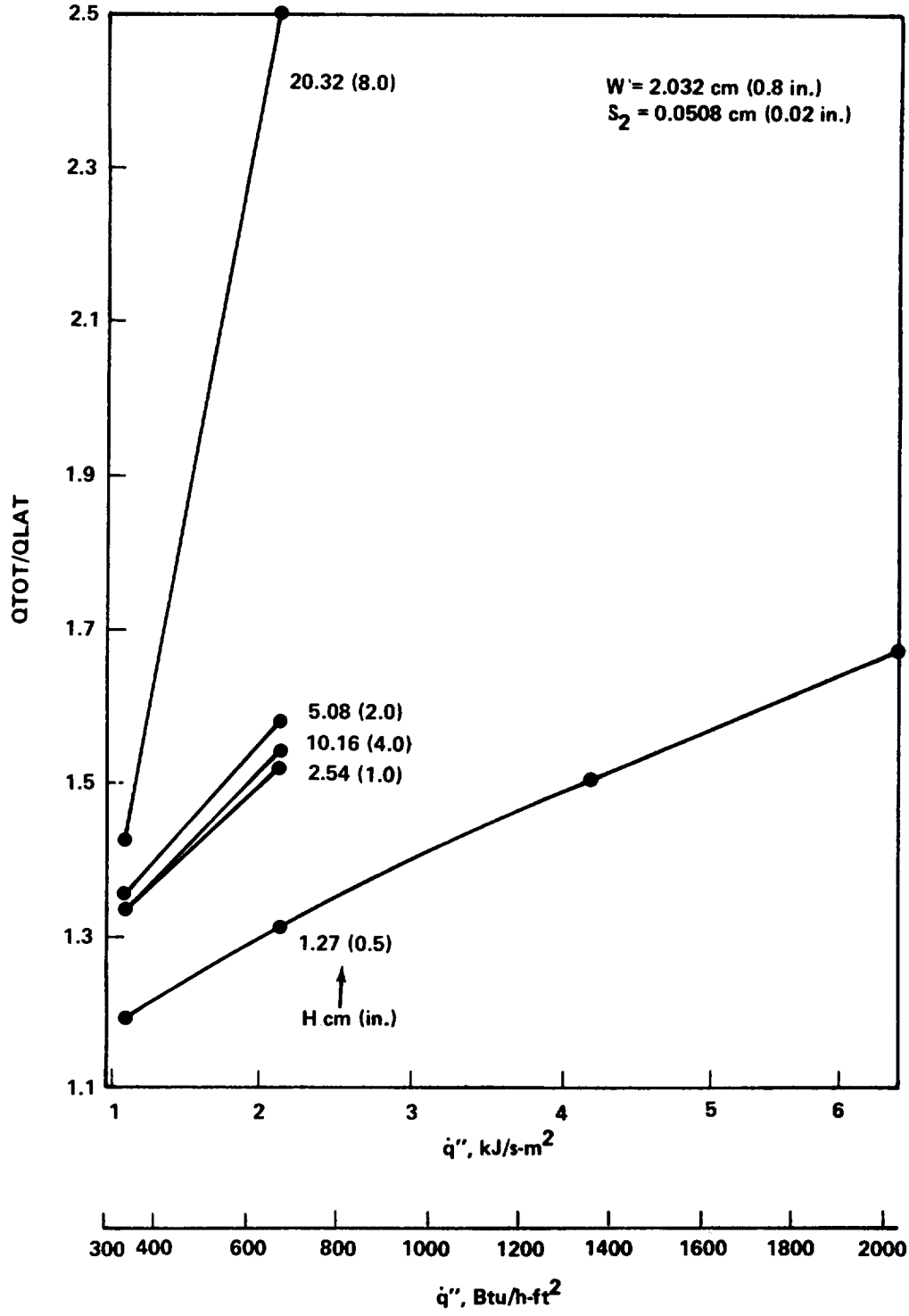

Figure 103. Energy ratio versus heat flux density for W = 2.032 cm (0.8 in.) and S_2 = 0.0508 cm (0.02 in.).

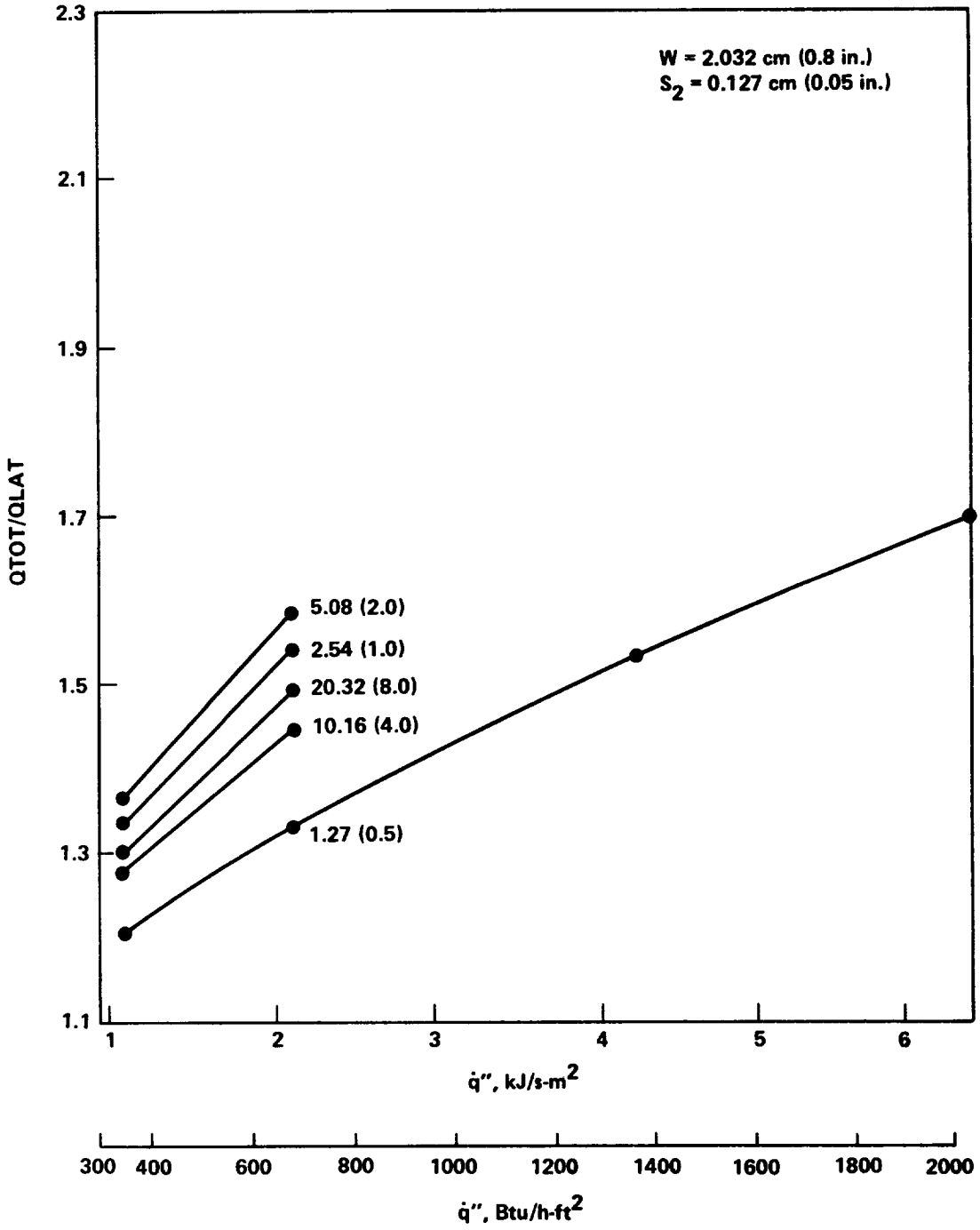

Figure 104. Energy ratio versus heat flux density for W = 2.032 cm (0.8 in.) and S_2 = 0.127 cm (0.05 in.).

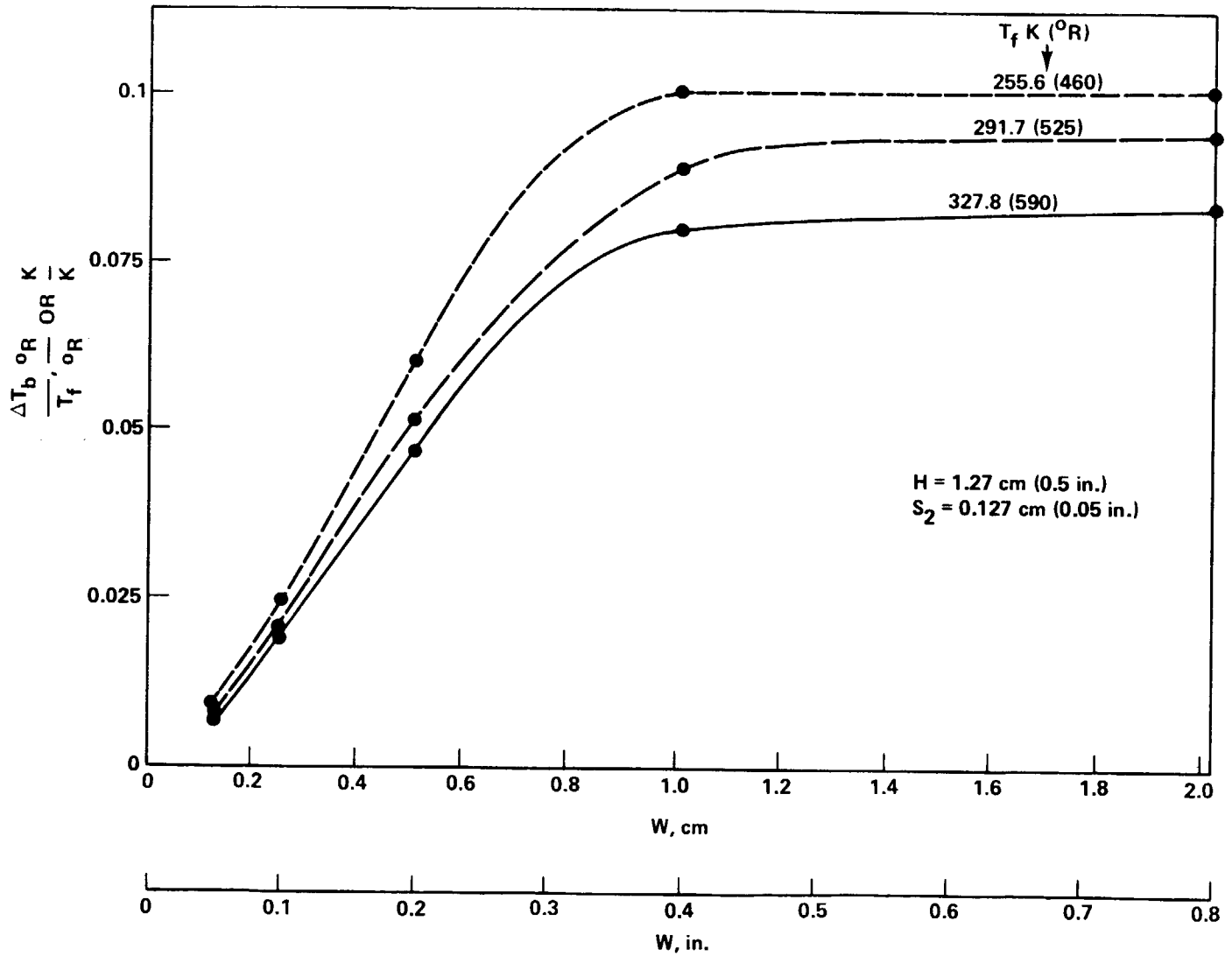

Figure 105. Base temperature rise versus W for three different fusion temperatures and H = 1.27 cm (0.5 in.) and S_2 = 0.127 cm (0.05 in.).

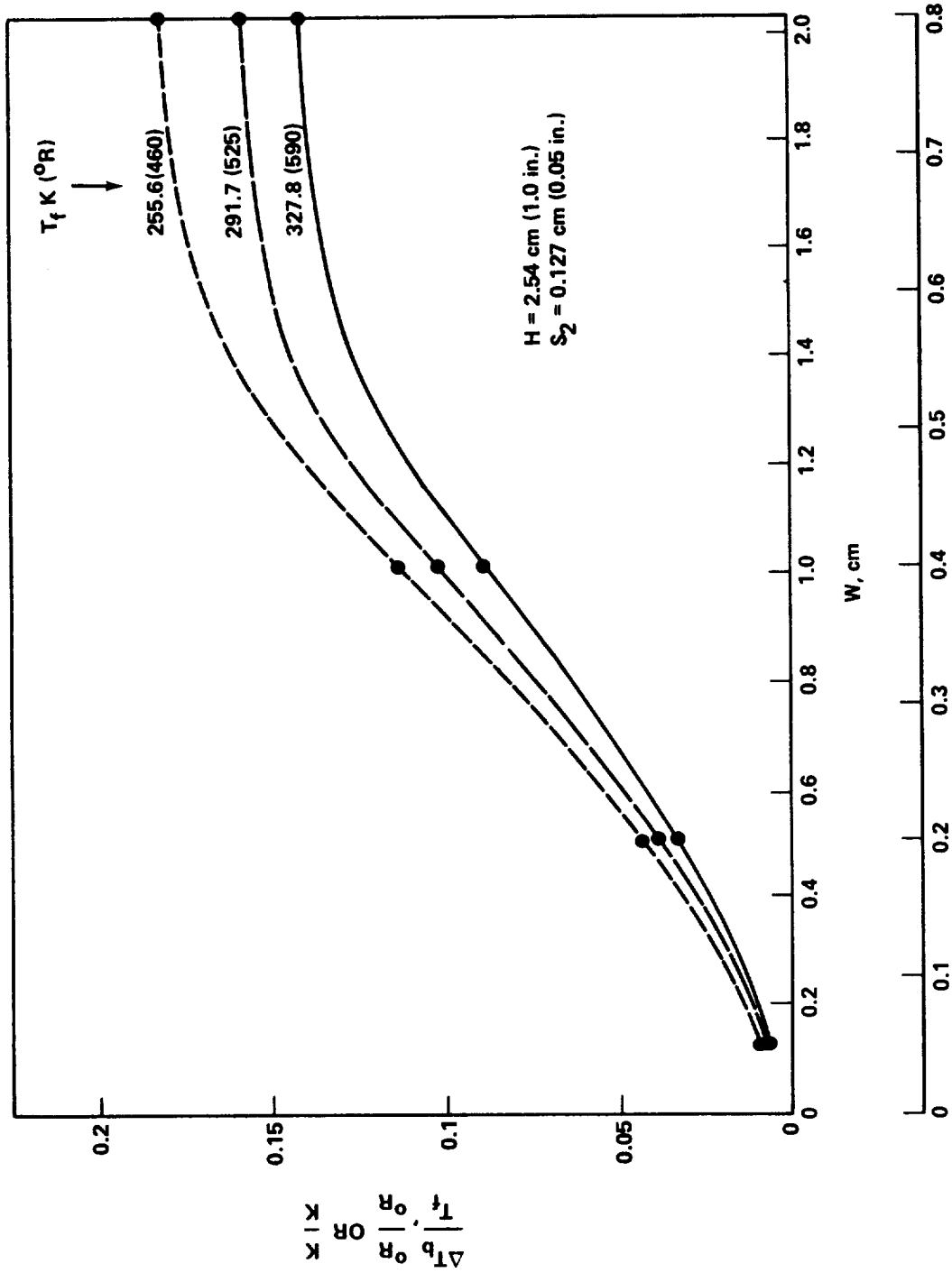

Figure 106. Base temperature rise versus W for three different fusion temperatures and H = 2.54 cm (1.0 in.) and S_2 = 0.127 cm (0.05 in.).

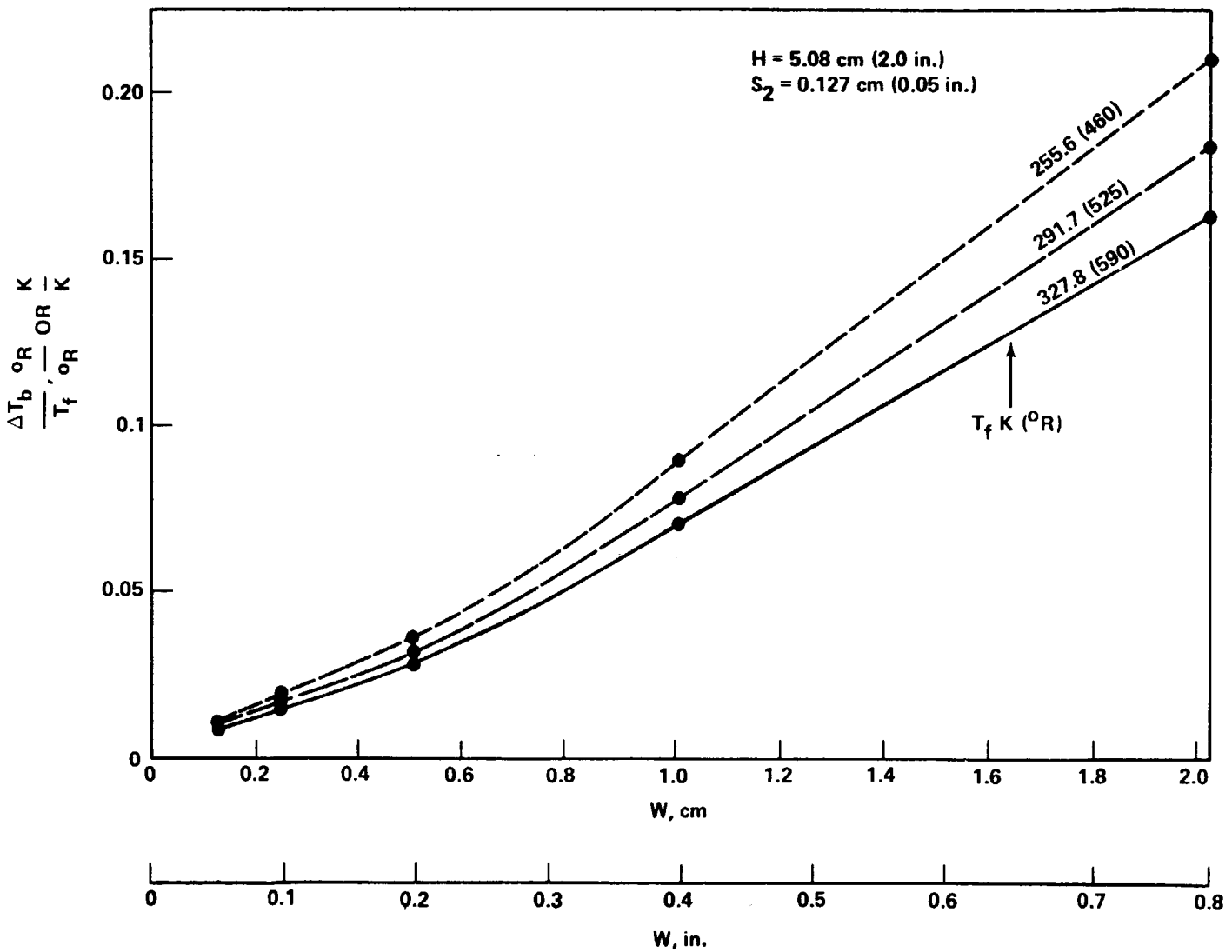

Figure 107. Base temperature rise versus W for three different fusion temperatures and H = 5.08 cm (2.0 in.) and S_2 = 0.127 cm (0.05 in.).

Some representative examples illustrating how the results can be used by a designer are given in the following section. For conditions significantly different from those used in the computations (Tables 14 and 15), it is suggested that the program described in Section III be used to determine the required design information.

D. Examples

Some hypothetical examples which a thermal designer may encounter illustrating use of the results are outlined as follows. All examples assume the designer has selected a housing design and materials as discussed earlier.

Example 1

Given: The heat flux density is specified to be 1076.4 J/s-m^2 (341.4 Btu/h-ft^2) and the designer wishes to limit the temperature increase to 5.56 K (10°R). The PCM melt temperature is 291.67 K (525°R), using these inputs the maximum permissable base temperature rise ratio is computed to be

$$\frac{\Delta T_b}{T_f} = \frac{5.56}{291.67} = 19.05 \times 10^{-3}$$

Case a – The designer wishes to use a fin thickness of 0.0127 cm (0.005 in.).

- Find an acceptable geometry to satisfy the given conditions. From Figure 51, a height of 2.54 cm (1 in.) can be used with a half-fin spacing of 0.127 cm (0.05 in.) to achieve the desired conditions.

- Determine the energy stored. From equation (22) or from Figure 33, the latent energy storage is 4506 kJ/m^2 (397 Btu/ft^2). The results shown in Figure 90 show that the total energy stored at the termination of melting for these conditions is approximately 5 percent higher than the latent energy stored, the difference being sensible energy storage.

Case b – The designer wishes to use a fin thickness of 0.127 cm (0.05 in.).

- Find an acceptable geometry. From Figure 53, it is seen that a fin height of 10.16 cm (4 in.) with a half-fin spacing of 0.254 cm (0.1 in.) can be used.

- Determine the energy stored. From equation (22) or from Figure 35, the corresponding latent energy storage is 15 128 kJ/m^2 (1333 Btu/ft^2). At the termination of melting, the total stored energy exceeds the latent value by approximately 5 percent as shown in Figure 95.

Example 2

Given: The designer is limited by space to a plan area for the phase change device of 0.0697 m^2 (0.75 ft^2); the heat flux density is specified to be 2152.8 J/s-m^2 (682.9 Btu/h-ft^2); the duty cycle of the controlled medium requires latent energy 948.9 kJ (900 Btu) of storage. For these conditions, latent energy storage per unit area is

$$E''_{\ell} = \frac{948.9}{0.0697} = 1.3614 \times 10^4 \text{ kJ/m}^2 \ (1200 \text{ Btu/ft}^2)$$

Case a – The designer wishes to use a fin thickness of 0.0127 cm (0.005 in.).

- Find the geometry. From Figure 33, it is noted that the required height is approximately 7.62 cm (3 in.) regardless of fin spacing over the range shown.

- Determine the base temperature rise. Assume a half-fin spacing of 0.254 cm (0.1 in.) and a height of 7.62 cm (3 in.). From Figure 54, the corresponding base temperature rise at the termination of melting is

$$\Delta T_b \simeq 0.132 \times 291.67 \simeq 38.5 \text{ K } (69^\circ\text{R})$$

Case b – The designer selects a fin thickness of 0.127 cm (0.05 in.).

- Find the geometry. From Figure 35, it can be seen that there is a wider range of fin height-spacing combinations which will satisfy the latent energy storage requirements.

- Determine the base temperature rise. First, assume a fin height of 10.92 cm (4.3 in.) and a half-fin spacing of 0.127 cm (0.05 in.). From Figure 56, the corresponding temperature rise of the base at the termination of melting is approximately

$$\Delta T_b \simeq 0.027 \times 291.67 \simeq 7.88 \text{ K } (14^\circ\text{R})$$

- Determine the base temperature rise for a second acceptable geometry. Second, assume a fin height of 8.38 cm (3.3 in.) and a half-fin spacing of 0.508 cm (0.2 in.). From Figure 56, the corresponding temperature rise of the base at the termination of melting is approximately

$$\Delta T_b \simeq 0.06 \times 291.67 \simeq 17.5 \text{ K } (32^\circ\text{R})$$

Example 3

Given: In a phase change device the designer wishes to utilize 0.0127 cm (0.005 in.) thick fins and he wants to limit the base temperature rise to 13.89 K (25°R). Consequently, the base temperature rise ratio is not to exceed

$$\frac{\Delta T_b}{T_f} = \frac{13.89}{291.67} = 48 \times 10^{-3}$$

Case a – A heat flux density of 1076.4 J/s-m^2 (341.4 Btu/h-ft^2) is required.

- Determine acceptable geometry and the corresponding latent energy storage capacity. From Figure 46, a height of 1.27 cm (0.5 in.) can be used with a half-fin spacing up to approximately 0.48 cm (0.19 in.). The corresponding latent energy storage capacity, from equation (22), is 2338 kJ/m^2 (206 Btu/ft^2).

- Determine acceptable geometry and the corresponding latent energy storage capacity. From Figure 51, heights up to 3.81 cm (1.5 in.) for a half-fin spacing of 0.254 cm (0.1 in.) and up to 9.65 cm (3.8 in.) can be used for a half-fin spacing 0.127 cm (0.05 in.). The corresponding upper limits on the latent energy storage capacity, from either equation (22) or Figure 33, are 6923 kJ/m^2 (610 Btu/ft^2) and 17 114 kJ/m^2 (1508 Btu/ft^2), respectively.

Case b - Assume an imposed heat flux density of 4305.6 J/s-m^2 (1365.7 Btu/h-ft^2).

- Determine an acceptable geometry and the corresponding latent energy storage capacity. From either Figure 46 or 57, the fin height cannot exceed 1.27 cm (0.5 in.) for a half-fin spacing 0.127 cm (0.05 in.). From equation (22) or Figure 33, the corresponding latent energy storage capacity is 2247 kJ/m^2 (198 Btu/ft^2).

Example 4

Given: A phase change device is required to have a fin height of no more than 5.08 cm (2.0 in.) and its base is to be exposed to a heat flux density of 2152.8 J/s-m^2 (682.9 Btu/h-ft^2).

Case a – The designer wishes to use a fin thickness of 0.0127 cm (0.005 in.) to store as much energy as possible.

- Determine the base temperature rise if the designer selects a half-fin spacing of 0.3175 cm (0.125 in). From Figure 48, the maximum base temperature rise is

$$\Delta T_b \simeq 0.21 \times 291.67 \simeq 61.3 \text{ K } (110.3°\text{R})$$

which is too large for most practical considerations.

- Determine the base temperature rise for a half-fin spacing of 0.127 cm (0.05 in.). From Figure 48, the maximum base temperature rise is

$$\Delta T_b \simeq 0.095 \times 291.67 \simeq 27.7 \text{ K } (49.9°\text{R})$$

Case b – Assume the designer selects a fin thickness of 0.0508 cm (0.02 in.)

- Determine the base temperature rise for a half-fin spacing of 0.3175 cm (0.125 in.). From Figure 43, the maximum base temperature rise is

$$\Delta T_b \simeq 0.088 \times 291.67 \simeq 25.7 \text{ K } (46.2°\text{R})$$

- Determine the base temperature rise for a half-fin spacing of 0.127 cm (0.05 in.). From Figure 43, the maximum base temperature rise is

$$\Delta T_b \simeq 0.043 \times 291.67 \simeq 12.5 \text{ K } (22.6°\text{R})$$

Case c – Assume a fin thickness of 0.127 cm (0.05 in) is selected.

- Determine the base temperature rise for a half-fin spacing of 0.3175 cm (0.125 in.). From Figure 38, the maximum base temperature rise is

$$\Delta T_b \simeq 0.060 \times 291.67 \simeq 17.5 \text{ K } (31.5°\text{R})$$

- Determine the base temperature rise for a half-fin spacing of 0.127 cm (0.05 in.). From Figure 38, the maximum base temperature rise is

$$\Delta T_b \simeq 0.030 \times 291.67 \simeq 8.8 \text{ K } (15.8°\text{R})$$

Example 5

Given: A phase change device is to be designed to have its base exposed to a heat flux density of 2152.8 J/s-m^2 (682.9 Btu/h-ft^2). Space constraints restrict the plan area

to 0.0557 m^2 (0.6 ft^2) and the maximum base temperature at 5400 s (1.5 h) is not to exceed the PCM fusion temperature by more than 8.33 K (15°R). Consequently,

$$\frac{\Delta T_b}{T_f} \simeq \frac{8.33}{291.67} \simeq 28.6 \times 10^{-3}$$

An estimate of the required latent energy storage capacity is

$$E''_{\ell} = 2152.8 \times 5400/1000 = 11\ 625\ kJ/m^2\ (1024\ Btu/ft^2)$$

Determine the acceptable geometry to satisfy these conditions. An examination of Figures 33 through 35 reveals that the maximum acceptable height is 6.35 cm (2.5 in.) and that the required height must be greater than this as the fin spacing is decreased and as the fin thickness is increased.

Case a – Consider a fin thickness of 0.0127 cm (0.005 in.). The specified conditions cannot be met for this case (at least considering geometries used herein) as can be seen in Figure 54.

Case b – Consider a fin thickness of 0.0508 (0.02 in.). Figure 55 shows that a fin height of 7.62 cm (3.0 in.) and a half-fin spacing of 0.127 cm (0.05 in.) will facilitate maintenance of the base temperature rise constraint. An examination of Figure 34 indicates that the latent energy storage capacity is also satisfied. Figure 67 shows that the time required for the PCM to melt is 5760 s (1.6 h.).

V. RELATED TOPICS

In the preceding section, attention has been given to certain properties of several paraffins and to an extensive numerical study of a particular phase change device. The results of the parametric study should be helpful to the designer of phase change devices for applications compatible with the model, but the user needs an awareness of features that may require more specialized treatment in a critical design. Some of these important features which are discussed in this section include: (1) filler, (2) convection, (3) solid-phase thermal conductivity, and (4) consideration of an application with a nonuniform thermal boundary condition.

A. Filler

The principal reason for using a filler is to improve the flow of energy to or from the PCM. Most nonmetallic PCM's, particularly the paraffins, have very low thermal

conductivities; consequently, large thermal gradients may be required to effect the desired heat transfer between the PCM and the heated or cooled surface of the phase change device. Incorporation of the metallic filler within the PCM region yields a composite medium with a higher effective thermal conductivity. If the application imposes a size limitation on the phase change device, utilization of a filler reduces the volume available for the PCM. Consequently, when considering the energy storage capacity, the large heat of fusion of the displaced PCM is replaced by the specific heat-temperature rise product for the filler.

Fillers are discussed in References 2, 15, and 16. Some types which have been considered are:

- Aluminum powder
- Aluminum foam
- Aluminum wool
- Aluminum honeycomb
- Copper foam
- Alumina (Al_2O_3) foam
- Alumina (Al_2O_3) powder
- Aluminum fins (straight).

Based on tests involving aluminum wool, aluminum foam, copper foam, and aluminum honeycomb, it is reported [15] that honeycomb offers distinct advantages over the other three types. The results of a number of performance tests on honeycomb are given.

Straight fins offer some advantage over honeycomb in certain cases since better thermal contact between the filler and the housing of the phase-change device may be possible. Fins can be welded to the housing or they may be provided integrally with the housing via milling or casting.

The numerical study treated in Sections III and IV applies specifically to straight-finned arrangements. Likewise the experimental work presented in Reference 2 pertains to applications with straight fins.

The designer should evaluate the advantages and penalties of using a filler. Fabrication, thermal contact resistance, added weight, reduced energy storage capacity, and improved effective thermal conductivity are all interrelated factors. The effects of straight-fin spacing, height, and width on the thermal performance of the model treated in Sections III and IV are reflected in the results. Some comparative insight into the effect of the use of honeycomb filler may be obtained from the results of tests presented in Reference 15.

B. Convection

The physical model and the parametric numerical study which are presented in Sections III and IV are based on the conductive mode of heat transfer only within the PCM. If motion occurs within the liquid phase of the PCM, the heat transfer is affected. This behavior may require special consideration for applications where the liquid is subjected to surface or body forces of sufficient magnitude to initiate and sustain the motion. For the considerations given herein, there appears to be no previous or contemporary treatment of the formidable problem of an exact analysis of convective motion in enclosed cells of liquid. Some experimental correlations exist for certain cases, and these have been applied with some success to phase change problems. A brief background review and some considerations related to PCM studies are presented in the following paragraphs to aid the user in his study of convective effects.

1. Brief Review of Convective Considerations. If one neglects body force fields other than gravity and surface forces other than surface tension, convective motion within the liquid of a PCM could still be due to one or more of the following effects:

- Buoyancy forces
- Surface tension forces
- Density change as the PCM undergoes a phase change.

In early studies of buoyancy driven convection, Lord Rayleigh [17] related the Nusselt numbers (Nu) to the product of the Grashoff number (Gr) and the Prandtl number (Pr). The product of the latter two is known as the Rayleigh number (Ra).

Numerous experimenters have conducted studies that were related to hydrodynamic instability caused by buoyancy as it effects the heat transfer process, including the studies cited in References 18 through 29. O'Toole and Silveston [30] verified the Nusselt number versus Rayleigh number correlation for a fluid confined between two parallel plates (Fig. 108). A number of authors, including Edwards and Catton [31] later showed the effect of L/d ratios for closed cells (Fig. 109), where L is the cell height and d represents fin cell spacings.

The critical Rayleigh number is defined as the value at which convection begins. In the region below the critical value, the heat transfer is substantially by conduction only (i.e., $Nu \cong 1$). The critical value, which depends on the boundary conditions, is 1708 for a fluid confined between two infinite horizontal, isothermal, conducting walls; it is 720 for the case of a fluid confined within a nonconducting walled container [29]. As shown for a bounded cell (Fig. 109a), this critical value tends to increase as the cell sides approach one another (i.e., as L/d increases), and it also tends to increase as the walls become more conducting (Fig. 109b).

Although scientists have been aware of surface tension driven convection for some time, quantitative studies of this phenomena appear to be scarce. The flow patterns created in Bénard's classic experiment [32], which produced cellular circulation patterns

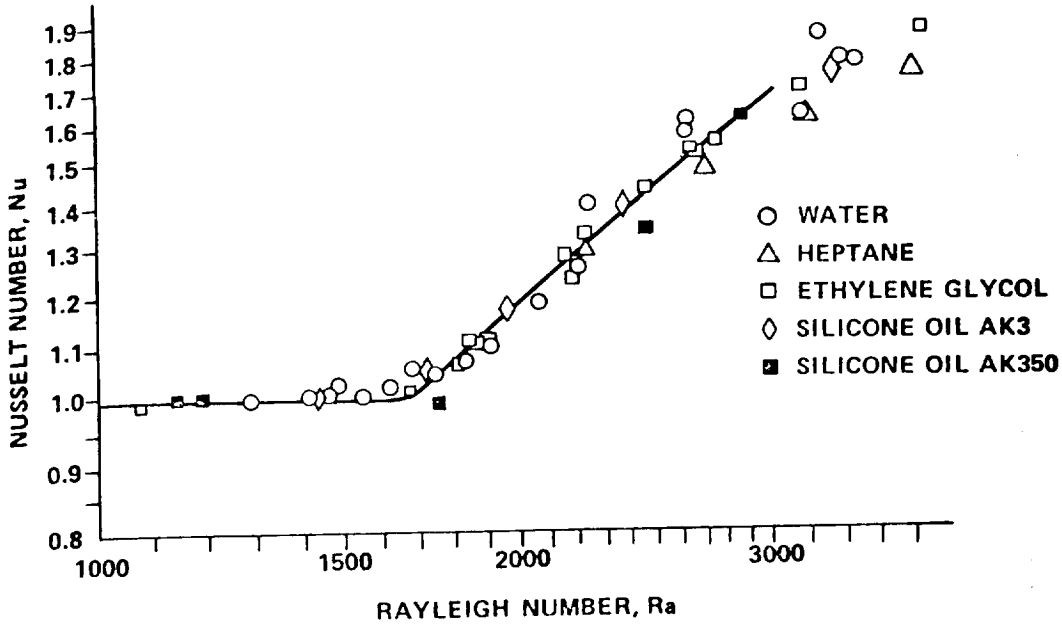

Figure 108. Silveston's experimental results in the neighborhood of instability in various liquids (Fig. 11 of Reference 2).

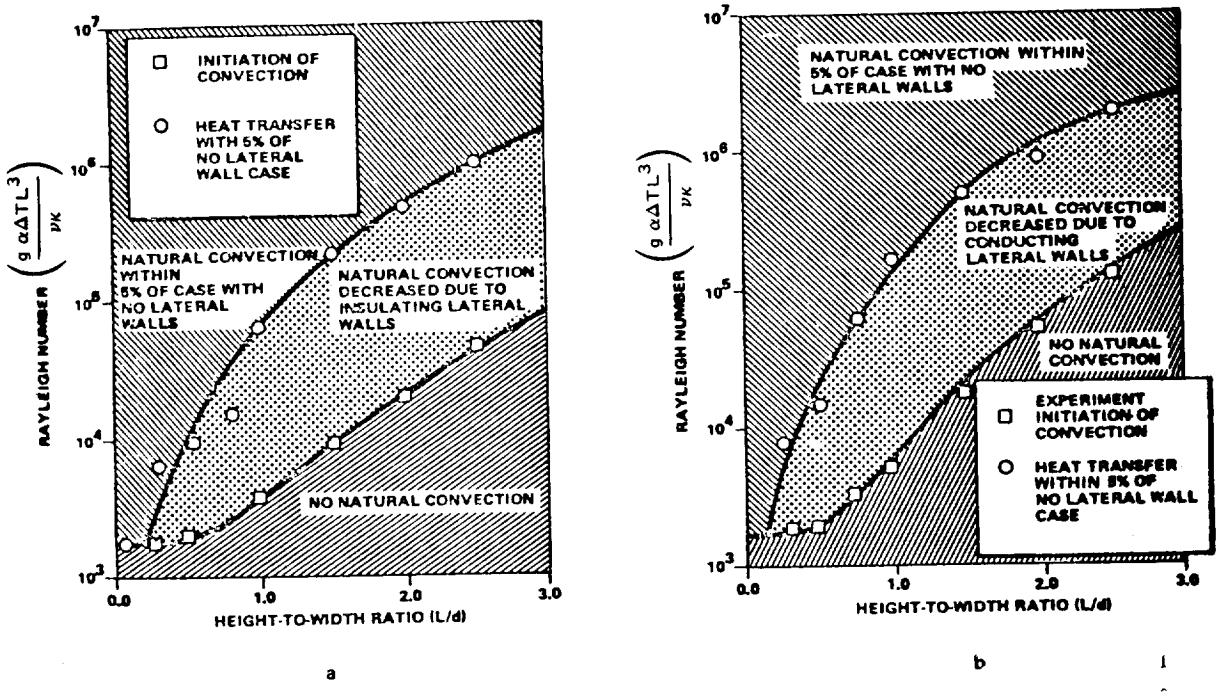

Figure 109. Region of influence of L/d on heat transfer (Fig. 12 of Reference 2).

in a very shallow liquid, were initially attributed to buoyancy effects; however, Block [33], Pearson [34], Scriven [35], and Sternling [36] later proved that this phenomenon was due to surface tension driven convection. The initial discovery of this phenomenon is attributed to Marangoni [37], and the term "Marangoni Flow" is commonly associated with this phenomenon.

The nature of the Marangoni flow, as discussed by Young, Goldstein and Block [38], is that temperature variations across a free gas/liquid interface produced variations in the shear force along the surface. This is due to the dependency of surface tension on temperature, which is estimated by Gambrill [39] to be linear:

$$\sigma = \sigma_0 + bT \tag{23}$$

Since the coefficient "b" is negative, an increase in temperature at the surface is accompanied by a subsequent decrease in the surface tension. Hershey [40] has shown qualitatively that a depression occurs in the surface at a local hot spot, causing the liquid to flow away from the hot zone and toward the cold zone (Fig. 110). McGrew and Larkin [41] photographed this effect for a number of configurations, producing dramatic verification of the phenomenon.

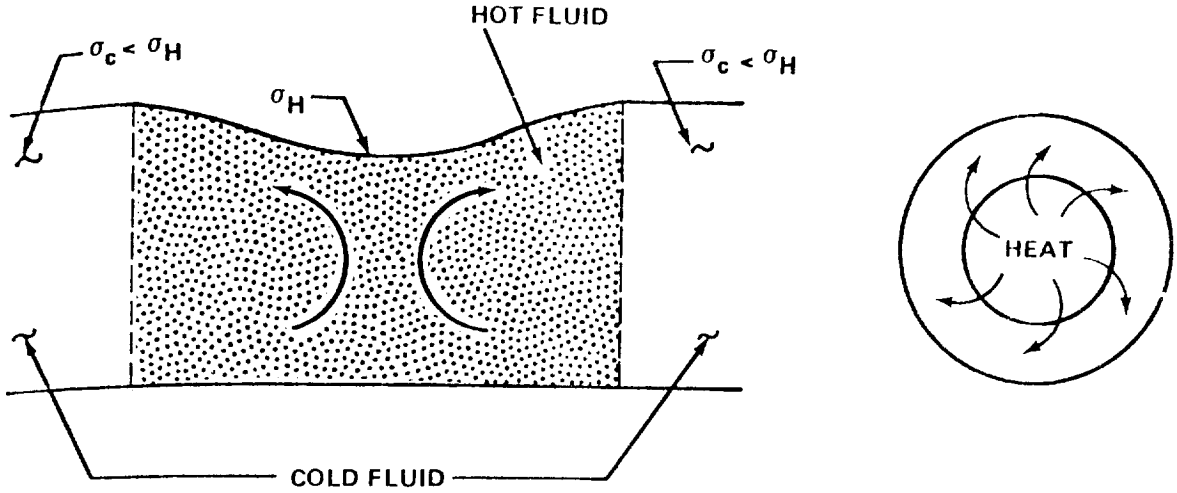

Figure 110. Surface tension convection patterns (Fig. 13 of Reference 2).

The level of surface tension driven convection is correlated by using the Marangoni number, Ma, which is given by

$$Ma = \frac{\frac{-d\sigma}{dT}\frac{dT}{dy} L^2}{\rho\nu\alpha} \tag{24}$$

The critical Marangoni number for a fluid fixed between a rigid and free surface is given as 80.

Nields [42] has stated that the onset of convection in a standard one-g field might be better determined by correlating the Nusselt number with a normalized parameter, R, given by

$$R = \frac{Ra}{Ra_{cr}} + \frac{Ma}{Ma_{cr}} \tag{25}$$

This assumes that buoyancy and Marangoni driven convection are additive. Grodzka [43], however, noted that experimental data on buoyancy and Marangoni surface effects indicated that such an additive relation does not hold. Regardless, the convective currents caused by Marangoni flow in a standard one-g gravitational field are usually small compared to those caused by buoyancy. For most fluids at normal temperatures, Pearson [34] has shown that a liquid thickness of 1 cm or less must be attained before Marangoni effects overshadow buoyancy effects.

For systems with small characteristic dimensions, the nondimensional Bond number, Bo, is given by

$$Bo = \frac{\text{Gravity Forces}}{\text{Surface Tension Forces}} = \frac{\rho g L^2}{\sigma} \tag{26}$$

This number is sometimes used to evaluate the relative importance of Marangoni effects as compared to buoyancy effects. From equation (26), it follows that a low Bond number indicates a high degree of surface tension effects.

Although surface tension effects exist at all unlike interfaces, only the liquid/gas interface (as opposed to liquid/liquid and liquid/solid interfaces) is expected to produce appreciable resulting flows. However, no proof of this conjecture was noted in the literature surveyed.

Volume change driven convection can be caused by the phase change process. During freezing, the new layer of frozen material at the interface tends to contract, since the solid density is usually greater than the liquid density. Consequently, the liquid near the front will flow toward the interface to fill the volume shrinkage caused by solidification. During melting, the liquid at the interface tends to flow away to allow for the volume created by melting. Tien and Koump [44] have stated that this effect will cause both the freezing and melting process to be retarded. This retardation is due to the ingress of warm fluid during freezing and the egress of warm fluid during melting (Fig. 111)

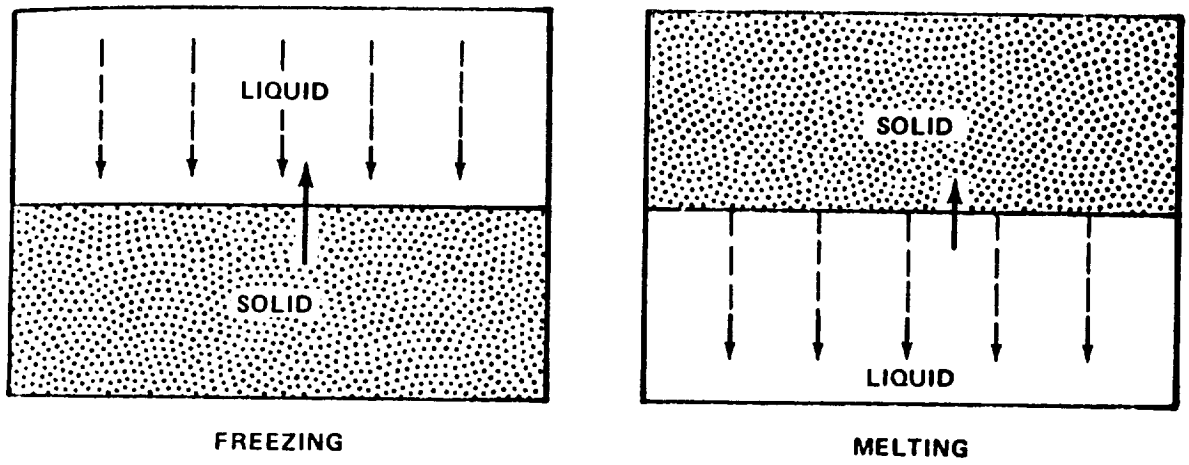

Figure 111. Volume change driven flow patterns (Fig. 14 of Reference 2).

If liquid circulation is created in the melting processes, warm fluid could be drawn into the interface, thereby, augmenting the melting process.

Tien and Koump [44] have also shown, in a computational exercise for a fictitious system where the solid density is 25 percent greater than the liquid density, that only a 10 percent reduction in the freezing rate occurs due to volume change effects. Since paraffins experience only a 5 to 10 percent volume increase on melting, it can be inferred that an even smaller effect can be expected in paraffins for similar conditions.

In summary, the principal modes of heat transfer that are involved in a typical one-g static phase change process are conduction and convection. Convection is caused only by buoyancy driven currents for reasonable container sizes. Surface tension effects are negligible, except for very thin films, and volume change effects may be ignored.

2. Zero Gravity. Since a number of applications of phase change devices [2] have been in space flight situations, some attention is devoted here to zero-g performance.

When comparing environs of near Earth orbital space with that of the Earth, several differences are noted in the heat transfer process. In Earth orbit, the reduced gravitational force is nearly balanced by the centripetal orbital force, creating an effective zero-g environment. Effects caused by reduced pressure, radiation field, meteoroid bombardment, and three-dimensional spacecraft maneuvers are also possible.

Restricting the hypothetical phase change device under consideration to be a hermetically sealed container that is isolated from exterior thermal effects by insulation and antipenetration shields and to be aboard a nonmaneuvering vehicle, then reduced gravity remains as the only important alien effect.

The primary effect of reduced gravity on the heat transfer mechanism is in the lessening or elimination of buoyancy convection. Typical measurements of the net

gravitational acceleration force on a spacecraft indicates acceleration levels of the order 1×10^{-7} g. Using nonadecane paraffin properties, a typical Rayleigh number of this low level of gravitational acceleration is

$$Ra = 0.01\ L^3\ \Delta T \tag{27}$$

Equation (27) indicates that, for reasonable container sizes (i.e., less than 15 cm (6 in.) cell depths), the temperature difference across the liquidus portion of the cell must be $\geqq$ 444°C (830°F) to produce buoyancy driven convection. Since this temperature difference is well in excess of normal operating values, buoyancy stimulated convection may be considered negligible.

At one-g, Marangoni flow or surface tension-driven convection is normally unimportant; however, at zero-g this is not necessarily true. As discussed earlier, liquid flow caused by surface tension at a liquid/vapor interface may occur.

A group of experiments, performed during the mission of NASA's Apollo-14, revealed that the surface tension driven phenomena in zero-g is a reality and can produce significant convection [45,46]. Using data from these experiments, Grodzka [46] has plotted the relation existing between the Marangoni number and the ratio of effective thermal conductivity to actual conductivity (Fig. 112). These data show a rapid increase in the convective level at a Marangoni number slightly greater than 300. The temperature difference in the Krytox test liquid was only 2.5°C (4.1°F) in this instance.

Close examination of these data stimulates some questions. Applying these data to nonadecane paraffin contained in a cell with a 15.24 cm (6 in.) characteristic dimension at a Marangoni number of 300, a K_{eff}/K of 12 is predicted in Figure 112. This is a very high convective level. The temperature difference across a parallel plate system required to reach this convective level is only 0.0011°C (0.002°F); however, for this same system, a Rayleigh number of 4.32×10^5 is predicted at one-g. From this, a K_{eff}/K of only 2.5 is indicated, which is a convective level well below that predicted by the tentative surface tension data. This conflicts with earlier investigators, who reported that for this condition at one-g, Marangoni driven convection is unimportant. This could be explained, at least partially, by the fact that the Apollo 14 data were taken for a free surface, whereas the Figure 108 correlations were taken for top and bottom bounded cells.

Using nonadecane paraffin properties, evaluated at the phase change temperature, the Marangoni number is given by

$$Ma = 2374\ \Delta TL \tag{28}$$

This indicates that for reasonably sized cells, a temperature difference of only 0.003 K (0.006°F) is necessary for the onset of Marangoni driven convection in a paraffin filled

device at zero-g. This fact, along with the high levels indicated in Figure 112, suggests that Marangoni convection can be appreciable at zero-g.

Since the magnitude of volume change effects discussed earlier were low for freezing (where buoyancy driven convection is negligible) as well as for melting, it may be implied that the volumetric effects are negligible for pure conduction as well as convective processes. Consequently, the volumetric effects on the heat transfer process are negligible for zero-g operation. Heat transfer modes occurring in a phase change device at zero-g are then reduced to Marangoni-driven convection and pure conduction.

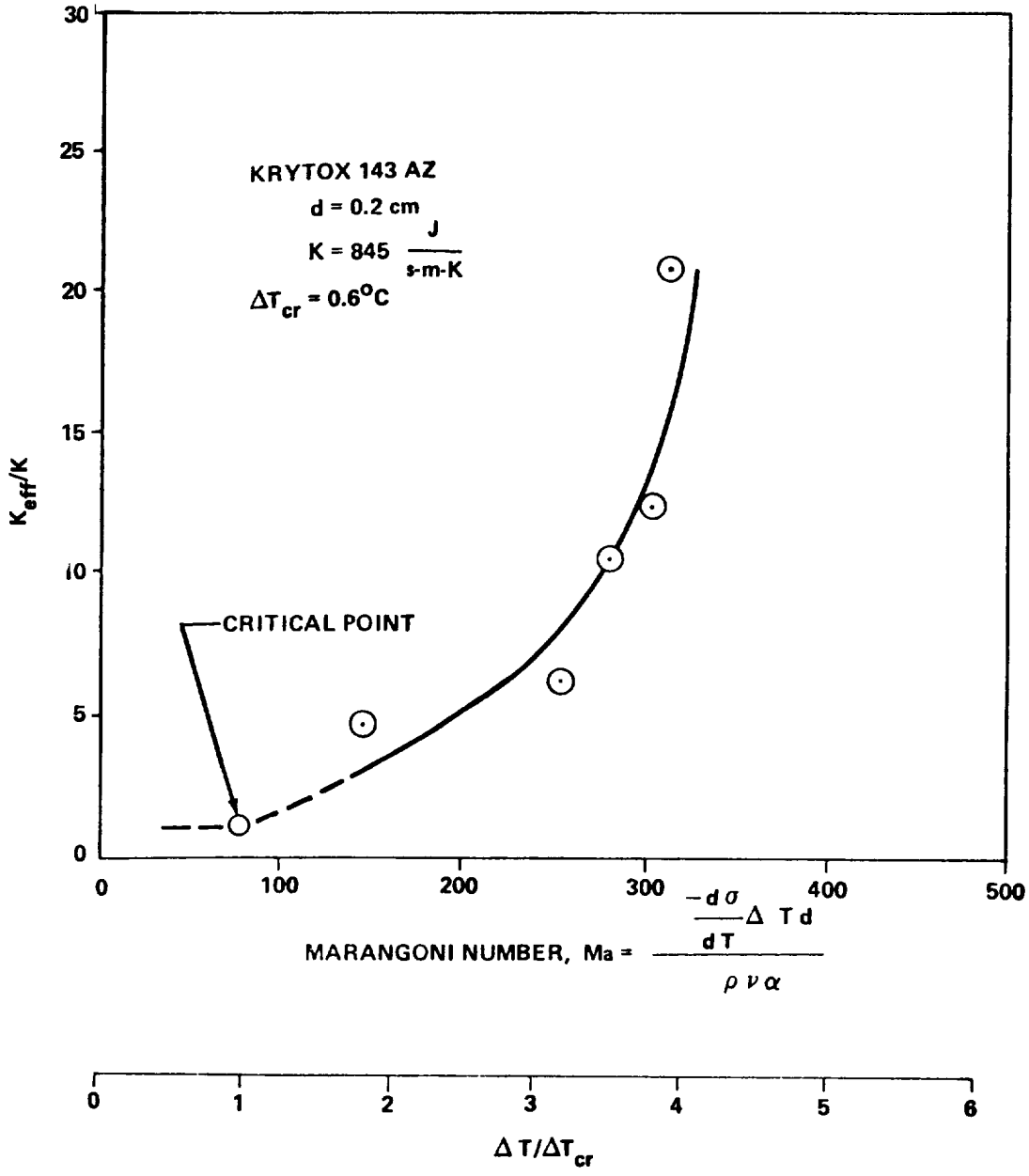

Figure 112. Heat transfer characteristics of Bénard cells (Fig. 15 of Reference 2).

A secondary effect of reduced gravity which can significantly alter the heat transfer process is the ullage gas position. In a typical rectangular cell containing ullage volume, the ullage gas may configure itself in any of a number of possible modes. A number of possible cell ullage locations are given by Reference 2, those of more importance are shown in Figure 113. When heating/cooling from the bottom, only configurations d and e (Fig. 113) would alter the normal process; however, when heating/cooling from the top or sides, configurations a, b, d, and e would all reduce the rate of heat transfer due to the insulating effect of the ullage gas. Small bubbles occurring in the liquid could induce convective currents. In a zero-g field, this motion could be caused by the Marangoni flow phenomon causing the bubbles to migrate toward warm zones. Also, bubbles could be entrapped in the freezing solid (configuration d of Fig. 113), thereby decreasing the apparent thermal conductivity of the PCM. Fortunately, paraffins have the property of being good surface wetters, which in zero-g tends to force the ullage to form in the center of the cell (configuration c of Fig. 113); however, insufficient quantitative data are available on these phenomena to determine the effect on the heat transfer process under given conditions.

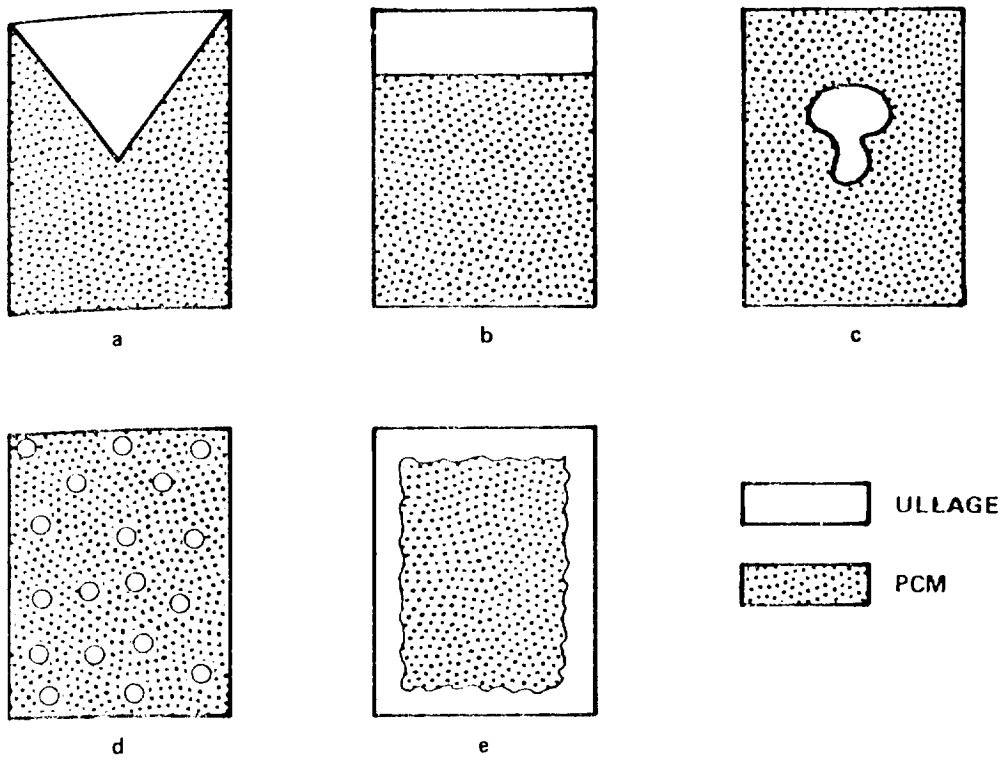

Figure 113. Zero-g ullage configurations (Fig. 16 of Reference 2).

Grodzka [4] has examined effects of the space environment on the microscopic processes. She concluded that complex coupling effects between phase change kinetics and various possible complex coupling effects between phase change kinetics and various possible modes of convective motion cannot be predicted accurately without actual flight data. She also concluded that the magnitude of magnetic and electric fields likely to be encountered in the Earth's orbit are not expected to alter phase change behavior significantly from that observed on Earth. Finally, she stated that radiation fields encountered in Earth orbit are expected to have little effect, except perhaps in the case of an organic PCM where long time exposures will result in the buildup of impurity. Although the later statement applies to a paraffin, no definitive information on this effect could be found in the literature surveyed.

Although insufficient reduced gravity data are available to corroborate these findings, some observations have been made as to the mechanisms of heat transfer in a phase change device. When a free surface is present and thermal conditions are proper, Marangoni convection may be present. Insufficient data are currently available to determine quantatively the influence of this phenomenon. In the absence of surface tension effects, conduction is the primary process governing heat transfer. The conduction process may, however, be altered by the ullage gas location. Furthermore, secondary effects of property degradation due to radiation may occur if the PCM is organic.

3. PCM Related Considerations. Regarding buoyancy-driven convective currents in the liquid during the melting of a PCM, a major factor is the positioning of the heated surface. If the heated surface is located at the bottom of a PCM cell during melting, convection may significantly augment the heat transfer. Conversely, the role of convection is minor, vanishing for one-dimensional cases, when the heated surface is at the top of the cell. The contribution of convection in the liquid to the heat transfer during solidification depends on positioning of the cooled surface, but it also depends on the amount by which the initial liquid temperature exceeds the fusion temperature of the PCM.

Prensner and Hsu [47] reported on studies of natural convection in air within closed cells. Their work revealed the possibility of a number of different geometry-dependent convective patterns, even under steady state conditions. Such studies attest to the formidable task of analytically predicting the transport mechanism occurring during natural convection within a bounded fluid. When considering convection within the liquid during melting of a PCM, the problem is further complicated by the fact that one of the boundaries is moving (i.e., the interface). Even if accurate predictions of the convective mechanism were possible, another unpredictable feature occurring in finned PCM devices is the tendency for the PCM to melt up the fin with the solid PCM core, subsequently, falling to the heated surface.

While the aforementioned difficulties appear pessimistic, some success has been reported [2, 48] on approximately accounting for convection during the melting of a paraffin. The approach made use of the correlations given by O'Toole and Silveston [30] which are:

$$
\begin{aligned}
1700 \leqslant Ra \leqslant 3500 \qquad & Nu = 0.00238\, Ra^{0.816} \\
3500 < Ra \leqslant 10^5 \qquad & Nu = 0.229\, Ra^{0.252} \\
10^5 < Ra < 19^9 \qquad & Nu = 0.104\, (Ra)^{0.305} (Pr)^{0.084}
\end{aligned} \tag{29}
$$

Although the correlations given by equation (29) were determined from data on steady state heat transfer through horizontal layers of fluid, they were used as a means of estimating the convective effect within the liquid of finned PCM cells similar to the one modeled in Section III. The scheme involved continuous replacement of the thermal conductivity of the liquid by an effective thermal conductivity, which was calculated by

$$K_{eff} = Nu \times k \tag{30}$$

It was recognized that this scheme would not yield true temperatures in the liquid because the convective mechanism therein was being artificially replaced by conduction in a hypothetical medium with a larger thermal conductivity than that of the liquid PCM.

Figure 114 shows some experimental data for the interface location during melting of a paraffin inside a cell similar to the one modeled in Section III. Also shown are numerical predictions for conduction only and for inclusion of convection in the manner previously described. The numerical predictions shown in Figure 114 were achieved with an explicit formulation which was subject to a stability requirement. For nodes located in the fin, this requirement demanded excessive computer time; consequently, temperatures along the fin were approximated with the aid of measurements from thermocouples attached to the fins. With the approximate inclusion of convection, the predictions were promising. The predicted interfacial positions followed the same trend as the experimental data. Although magnitudes did not exactly agree, the difference appeared to be due to a shift in time and might have been associated with starting conditions. Use of this approach for including convection is discussed more extensively in Reference 2. Also presented is a more detailed discussion of the computer program and several comparisons between predictions and experimental data. The computer program is also listed and briefly discussed in Appendix D.

4. Solid Phase Thermal Conductivity. Nearly all published thermal conductivity values for paraffins apply to the liquid phase. Since the mechanism of heat conduction is typically different in solids than in liquids, one should expect some difference between the thermal conductivity value for the solid phase and that for the liquid phase of a PCM.

In studies reported in References 2 and 49, attempts to analytically predict the transient interfacial location during the phase change of a paraffin were more successful

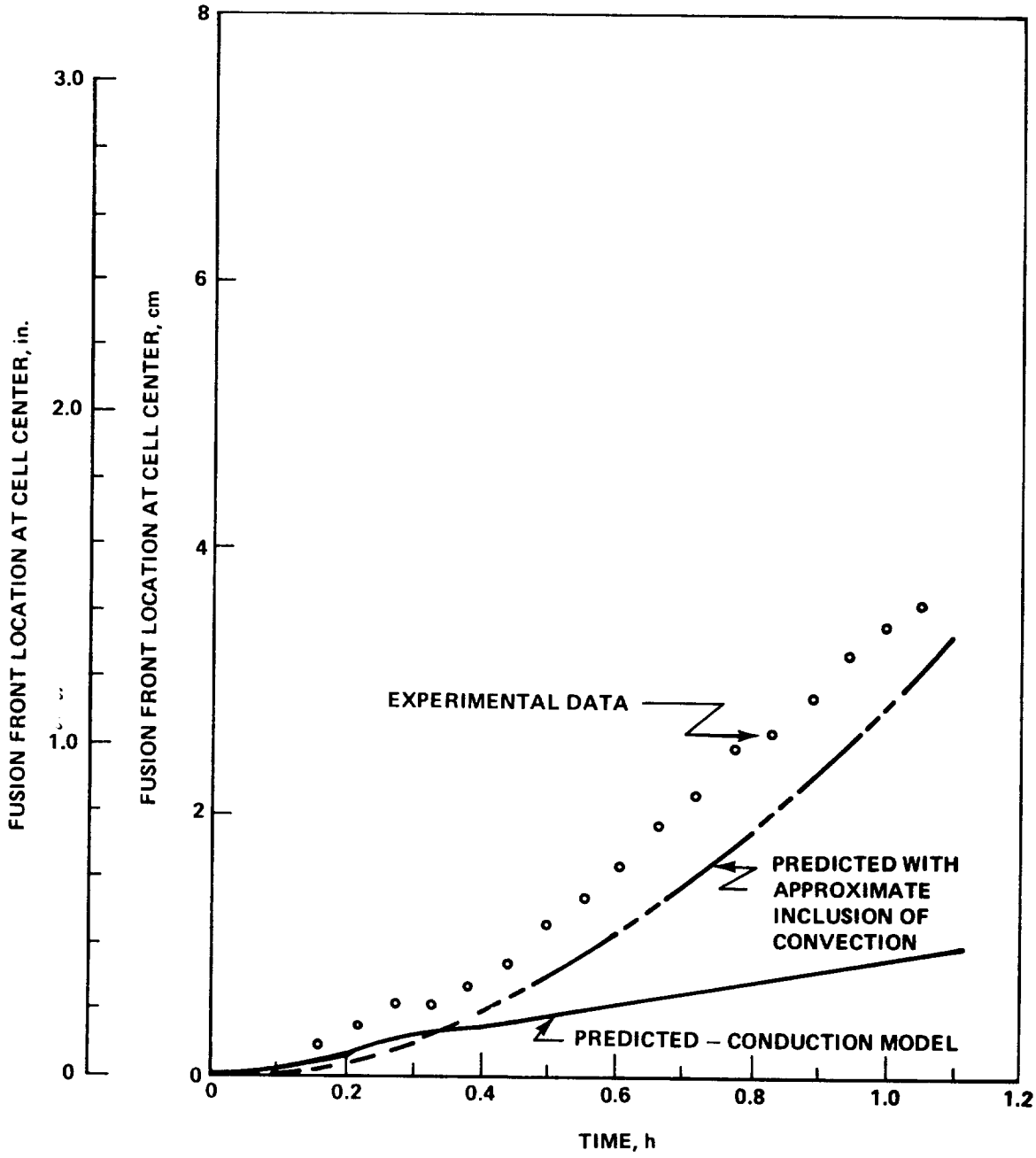

Figure 114. Comparison between predicted and measured fusion front location for an example melt run.

for the case of melting than for the case of solidification. Two plausible explanations for the lack of success with solidification existed. One explanation was simply that the true value of the thermal conductivity of the solid phase may not have been used in the analysis. Knowledge of the thermal conductivity of the solid is more critical in analyses of solidification than in those of melting. Another possible explanation was related to the character of the solid-liquid interface during the phase transition. During melting, the interface appeared smooth. During solidification, however, it was covered with numerous projections called dendrites. Their presence may have affected the interfacial heat transfer rate. The discrepancy may also have been due to a combination of both effects.

Thomas and Westwater [50] studied the nature of the interface during freezing and melting of n-octadecane. Measured interfacial velocities exceeded analytical predictions by as much as 100 percent; the difference was attributed to irregularities at the interface.

Bailey and Davila [51] monitored the position of the solid-liquid interface during solidification of hexadecane and octadecane. Bailey and Liao [52] found that effective solid thermal conductivities, which yielded agreement between predictions and experimental measurements, exceeded published values by factors ranging from 2.5 to 3.

Dyer and Griggs [49] measured interfacial positions during solidification of nonadecane and hexadecane; they also determined the values of solid thermal conductivity which forced agreement between the measurements and numerical predictions. The work was extended to include measurement of the thermal conductivities of solid nonadecane and hexadecane. The measured values did not agree with the values required to force agreement between experimental and analytical results (Table 16).

As previously mentioned, values of thermal conductivity for the solid phase of paraffins are less prominent in the literature than are those for the liquid phase. Some of the available values are summarized in Table 16 for reference.

In summary, analytical predictions of the solidification of paraffins suffer accuracy due to the aforementioned effects. The designer needs to exercise some judgement in the selection of an appropriate thermal conductivity value to use for the solid phase. Uncertainty associated with the effect of interfacial irregularities (i.e., dendrites) renders the problem less amenable to an exact treatment.

C. Example Application with a Nonuniform Thermal Boundary Condition

The parametric study, which is presented in Section IV, pertains to a numerical analysis of a symmetrical half of a single PCM cell. The results can be extended to multicell phase change devices by appropriate scaling provided that the thermal boundary condition imposed on the full-scale device is uniform and agrees with the type analyzed.

TABLE 16. SOME REPORTED THERMAL CONDUCTIVITY VALUES FOR THE SOLID PHASE OF CERTAIN PARAFFINS IN W/m-°C (Btu/h-ft-°F)

Source \ Paraffin	Paraffin Wax	Nonadecane	Hexadecane	Octadecane
McAdams [53]	0.24 (0.14)	–	–	–
Bailey and Liao [52][a]	–	–	0.49 (0.28)	0.41 (0.24)
Dyer and Griggs [49][a]	–	0.35 (0.20)	0.52 (0.30)	–
Dyer and Griggs [49]	–	0.26 (0.15)	0.35 (0.20)	–
Powell and Challar [54]	–	–	–	≃0.19 (≃0.11)

a. Value used to force agreement between analytical and experimental results.

One application of phase change devices involves heat transfer between the device and a flowing fluid. In such applications, the thermal condition existing at the separating surface between the PCM and the fluid is not necessarily uniform. An analysis of the heat transfer between the fluid and the PCM is not a simple problem. The entire apparatus including PCM, housing, and flow passage could be subdivided into a thermal network of nodes and interconnecting thermal resistances, and an appropriate numerical study could be performed. Such an approach, however, could involve a large number of nodes, particularly if much internal detail is needed. For a specific case, this approach may be the most desirable as well as productive; however, it certainly does not appear feasible to attempt to generalize it into an extensive parametric study, not only because of the vast nature of the task but also because of the large number of parameters which would be involved. The unwieldiness of the problem is evident from the integral analysis presented by Baily and Liao [55] even where some simplifying assumptions were incorporated. An approximate approach which utilizes input from the parametric study is outlined in the following paragraphs.

The model under consideration is depicted in Figure 115. Fluid flows through the flow passage and makes intimate thermal contact with a surface separating it from a device filled with a PCM. For this model, it is assumed that the lower side of the flow passage is insulated or that a symmetrical PCM device is also located on the other side.

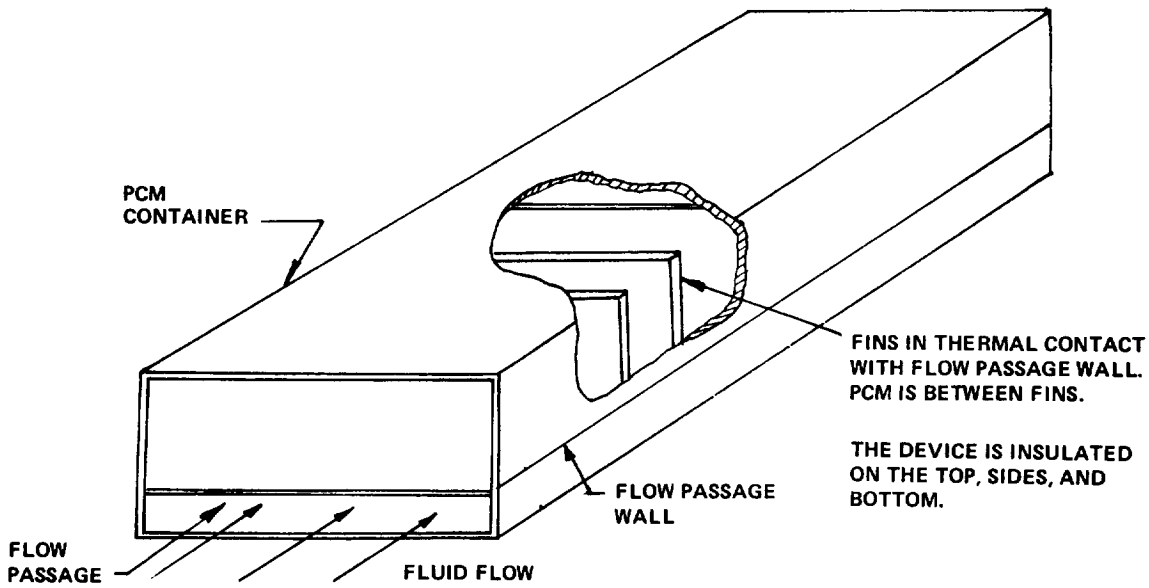

Figure 115. Physical model for heat transfer between a phase change device and a flowing fluid.

An energy balance on a differential length of the flow passage yields the following differential equation:

$$\rho A_p c_p \frac{\partial T_m}{\partial t} + \dot{m} c_p \frac{\partial T_m}{\partial x} = k A_p \frac{\partial^2 T_m}{\partial x^2} - k B(T_m - T_s) \tag{31}$$

Neglecting any effect due to the surface separating the PCM and fluid, the instantaneous heat transfer between the surface and the PCM can be equated to the instantaneous heat transfer between the flowing fluid and the surface. This equality can be expressed by

$$h(T_m - T_s) = U_0(T_s - T_f) \tag{32}$$

The right-hand side of equation (32) represents the instantaneous heat transfer per unit area between the surface and the PCM. The two-dimensional character of the problem has been masked by use of an overall heat transfer coefficient based on the difference between the surface temperature and the PCM fusion temperature. Equation (32) can be rearranged to yield the surface temperature as

$$T_s = \frac{T_m}{1 + (U_0/h)} + \frac{T_f}{1 + h/U_0} \tag{33}$$

Equation (33) implies that $T_s \simeq T_m$ when h greatly exceeds U_0 and $T_s \simeq T_f$ when U_0 greatly exceeds h.

The elimination of T_s in equation (31) with the aid of equation (33) and the neglection of heat conduction in the flowing fluid give

$$\rho c_p A \frac{\partial T_m}{\partial t} + \dot{m} c_p \frac{\partial T_m}{\partial x} = hB\left(\frac{T_f}{1 + h/U_0} - \frac{T_m}{1 + h/U_0}\right) \tag{34}$$

Equation (34) can be solved numerically for both spatial and temporal variations of T_m; the solution, however, requires input of the convective heat transfer coefficient h for the flowing fluid and the overall coefficient U_0 for heat transfer with the PCM. The computer programs (listed in Section IV) provided a value of U_0 as part of the output. This value is determined by dividing the instantaneous heat transfer per unit area between the surface and the PCM by the difference in the surface temperature and the fusion temperature of the PCM. Although the computations apply to a symmetrical cell, use of the U_0 values may be acceptable since lateral heat conduction between adjacent PCM cells is probably much less significant that heat transfer between the surface and the PCM. If this hypothesis is valid, the U_0 values may serve as a convenient aid in analyzing the variation of T_m. The solutions discussed in the following paragraphs are restricted to those cases for which the aforementioned assumptions are meaningful.

The time derivative can be approximated by

$$\frac{\partial T_m}{\partial t} \simeq \frac{T_{m_{i+1,n}} - T_{m_{i,n}}}{\Delta t} \tag{35}$$

The space derivative can be approximated by

$$\frac{\partial T_m}{\partial x} \simeq \frac{T_{m_{i+1,n}} - T_{m_{i+1,n-1}}}{\Delta x} \tag{36}$$

The first subscript denotes time while the second subscript denotes space.

Insertion of the difference expressions given in equations (35) and (36) into equation (34) and some rearrangement result in

$$T_{m_{i+1,n}} = \left[\frac{1}{\frac{\rho c_p A}{\Delta t} + \frac{\dot{m} c_p}{\Delta x} + \frac{hB}{1 + h/U_0}}\right]\left(\frac{h B T_f}{1 + h/U_0}\right) = \frac{\dot{m} c_p}{\Delta T} T_{m_{i+1,n-1}} + \frac{\rho c_p A}{\Delta t} T_{m_{i,n}} \quad (37)$$

Equation (37) facilitates computation of the temperature of a node in the fluid at time $t + \Delta t$ from the previous temperature of that node at time t and the temperature of the adjacent node at $x - \Delta x$ and at time $t + \Delta t$. The nodal pattern is illustrated in Figure 116. The computations require input of the initial temperature distribution in the fluid (i.e., temperatures along the horizontal axis of Figure 116) and the transient variation of the fluid temperature at the inlet to the flow passage (i.e., temperatures along the vertical axis of Fig. 116). The internal convective heat transfer coefficient for the flowing fluid must be estimated from knowledge of the character of the flow (e.g., laminar, fully-developed, turbulent, etc.). The value of U_0 is dependent on the amount of PCM which has undergone phase change; consequently, the computational scheme should incorporate sequential alteration of U_0. One method employed in the following computations involved representing U_0 as a function of the fraction of PCM which has undergone phase change. The fraction is determined at each location and used in the functional representation to determine U_0 for use in the computation of T_m.

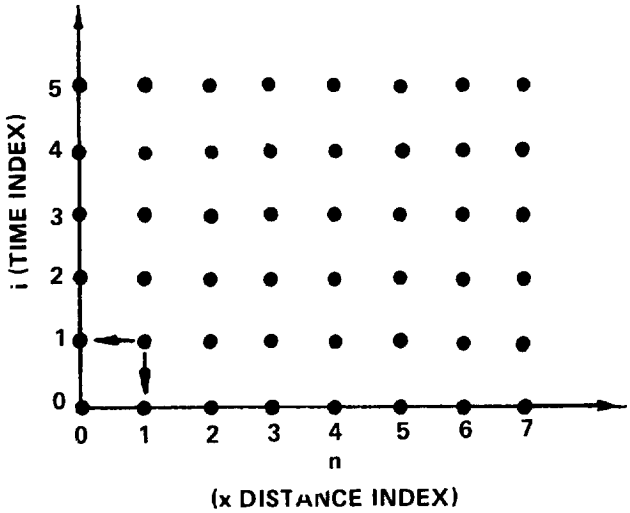

Figure 116. Nodal pattern for calculating bulk temperature of flowing fluid.

A computer program which facilitates computations of the type previously outlined is listed in Appendix C. Exploratory calculations have been made, but the predictions have not been corroborated by any experimental data. The program was developed and intended as a tool for investigating the effect of the phase change process, flow rate, and internal convective heat transfer coefficient on the temperature at the exit of a flow passage which exchanges energy with the phase change device. Without some history of comparison with experimental data, the integrity of the results can only be conjectured at this stage.

The following parameters were used in two computer runs to examine the influence of the internal convective heat transfer coefficient inside the flow passage. The results were generated for the case of a sinusoidal variation of the fluid temperature at the inlet of the flow passage. Initially, the flow was stagnant with the fluid in the passage and the entire phase change device considered to be at the fusion temperature of the PCM.

- Length of phase change device – 31.7 cm (1.04 ft)
- Width of phase change device – 7.6 cm (3 in.)
- PCM thickness – 3.8 cm (1.5 in.)
- Flowing fluid – Water
- Flow rate – 1.89 gm/s (15 lb/h)
- PCM fusion temperature – 32.2°C (90°F)
- U_0 variation with fraction of PCM melted, f – $U_0 = 86.02 - 76.45$ f Btu/h-ft^2-°F or $U_0 = 488.36 - 434.03$ f J/s-m^2-°C
- Temperature variation of fluid at passage inlet – $T_{inlet} = 110 + 10 \sin (6.283\ t)$ °F with t (h) or $T_{inlet} = 43.33 + 5.56 \sin (2.26 \times 10^4\ t)$ °C with t (s)
- Convective heat transfer coefficient inside flow passage – 1st Run: h = 283.86 J/s-m^2-°C (50 Btu/h-ft^2-°F); 2nd Run: h = 28.39 J/s-m^2-°C (5 Btu/h-ft^2-°F).

The results for the fluid temperature at the exit of the flow passage are shown in comparison to the inlet temperature variation in Figure 117. For both heat transfer coefficients, the temperature drop across the passage decreases as the PCM melts (as would be expected). The relative influence of the heat transfer coefficient on the temperature drop across the passage is evident.

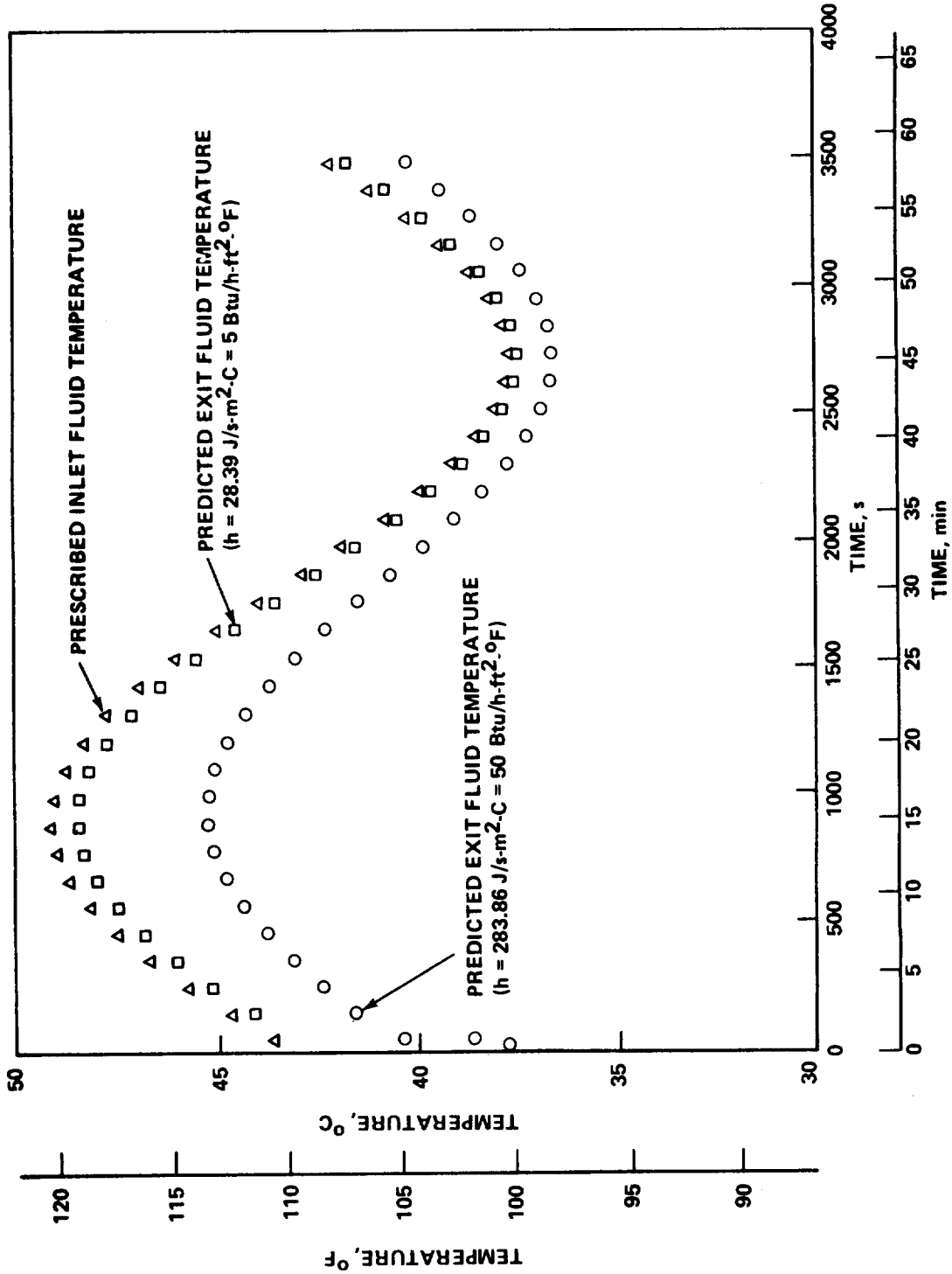

Figure 117. Example exit temperature variations for a sinusoidal temperature at inlet.

APPENDIX A

PROPERTY APPENDIX

Tabulations of certain properties for a number of phase change materials are given in this appendix. They have been included principally to serve as a convenient reference for the user; they are not intended to be exhaustive. For more detail regarding the advantages and disadvantages of the listed materials, the referenced literature should be consulted.

Following is an index for the tabulations:

Table A-1. Fusible Materials with a Heat of Fusion Greater than 185.96 kJ/kg (80 Btu/lb) Listed in Order of Increasing Melt Temperature from 4.4 to 65°C (40 to 150°F). (Table 3-1 of Reference 15).

Table A-2. Comparisons of Fusion Properties of Selected PCM's Reported in Reference 56 (From Table 3 of Reference 56)

Table A-3. Properties of Six PCM's Studied in Reference 57 with a Fusion Temperature Between 273 and 373 K (From Table 2 of Reference 57)

Table A-4. Melt Temperatures of Fifteen Low Temperature PCM Candidates (From Table 6 of Reference 57)

Table A-5. Four Low Temperature PCM's Recommended in Reference 57 (From Table 7 of Reference 57)

Table A-6. PCM's Used in Tests Reported in Reference 58 (From Table 1 of Reference 58)

Table A-7. Comparative Data on Waxes and Inorganic Hydrates (From Reference 59)

Table A-8. Melting Temperature of Some Mixtures Investigated for Air Conditioning Thermal Energy Storage (From Table 3-1 of Reference 1)

Table A-9. Melting Temperature and Heat of Fusion of Inorganic Salt Hydrates (From Table 3-3 of Reference 1)

Table A-10. Melting Point, Heat of Fusion, and Latent Heat Density of Some Inorganic Hydrates (From Table 3-4 of Reference 1)

Table A-11. Melting Temperature and Heat of Fusion of Some Inorganic Hydrate Eutectics (From Table 3-5 of Reference 1)

Table A-12. Calorimetric Data for Some Organic Thermal Energy Storage Materials for Solar Heating (From Table 3-6 of Reference 1)

Table A-13. Melting Temperature and Heat of Fusion of Organic Materials for Air Conditioning-Hydrocarbons and Halogenated Hydrocarbons (From Table 3-7 of Reference 1)

Table A-14. Melting Point and Heat of Fusion for Some Organic Eutectics (From Table 3-7 of Reference 1)

Table A-15. Melting Temperature and Heat of Fusion for Some Acetamide-Organic Eutectics and Compounds (From Table 3-7 of Reference 1)

Table A-16. PCM Data for Some Alcohols, Phenols, Aldehydes, Ketones, and Ethers (From Table 3-7 of Reference 1)

Table A-17. PCM Data for Organic Acids and Miscellaneous Organics (From Table 3-7 of Reference 1)

Table A-18. Calorimetric Data for Air Conditioning Organic Materials (From Table 3-8 of Reference 1)

Table A-19. Melting Point and Heat of Fusion for Clathrates and Semi-Clathrates Melting Congruently Above 0°C (32°F) (From Table 3-9 of Reference 1)

Table A-20. Melting Point for Organic-Inorganic Eutectics (From Table 3-10 of Reference 1).

TABLE A-1. FUSIBLE MATERIALS WITH A HEAT OF FUSION GREATER THAN 185.96 kJ/kg (80 Btu/lb) LISTED IN ORDER OF INCREASING MELT TEMPERATURE FROM 4.4 TO 65°C (40 TO 150°F). (FROM TABLE 3-1 OF REFERENCE 15).

Material	Melting Point °C (°F)	Heat of Fusion kJ/kg (Btu/lb)
Tetradecane $C_{14}H_{30}$	5.6 (42)	227.6 (98)
Formic Acid HCOOH	7.8 (46)	246.1 (106)
Pentadecane $C_{15}H_{32}$	10 (50)	206.7 (89)
Myristic Acid Ethyl Ester $CH_3(CH_2)_{12}COOC_2H_5$	11 (51)	185.8 (80)
Acetic Acid CH_3CO_2H	17 (62)	185.8 (80)
Hexadecane $C_{16}H_{34}$	18 (64)	236.8 (102)
Lithium Chloride Ethanolate $LiCl{\cdot}4C_2H_{60}$	21 (69)	185.8 (80)
n-Heptadecane $C_{17}H_{36}$	22 (71)	213.6 (92)
d-Lactic Acid $CH_3CHOHCOOH$	26 (79)	185.8 (80)
Octadecane $C_{18}H_{38}$	28 (82)	243.8 (105)
13-Methyl Pentacosane $C_{26}H_{54}$	29 (84)	195.1 (84)
Methyl Palmitate $C_{27}H_{34}O_2$	29 (84)	104.3 (88)
Nonadecane $C_{19}H_{40}$	32 (90)	220.6 (95)
Trimyristin $(C_{13}H_{27}COO)_3C_3H_3$	33 (91)	202.0 (87)
2-Dimethyl-n-docosane $C_{24}H_{50}$	35 (95)	197.4 (85)
Eicosane $C_{20}H_{42}$	37 (98)	246.1 (106)
1-Tetradecanol $CH_3(CH_2)_{12}CH_2OH$	38 (100)	229.9 (99)
Camphenilone $C_9H_{14}O$	39 (102)	204.3 (88)
Caprylone $(CH_3(CH_2)_6)_2CO$	40 (104)	257.7 (111)
Docosyl Bromide $C_{22}H_{45}BR$	40 (104)	202.0 (87)
Heneicosane $C_{21}H_{44}$	41 (105)	213.6 (92)
7-Heptadecamone $C_{17}H_{34}O$	41 (105)	199.7 (86)
1-Cyclohexyloctadecane $C_{24}H_{28}$	41 (106)	218.3 (94)
4-Heptadecanone $C_{17}H_{34}O$	41 (106)	197.4 (85)

TABLE A-1. (Concluded)

Material	Melting Point °C (°F)	Heat of Fusion kJ/kg (Btu/lb)
8-Heptadecanone $C_{17}H_{34}O$	42 (107)	202.0 (87)
Cyanamide CH_2N_2	44 (111)	209.0 (90)
Docosane $C_{22}H_{46}$	44 (112)	248.5 (107)
Methyl Eicosanate $C_{21}H_{42}O_2$	45 (113)	227.6 (98)
Tricosane $C_{23}H_{48}$	47 (117)	232.2 (100)
3-Heptadecanone $C_{17}H_{34}O$	48 (118)	216.0 (93)
2-Eptadecanone $C_{17}H_{34}O$	48 (119)	216.0 (93)
Camphene $C_{10}H_{16}$	50 (122)	239.2 (103)
9-Heptadecanone $C_{17}H_{34}O$	51 (123)	211.3 (91)
Tetracosane $C_{24}H_{50}$	51 (124)	253.1 (109)
Elaidic Acid $C_{18}H_{34}O_2$	51 (124)	218.3 (94)
Methyl Behenate $C_{24}H_{46}O_2$	52 (126)	232.2 (100)
Pentacosane $C_{25}H_{52}$	54 (129)	236.8 (102)
Ethyl Lignocerate $C_{26}H_{52}O_2$	54 (129)	216.0 (93)
Hypo Phosphoric Acid $H_4P_2O_6$	55 (131)	213.6 (92)
n-Hexacosane $C_{26}H_{54}$	56 (133)	255.4 (110)
Myristic Acid $C_{13}H_{27}COOH$	57 (135)	199.7 (86)
Heptacosane $C_{27}H_{56}$	59 (138)	234.5 (101)
Ethyl Cerotate $C_{28}H_{56}O_2$	60 (140)	222.9 (96)
Octacosane $C_{28}H_{58}$	61 (142)	253.1 (109)
Nonacosane $C_{29}H_{60}$	64 (147)	239.2 (103)
Stearic Acid $C_{17}H_{35}CO_2H$	64 (148)	199.7 (86)
Triacontane $C_{30}H_{62}$	65 (150)	250.8 (108)

TABLE A-2. COMPARISONS OF FUSION PROPERTIES AND MELT TEMPERATURE OF SELECTED PCM'S REPORTED IN REFERENCE 56 (FROM TABLE 3 AND MELT TEMPERATURE OF REFERENCE 56)

	Formic Acid	Tetradecane	Damphene	Eicosane	Hexadecane	Octadecane
Heat of Fusion kJ/kg (Btu/lb)						
From Literature	246.1 (106)	227.6 (98)	239.2 (103)	246.1 (106)	236.8 (102)	243.8 (105
Melt Temperature °C (°F)						
From Literature	7.8 (46)	5.6 (42)	50 (122)	36.7 (98)	17.8 (64)	27.8 (82)
Supplier[a]	—	1.7-3.9 (35-39)	35-45 (95-113)	36.1-37.8 (97-100)	16.7-17.8 (62-64)	27.2-28.9 (81-84)
Tests[a]	8.3 (47)	5 (41)	40.6-46.1 (105-115)	36.7 (98)	16.1 (98)	27.2 (81)
Supercooling to	0.6-1.7 (33-35)	None Observed	No Sharp Complete Crystallization Point	None Observed	None Observed	None Observed

a. As reported in Reference 56.

TABLE A-3. PROPERTIES OF SIX PCM'S STUDIED IN REFERENCE 57 WITH A FUSION TEMPERATURE BETWEEN 273 AND 373 K (FROM TABLE 2 OF REFERENCE 57)

PCM	Formula	Melt Temperature K (°R)	Heat of Fusion $\frac{kJ}{kg}\left(\frac{Btu}{lb}\right)$	Phase	Density $\frac{kg}{m^3}\left(\frac{lbm}{ft^3}\right)$	Thermal Conductivity $\frac{W}{m\text{-}^\circ C}\left(\frac{Btu}{h\text{-}ft\text{-}^\circ F}\right)$	Constant Pressure Specific Heat $\frac{kJ}{kg\text{-}^\circ C}$ $\frac{Btu}{lbm\text{-}^\circ F}$
Octadecane	$C_{18}H_{38}$	301 (541.8)	242.2 (104.4)	Solid Liquid	810 (50.6) 770 (48.1)	0.15 (0.087) 0.15 (0.087)	2.18 (0.52) 2.18 (0.52)
Lithium Nitrate Trihydrate	$LiNO_3 \cdot 3H_2O$	303 (545.4)	296.5 (127.8)	Solid Liquid	1550 (96.8) 1430 (89.3)	0.50 (0.29) 0.50 (0.29)	2.09 (0.50) 2.09 (0.50)
Sodium Hydrogen Phosphate Dodecahydrate	$Na_2HPO_4 \cdot 12H_2O$	309 (556.2)	279.8 (120.6)	Solid Liquid	1520 (94.9) 1450 (90.5)	0.51 (0.30) 0.48 (0.28)	1.67 (0.40) 1.93 (0.46)
Myristic Acid	$CH_3(CH_2)_{12}COOH$	331 (595.8)	200.5 (86.4)	Solid Liquid	860 (53.7) 860 (53.7)	0.10 (0.058) 0.10 (0.058)	1.59 (0.38) 2.26 (0.54)
Cerrobend	Alloy	343 (617.4)	33.4 (14.4)	Solid Liquid	9400 (586.8) 9200 (574.3)	18.8 (10.89) 18.8 (10.89)	0.17 (0.04) 0.17 (0.04)
Acetamide	CH_3CONH_2	354 (637.2)	242.2 (104.4)	Solid Liquid	1160 (72.4)	0.25 (0.15) 0.25 (0.15)	2.80 (0.67) 2.80 (0.67)

TABLE A-4. MELT TEMPERATURES OF FIFTEEN LOW TEMPERATURE PCM CANDIDATES (FROM TABLE 6 OF REFERENCE 57)

PCM	Melt Temperature K (°R)
n-Dodecane	263.4 (474.1)
Transit-Heat	257.2 (463.0)
Formic Acid/Formamide (75.5/24.5)	256.4 (461.5)
Transit-Heat	252.2 (414.0)
Acetic Acid/Formic Acid (53.1/46.9)	250.7 (451.3)
Acetic Acid/Water (58%)	246.8 (444.2)
n-Decane	243.3 (437.9)
Formic Acid/Potassium Formate (75/25)	241.7 (435.1)
Heptanone-4	240.2 (432.4)
Hydrazine Hydrate ($N_2H_4 \cdot H_2O$)	233.2 (419.8)
Monomethylhydrazine	220.8 (397.4)
Tricaproin	213 (383.4)
Tributyrin	198 (356.4)
Ammonia	195 (351.0)
Ammonia Hydrate ($NH_3 \cdot H_2O$)	194 (349.2)

TABLE A-5. FOUR LOW TEMPERATURE PCM'S RECOMMENDED IN REFERENCE 57
(FROM TABLE 7 OF REFERENCE 57)

PCM	Melt Temperature K (°R)	Heat of Fusion $\frac{kJ}{kg}\left(\frac{Btu}{lb}\right)$	Phase	Density $\frac{kg}{m^3}\left(\frac{lb}{ft^3}\right)$	Thermal Conductivity $\frac{W}{m\text{-}°C}\left(\frac{Btu}{h\text{-}ft\text{-}°F}\right)$	Constant Pressure Specific Heat $\frac{kJ}{kg\text{-}°C}\left(\frac{Btu}{lb\text{-}°F}\right)$
n-Dodecane	263 (473.4)	214.6 (92.3)	Solid Liquid	800[a] (49.9) 750 (46.8)	>0.146[a] (>0.085)[a] 0.138 (0.080)	2.18[a] (0.521)[a] 2.18[a] (0.521)[a]
Heptanone-4	240 (432)	>209.2[a] (90.0)[a]	Solid Liquid	Unknown 822 (51.3)	Unknown 0.142[a] (0.082)[a]	Unknown 2.18[a] (0.522)[a]
Tricaproin	213 (383.4)	>209.2[a] (90.0)[a]	Solid Liquid	Unknown 987 (61.6)	Unknown 0.088[a] (0.051)[a]	Unknown 1.8[a] (0.430)[a]
Ammonia	195 (351)	334.7 (144)	Solid Liquid	720 (44.9) 817 (51.0)	Unknown 0.502 (0.29)	Unknown 4.38 (1.046)

a. Represents estimated data.

TABLE A-6. PCM'S USED IN TESTS REPORTED IN REFERENCE 58
(FROM TABLE 1 OF REFERENCE 58)

Pairings	Name	Formula	Melting Point °C (°F)	Density $\frac{kg}{m^3}\left(\frac{lb}{ft^3}\right)$	Surface Tension $\frac{N}{m}\left(\frac{lb}{ft}\right)$
	n-Octadecane	$C_{18}H_{38}$	28.0 (82.4)	774 (48.3)	27.45×10^{-3} (18.80×10^{-6})
1	Tripalmitin	$C_{51}H_{98}O_6$	65.1 (149.2)	866 (54.1)	28.78×10^{-3} (19.71×10^{-6})
	m-Phenylenediamine	$C_6H_8O_2$	62.8 (145.1)	1107 (49.1)	42.2×10^{-3} (28.90×10^{-6})
2	Trilavrin	$C_{39}H_{74}O_6$	46.5 (115.7)	891 (55.6)	20.0×10^{-3} (20.55×10^{-6})
	O-Iodonitro	$C_6H_4INO_2$	49.4 (120.9)	1810 (113.0)	43.1×10^{-3} (29.52×10^{-6})
3	n-Tetracosane	$C_{24}H_{50}$	54.0 (129.2)	779 (48.6)	30.0×10^{-3} (20.55×10^{-6})
	Tristearin	$C_{57}H_{110}O_6$	54.5 (130.1)	862 (53.8)	—
4	n-Octacosane	$C_{28}H_{58}$	65.0 (149.0)	779 (48.6)	—
	Tripalmitin	$C_{51}H_{98}O_6$	65.1 (149.2)	866 (54.1)	28.78×10^{-3} (19.71×10^{-6})

TABLE A-7. COMPARATIVE DATA ON WAXES AND INORGANIC HYDRATES (FROM REFERENCE 59)

	Candidate Materials	
	Waxes (Paraffins and Microcrystalline)	Inorganic Hydrates
Materials Compatibility	Compatible with most metals and plastics, waxes generally nonreactive and stable	Unknown, material composition proprietary
Thermal Properties	Heat of Fusion: ~1.67 (10^5)J/kg (~71.8 Btu/lb) Specific Heat: Solid – 1886-2019 J/kg°C (0.45-0.48 Btu/lb-°F) Liquid – 2019-2837 J/kg°C (0.48-0.68 Btu/lb-°F) Thermal Conductivity: ~0.146 J/m-s-°C (~0.085 Btu/h-ft-°F) Expansion on Liquification: 15-20%	Heat of Fusion: ~2.6 (10^5)J/kg (~111.9 Btu/lb) Specific Heat: Solid – 1464-2092 J/kg°C (0.35-0.50 Btu/lbm-°F) Liquid – 2092-3347 J/kg°C (0.50-0.80 Btu/lb-°F) Thermal Conductivity: Unknown Expansion on Liquification: Unknown
Maximum Allowable Temperature	200°C (400°F) (Higher with oxidation inhibitor)	104°C (220°F) (Limited by decomposition/Vapor generation)
Phase Change Reversibility	High melting temperature paraffins should exhibit minimal supercooling, based on tests of low melting paraffins for many cycles. Microcrystallines should have similar behavior	Unknown, limited test conducted, data insufficient
Fabricability	Small sample fabricated to examine PCM behavior, no special problems	Unknown, proprietary to Royal Industries
Cost/Availability	Cheap, readily available	Uncertain

TABLE A-8. MELTING TEMPERATURE OF SOME MIXTURES INVESTIGATED FOR AIR CONDITIONING THERMAL ENERGY STORAGE (FROM TABLE 3-1 OF REFERENCE 1)

Composition	Mole Weight (gram)	Relative Weight (%)	Melting Point °C (°F)
NA_2SO_4	142.04	37.2	
$10\ H_2O$	180.15	47.4	18 (64)
NaCl	58.44	15.4	
Total	380.63	100.0	
Na_2SO_4	142.04	37.8	
$10\ H_2O$	180.15	48.0	10 (50)
NH_4Cl	53.49	14.2	
Total	375.68	100.0	
Na_2SO_4	142.04	37.6	
$10\ H_2O$	180.15	47.6	
1/2 NaCl	29.22	7.7	13 (55)
1/2 NH_4Cl	26.75	7.1	
Total	378.16	100.0	
Na_2SO_4	142.04	35.8	
$10\ H_2O$	180.15	45.4	7 (45)
KCl	74.55	18.8	
Total	396.74	100.0	

TABLE A-9. MELTING TEMPERATURE AND HEAT OF FUSION OF INORGANIC SALT HYDRATES (FROM TABLE 3-3 OF REFERENCE 1)

Compound	Melting Point °C (°F)	Heat of Fusion $\frac{kJ}{kg}\left(\frac{Btu}{lb}\right)$	Remarks
$LiClO_3 \cdot 3H_2O$	8.1 (46.5)	253.1 (108.9)	Needs cold finger to prevent supercooling. Not available commercially The least expensive lithium salt is the carbonate: 1971 carlot price $0.52-$0.46 per lb
$H_2SO_4 \cdot H_2O$	8.6 (47.5)	163.6 (70.4)	Safety hazard. Containerization difficult
$ZnCl_2 \cdot 3H_2O$	10.0 (50.0)		Strong tendency to form glasses
$ZnCl_2 \cdot 5/2H_2O$	13.0 (55.4)		Crystallization velocity at all temperatures very slow. Cold finger needed to prevent glass formation
$K_2HPO_4 \cdot 6H_2O$	11.1-13.3 (52-56)	108.8 (46.8)	Cold finger needed to prevent supercooling
$NaOH \cdot 7/2H_2O$	15.0 (59)	192.5 (82.9)	Safety hazard, containerization difficult
$Na_2CrO_4 \cdot 10H_2O$	18.9 (66)	164.0 (70.6)	Temperature rather high. Requires cold finger to prevent nucleation of different hydrates. 1971 carlot price $0.17 per lb for the anhydrous salt
$CaCl_2 \cdot 6H_2O$	30.0 (86)	170.3 (73.3)	Congruent only if melted quickly. Slow melting forms metastable α-$CaCl_2 \cdot 4H_2O$ incongruently
$LiNO_3 \cdot 3H_2O$	30.0 (86)	295.8 (127.3)	See remarks on $LiClO_3 \cdot 3H_2O$
$Na_2SO_4 \cdot 10H_2O$	(90.3)	(108.0)	Reduction in apparent latent with freeze/melt cycling
$FeCl_3 \cdot 6H_2O$	36.1 (97)	225.9 (97.3)	Forms complex system with HCl. Crystallization velocities at all temperatures very slow Requires cold finger to prevent supercooling

TABLE A-9. (Concluded)

Compound	Melting Point °C (°F)	Heat of Fusion $\frac{kJ}{kg}\left(\frac{Btu}{lb}\right)$	Remarks
$Zn(NO_3)_2 \cdot 6H_2O$	36.1 (97)	133.9 (57.6)	Nucleating agent available; expensive
$Na_2HPO_4 \cdot 12H_2O$	36.1 (97)	279.5 (129.3)	Supercools; nucleates unstable heptahydrate
$Na_2S_2O_3 \cdot 5W$	45 (113)	200.0 (86.1)	Supercools; unstable relative to sulfur and sodium sulfate
$Ca(NO_3)_2 \cdot 4H_2O$	47.2 (117)	161.9 (69.7)	Supercools
$Mg(NO_3)_2 \cdot 6H_2O$	90.0 (194)	159.0 (68.4)	Corrosive
$MgCl_2 \cdot 6H_2O$	115.0 (239)	164.9 (71.0)	Corrosive

TABLE A-10. MELTING POINT, HEAT OF FUSION, AND LATENT HEAT DENSITY OF SOME INORGANIC HYDRATES (FROM TABLE 3-4 OF REFERENCE 1)

Material	Melting Point °C (°F)	Heat of Fusion (Literature) $\frac{kJ}{kg}\left(\frac{Btu}{lb}\right)$	Latent Heat Density $\frac{kJ}{m^3}\left(\frac{Btu}{ft^3}\right)$
$CaCl_2 \cdot 6H_2O$	28.9 (84)	170.2 (73.3)	2.86×10^5 (7688)
$MgCl_2 \cdot 6H_4O$	117.2 (243)	172.3 (74.2)	2.69×10^5 (7226)
$Ca(NO_3)_2 \cdot 4H_2O$	42.8 (109)	142.1 (61.2)	2.59×10^5 (6954)
$Mg(NO_3)_2 \cdot 6H_2O$	95.0 (203)	159.8 (68.8)	2.34×10^5 (6271)
$Zn(NO_3)_2 \cdot 6H_2O$	36.1 (97)	130.0 (56.0)	2.69×10^5 (7219)
$Al(NO_3)_3 \cdot 9H_2O$	70.1 (158)	155.6 (67)[a]	

a. Experimental value

TABLE A-11. MELTING TEMPERATURE AND HEAT OF FUSION OF SOME INORGANIC HYDRATE EUTECTICS (FROM TABLE 3-5 OF REFERENCE 1)

Composition	Wt.%	Melting Point °C (°F)	Heat of Fusion $\frac{kJ}{kg}\left(\frac{Btu}{lb}\right)$
$CaCl_2$ $Ca(NO_3)_2$ H_2O	37 23 approx. 40	13 (56)	
$CaCl_2$ $MgCl_2$ H_2O	41 10 49	25 (57)	174.5 (75.1) Experimental
$CaCl_2$ K Cl NaCl H_2O	48.0 4.3 0.4 47.3	27 (81)	
$Ca(NO_3)_2 \cdot 4H_2O$ $2n(NO_3)_2 \cdot 6H_2O$	45 55	25 (77)	129.7 (55.8) Calculated
$Ca(NO_3)_2 \cdot 4H_2O$ $Mg(NO_3)_2 \cdot 6H_2O$	67 33	30 (86)	136.0 (58.5) Calculated
$Ca(NO_3)_2 \cdot 4H_2O$ $Al(NO_3)_2 \cdot 9H_2O$	72 28	35 (95)	138.9 (59.8) Calculated
$Mg(NO_3)_2 \cdot 6H_2O$ $Al(NO_3)_2 \cdot 9H_2O$	53 47	61 (142)	148.1 (63.8) Calculated
$Mg(NO_3)_2 \cdot 6H_2O$ $2n(NO_3)_2 \cdot 6H_2O$	18 82	32 (90)	130.1 (56.0) Calculated

TABLE A-12. CALORIMETRIC DATA FOR SOME ORGANIC THERMAL ENERGY STORAGE MATERIALS FOR SOLAR HEATING (FROM TABLE 3-6 OF REFERENCE 1)

Material	Supplier	Measurement Temperature Range °C (°F)	Heat of Fusion[a] $\frac{kJ}{kg}\left(\frac{Btu}{lb}\right)$	Heat Storage Density $\frac{kJ}{m^3}\left(\frac{Btu}{ft^3}\right)$
Artificial Spermaceti	Lipo Chemicals	35-47.8 (95-118)	195.0 (84)	1.86×10^5 (5000)
Artificial Spermaceti	Lipo Chemicals	40-47.8 (104-118)	133.9 (58)	1.27×10^5 (3400)
Paraffin Wax +25% Wt. CCl	Arthur H. Thomas	40-50 (104-122)	95.2 (41)	0.89×10^5 (2400)
Paraffin Wax +33% Wt. CCl	Arthur H. Thomas	40-17.18 (104-118)	104.5 (45)	0.93×10^5 (2500)
P116 Paraffin Wax	Sun Oil Company	45.6-46.7 (114-116)	209.0 (90)	1.64×10^5 (4400)

a. Includes specific heat contribution over the indicated temperature range.

TABLE A-13. MELTING TEMPERATURE AND HEAT OF FUSION OF ORGANIC MATERIALS FOR AIR CONDITIONING-HYDROCARBONS AND HALOGENATED HYDROCARBONS (FROM TABLE 3-7 OF REFERENCE 1)

Compound	Melting Point °C (°F)	Heat of Fusion $\frac{kJ}{kg}\left(\frac{Btu}{lb}\right)$
n-Tetradecane	5.9 (42.6)	225.5 (97.1)
n-Pentadecane	9.0 (48.2)	162.9 (70.1)
n-Hexadecane	18.2 (64.8)	233.9 (100.7)
n-Hexadecylbromide	14 (57.2)	—
l-Heptadecane	11.2 (52.2)	131.1 (56.5)
l-Octadecane	17.9 (64.2)	129.1 (55.6)
l-Pentadecyne	10 (50)	—
l-Hexodecyne	15 (59)	—
p-Xylene	13.2 (55.8)	159.9 (68.9)
Tridecylbenzene	10 (50)	168.3 (72.5)
Tetradecylbenzene	16 (60.8)	173.3 (74.6)
2-Nonyl naphthaleno	12 (53.6)	—
3-Chlorobiophenyl	17 (62.6)	—

TABLE A-14. MELTING POINT AND HEAT OF FUSION FOR SOME ORGANIC EUTECTICS (FROM TABLE 3-7 OF REFERENCE 1)

Compound	Mole %	Melting Point °C (°F)	Heat of Fusion $\frac{kJ}{kg}\left(\frac{Btu}{lb}\right)$
α Chloroacetic Acid Phenol	31.0 69.0	16.5 (61.7)	144.1 (62.1)
β Chloroacetic Acid Phenol	35.0 65.0	11.8 (53.2)	138.2 (59.5)
α Chloroacetic Acid p Cresol	28.0 72.0	13.4 (56.1)	141.6 (61.0)
α Chloroacetic Acid o Cresol	30.9 69.1	15.8 (60.4)	189.6 (81.7)
Acetic Acid Benzoic Acid	88.0 12.0	9.5 (49.1)	184.6 (79.5)
Naphthalene Diphenyl Methane	25.0 75.0	14.5 (58.1)	109.0 (46.9)

TABLE A-15. MELTING TEMPERATURE AND HEAT OF FUSION FOR SOME ACETAMIDE-ORGANIC EUTECTICS AND COMPOUNDS (FROM TABLE 3-7 OF REFERENCE 1)

A	Mole % A	Wt. % A	Melting Point °C (°F)	Heat of Fusion $\frac{kJ}{kg}\left(\frac{Btu}{lb}\right)$
Urea	37	37	56.5 (133)	181.3 (78.1) Literature
o-Cresol	46	61	26 (78)	—
Phenol	42	53.5	26.5 (79)	164.5 (70.9) Calculated
Stearic Acid	50	83	65.4 (150)	206.7 (89.0) Calculated 217.2 (93.5) Experimental
Palimtic Acid	50	81	59.1 (138)	178.3 (76.8) Calculated
Palimtic Acid	64.8	89	57.2 (135)	172.1 (74.1) Calculated
Myristic Acid	69.0	89	48.7 (120)	198.8 (85.6) Calculated
Lauric Acid	75.8	91	39.4 (103)	182.9 (78.8) Calculated

TABLE A-16. PCM DATA FOR SOME ALCOHOLS, PHENOLS, ALDEHYDES, KETONES, AND ETHERS (FROM TABLE 3-7 OF REFERENCE 1)

Compound	Melting Point °C (°F)	Heat of Fusion $\frac{kJ}{kg}\left(\frac{Btu}{lb}\right)$
Alcohols and Phenols		
1-Decanol	6.1 (43.0)	
1-Undecanol	15 (59.0)	
Glycerol	18 (64.4)	200.4 (86.2)
m-Cresol	12 (53.6)	94.0 (40.5)
2-Chlorophenol	7 (44.6)	
3,3 Dimethyl Cyclohexanol	11 (51.8)	
Aldehydes, Ketones, and Ethers		
1,4 Dioxane	11.8 (53.2)	145.3 (62.6)
2-Decanone	14 (57.2)	
n-Tridecanol	15 (59.0)	
Parahlehyde	12.6 (54.7)	104.4 (45.0)
2,5 Dichloroaceiophenone	14 (57.2)	

TABLE A-17. PCM DATA FOR ORGANIC ACIDS AND MISCELLANEOUS ORGANICS (FROM TABLE 3-7 OF REFERENCE 1)

Compound	Melting Point °C (°F)	Heat of Fusion $\frac{kJ}{kg}\left(\frac{Btu}{lb}\right)$
Organic Acids		
Formic Acid	8.4 (47.1)	276.7 (119.0)
Acetic Acid	16.6 (61.9)	201.3 (86.6)
Acrylic Acid	12.3 (54.1)	154.9 (66.6)
n-Octanoic Acid	16.3 (61.3)	148.2 (63.7)
n-Nonanoic Acid	12.3 (54.1)	128.1 (55.1)
Oleic Acid	14 (57.2)	
Other		
Diethyl Isophthalate	11.5 (52.7)	
Dimethyl Adipate	8.5 (47.3)	
1,2 Ethylene Diamine	8.5 (47.3)	
m-Cresyl Acetate	12 (53.6)	
2,5 Dimethyl Analine	14.2 (57.7)	

TABLE A-18. CALORIMETRIC DATA FOR AIR CONDITIONING ORGANIC MATERIALS (FROM TABLE 3-8 OF REFERENCE 1)

Material	Supplier	Freezing Point °C (°F)	Melting Point °C (°F)	Heat of Fusion[a] $\frac{kJ}{kg}\left(\frac{Btu}{lb}\right)$	Heat Storage Density $\frac{kJ}{m^3}\left(\frac{Btu}{ft^3}\right)$
C_{14}-C_{16} Paraffin	Conoco	5.6-6.1 (42-43)	1.7-7.2 (35-45)	151.9 (65.4)	1.19×10^5 (3185)
C_{15}-C_{16} Paraffin	Enjay				
Batch No. 1		8.3 (47)	4.4-10 (40-50)	152.6 (65.7)	1.19×10^5 (3200)
Batch No. 2		8.3 (47)	4.4-10 (40-50)	147.2 (63.4)	1.15×10^5 (3080)
1-Decanol	Eastman	5.6 (42)	4.4-7.2 (40-45)	205.7 (88.6)	1.71×10^5 (4590)
C_{15}-C_{18} Olegins	Chevron	3.3 (38)		35.5 (15.3)	0.98×10^5 (780)
C_{14} Paraffin	Humphrey	4.4 (40)	1.7-4.4 (35-40)	165.1 (71.1)	1.27×10^5 (3420)
C_{16} Paraffin	Humphrey	17.8 (64)	14.4-18.3 (58-65)	200.2 (86.2)	1.56×10^5 (4190)

a. Not including any specific heat contribution; the average specific heat of the paraffins between 1.7°C (35°F) and room temperature is 2.8 kJ/kg-°C (0.52 Btu/lb-°F).

TABLE A-19. MELTING POINT AND HEAT OF FUSION FOR CLATHRATES AND SEMI-CLATHRATES MELTING CONGRUENTLY ABOVE 0°C (32°F) (FROM TABLE 3-9 OF REFERENCE 1)

Composition	Melting Point °C (°F)	Heat of Fusion $\frac{kJ}{kg}\left(\frac{Btu}{lb}\right)$
Type I Clathrate Hydrates		
$H_2S \cdot 6.1\ H_2O$	0.4 (33)	
$H_2S \cdot 6.1\ H_2O$	29.5 (85)	
$CO_2 \cdot 6.0\ H_2O$	9.9 (50)	
$Cl_2 \cdot 7.3\ H_2O$	9.7 (50)	
$SO_2 \cdot 6.0\ H_2O$	7.0 (45)	246.9 (106.3) Calculated
$SO_2 \cdot 6.1\ H_2O$	12.1 (54)	
$C_2H_4O \cdot 6.9\ H_2O$	11.1 (52)	
Type II Clathrate Hydrates		
$C_4H_8O \cdot 17.2\ H_2O$ (Tetrahydrofuran)	4.4 (40)	255.2 (109.0) Experimental
$C_4H_8O \cdot 2H_2S \cdot 17\ H_2O$	21.3 (70)	276.1 (118.9) Experimental
$(CH_3)_3COH \cdot 2H_2S \cdot 17H_2O$	7.3 (45)	
Amine Semi-Clathrate Hydrate		
$(CH_3)_3N \cdot 10\ 1/4\ H_2O$	5.9 (43)	238.5 (102.7) Experimental
Tetrabutylammonium Salt Semi-Clathrate Hydrates		
$Bu_4NF \cdot 32H_2O$	24.9 (77)	
$Bu_4NCl \cdot 32H_2O$	15.7 (60)	
$Bu_4NBr \cdot 32H_2O$	12.5 (54)	
$Bu_4NNO_3 \cdot 32H_2O$	5.8 (42)	
$Bu_4NOH \cdot 32H_2O$	30.2 (86)	
$Bu_4NHCO_3 \cdot 32H_2O$	17.8 (64)	
$(Bu_4N)_2HPO_4 \cdot 64H_2O$	17.2 (63)	
$(Bu_4N)_2C_2O_4 \cdot 64H_2O$	16.8 (62)	
$Bu_4NCHO_2 \cdot 32H_2O$	12.5 (54)	184.1 (79.3) Experimental
$Bu_4NCH_3CO_2 \cdot 32H_2O$	15.1 (59)	209.2 (90.1) Experimental
$Bu_4NC_6H_5CO_2 \cdot 32H_2O$	3.5 (38)	
Tetraisoamylammonium Salt Semi-Clathrate Hydrates		
$i\text{-}Am_4NF \cdot 40\ H_2O$	31.2 (88)	
$i\text{-}Am_4NCl \cdot 38\ H_2O$	29.8 (86)	
$i\text{-}Am_4NOH \cdot 40\ H_2O$	31 (88)	
$i\text{-}Am_4NCHO_2 \cdot 40\ H_2O$	15-20 (59-68)	

TABLE A-20. MELTING POINT FOR ORGANIC-INORGANIC EUTECTICS
(FROM TABLE 3-10 OF REFERENCE 1)

Urea Eutectics-Binary			
A	Mole % A	Wt. % A	Melting Point °C (°F)
NH_4Cl	17.5	15.9	101 (214)
NH_4Br	23.5	33.4	76 (169)
NH_4I	25.5	45.2	66 (151)
NH_4NO_3	47.5	54.7	46 (115)
NH_4SCN	39.5	48.4	32 (90)
$LiNO_3$	16	18	76 (169)
$LiNO_3$	45.5	48.1	104 (219)
$NaNO_3$	23	29.5	84 (183)
KNO_3	16	24.3	110 (230)
$Ca(NO_3)_2$	9.4	22	92 (198)
$Ca(NO_3)_2$	25	48	140 (286)
$Sr(NO_3)_2$	15	38	67 (153)
$Ba(NO_3)_2$	10.5	33.8	96 (205)
K_2CO_3	7	14.8	102 (216)

Urea Eutectics-Ternary						
A	B	Mole % A	Wt. % A	Mole % B	Wt. % B	Melting Point °C (°F)
NH_4Cl	NH_4NO_3	4	2.4	46	53	35 (95)
NH_4Cl	NH_4SCN	4	2.5	40	46	20 (68)
NH_4NO_3	$LiNO_3$	34	40	7	7.1	34 (93)
NH_4NO_3	$LiNO_3$	46	51	32	31	65 (149)
NH_4NO_3	$NaNO_3$	41	47	8	9.7	35 (95)
NH_4NO_3	KNO_3	44	49.9	4	5.7	43 (109)
$LiNO_3$	$NaNO_3$	24	26	10	13	56 (133)
$LiNO_3$	$NaNO_3$	45	49	3.5	4.6	100 (212)
$LiNO_3$	KNO_3	16	17	6	9.5	62 (144)
$LiNO_3$	KNO_3	45	43	19	27	96 (205)
$LiNO_3$	$Ca(NO_3)_2$	16.5	18.1	1.5	4	62 (144)
$LiNO_3$	$Ca(NO_3)_2$	41	44.5	4	9.2	82 (180)
$LiNO_3$	$Sr(NO_3)_2$	12	11	8	23	45 (113)
$LiNO_3$	$Ba(NO_3)_2$	16	17	1	4	68 (154)
$LiNO_3$	$Ba(NO_3)_2$	44	46	1	4	92 (198)
$NaNO_3$	KNO_3	22.3	27.7	7	10.3	73 (163)
$NaNO_3$	$Ba(NO_3)_2$	17.5	20.5	4	14.4	68 (154)
KNO_3	$Ca(NO_3)_2$	3	4	14	20	89 (192)
KNO_3	$Ca(NO_3)_2$	18	20	24	42.5	125 (257)
KNO_3	$Ba(NO_3)_2$	8.5	11.5	5.5	19.3	80 (176)

TABLE A-20. (Concluded)

Acetamide Eutectics			
A	Mole % A	Wt. % A	Melting Point °C (°F)
NH_4NO_3	32	39	38 (100)
$LiNO_3$	20	23	25 (77)
$NaNO_3$	15	20	59 (138)
KNO_3	6	9.8	72 (162)

APPENDIX B

THERMAL RESISTANCE VARIATION

Some of the results of the parametric study which are shown in Section V exhibit interesting trends. Specifically, some plots of the temperature rise at the termination of melting versus fin height demonstrate a relative maximum, a relative minimum, or both. Several curves in Figures 51 through 62 indicate this behavior. A plausible explanation of this behavior is presented in this appendix.

The physical model, which was treated in Section IV, is shown in Figure B-1. Heat flows directly from the bottom into the PCM. Heat also flows into the PCM through the fin and top. The relative thermal resistances of these paths is dependent on the geometry.

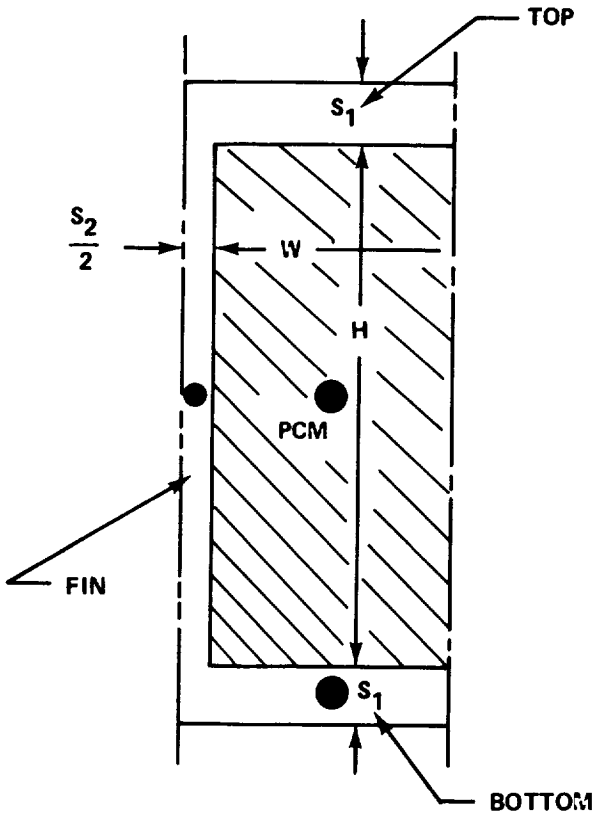

Figure B-1. Physical model.

Some insight into the thermal resistance behavior may be gained by means of a simple but nonexact viewpoint. Suppose the effect of the top is ignored and the PCM and fin are each represented by a single node. The resulting thermal network, including thermal resistances, for the heat flow between the bottom and the PCM is indicated in Figure B-2. The equivalent thermal resistance for this arrangement is related to the parameters by

$$K_{eq} K_w B = 1.0/[2W/H + 2 (K/K_w)HS/(2H^2 + WS(K/K_w)] \quad \text{(B-1)}$$

The right-hand side of equation (B-1) was evaluated for the range of geometrical parameters covered in the parametric study. The thermal conductivity ratio (K/K_w) of 1069 was also used. The results are plotted in Figures B-3 through B-5. The effect of geometry on the equivalent thermal resistance for the simplified network is shown by the curves.

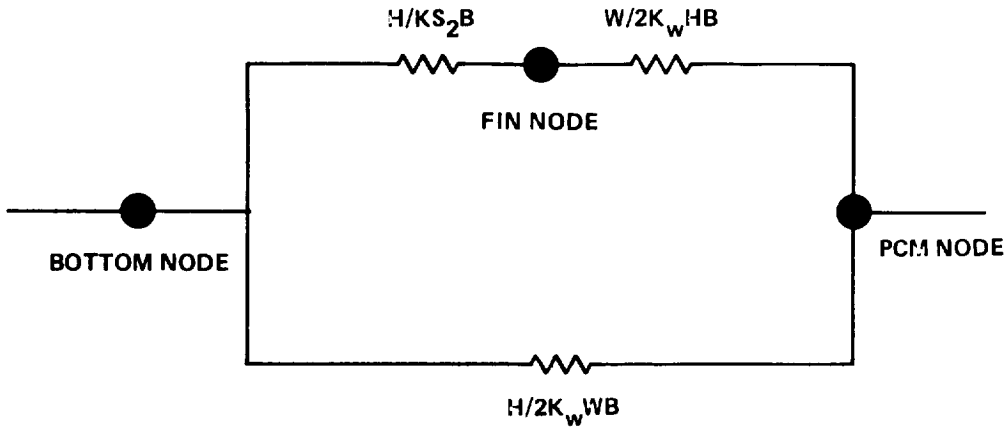

Figure B-2. Simplified thermal network.

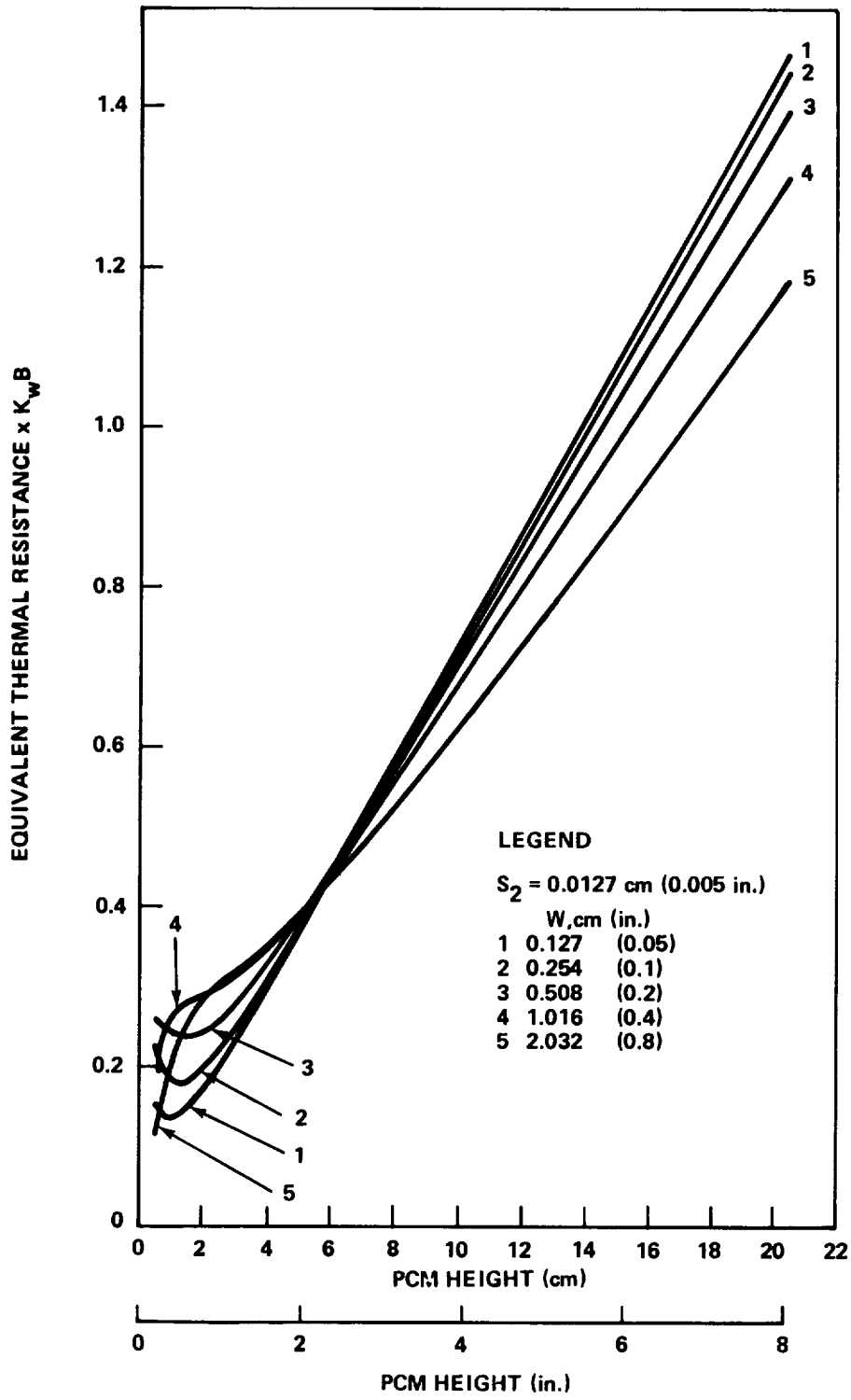

Figure B-3. Variation of equivalent thermal resistance with height for a fin thickness of 0.0127 cm (0.005 in.).

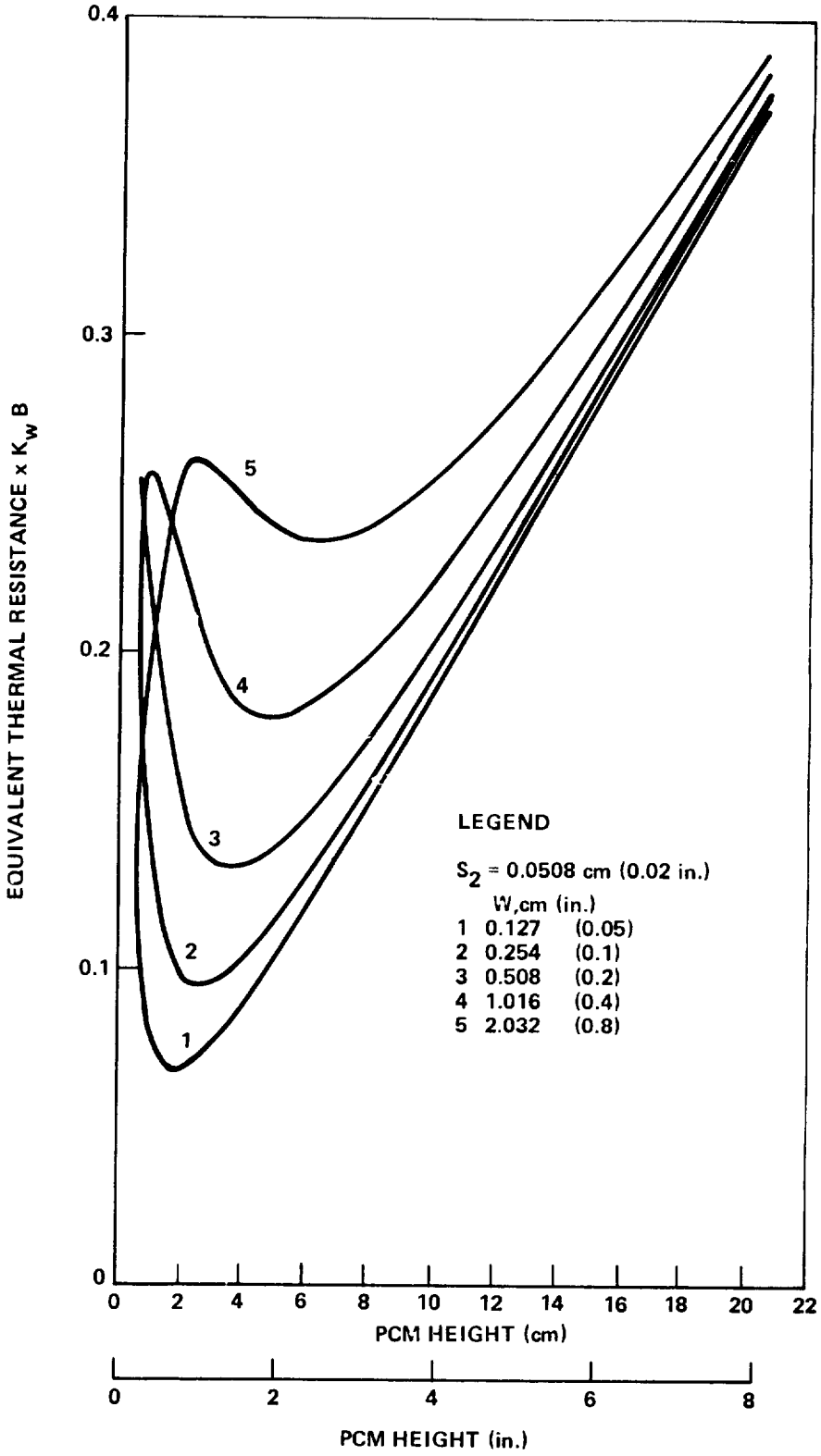

Figure B-4. Variation of equivalent thermal resistance with height for a fin thickness of 0.0508 cm (0.02 in.).

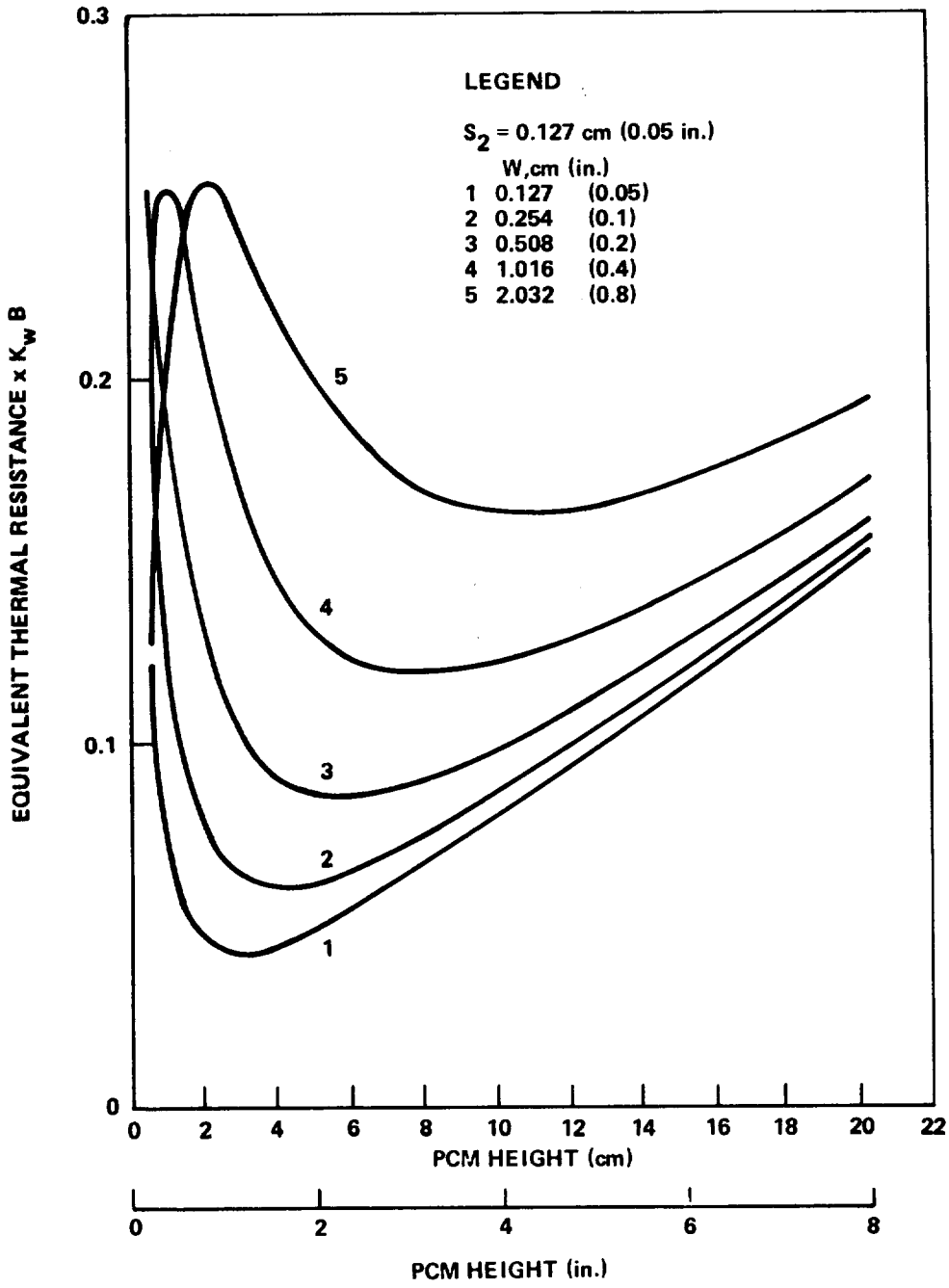

Figure B-5. Variation of equivalent thermal resistance with height for a fin thickness of 0.127 cm (0.05 in.).

APPENDIX C

COMPUTER PROGRAM FOR EXAMPLE DESCRIBED IN SECTION V

An example application of a phase change device with a nonuniform thermal boundary condition is discussed in Section V. The equation used to compute the temperature variation of the flowing fluid is equation (37). The computer program shown in Table C-1 was written to facilitate the calculation of the mean fluid temperature from equation (37). This program occupies approximately 7 K words of storage. The data shown in Table C-2 is required for each run. In addition, the user must supply routines in the function subroutines COEFF and TEMP. COEFF calculates U_0 and TEMP generates the inlet temperature of the fluid. Note that there are provisions for up to three different functions for U_0 and the inlet temperature. The function used during any run is chosen by the data entered in the data card (Table C-2). There are provisions for multiple runs within one computer job. The program reads nine cards, processes the run, and then returns to read nine more. If none are present, the program terminates. For each run, header information is printed, such as flow rates, and fluid and PCM properties. Two time steps are printed simultaneously, one on the left-hand side of the page, the other on the right-hand side of the page. A description of the output data is given in Table C-3. At the end of each run, the total energy stored, QTOT, is printed.

TABLE C-1. COMPUTER PROGRAM USED TO COMPUTE FLUID TEMPERATURE VARIATION AS IT FLOWS THROUGH A PHASE CHANGE DEVICE

```
      REAL LENGTH,MLUMP,MDOT
      INTEGER TIME,TIMECT
      DIMENSION TMEAN(2,500),QTAB(500),OLD2(500),TLUMP(2
     1,500)
      COMMON IBUFF,LINCT,OLDTME,NODECT
 9998 READ (5,100,END=9999) TFREEZ
  100 FORMAT (F10.2)
      READ (5,110) SPHEAT,MDOT,HTXFER,WIDTH,LENGTH,XSTEP
     1,TIMELN,TMESTP
  110 FORMAT (3F10.2/2F10.2,F10.5/F10.2,F10.5)
      READ (5,150) RHO,XSECT
  150 FORMAT (2F10.2)
      READ (5,190) SPAC,VISC,PRAN,COND
  190 FORMAT (4F10.2)
      READ (5,160) HEIGHT,HTFUS,SPHLMP,CONLMP,RHOLMP
  160 FORMAT (F10.5,4F10.2)
      READ (5,170) IWRIT,ISUPX
  170 FORMAT (2I10)
      READ (5,180) ITMPIN,IUORTN
  180 FORMAT (2I10)
      WRITE (6,199)
  199 FORMAT ('1')
      WRITE (6,200)
  200 FORMAT ('0',T49,'*************************************
     1**********************')
      WRITE (6,220) LENGTH,XSECT
  220 FORMAT (' ',T38,'CAPACITOR  * LENGTH ='F7.3,' FT.',T8(
     1,'FLOW PASS.AREA ='F7.4,' SQ.FT.',T115,'*')
      WRITE (6,230) HEIGHT,SPAC
  230 FORMAT (' ',T38,'DIMENSIONS * PCM HEIGHT =',F7.3,'
     1 FT.',T80,'FLOWPASS HEIGHT =',F7.4,' FT.',T115,'*')
      WRITE (6,240) WIDTH
  240 FORMAT (' ',T49,'* H=WIDTH ='F7.4,' FT.',T115,'*')
      WRITE (6,210)
  210 FORMAT (' ',T49,'*************************************
     1*****************************')
      WRITE (6,200)
      WRITE (6,250) MDOT,VISC
  250 FORMAT (' ',T38,'FLUID       * FLOW RATE =',F7.3,' LB
     1/HR.',T80,'VISCOSITY =',F7.4,' LB/FT-HR.',T115,'*')
      WRITE (6,260) SPHEAT,PRAN
  260 FORMAT (' ',T38,'PROPERTIES * SPECIFIC HT =',F5.3,'
     1 BTU/LB-F',T80,'PRAND NO =',F7.3,T115,'*')
      WRITE (6,270) RHO,COND
  270 FORMAT (' ',T49,'* DENSITY =',F7.3,' LB/CUB FT',T80
     1,'THERM COND =',F7.3,' BTU/HR-FT-F',T115,'*')
      WRITE (6,210)
      WRITE (6,200)
      WRITE (6,280) HTFUS,CONLMP
  280 FORMAT (' ',T38,'PCM         * HEAT OF FUS =',F5.0,'
     1 BTU/CUB FT',T80,'THERM COND =',F7.3,' BTU/HR-FT-F'
```

TABLE C-1. (Continued)

```
   2,T115,'*')
    WRITE (6,290) SPHLMP,TFREEZ
290 FORMAT (' ',T38,'PROPERTIES * SPECIFIC HT =',F5.3,'
   1 BTU/LB-F',T80,'FREEZE TEMP =',F5.3,' F',T115,'*')
    WRITE (6,300) RHOLMP
300 FORMAT (' ',T49,'DENSITY =',F7.3,' LB/CUB FT',T115,'
   1*')
    WRITE (6,210)
    WRITE (6,200)
    WRITE (6,310) XSTEP,ITMPIN
310 FORMAT (' ',T38,'RUN        * K-STEP =',F7.4,' FT',T80
   1,'TEMP-IN RTN : ',I1,T115,'*')
    WRITE (6,320) TMESTP,IUORTN
320 FORMAT (' ',T38,'PARAMETERS * TIME-STEP =',F7.3,' HRS
   1',T80,'UO-RTN : ',I1,T115,'*')
    WRITE (6,330) TIMELN
330 FORMAT (' ',T49,'* TIME LENGTH =',F7.3,' HRS',T115,'*'
    WRITE (6,210)
    C1=RHO*XSECT*SPHEAT/TMESTP
    C2=MDOT*SPHEAT/XSTEP
    NODECT=LENGTH/XSTEP+2
    TIMECT=TIMELN/TMESTP
    VOLUME=WIDTH*XSTEP*HEIGHT
    MLUMP=RHOLMP*VOLUME
    UCONST=1/(HEIGHT/(2*CONLMP))
    DIA=2.*SPAC
    REYNO=DIA*MDOT/(RHO*XSECT*VISC)
    IHTSW=1
    IF (HTXFER.EQ.0.0) IHTSW=0
    DO 1 J=1,NODECT
    TMEAN(1,J)=TFREEZ
    TLUMP(1,J)=TFREEZ
  1 QTAB(J)=0.
    IRITSW=IWRIT=1
    IBUFF=0
    LINCT=25
    OLDTME=999.0
    DO 3 TIME=1,TIMECT
    T=TIME*TMESTP
    IF (IRITSW.EQ.IWRIT) IRITSW=0
    IRITSW=IRITSW+1
    TMEAN(2,1)=TEMPIN(ITMPIN,T)
    DO 4 NODE=2,NODECT
    X=(NODE-1)*XSTEP
    UO=COEFF(QTAB(NODE),VOLUME,HTFUS,FRACTN,IUORTN)
    IF (FRACTN.LT.0.99) GO TO 30
    TLUMP(2,NODE)=OLDQ(NODE)/(MLUMP*SPHLMP)+TLUMP(1,NODE)
    TMPPCM=TLUMP(2,NODE)
    UO=UCONST
    GO TO 40
 30 TMPPCM=TFREEZ
```

TABLE C-1. (Continued)

```
   40 IF (IHTSW.EQ.1) GO TO 20
      GRATZ=X/(DIA*REYNO*PRAN)
      HTXFER=(COND/DIA)*HEAT(GRATZ)
   20 C4=(HTXFER*WIDTH*UO)/(UO+HTXFER)
      C5=1/(C1+C2+C4)
      TMEAN(2,NODE)=C5*(C4*TMPPCM+C2*TMEAN(2,NODE-1)+C1
     1*TMEAN(1,NODE))
      QA=C2*(TMEAN(2,NODE)-TMEAN(2,NODE-1))
      QB=C1*(TMEAN(2,NODE)-TMEAN(1,NODE))
      Q=-1*(QA+QB)*TMESTP*XSTEP
      QTAB(NODE)=QTAB(NODE)+Q
      OLDQ(NODE)=Q
      IF (IRITSW.EQ.IWRIT) CALL PRNTIT(TMEAN(2,NODE),QTAB
     1(NODE),FRACTN,UO,T,TMEAN(2,1),X,NODE,HTXFER,ISUPX)
    4 CONTINUE
      DO 2 J=1,NODECT
      TLUMP(1,J)=TLUMP(2,J)
    2 TMEAN(1,J)=TMEAN(2,J)
    3 CONTINUE
      QTOT=0
      DO 10 J=2,NODECT
   10 QTOT=QTOT+QTAB(J)
      WRITE (6,140) QTOT
  140 FORMAT (5X,'QTOT =',F10.2)
      GO TO 9998
 9999 CALL EXIT
      END
      SUBROUTINE PRNTIT(TMEAN,QTAB,FRCTN,JJ,T,TEMPIN,X,NODE
     1,HTXFR,ISUPX)
      DIMENSION TMEAN1(500),QTAB1(500),FRCTN1(500),UO1(500)
     1,HTXFR1(500)
      COMMON IBUFF,LINCT,OLDTME,NODECT
      IF (ISUPX.EQ.0.AND.NODE.NE.NODECT) RETURN
      IF (FRCTN.GT.1.0) FRCTN=1.0
      IF (IBUFF.EQ.0) GO TO 10
      IF (OLDTME.EQ.T) GO TO 20
      IBUFF=0
      OLDTME=T
      GO TO 30
   20 TMEAN1(NODE)=TMEAN
      QTAB1(NODE)=QTAB
      FRCTN1(NODE)=FRCTN
      UO1(NODE)=UO
      HTXFR1(NODE)=HTXFR
      RETURN
   10 IF (OLDTME.EQ.T) GO TO 40
      IBUFF=1
      OLDTME=T
      PRNTTM=OLDTME
      PRNTTP=TEMPIN
      GO TO 20
```

TABLE C-1. (Continued)

```
   30 IF (LINCT.GE.65) GO TO 50
      WRITE (6,100) PRNTTM,PRNTTP,T,TEMPIN
  100 FORMAT ('0',T9,'TIME =',F6.3,T28,'TEMPIN =',F7.2,T84
     1,'TIME =',F6.3,T103,'TEMPIN =',F7.2)
      WRITE (6,140)
      GO TO 40
   50 WRITE (6,110) PRNTTM,PRNTTP,T,TEMPIN
  110 FORMAT ('1',T9,'TIME =',F6.3,T28,'TEMPIN =',F7.2,T84
     1,'TIME =',F6.3,T103,'TEMPIN =',F7.2)
      WRITE (6,140)
  140 FORMAT ('0',T9,'X',T16,'TEMP',T28,'Q',T36,'CHANGE',T47
     1,'UO',T55,'HTXFER',T80,'X',T88,'TEMP',T100,'Q',T109
     2,'CHANGE',T119,'UO',T126,'HTXFER')
      LINCT=4
   40 IF (LINCT.LT.73) GO TO 60
      WRITE (6,160)
  160 FORMAT ('1',T9,'X',T16,'TEMP',T28,'Q',T36,'CHANGE',T47
     1,'UO',T55,'HTXFER',T80,'X',T88,'TEMP',T100,'Q',T109
     2,'CHANGE',T119,'UO',T126,'HTXFER')
      LINCT=2
   60 LINCT=LINCT+1
      WRITE (6,150) X,TMEAN1(NODE),QTA31(NODE),FRCTN1(NODE)
     1,UO1(NODE),HT XFR1(NODE),X,TMEAN,QTA3,FRCTN,UO,HTXFR
  150 FORMAT (' ',6F10.2,11X,6F10.2)
      RETURN
      END
      FUNCTION COEFF(QTAB,VOLUME,HTFUS,FRACTN,IUORTN)
      VOLMLT=QTAB/HTFUS
      FRACTN=ABS(VOLMLT/VOLUME)
      IF (FRACTN.GE.0.99) RETURN
      GO TO (1,2,3),IUORTN
    1 CONTINUE
C     *** USER SUPPLIED UO VARIATION ROUTINE
C     *** GOES BETWEEN STATEMENTS 1&2.
C     *** SELECTED WHEN IUORTN=1.
      IF (FRACTN.GT..25) GO TO 10
      COEFF=106.12-242.56*FRACTN
      RETURN
   10 COEFF=54.32-35.37*FRACTN
      RETURN
    2 CONTINUE
C     *** A SECOND UO VARIATION ROUTINE
C     *** MAY GO BETWEEN STATEMENTS 2&3.
C     *** SELECTED WHEN IUORTN=2.
      COEFF=500.0
      RETURN
    3 CONTINUE
C     *** A THIRD UO VARIATION ROUTINE CAN GO
C     *** AFTER STATEMENT 3.
C     *** SELECTED WHEN IUORTN=3.
      RETURN
```

TABLE C-1. (Concluded)

```
      END
      FUNCTION TEMPIN(ITMPIN,T)
      GO TO (1,2,3),ITMPIN
    1 CONTINUE
C     *** USER SUPPLIED INLET TEMPERATURE
C     *** ROUTINE GOES BETWEEN STATEMENTS
C     *** 1&2. SELECTED WHEN ITEMPIN=1.
      IF (T.GT.1.5) GO TO 10
      TEMPIN=1.38*T
      RETURN
   10 IF (T.GT.5.5) GO TO 20
      TEMPIN=-0.644-12.927*T+9.826*T*T
      RETURN
   20 IF (T.GT.10.5) GO TO 30
      TEMPIN=208.0*SIN((3.1415/15)*T)
      RETURN
   30 IF (T.GT.14.0) GO TO 40
      TEMPIN=1485.165-157.533*T+3.898*T*T
      RETURN
   40 TEMPIN=614.7-40.98*T
      RETURN
    2 CONTINUE
C     *** A SECOND TEMPERATURE VARIATION
C     *** ROUTINE MAY GO BETWEEN STATEMENTS
C     *** 2&3. SELECTED WHEN ITEMPIN=2.
      TEMPIN=100.0+20.0*T
      RETURN
    3 CONTINUE
C     *** A THIRD INLET TEMPERATURE VARIATION
C     *** ROUTINE MAY GO AFTER STATEMENT
C     *** 3. SELECTED WHEN ITEMPIN=3.
      RETURN
      END
      FUNCTION HEAT(GRATZ)
      IF (GRATZ.GT..01) GO TO 10
      EX=-0.26
      HEAT=2.27*GRATZ**EX
      RETURN
   10 IF (GRATZ.GT..03) GO TO 20
      EX=-0.01
      HEAT=7.26*GRATZ**EX
      RETURN
   20 HEAT=7.541
      RETURN
      END
```

TABLE C-2. REQUIRED INPUT DATA FOR THE PROGRAM LISTED IN TABLE C-1

Card Number	Punch Position	Data Description	Units
1	1-10	Freezing temperature of the PCM	°F
2	1-10	Specific heat of working fluid	Btu/lbm-°F
	11-20	Mass flow rate of working fluid	lbm/h
	21-30	Heat transfer coefficient between working fluid and the flow passage wall Note: If this piece of data is omitted, a heat transfer coefficient will be calculated by the program for flow between parallel flat plates	Btu/h-ft^2
3	1-10	Area of flow passage wall over which heat transfer takes place	ft^2
	11-20	Length of the capacitor	ft
	21-30	Length of X increment used in finite difference formula	ft
4	1-10	Duration of the simulation run	h
	11-20	Length of time increment used in finite difference formula	h
5	1-10	Density of the working fluid	lbm/ft^3
	11-20	Cross-sectional area of flow passage	ft^2
6	1-10	Height of the flow passage	ft
	11-20	Viscosity of the working fluid	lbm/ft-h
	21-30	Prandtl number of the working fluid	N/A
	31-40	Thermal conductivity of the working fluid	Btu/h-ft-°F
7	1-10	Height of the PCM	ft
	11-20	Heat of fusion of the PCM	Btu/ft^3
	21-30	Specific heat of the PCM	Btu/lbm-°F
	31-40	Thermal conductivity of the PCM	Btu/h-ft-°F
	41-50	Density of the PCM	lbm/ft^3
8	10	An integer number, N, that specifies the number of time increments between prints	N/A
	20	A blank here will cause only information about the last node to be printed. An integer 1 will cause information about all nodes to be printed	N/A

TABLE C-2. (Concluded)

Card Number	Punch Position	Data Description	Units
9	10	An integer 1, 2, or 3. This number selects which inlet temperature routine will be used	N/A
	20	An integer 1, 2, or 3 that selects the U_0 generator routine that will be used	N/A
		Note: These routines must be user supplied. They will go in the COEFF and the TEMPIN function subroutines	

TABLE C-3. DESCRIPTION OF OUTPUT DATA FROM PROGRAM LISTED IN TABLE C-1

Data Name	Description	Units
TEMP IN	Fluid inlet temperature	°F
X	X location in the capacitor	ft
TEMP	Temperature at X	°F
Q	Accumulated heat transfer into the PCM at X	Btu
CHANGE	Fraction undergone change of phase	
UO	U_0	$\frac{\text{Btu}}{\text{h-ft}^2\text{-°F}}$
HTXFER	Convective heat transfer coefficient between fluid and flow passage wall	$\frac{\text{Btu}}{\text{h-ft}^2\text{-°F}}$

APPENDIX D

COMPUTER PROGRAM USED TO FACILITATE THE EXPLICIT NUMERICAL STUDY

The computer program used to facilitate the explicit numerical study is outlined and described in this appendix. A copy of the program for a melting run with inclusion of convective effects is given in Section D.1; the corresponding notation is described in Section D.2; and the steps are discussed in Section D.3.

After listing this program, it was discovered that the program described in Section D.1 would not run for the case of M = 1. The statements causing this incompatibility are indicated in Section D.1 by an arrow placed at the left of the appropriate statement.

A copy of the computer program for a solidification case is given in Section D.4. A comparison of the appropriate statements with those shown in Section D.3 generally illustrates the modification to accommodate M = 1.

The statements which were included in the solidification program to allow for changing the effective interfacial area for nodes experiencing melting are underlined.

D.1. COMPUTER PROGRAM FOR MELTING

```
      DIMENSION  RV(5,31) , RH(5,31) , C(5,31) , QS(5,31), T1(5,31)
      DIMENSION T2(5,31) , F(5,31) , Q(5,31) , QRAT(5,31), T3(1,31)
      DIMENSION TM1(9), TM2(9), TM3(9), TM4(9), TIM(9)
      DIMENSION QRA2(5, 31)
 COMPUTATIONAL PARAMETERS
      N=27
      M=4
      AM=M
      MM=M+1
      NN=N+2
      NJ=N+3
      NI=N+4
      ND=9
      NDP=8
      TAU=1.1
      KCOUNT=1
      MCOUNT=1
      MFIN=500
      EPS=1.E-06
      KCHK=1000
      JOE=1
      DT=1.0E-04
      TAU2=(10.*DT)+(DT/3.)
 PHYSICAL PROPERTIES
      TAMB=80.
      TIN=73.5
      HTOP=1.E-08
      HBOT=5.0
      G=(32.2*3600.*3600.)
  WAX
      DEN=47.2
      TK=0.087
      CP=0.5
      TTR=73.04
      HTR=22.108
      TMELT=89.8
      HMELT=73.357
      TREF=50.0
      BETA=0.00045
      VIS=14.3
      CL=CP
      TKL=TK
  BOTTOM PLATE DENOTED BY 1
      DEN1=171.0
      TK1=93.0
      CP1=0.22
  FIN DENOTED BY 2
      DEN2=171.0
      TK2=93.0
      CP2=0.22
  TOP PLATE DENOTED BY 3
      DEN3=72.5
      TK3=0.09
      CP3=0.33
```

```
      GEOMETRY PARAMETERS
         W=0.75/12.0
         H=2.625/12.0
         B=5.0/12.0
         S=W/(2.0*AM)
         S1=0.032/12.0
         S2=0.008/12.0
         S3=0.25/12.0
         F2JM=1.0/(32.0*S*12.0)
       VERTICAL RESISTANCES
         RV(1,2)=(S1/(TK1*S2*B))+(2./(HBOT*S2*B))
         DO 10 I=2,MM
      10 RV(I,2)=(S1/(2.*TK1*S*B))+(1./(HBOT*S*B))
         RV(1,3)=(S/(TK2*S2*B))+(S1/(TK1*S2*B))
         DO 20 I=2,MM
      20 RV(I,3)=(1./(2.*TK*B))+(S1/(2.*TK1*S*B))
         DO 30 J=4,NN
      30 RV(1,J)=((2.*S)/(TK2*S2*B))
         DO 40 J=4,NN
         DO 40 I=2,MM
      40 RV(I,J)=(1./(TK*B))
         RV(1,N+3)=(S3/(TK3*S2*B))+(S/(TK2*S2*B))
         DO 50 I=2,MM
      50 RV(I,N+3)=(S3/(2.*TK3*S*B))+(1./(2.*TK*B))
         RV(1,N+4)=(S3/(TK3*S2*B))+(2./(HTOP*S2*B))
         RV(2,N+4)=(S3/(2.*TK3*B*(S+(S2/2.))))+(1./(HTOP*B*(S+(S2/2.))))
         DO 60 I=3,MM
      60 RV(I,N+4)=(S3/(2.*TK3*S*B))+(1./(HTOP*S*B))
       HORIZONTAL RESISTANCES
         RH(2,N+3)=((S2+S)/(2.*TK3*S3*B))
         DO 70 I=3,MM
      70 RH(I,N+3)=(S/(TK3*S3*B))
         DO 80 J=3,NN
      80 RH(2,J)=(S2/(2.*TK2*S*B))+(1./(2.*TK*B))
         DO 90 J=3,NN
         DO 90 I=3,MM
      90 RH(I,J)=(1./(TK*B))
         RH(2,2)=((S2+S)/(2.*TK1*S1*B))
         DO 100 I=3,MM
     100 RH(I,2)=(S/(TK1*S1*B))
         RH(2,N+3)=RH(2,N+3)+RV(1,N+3)
      NODAL CAPACITANCES
         C(1,2)=((DEN1*S1*S2*B*CP1)/2.)
         DO 110 I=2,MM
     110 C(I,2)=(DEN1*S1*S*B*CP1)
         DO 120 J=3,NN
     120 C(1,J)=((DEN2*S2*S*B*CP2)/2.)
         C(1,N+3)=((DEN3*S2*S3*B*CP3)/2.)
         C(2,N+3)=(S3*B*(S+(S2/2.))*DEN3*CP3)
         DO 130 I=3,MM
     130 C(I,N+3)=(DEN3*S3*S*B*CP3)
         DO 140 J=3,NN
         DO 140 I=2,MM
     140 C(I,J)=(DEN*(S**2)*B*CP)
         Q1=(C(3,4)*(TTR-TREF))
         Q2=Q1+((DEN*(S**2)*B*HTR))
```

```
      Q3=Q2+((C(3,4))*(TMELT-TTR))
      Q4=Q3+((DEN*(S**2)*B*HMELT))
C  INITIALIZATION OF PERTINENT QUANTITIES
      TIME=0.0
      QWAX=0.0
      QBW=0.0
      QSW=0.0
      QTW=0.0
      QTOP=0.0
      QFTR=0.0
      QTTR=0.0
      V1=0.0
      V2=0.0
      DMO=0.0
      DO 150 J=2,NJ
      DO 150 I=1,MM
  150 T1(I,J)=TIN
      IF(TIN.LT.TTR)QSIN=(C(3,4)*(TIN-TREF))
      IF(TIN.GT.TTR.AND.TIN.LT.TMELT) QSIN=Q2+((C(3,4))*(TIN-TTR))
      IF(TIN.GT.TMELT)QSIN=Q4+((C(3,4))*(TIN-TMELT))
      DO 160 I=1,MM
  160 T1(I,N+4)=TAMB
      DO 170 J=3,NN
      DO 170 I=2,MM
  170 QS(I,J)=QSIN
      DO 180 I=1,MM
      Q(I,2)=0.0
  180 Q(I,N+3)=0.0
      DO 190 J=3,NN
  190 Q(1,J)=0.0
      DO 199 J=2,NI
      DO 199 I=1,MM
      F(I,J)=0.0
  199 QRAT(I,J)=0.0
      READ(5,11) (TM1(I), I=1,ND)
      READ(5,11) (TM2(I), I=1,ND)
      READ(5,11) (TM3(I), I=1,ND)
      READ(5,11) (TM4(I), I=1,ND)
      READ(5,11) (TIM(I), I=1,ND
   11 FORMAT(8F10.0)
      WRITE(6,22) TIME,W,H,N,M
   22 FORMAT(1X,5HTIME=,E15.8,10X,2HW=,E15.8,10X,2HH=,E15.8,10X,2HN=,I2,
     15X,2HM=,I2)
      WRITE(6,33)Q1,Q2,Q3,Q4
   33 FORMAT(1X,3HQ1=,E15.8,10X,3HQ2=,E15.8,10X,3HQ3=,E15.8,10X,3HQ4=,E1
     5.8)
      WRITE(6,44)
   44 FORMAT(2X,4HI J,5X,19HVERTICAL RESISTANCE,6X,21HHORIZONTAL RESIST
     ANCE,6X,17HNODAL CAPACITANCE,6X,11HTEMPERATURE,5X,7HQS(I,J))
      DO 200 J=2,NI
      DO 200 I=1,MM
      IF(J.EQ.N+4) GO TO 1
      GO TO 2
    1 QS(1,J)=0.0
      RH(I,J)=1.E08
      C(I,J)=0.0
```

```
167      2 IF(I.EQ.1)RH(I,J)=1.E08
168        IF(J.EQ.2.OR.J.EQ.N+3)QS(I,J)=0.0
169        IF(I.EQ.1)QS(I,J)=0.0
170        WRITE(6,55)I,J,RV(I,J),RH(I,J),C(I,J),T1(I,J),QS(I,J)
171     55 FORMAT(1X,I2,1X,I2,5X,E15.8,10X,E15.8,10X,E15.8,6X,E16.8,4X,E15.8)
172    200 CONTINUE
173        DO 889 J=3,NN
174    889 T3(1,J)=T1(1,J)
175    COMPUTATION SECTION  COMPUTATION SECTION COMPUTATION SECTION
176      3 TIME=TIME+DT
177        DO 210 J=3,NJ
178        QRAT(1,J)=((T1(2,J)-T1(1,J))/RH(2,J))+((T1(1,J-1)-T1(1,J))/RV(1,J)
179        +((T1(1,J+1)-T1(1,J))/RV(1,J+1))
180        QRAT(MM,J)=((T1(M,J)-T1(MM,J))/RH(MM,J))+((T1(MM,J-1)-T1(MM,J))/RV
181        (MM,J))+((T1(MM,J+1)-T1(MM,J))/RV(MM,J+1))
182    210 CONTINUE
183        DO 211 J=3,NJ
184  ----> DO 211 I=2,M
185        QRAT(I,J)=((T1(I-1,J)-T1(I,J))/RH(I,J))+((T1(I+1,J)-T1(I,J))/RH(I+
186        1,J))+((T1(I,J-1)-T1(I,J))/RV(I,J))+((T1(I,J+1)-T1(I,J))/RV(I,J+1)
187        )
188    211 CONTINUE
189    212 DO 220 J=3,NJ
190        DO 220 I=1,MM
191    220 QS(I,J)=QS(I,J)+(QRAT(I,J)*DT)
192        DO 240 I=2,MM
193    240 T2(I,N+3)=T1(I,N+3)+((QRAT(I,N+3)*DT)/C(I,N+3))
194        T2(1,N+3)=T2(2,N+3)
195        DO 250 J=3,NN
196        DO 250 I=2,MM
197        IF(QS(I,J).LT.Q1)T2(I,J)=TREF+(QS(I,J)/C(I,J))
198        IF(QS(I,J).GE.Q1.AND.QS(I,J).LE.Q2) T2(I,J)=TTR
199        IF(QS(I,J).GT.Q2.AND.QS(I,J).LT.Q3) T2(I,J)=TTR+((QS(I,J)-Q2)/C(I,
           J))
200        IF(QS(I,J).GE.Q3.AND.QS(I,J).LE.Q4) T2(I,J)=TMELT
201      WHEN GOING FROM MELT TO FREEZE OR VICE-VERSA CHANGE THE FOLLOWING CARD
202        IF(QS(I,J).GT.Q3.AND.QS(I,J).LT.Q4) F(I,J)=(QS(1,J)-Q3)/(DEN*(S**2
203        )*B*HMELT)
204        IF(QS(I,J)GT.Q4)  T2(I,J)=TMELT+((QS(I,J)-Q4)/C(I,J))
205      WHEN GOING FROM MELT TO FREEZE OR VICE-VERSA CHANGE THE FOLLOWING CARD
206        IF(QS(I,J).GE.Q4)F(I,J)=1.0
207        IF(QS(I,J).LE.Q3) F(I,J)=0.0
208    250 CONTINUE
209    SPECIFICATION AND/OR DETERMINATION OF FIN TEMPERATURES
210             THE FOLLOWING DO LOOP ASSUMES FIN TEMPERATURES FOR ITERATION
211        DO 255 J=3,NN
212    255 T2(1,J)=T3(1,J)
213        DO 260 L=1,NDP
214        IF(TIME.GE.TIM(L).AND.TIME.LE.TIM(L+1)) GO TO 4
215    260 CONTINUE
216      4 FAC=(TIME-TIM(L))/(TIM(L+1)-TIM(L))
217        T2(1,2)=TM1(L)+((TM1(L+1)-TM1(L))*FAC)
218        T2(1,8)=TM2(L)+((TM2(L+1)-TM2(L))*FAC)
219        T2(1,15)=TM3(L)+((TM3(L+1)-TM3(L))*FAC)
220        T2(1,21)=TM4(L)+((TM4(L+1)-TM4(L))*FAC)
221        DO 270 I=1,MM
```

```
  270 T2(I,2)=T2(1,2)
UNSPECIFIED FIN TEMPERATURES DETERMINED BY STEADY STATE EQUATIONS
  256 MCOUNT=MCOUNT+1
      DO 280 J=3,NN
      T3(1,J)=T2(1,J)
      IF(J.EQ.8.OR.J.EQ.15) GO TO 5
      IF(J.EQ.21) GO TO 5
      T2(1,J)=((T2(1,J-1)/RV(1,J))+(T2(2,J)/RH(2,J))+(T2(1,J+1)/RV(1,J+1
      )))/((1./RV(1,J))+(1./RH(2,J))+(1./RV(1,J+1)))
    5 CONTINUE
  280 CONTINUE
      IF(MCOUNT.GT.MFIN) GO TO 8
      DO 281 J=3,NN
      DIF=T2(1,J)-T3(1,J)
      IF(ABS(DIF).GT.EPS) GO TO 256
  281 CONTINUE
      IF(JOE.EQ.2) GO TO 285
      JOE=JOE+1
      DO 888 J=3,NJ
      DO 888 I=1,MM
  888 QS(I,J)=QS(I,J)-(QRAT(I,J)*DT)
      DO 282 J=3,NJ
      QRA2(1,J)=((T2(2,J)-T2(1,J))/RH(2,J))+((T2(1,J-1)-T2(1,J))/RV(1,J)
      )+((T2(1,J+1)-T2(1,J))/RV(1,J+1))
      QRA2(MM,J)=((T2(M,J)-T2(MM,J))/RH(MM,J))+((T2(MM,J-1)-T2(MM,J))/RV
      (MM,J))+((T2(MM,J+1)-T2(MM,J))/RV(MM,J+1))
  282 CONTINUE
      DO 283 J=3,NJ
      DO 283 I=2,M
      QRA2(I,J)=((T2(I-1,J)-T2(I,J))/RH(I,J))+((T2(I+1,J)-T2(I,J))/RH(I+
      1,J))+((T2(I,J-1)-T2(I,J))/RV(I,J))+((T2(I,J+1)-T2(I,J))/RV(I,J+1)
      )
  283 CONTINUE
      DO 284 J=3,NJ
      DO 284 I=1,MM
  284 QRAT(I,J)=(QRAT(I,J)+QRA2(I,J))/2.0
      GO TO 212
  285 MCOUNT=1
      DO 286 I=1,MM
  286 QRAT(I,2)=((T2(I,2)-T1(I,2))*C(I,2)/DT)
      DO 287 I=1,MM
  287 QS(I,2)=QS(I,2)+(C(I,2)*(T2(I,2)-T1(I,2)))
      DO 290 I=2,MM
      QBW=(T2(I,2)-T2(I,3))/RV(I,3)+QBW
  290 QTW=(T2(I,N+3)-T2(I,N+2))/RV(I,N+3)+QTW
      QBT=QBW+((T2(1,2)-T2(1,3))/RV(1,3))
      DO 300 J=3,NN
  300 QSW=QSW+((T2(1,J)-T2(2,J))/RH(2,J))
      DO 310 I=1,MM
  310 QTOP=((T2(I,N+3)-TAMB)/RV(I,N+4))+QTOP
      DO 311 J=3,NN
  311 QFTR=QFTR+QRAT(1,J)
      DO 312 I=1,MM
  312 QTTR=QTTR+QRAT(1,NJ)
      QWAX=(QBW+QTW+QSW)*DT+(QWAX)
      RATIO=QSW/QBW
```

```
      ERROR=((QBT-(QBW+QSW+QTW+QTOP+QFTR+QTTR))*100.0)/QBT
      DO 930 J=3,NN
      DO 930 I=2,MM
      V2=V2+(F(I,J)*(S**2)*B)
  930 CONTINUE
      DAVG=((2.0*V2)/(W*B))*12.0
      QMELT=((V2-V1)*DEN*HMELT)/DT
      V1=V2
      V2=0.0
      DELT=ABS(T2(1,2)-TMELT)
      PR=(VIS*CL)/TKL
      RA=((DEN**2)*G*CL*BETA*DELT*(DAVG**3))/(VIS*TKL*1728.0)
      IF(T2(1,2).LE.TMELT) RA=0.0
      IF(RA.GT.1.E05)TK=(TKL*0.104*(RA**0.305)*(PR**0.084))
      IF(RA.GE.3500.0.AND.RA.LE.1.E05) TK=(TKL*0.229*(RA**0.252))
      IF(RA.GE.1700.0.AND.RA.LT.3500.0) TK=(TKL*0.00238*(RA**0.816)
      TKR=TK/TKL
      DO 945 I=2,MM
      IF(F(I,3).LT.0.25) GO TO 945
      RV(I,3)=(1./(2.*TK*B))+(S1/(2.*TK1*S*B))
  945 CONTINUE
      DO 946 J=4,NN
      DO 946 I=2,MM
      IF(F(I,J).LT.EPS) GO TO 946
      RV(I,J)=(1./(TK*B))
  946 CONTINUE
      DO 947 I=2,MM
      IF(F(I,NN).LT.0.75) GO TO 947
      RV(I,N+3)=(S3/(2.*TK3*S*B))+(1./(2.*TK*B))
  947 CONTINUE
      DO 950 J=3,NN
      IF(F(2,J).LT.0.25) GO TO 949
      RH(2,J)=(S2/(2.*TK2*S*B))+(1./(2.*TK*B))
  949 CONTINUE
      DO 950 I=3,MM
      IF(F(I,J).LT.EPS) GO TO 950
      RH(I,J)=(1./(TK*B))
  950 CONTINUE
      IF(KCOUNT.EQ.KCHK) GO TO 6
      KCOUNT=KCOUNT+1
      GO TO 7
    6 WRITE(6,66) TIME, QWAX, ERROR
   66 FORMAT(1X,5HTIME=,E15.8,10X,5HQWAX=,E15.8,10X,6HERROR=,E15.8)
      DO 313 J=3,NN
      AJ=J-3
      BJ=J-2
      IF(F(2,J).GT.F2JM) DFLO=(BJ*S*12.0)
      DFIN=(AJ*S*12.0)
      IF(F(2,J).LT.EPS) GO TO 314
  313 CONTINUE
  314 DO 315 J=3,NN
      AJ=J-3
      IF(F(MM,J).LT.1.0) DMID=((AJ*S)+(F(MM,J)*S))*12.0
      IF(F(MM,J).LT.1.0) GO TO 316
  315 CONTINUE
  316 WRITE(6,67) DFIN, DFLO, DAVG, DMID
```

```
334     67 FORMAT(1X,5HDFIN=,E15.8,10X,5HDFLO=,E15.8,10X,5HDAVG=,E15.8,10X,5H
335        DMID=,E15.8)
336        DDOT=(DMID-DMO)/DT
337        DMO=DMID
338        WRITE(6,68) RA, TKR, QMELT, DDOT
339     68 FORMAT(1X,3HRA=,E15.8,10X,4HTKR=,E15.8,10X,6HQMELT=,E15.8,10X,5HDD
340        OT=,E15.8)
341        WRITE(6,77) QBW, QSW, QTW, QBT, RATIO
342     77 FORMAT(1X,4HQBW=,E15.8,3X,4HQSW=,E15.8,3X,4HQTW=,E15.8,3X,4HQBT=,E
343        15.8,3X,6HRATIO=,E15.8)
344        WRITE(6,88)
345     88 FORMAT(2X,1HI,2X,1HJ,10X,11HTEMPERATURE,10X,15HFRACTION MELTED,10X
346        ,11HENERGY RATE,10X,13HENERGY STORED)
347        DO 320 J=2,NJ
348        DO 320 I=1,MM
349        WRITE(6,99)I,J,T2(I,J),F(I,J),QRAT(I,J),QS(I,J)
350     99 FORMAT(1X,I2,1X,I2,8X,E15.8,8X,E15.8,8X,E15.8,8X,E15.8)
351    320 CONTINUE
352        KCOUNT=1
353      7 QBW=0.0
354        QSW=0.0
355        QTW=0.0
356        QTOP=0.0
357        QTTR=0.0
358        QFTR=0.0
359        DO 330 J=2,NJ
360        DO 330 I=1,MM
361    330 T1(I,J)=T2(I,J)
362        JOE=1
363        IF(TIME.LT.TAU) GO TO 3
364      8 WRITE(6,111) MCOUNT
365    111 FORMAT(1X,I3)
366        STOP
367        END
```

D.2. DESCRIPTION OF PROGRAM NOTATION

AJ	J-3, used in computing interface location
AM	value of integer M converted to floating point
B	length of section, ft
BETA	volume expansivity of wax, R^{-1}
BJ	J-2, used in computing interface location
C(I,J)	thermal capacitance of node (I,J), Btu/°F
CL	constant pressure specific heat of wax, Btu/lbm°F
CP	constant pressure specific heat of wax, Btu/lbm°F
CP1	constant pressure specific heat of bottom plate, Btu/lbm°F
CP2	constant pressure specific heat of fin, Btu/lbm°F
CP3	constant pressure specific heat of top plate, Btu/lbm°F
DAVG	average height of liquid based on amount melted, in.
DDOT	interfacial velocity for nodes adjacent to centerline (I = MM), in./h
DELT	absolute value of temperature difference between bottom plate and interface, °F
DEN	wax density, lbm/ft^3
DEN1	bottom plate density, lbm/ft
DEN2	fin density, lbm/ft^3
DEN3	top plate density, lbm/ft^3
DFLO[a]	approximate interfacial location for nodes adjacent to fin (I = 2) based on amount melted being equal to F2JM, in.
DFIN	interfacial position for nodes adjacent to fin (I = 2) based on any amount being melted, in.

DIF	temperature difference used in comparing new and old temperatures during iteration when solving steady state equations for unspecified fin temperatures, °F.
DMID	interfacial position for node adjacent to centerline, in.
DMO	DMID evaluated at previous time, in.
DT	time increment, h.
EPS	arbitrarily set small number used as a comparator
ERROR	percent error in computed energy balance based on transfer rates, percent.
F(I,J)	mass fraction of node (I,J) which has undergone phase change since start of process
FAC	time ratio used in linearly interpolating specified fin temperatures at a particular time in terms of bracketed data values.
F2JM	fraction of S which corresponds to 1/32 in. (arbitrary)
G	acceleration of gravity, ft/h^2
H	PCM section height (see Fig. 40), ft.
$HBOT^2$	heat transfer coefficient between external fluid and bottom plate, $Btu/h\text{-}ft^2\text{-}°F$
HMELT	heat of fusion, Btu/lbm
$HTOP^3$	heat transfer coefficient between external fluid and top plate, $Btu/h\text{-}ft^2\text{-}°F$
HTR	heat of transition, Btu/lbm.
I	integer designation of vertical column in which a mode is located (see Fig. 40)
J	integer designation of horizontal row in which a mode is located (see Fig. 40)
JOE	counter used in refining the heat transfer computation before progressing in time
KCHK	integer used to control printing of results at desired times (see definition of KCOUNT)

KCOUNT	integer counter used to print our results at times when KCOUNT = KCHK
M	number of wax nodes in a horizontal row
MCOUNT	counter used in determining unspecified fin temperatures
MFIN	maximum value of MCOUNT which when exceeded causes program to stop
MM	M+1 (see Fig. 40)
N	number of wax nodes in a vertical column
ND	number of data points for measured fin temperatures
NDP	ND-1
NI	N+4
NJ	N+3
NN	N+2
PR	Prandtl number
Q(I,J)	unnecessary variable – replaced where needed by QS(I,J)
QBT	instantaneous heat transfer rate through bottom, Btu/h
QBW	instantaneous heat transfer rate through bottom to wax only, Btu/h
QFTR	instantaneous rate of heat transfer to fin, Btu/h
QMELT	energy which accounts for amount of wax melted at any time, Btu
QRAT(I,J)	the instantaneous net rate of heat transfer to node I,J, Btu/h
QS(I,J)	the energy stored by node I,J above TREF for wax and above 0 for metal nodes, Btu
QSIN	the energy stored by node I,J above TREF corresponding to initial temperature throughout network, Btu
QSW	instantaneous heat transfer rate from fin to wax, Btu/h

TIME	instantaneous value of time, h.
TIN	initial temperature of all nodes, °F
TK	wax thermal conductivity (artificially allowed to vary in liquid to account for convection), Btu/h-ft-°F
TKL	thermal conductivity of liquid, Btu/h-ft-°F
TKR	ratio of effective thermal conductivity to thermal conductivity
TMELT	fusion temperature of wax, °F
TREF	arbitrary reference temperature (should be less than TIN), °F
TTR	transition temperature, °F
T1(I,J)	temperature of node I,J at time t, °F
T2(I,J)	temperature of node I,J at time t+Δt, °F
T3(I,J)	temperature of node I,J in fin at beginning of each iterative step used in finding steady state solution, °F
TAU2	arbitrarily defined time value used in print-out control, h.
TK1	thermal conductivity of bottom plate, Btu/h-ft-°F
TK2	thermal conductivity of fin, Btu/h-ft-°F
TK3	thermal conductivity of top plate, Btu/h-ft-°F
TIM(L)	time value corresponding to input data of measured fin temperatures, h
TM1(L)	measured bottom plate temperature (input data), °F
TM2(L)	first measured fin temperature (input data), °F
TM3(L)	second measured fin temperature (input data), °F
TM4(L)	third measured fin temperature (input data), °F
VIS	viscosity of liquid, lbm/h-ft

V1 volume of wax melted at time t, ft^3

V2 volume of wax melted at time $t+\Delta t$, ft^3

W width of wax cell, ft

1. This assumes that some finite thickness must have melted before it could be detectable on the film. The number DFIN is the height corresponding to a node with any amount melted.

2. This was included to be general but has not been used to date as bottom plate temperatures were specified as input data.

3. This has been included but set at a small value to essentially correspond to the top being insulated.

D.3. DISCUSSION OF COMPUTER PROGRAM FOR MELTING

In the following discussion, references are made to line numbers corresponding to those designated on the copy of the program.

LINES	DISCUSSION
1–4	required dimension statements for subscripted variables; values should be (MM, NI) for all double subscripted variables except T3 for which they should be (1, NJ); values should be ND for single subscripted variables. NOTE: Q(MM,NI) is superfluous and can be omitted with lines 136-140.
5–23	specification of computational parameters
24–54	specification of physical properties
55–63	specification of geometry parameters
64–82	computation of all vertical thermal resistance values RV (I,J)
83–95	computation of all horizontal thermal resistance values RH(I,J);note that line 95 is a special definition which amounts to bypassing node (1,N+3) which was done to overcome stability criterion required by this small corner node
96–108	computation of all nodal capacitance values C(I,J)
109–112	computation of energy stored by a wax node relative to TREF for the start and end of phase transition and the start and end of fusion, respectively
113–144	initialization of pertinent quantities; the initial value of the stored energy depends on the relationship of the initial temperature to the reference temperature TREF; note that lines 136–140 are superfluous and can be omitted; some initialization of certain parameters is done in the DO loop between lines 160 and 172 which are set primarily to avoid random printout and are not essential to the computation done in the heart of the program
145–150	input data values for measured fin and bottom plate temperatures and corresponding time values
151–172	printout of initial values for checking purposes and printout of certain computed quantities for informational purposes
173–174	initially defines T3(1,J) for all fin nodes and sets these equal to the initial temperatures T1(1,J)

175 beginning of main computation scheme

176 time is stepped forward by Δt

177–188 loops which compute and store the net rate of heat transfer to nodes (I,J) based on old temperatures T1(I,J); the rate of heat transfer to node (I,J) is given by

$$\dot{q}(I,J) = \frac{T(I-1,J)-T(I,J)}{RH(I,J)} + \frac{T(I+1,J)-T(I,J)}{RH(I,J)} + \frac{T(I,J-1)-T(I,J)}{RV(I,J)} + \frac{T(I,J+1)-T(I,J)}{RV(I,J+1)}$$

this expression must be modified accordingly for nodes near a boundary which are not surrounded by four neighbors

189–191 computation of total energy stored by node (I,J) since the start which is given by

$$Q_{stored} = \sum_{time} \dot{q}\Delta t$$

192–193 computation of new top plate temperatures T2(I,N+3) from the expression

$$T2(I,J) = T1(I,J) + \frac{\dot{q}(I,J)\Delta t}{C(I,J)}$$

194 sets the corner plate node (1,N+3) temperature equal to that of the second node (2,N+3); omission of the corner node in the computation scheme was done to avoid stability problems due to its small size

195–208 computation of new wax node temperatures from the energy stored by the nodes and their capacity and/or phase change enthalpy values; when the stored energy lies between Q1 and Q2 the new temperature is forced to be the transition temperature and when it lies between Q3 and Q4 the new temperature; is forced to be the fusion temperature; also the fraction of the node which has undergone phase change is calculated from the relationship of the stored energy to Q3 and Q4; note that certain designated cards need to be changed when running the program for freezing as contrasted to melting

209–210 beginning of determination of fin temperatures

211–212 all new fin temperatures are set to T3(1,J) which simply represents an assumed value always corresponding to the previously computed value except at the very beginning at which time it is set as the initial temperature

213–220 interpolation scheme which assigns new temperatures to the three nodes on the fin and one on the bottom plate corresponding to positions where temperature measurements were made; the new temperatures are linearly interpolated from the input data

221–222 assigns all nodes along the bottom plate the same value of new temperature

223 beginning of iteration process to determine unspecified fin temperatures from steady state equation; fin nodes were not treated as transient cases due to their extremely small capacitances that would impose a severe stability criterion

224–237 iteration process used to determine unspecified fin temperatures; in each iteration, T2(1,J) is computed from steady state equations and then compared with T3(1,J) which corresponds to the calculated temperatures during the previous iterative step; the interation is continued until the differences between computed fin temperatures and their corresponding values for the previous iterative step are all acceptably small; should the iteration exceed MFIN counts the program is directed to stop

238 when counter JOE equals 2, the new temperatures at all nodes are considered to be the solution at the particular time and the program advances to line 259

239 increase of counter JOE to 2

240–242 the energy stored at each node (I,J) is reset back to its original value; this is to allow for an improved computation of the net heat transfer rate to each node to be made and then a recomputation of the stored energy and the corresponding new temperatures

243–254 computation of net heat transfer rate to each node using new temperatures T2

255–257 calculation of net heat transfer rate to each node as the average of that based on old temperatures T1 and new temperatures T2

258 return to line 189 which consists of redirecting the computation through that of computing improved new temperatures, energy storage values, and fractional melted values by using the improved (averaged) heat transfer rate (Lines 255-257); this corrective technique is only employed once

259–278	computation of various heat transfer quantities from the new temperatures obtained at time $t+\Delta t$
279–282	computation of volume of melted wax
283	computation of average liquid depth from the volume melted
284	computation of energy required to melt the wax which has melted
285–286	resetting of V1 and V2 for next time step
287	determination of absolute value of temperature difference between bottom plate and the fusion temperature
288	computation of the Prandtl number
289–290	computation of the Rayleigh number
291–293	determination of effective liquid conductivity due to convection by using correlations of O'Toole and Silveston
294	computation of ratio of effective liquid conductivity to actual value
295–315	recomputation of thermal resistances in the liquid by using the effective thermal conductivity rather than the actual value
316	counter check which controls printing out of desired results as well as computation of interfacial position
317	counter advance
318	by-pass of printing results except when line 316 is executed
319–320	write statement for printing results
321–332	computation of interface position for columns next to fin and next to centerline
333–335	write statement for printing results
336–337	calculation of interfacial velocity and renaming interfacial position to provide for determining its change at the next time step
338–351	write statements and corresponding formats for printing results

352–358 reinitialization of pertinent quantities for next time step

359–361 setting new temperatures for current time step to be old temperatures for the next time step

361 reinitialization of counter

363 comparison of time to upper limit value which when exceeded results in stopping the program

364–365 printing out of value of counter used in fin temperature iteration

366 STOP

367 END

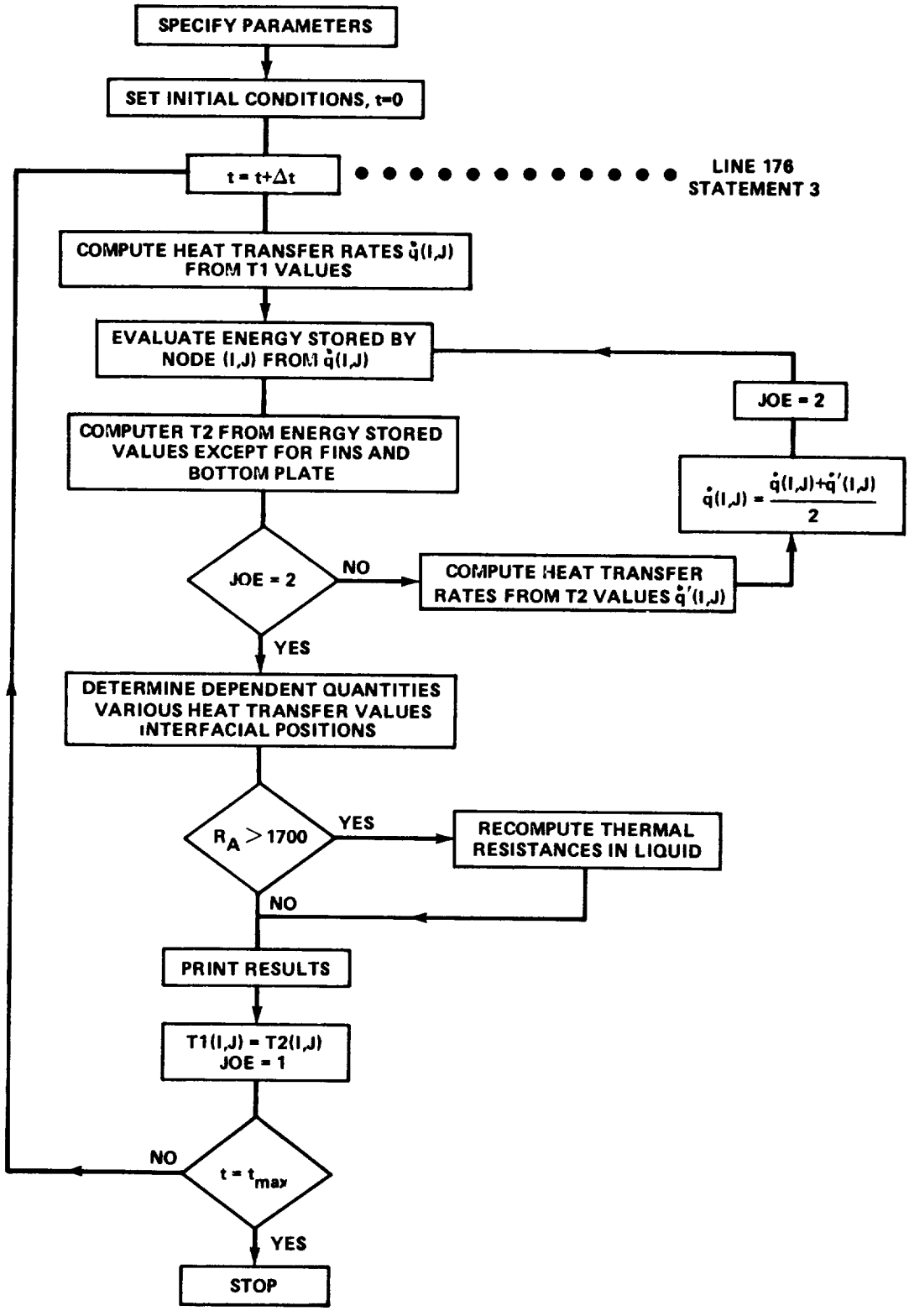

Figure D-1. Skelton flow chart.

D.4. COMPUTER PROGRAM FOR SOLIDIFICATION

```
C       TEST 230-15 FREEZE TEST 3/4 INCH CELL
        DIMENSION RV(5,31), RH(5,31), C(5,31), QS(5,31), T1(5
       1,31)
        DIMENSION T2(5,31), F(5,31), QRAT(5,31), T3(1,31),QRA2
       1(5,31)
        DIMENSION TM1(25), TM2(25), TM3(25), TM4(25), TIM(25)
        DIMENSION VR(5,31), HR(5,31)
C COMPUTATIONAL PARAMETERS
        N=27
        M=4
        AM=M
        MM=M+1
        NN=N+2
        NJ=N+3
        NI=N+4
        ND=23
        NDP=22
        TAU=1.5
        KCOUNT=1
        MCOUNT=1
        MFIN=500
        EPS=1.E-06
        KCHK=1000
        JOE=1
        DT=0.00005
        TAU2=(10.*DT)+(DT/3.)
        AF=40.
        UN=1.0-EPS
C PHYSICAL PROPERTIES
        TAMB=80.
        TIN=100.
        HTOP=1.E-08
        HBOT=5.
        G=(32.174*3600.*3600.)
C    WAX
        DEN=47.2
        TK=0.087
        CP=0.5
        TTR=73.04
        HTR=22.108
        TMELT=89.8
        HMELT=73.357
        TREF=50.
        BETA=0.00045
        VIS=14.3
        CL=CP
        TKL=TK
C    BOTTOM PLATE DENOTED BY 1
        DEN1=171.
        TK1=93.
        CP1=0.22
```

```
C    FIN DENOTED BY 2
       DEN2=171.
       TK2=93.
       CP2=0.22
C    TOP PLATE DENOTED BY 3
       DEN3=72.5
       TK3=0.09
       CP3=0.33
C GEOMETRY PARAMETERS
       W=0.75/12.0
       H=2.625/12.0
       B=5.0/12.0
       S=W/(2.*AM)
       S1=0.032/12.0
       S2=0.008/12.0
       S3=0.25/12.0
       F2JM=1.0/(32.0*S*12.0)
C    VERTICAL RESISTANCES
       RV(1,2)=(S1/(TK1*S2*B))+(2./(HBOT*S2*B))
       DO 10 I=2,MM
    10 RV(I,2)=(S1/(2.*TK1*S*B))+(1./(HBOT*S*B))
       RV(1,3)=(S/(TK2*S2*B))+(S1/(TK1*S2*B))
       DO 20 I=2,MM
    20 RV(I,3)=(1./(2.*TK*B))+(S1/(2.*TK1*S*B))
       DO 30 J=4,NN
    30 RV(1,J)=((2.*S)/(TK2*S2*B))
       DO 40 J=4,NN
       DO 40 I=2,MM
    40 RV(I,J)=(1./(TK*B))
       RV(1,N+3)=(S3/(TK3*S2*B))+(S/(TK2*S2*B))
       DO 50 I=2,MM
       RV(I,N+4) = (S3/(2.*TK3*S*B)) + (1./(HTOP*S*B))
    50 RV(I,N+3)=(S3/(2.*TK3*S*B))+(1./(2.*TK*B))
       RV(1,N+4)=(S3/(TK3*S2*B))+(2./(HTOP*S2*B))
       RV(2,N+4)=(S3/(2.*TK3*B*(S+(S2/2.))))+(1./(HTOP*B*(S+
      1(S2/2.))))
C    HORIZONTAL RESISTANCES
       DO 70 I=2,MM
       RH(I,2) = (S/(TK1*S1*B))
    70 RH(I,N+3)=(S/(TK3*S3*B))
       DO 80 J=3,NN
       DO 80 I=2,MM
    80 RH(I,J) = (1./(TK*B))
       DO 90 J=3,NN
    90 RH(2,J)= (S2/(2.*TK2*S*B)) + (1./(2.*TK*B))
       RH(2,2)=((S2+S)/(2.*TK1*S1*B))
       RH(2,N+3)=((S2+S)/(2.*TK3*S3*B))
       RH(2,N+3)=RH(2,N+3)+RV(1,N+3)
C NODAL CAPACITANCES
       C(1,2)=((DEN1*S1*S2*B*CP1)/2.)
       DO 110 I=2,MM
```

```
  110 C(I,2)=(DEN1*S1*S*B*CP1)
      DO 120 J=3,NN
  120 C(1,J)=((DEN2*S2*S*B*CP2)/2.)
      C(1,N+3)=((DEN3*S2*S3*B*CP3)/2.)
      DO 130 I=2,MM
  130 C(I,N+3)=(DEN3*S3*S*B*CP3)
      C(2,N+3)=(S3*B*(S+(S2/2.))*DEN3*CP3)
      DO 140 J=3,NN
      DO 140 I=2,MM
  140 C(I,J)=(DEN*(S**2)*B*CP)
      Q1 = (C(2,3)*(TTR-TREF))
      Q2=Q1+((DEN*(S**2)*B*HTR))
      Q3 = Q2 + ((C(2,3))*(TMELT-TTR))
      Q4=Q3+((DEN*(S**2)*B*HMELT))
C INITIALIZATION OF PERTINENT QUANTITIES
      TIME=0.0
      QWAX=0.0
      QBW=0.0
      QSW=0.0
      QTW=0.0
      QTOP=0.0
      QFTR=0.0
      QTTR=0.0
      V1=0.0
      V2=0.0
      DMO=0.0
      DO 150 J=2,NJ
      DO 150 I=1,MM
  150 T1(I,J)=TIN
      IF(TIN.LT.TTR)QSIN=(C(2,3)*(TIN-TREF))
      IF(TIN.GT.TTR.AND.TIN.LT.TMELT) QSIN=Q2+(C(2,3)*(TIN
     1-TTR))
      IF(TIN.GT.TMELT)QSIN=Q4+((C(2,3))*(TIN-TMELT))
      DO 160 I=1,MM
  160 T1(I,N+4)=TAMB
      DO 170 J=3,NN
      DO 170 I=2,MM
  170 QS(I,J)=QSIN
      DO 199 J=2,NI
      DO 199 I=1,MM
      F(I,J)=0.0
  199 QRAT(I,J)=0.0
      READ(5,11) (TM1(I), I=1,ND)
      READ(5,11) (TM2(I), I=1,ND)
      READ(5,11) (TM3(I), I=1,ND)
      READ(5,11) (TM4(I), I=1,ND)
      READ(5,11) (TIM(I), I=1,ND)
   11 FORMAT(8F10.0)
      DO 910 KTC=1, ND
  910 TIM(KTC)=TIM(KTC)/3600.
      WRITE(6,22) TIME,W,H,N,M
```

```
   22 FORMAT(1X,5HTIME=,E15.8,10X,2HW=,E15.8,10X,2HH=,E15.8
     1,10X,2HN=,I2,15X,2HM=,I2)
      WRITE(6,33)Q1,Q2,Q3,Q4
   33 FORMAT(1X,3HQ1=,E15.8,10X,3HQ2=,E15.8,10X,3HQ3=,E15.8
     1,10X,3HQ4=,E15.8)
      WRITE(6,44)
   44 FORMAT(2X,4HI  J,5X,19HVERTICAL RESISTANCE,6X
     1,21HHORIZONTAL RESISTANCE,6X,17HNODAL CAPACITANCE,6X
     2,11HTEMPERATURE,5X,7HQS(I,J))
      DO 200 J=2,NI
      DO 200 I=1,MM
      IF(J.EQ.N+4) GO TO 1
      GO TO 2
    1 QS(I,J)=0.0
      RH(I,J)=1.E08
      C(I,J)=0.0
    2 IF(I.EQ.1) RH(I,J)=1.E08
      IF(J.EQ.2.OR.J.EQ.N+3) QS(I,J)=0.0
      IF(I.EQ.1) QS(I,J)=0.0
      WRITE(6,55)I,J,RV(I,J),RH(I,J),C(I,J),T1(I,J),QS(I,J)
   55 FORMAT(1X,I2,1X,I2,5X,E15.8,10X,E15.8,10X,E15.8,6X
     1,E15.8,4X,E15.8)
  200 CONTINUE
      DO 400 J=3,NJ
      DO 400 I=2,MM
      VR(I,J)=RV(I,J)
  400 HR(I,J)=RH(I,J)
      DO 889 J=3,NN
  889 T3(1,J)=T1(1,J)
C COMPUTATION SECTION   COMPUTATION SECTION COMPUTATION
C       SECTION
    3 TIME=TIME+DT
      DO 210 J=3,NJ
      QRAT(1,J)=((T1(2,J)-T1(1,J))/RH(2,J))+((T1(1,J-1)-T1(1
     1,J))/RV(1,J))+((T1(1,J+1)-T1(1,J))/RV(1,J+1))
      QRAT(MM,J)=((T1(M,J)-T1(MM,J))/RH(MM,J))+((T1(MM,J-1)
     1-T1(MM,J))/RV(MM,J))+((T1(MM,J+1)-T1(MM,J))/RV(MM,J
     2+1))
  210 CONTINUE
      IF(M.EQ.1)GO TO 212
      DO 211 J=3,NJ
      DO 211 I=2,M
      QRAT(I,J)=((T1(I-1,J)-T1(I,J))/RH(I,J))+((T1(I+1,J)-T1
     1(I,J))/RH(I+1,J))+((T1(I,J-1)-T1(I,J))/RV(I,J))+((T1(I
     2,J+1)-T1(I,J))/RV(I,J+1))
  211 CONTINUE
  212 DO 220 J=3,NJ
      DO 220 I=1,MM
  220 QS(I,J)=QS(I,J)+(QRAT(I,J)*DT)
      DO 240 I=2,MM
  240 T2(I,N+3)=T1(I,N+3)+((QRAT(I,N+3)*DT)/C(I,N+3))
```

```
      T2(1,N+3)=T2(2,N+3)
      DO 250 J=3,NN
      DO 250 I=2,MM
      IF(QS(I,J).LT.Q1) T2(I,J)=TREF+(QS(I,J)/C(I,J))
      IF(QS(I,J).GE.Q1.AND.QS(I,J).LE.Q2) T2(I,J)=TTR
      IF(QS(I,J).GT.Q2.AND.QS(I,J).LT.Q3) T2(I,J)=TTR+((QS(I
     1,J)-Q2)/C(I,J))
      IF(QS(I,J).GE.Q3.AND.QS(I,J).LE.Q4) T2(I,J)=TMELT
C    WHEN GOING FROM MELT TO FREEZE OR VICE-VERSA CHANGE THE
C       FOLLOWING CA
      IF(QS(I,J).GT.Q3.AND.QS(I,J).LT.Q4) F(I,J)=(Q4-QS(I
     1,J))/(DEN*(S**2)*3*HMELT)
      IF(QS(I,J).GE.Q4) F(I,J)=0.0
      IF(QS(I,J).GT.Q4) T2(I,J)=TMELT+((QS(I,J)-Q4)/C(I,J))
C    WHEN GOING FROM MELT TO FREEZE OR VICE-VERSA CHANGE THE
C       FOLLOWING CA
      IF(QS(I,J).LE.Q3) F(I,J)=1.0
  250 CONTINUE
C SPECIFICATION AND/OR DETERMINATION OF FIN TEMPERATURES
C           THE FOLLOWING DO LOOP ASSUMES FIN TEMPERATURES
C       FOR ITERATION
      DO 255 J=3,NN
  255 T2(1,J)=T3(1,J)
      DO 260 L=1,NDP
      IF(TIME.GE.TIM(L).AND.TIME.LE.TIM(L+1)) GO TO 4
  260 CONTINUE
    4 FAC=(TIME-TIM(L))/(TIM(L+1)-TIM(L))
      T2(1,2)=TM1(L)+((TM1(L+1)-TM1(L))*FAC)
      T2(1,8)=TM2(L)+((TM2(L+1)-TM2(L))*FAC)
      T2(1,15)=TM3(L)+((TM3(L+1)-TM3(L))*FAC)
      T2(1,21)=TM4(L)+((TM4(L+1)-TM4(L))*FAC)
      DO 270 I=1,MM
  270 T2(I,2)=T2(1,2)
C UNSPECIFIED FIN TEMPERATURES DETERMINED BY STEADY STATE
C       EQUATIONS
  256 MCOUNT=MCOUNT+1
      DO 280 J=3,NN
      T3(1,J)=T2(1,J)
      IF(J.EQ.8.OR.J.EQ.15) GO TO 5
      IF(J.EQ.21) GO TO 5
      T2(1,J)=((T2(1,J-1)/RV(1,J))+(T2(2,J)/RH(2,J))+(T2(1,J
     1+1)/RV(1,J+1)))/((1./RV(1,J))+(1./RH(2,J))+(1./RV(1,J
     2+1)))
    5 CONTINUE
  280 CONTINUE
      IF(MCOUNT.GT.MFIN) GO TO 8
      DO 281 J=3,NN
      DIF=T2(1,J)-T3(1,J)
      IF(ABS(DIF).GT.EPS) GO TO 256
  281 CONTINUE
      IF(JOE.EQ.2) GO TO 285
```

```
      JOE=JOE+1
      DO 888 J=3,NJ
      DO 888 I=1,MM
  888 QS(I,J)=QS(I,J)=(QRAT(I,J)*DT)
      DO 282 J=3,NJ
      QRA2(1,J)=((T2(2,J)-T2(1,J))/RH(2,J))+((T2(1,J-1)-T2(1
     1,J))/RV(1,J))+((T2(1,J+1)-T2(1,J))/RV(1,J+1))
      QRA2(MM,J)=((T2(M,J)-T2(MM,J))/RH(MM,J))+((T2(MM,J-1)
     1-T2(MM,J))/RV(MM,J))+((T2(MM,J+1)-T2(MM,J))/RV(MM,J
     2+1))
  282 CONTINUE
      IF(M.EQ.1)GO TO 283
      DO 283 J=3,NJ
      DO 283 I=2,M
      QRA2(I,J)=((T2(I-1,J)-T2(I,J))/RH(I,J))+((T2(I+1,J)-T2
     1(I,J))/RH(I+1,J))+((T2(I,J-1)-T2(I,J))/RV(I,J))+((T2(I
     2,J+1)-T2(I,J))/RV(I,J+1))
  283 CONTINUE
      DO 284 J=3,NJ
      DO 284 I=1,MM
  284 QRAT(I,J)=(QRAT(I,J)+QRA2(I,J))/2.0
      GO TO 212
  285 MCOUNT=1
      DO 401 J=3,NJ
      DO 401 I=2,MM
      IF(F(I,J).GT.EPS.AND.F(I,J).LT.UN) GO TO 402
      IF(F(I,J).GT.UN) GO TO 403
      GO TO 401
  403 RV(I,J)=VR(I,J)
      RH(I,J)=HR(I,J)
      GO TO 401
  402 RV(I,J)=VR(I,J)/AF
      RH(I,J)=HR(I,J)/AF
      RV(I,J+1)=VR(I,J+1)/AF
      RH(I+1,J)=HR(I+1,J)/AF
  401 CONTINUE
      DO 286 I=1,MM
  286 QRAT(I,2)=((T2(I,2)-T1(I,2))*C(I,2)/DT)
      DO 287 I=1,MM
  287 QS(I,2)=QS(I,2)+(C(I,2)*(T2(I,2)-T1(I,2)))
      DO 290 I=2,MM
      QBW=(T2(I,2)-T2(I,3))/RV(I,3)+QBW
  290 QTW=(T2(I,N+3)-T2(I,N+2))/RV(I,N+3)+QTW
      QBT=QBW+((T2(1,2)-T2(1,3))/RV(1,3))
      DO 300 J=3,NN
  300 QSW=QSW+((T2(1,J)-T2(2,J))/RH(2,J))
      DO 310 I=1,MM
  310 QTOP=((T2(I,N+3)-TAMB)/RV(I,N+4))+QTOP
      DO 311 J=3,NN
  311 QFTR=QFTR+QRAT(1,J)
      DO 312 I=1,MM
```

```
312 QTTR=QTTR+QRAT(I,NJ)
    QWAX=(QBW+QTW+QSW)*DT+(QWAX)
    RATIO=QSW/QBW
    ERROR=((QBT-(QBW+QSW+QTW+QTOP+QFTR+QTTR))*100.0)/QBT
    DO 930 J=3,NN
    DO 930 I=2,MM
    V2=V2+(F(I,J)*(S**2)*B)
930 CONTINUE
    DAVG=((2.0*V2)/(W*B))*12.0
    QMELT=((V2-V1)*DEN*HMELT)/DT
    QFREZ=QMELT
    V1=V2
    V2=0.0
    IF(KCOUNT.EQ.KCHK) GO TO 6
    KCOUNT=KCOUNT+1
    GO TO 7
  6 WRITE(6,66) TIME, QWAX, ERROR
 66 FORMAT(1X,5HTIME=,E15.8,10X,5HQWAX=,E15.8,10X,6HERROR=
   1,E15.8)
    DO 313 J=3,NN
    AJ=J-3
    BJ=J-2
    IF(F(2,J).GT.F2JM) DFLO=(BJ*S*12.0)
    DFIN=(AJ*S*12.0)
    IF(F(2,J).LT.EPS) GO TO 314
313 CONTINUE
314 DO 315 J=3,NN
    AJ=J-3
    IF(F(MM,J).LT.1.0) DMID=((AJ*S)+(F(MM,J)*S))*12.0
    IF(F(MM,J).LT.1.0) GO TO 316
315 CONTINUE
316 WRITE(6,67) DFIN, DFLO, DAVG, DMID
 67 FORMAT(1X,5HDFIN=,E15.8,10X,5HDFLO=,E15.8,10X,5HDAVG=
   1,E15.8,10X,5HDMID=,E15.8)
    DDOT=(DMID-DMO)/DT
    DMO=DMID
    WRITE(6,69) QFREZ, DDOT
 69 FORMAT(1X,6HQFREZ=,E15.8,10X,5HDDOT=,E15.8)
    WRITE(6,77) QBW, QSW, QTW, QBT, RATIO
 77 FORMAT(1X,4HQBW=,E15.8,3X,4HQSW=,E15.8,3X,4HQTW=,E15.8
   1,3X,4HQBT=,E15.8,3X,6HRATIO=,E15.8)
    WRITE(6,88)
 88 FORMAT(2X,1HI,2X,1HJ,10X,11HTEMPERATURE,10X,15HFRACTIO
   1N MELTED,10X,11HENERGY RATE,10X,13HENERGY STORED)
    DO 320 J=2,NJ
    DO 320 I=1,MM
    WRITE(6,99)I,J,T2(I,J),F(I,J),QRAT(I,J),QS(I,J)
 99 FORMAT(1X,I2,1X,I2,8X,E15.8,8X,E15.8,8X,E15.8,8X
   1,E15.8)
320 CONTINUE
    KCOUNT=1
```

```
  7 QBW=0.0
    QSW=0.0
    QTW=0.0
    QTOP=0.0
    QTTR=0.0
    QFTR=0.0
    DO 330 J=2,NJ
    DO 330 I=1,MM
330 T1(I,J)=T2(I,J)
    JOE=1
    IF(TIME.LT.TAU) GO TO 3
  8 WRITE(6,111) MCOUNT
111 FORMAT(1X,I3)
    STOP
    END
```

REFERENCES

1. Lorsch, H.: NSF Phase O; Feasibility and Planning Study Final Report. Appendix B-9. Vol. 3, Book 1, NSF-RA-N-74-021C, May 1974.

2. Humphries, W. R.: Performance of Finned Thermal Capacitors. NASA TN D-7690, July 1974.

3. Grodzka, P. B. and Fan, C.: Thermal Control by Freezing and Melting; First Interim Report on Space Thermal Control Study. Lockheed Missiles and Space Company, A791342, NASA Contract NAS8-21123, March 1968.

4. Grodzka, P. B.: Thermal Control by Freezing and Melting; Second Interim Report on Space Thermal Control Study. Lockheed Missiles and Space Company, D148619, NASA Contract NAS8-21123, May 1969.

5. Chalmers, B.: Principles of Solidification. John Wiley and Sons, New York, New York, 1964.

6. Bailey, J. A. and Liao, C.: Thermal Capacitor Design Rationale; Part I; Thermal and Mechanical Property Data for Selected Material Potentially Useful in Thermal Capacitor Design and Construction. Final Report submitted to NASA-MSFC under Cooperative Agreement NCA8-52 with North Carolina State University, 1975.

7. API 44 Tables, Selected Values of Properties of Hydrocarbons and Related Compounds. Volumes I-IV, American Petroleum Institute Research Project 44, Thermodynamics Research Center, Texas A&M University, June 1972.

8. Timmermans, J.: Physico-Chemical Constants of Pure Organic Compounds. Vol. 2, Elsevier Publishing Co., New York, 1965.

9. Research and Development Study on Thermal Control by Use of Fusible Materials. Northrop Corporation Interim Report NSL 65-16 to NASA-MSFC on Contract No. NAS 8-11163, February 1965.

10. Muehlbauer, J. C. and Sunderland, J. E.: Heat Conduction with Freezing or Melting. Applied Mechanics Review, vol. 18, no. 12, December 1965, pp. 951-955.

11. Chapman, A. J.: Heat Transfer. Second Edition, The Macmillan Company, 1967.

12. Rathjen, K. A. and Jiji, L. M.: Heat Conduction with Melting or Freezing in a Corner. Trans. ASME, J. Heat Transfer, February 1971.

13. Özisk, M. N.: Boundary Value Problem of Heat Conduction. International Textbook Company, 1968.

14. Funderlic, R. E.: The Programmer's Handbook, AEC Research and Development Report K-1729. Union Carbide Corporation Nuclear Division, February 9, 1968.

15. Bentilla, E. W.; Sterrett, K. F.; and Karre, L. E.: Research and Development Study on Thermal Control by Use of Fusible Materials. Northrop Space Laboratories, Final Report under Contract No. NAS 8-11163, NSL 65-16-1, April 1966.

16. Hale, D. V.; Hoover, M. J.; and O'Neill, M. J.: Phase Change Materials Handbook. NASA Contractor Report NASA CR-61363 by Lockheed Missiles and Space Company, September 1971.

17. Rayleigh, Lord: On Convection Currents in a Horizontal Layer of Fluid, When the Higher Temperature is on the Under Side. Phil. Mag. and Journal of Science, vol. 32, no. 192, December 1916.

18. Schmidt, E. and Silveston, P. L.: Natural Convection in Horizontal Fluid Layers. Chemical Engineering Progress Symposium Series, vol. 55, no. 29, 1959.

19. Glober, S. and Dropkin, D.: Natural-Convection Heat Transfer in Liquids Confined by Two Horizontal Plates and Heated From Below. Journal of Heat Transfer, vol. 81, 1959.

20. Silveston, P. L.: Warmedurchgarg in Waagerechten Flussighkeitsschichten. Part 1. Forsch Ing. Wes., vol. 24, 1958.

21. Edwards, D. K.: Suppression of Cellular Convection by Lateral Walls. Journal of Heat Transfer, Trans. ASME, Series C, vol. 91, no. 1, February 1969, pp. 145-150.

22. Sammuels, M. R. and Churchill, S. W.: Stability of a Fluid in a Rectangular Region Heated from Below. AlCHe Journal, vol. 13, no. 1, 1967, pp. 77-85.

23. Davis, S. H.: Convection in a Box, Linear Theory. Journal of Fluid Mechanics, vol. 30, part 3, 1967, pp. 465-478.

24. Sun, W. M. and Edwards, D. K.: Natural Convection in Cells with Finite Conducting Wide Walls Heated from Below, Heat Transfer. Fourth International Heat Transfer Conference, vol. 4, paper NC 23, Elsevier Publishing Co., Amsterdam, 1970. pp. 1-11.

REFERENCES (Continued)

25. Ostrach, S. and Pmueli, D.: The Thermal Instability of Completely Confined Fluids Inside Some Particular Configurations. Journal of Heat Transfer, Trans. ASME, vol. 4, series c, November 1963, pp. 346-354.

26. Sherman, M. and Ostrach, S.: Lower Bounds to the Critical Rayleigh Number in Completely Confined Regions. Journal of Applied Mechanics, Trans. ASME, vol 34, series E, no. 2, June 1967, pp. 308-312.

27. Catton, I. and Edwards, D. K.: Effect of Side Walls on Natural Convection Between Horizontal Plates Heated from Below. Journal of Heat Transfer, Trans. ASME, vol. 80, series c, no. 4, November 1967, pp. 295-299.

28. Heitz, W. L. and Westwater, J. W.: Critical Rayleigh Numbers for Natural Convection of Water Confined in Square Cells with L/D from 0.5 to 8. Journal of Heat Transfer, Trans. ASME, May 1971, pp. 188-196.

29. Gershuni, G. Z. and Zhuklovitskii, E. M.: Convection Instability of Horizontal Fluid Layers Bounded by Thermal Interaction. PPM, vol. 32, no. 3, 1968.

30. O'Toole, J. L. and Silveston, P. L.: Correlation of Convective Heat Transfer in Confined Horizontal Layers. Chemical Engineering Progress Symposium Series, vol. 57, no. 32, 1961.

31. Edwards, D. K. and Catton, I.: Prediction of Heat Transfer in Liquids Confined by Two Horizontal Plates and Heated From Below. Journal of Heat Transfer, vol. 81, 1959.

32. Bénard, H.: Les Tourbillion Cellulaires Dans Une Nappe Liquide Transport-Aut de La chaleur Par Convection in Regime Permanent. Ann. Chem. Phy., vol. 23, 1901, pp. 62-144.

33. Block, M. J.: Surface Tension as the Cause of Benard Cells and Surface Deformation in a Liquid Film. Nature, vol. 178, September 1956.

34. Pearson, J. R. A.: On Convection Induced by Surface Tension. Journal of Fluid Mechanics, vol. 4, 1958.

35. Scriven, L. E. and Sternling, C. V.: The Marangoni Effects. Nature, vol. 187, July, 1960.

36. Sternling, C. V. and Scriven, L. E.: Interfacial Turbulence; Hydrodynamic Instability and the Marangoni Effect. American Institute of Chemical Engineers Journal, December 1956.

37. Marangoni, C. S. M.: Il Nuovo Cimento Journal, series 2.516, 1872, p. 239.

38. Young, N. O.; Goldstein, J. S.; and Block, M. J.: The Motion of Bubbles in a Vertical Temperature Gradient. Journal of Fluid Mechanics, vol. 6, 1959.

39. Gambrill, W. R.: Surface Tension for Pure Liquids. Chem. Eng., April 1958.

40. Hershey, A. V.: The Physical Review, vol. 56, 1939, p. 204.

41. McGrew, J. L. and Larkin, B. K.: Cryogenic Liquid Experiments in Orbit. Vol. III. Bubble Mechanics. Boiling Heat Transfer and Propellant Tank Venting in a Zero Gravity Environment. NASA Report CR 652, December 1966.

42. Nields, D. A.: Surface Tension and Buoyance Effects in Cellular Convection. Journal of Fluid Mechanics, vol. 19, 1964.

43. Grodzka, P. G.: Zero Gravity Solidification. Lockheed Final Report D148619, NASA Contract NAS8-21123, March 1970.

44. Tien, R. H. and Koump, V.: Effect of Density Change or the Solidification of Alloys. Trans. ASME Journal of Heat Transfer, February 1970, pp. 11-16.

45. Bannister, T. C.: Heat Flow and Convection Demonstration (Apollo 14). Marshall Space Flight Center Internal Report, July 1971.

46. Grodzka, P. G.; Fan, C.; and Hedden, R. O.: The Apollo 14 Heat Flow Convection Demonstration Experiments – Final Results of Data Analysis. Lockheed Missiles and Space Company Report D225333, NASA Contract NAS8-25577, September 1971.

47. Prensner, D. S. and Hsu, G. R.: Thermal Conveciton in Laterally Bounded Air Spaces. Proceedings of the Eighth Southeastern Seminar on Thermal Sciences, 1972, pp. 339-368.

48. Griggs, E. I.: Thermal Capacitor Study. Research Reports, 1971 NASA-ASEE Summer Faculty Fellowship Research Program, September 1971, pp. 208-220.

49. Dyer, J. D. and Griggs, E. I.: Study of the Solidification and Melting of Nonadecane and Hexadecane Including Solid Phase Thermal Conductivity Measurements. Report ME-49, Tennessee Technological University, College of Engineering, June 1975.

50. Thomas, L. J. and Westwater, J. W.: Microscopic Study of Solid-Liquid Interface During Melting and Freezing. Chemical Engineering Progress Symposium Series, vol. 59, no. 41, 1963, pp. 155-164.

51. Bailey, J. A. and Davila, J. R.: An Investigation of the Solidification of a Metal and Two n-Paraffins Using an Acoustic Technique. Applied Science Research, no. 25, 1971, pp. 245-261.

52. Bailey, J. A. and Liao, C.: Thermal Capacitor Design Rationale. Interim Report No. 5. Submitted to Astronautics Laboratory, George C. Marshall Space Flight Center, Huntsville. Alabama, 1973.

53. McAdams, W. H.: Heat Transmission. McGraw-Hill Series in Chemical Engineering, 1954, p. 450.

54. Powell, R. W. and Challar, A. R.: Thermal Conductivity of n-Octadecane. Ind. Engr. Chem., vol. 53, no. 7, July 1961, pp. 581-582.

55. Bailey, J. A. and Liao, C. K.: Thermal Capacitor Design Rationale; Part II-Thermal Analysis. Final Report submitted to NASA-MSFC under Cooperative Agreement NCA8-52 with North Carolina State University.

56. Bentilla, E. W. and Shlosinger, A. P.: Research and Development Study on Thermal Control by Use of Fusible Materials. Northrop Corporation Report No. NSL 65-16, Interim Report under Contract NAS 8-11163 to NASA-MSFC, February 1965.

57. Pizzolato, P. J. and Farmer, R. A.: Phase Change Thermal Control Development. Martin Marietta Corporation, March 1973.

58. Young, C. T. K.; Harper, T. D.; and Ingram, E. H.: PCM-Heat Transfer Improvement Study, Brown Engineering, February 1973.

59. Anonymous: Study of Structural Active Cooling and Heating Heat Sink Systems for Space Shuttle. McDonnell Douglass Corporation, MDC E0479, October 1971

TECHNICAL REPORT STANDARD TITLE PAGE

1. REPORT NO.	2. GOVERNMENT ACCESSION NO.	3. RECIPIENT'S CATALOG NO.
NASA TP-1074		

4. TITLE AND SUBTITLE	5. REPORT DATE
A Design Handbook for Phase Change Thermal Control and Energy Storage Devices	November 1977
	6. PERFORMING ORGANIZATION CODE

7. AUTHOR(S)	8. PERFORMING ORGANIZATION REPORT #
William R. Humphries and Edwin I. Griggs*	M-230

9. PERFORMING ORGANIZATION NAME AND ADDRESS	10. WORK UNIT NO.
George C. Marshall Space Flight Center Marshall Space Flight Center, Alabama 35812	11. CONTRACT OR GRANT NO.
	13. TYPE OF REPORT & PERIOD COVERED
12. SPONSORING AGENCY NAME AND ADDRESS National Aeronautics and Space Administration Washington, D.C. 20546	Technical Paper
	14. SPONSORING AGENCY CODE

15. SUPPLEMENTARY NOTES

Prepared by Structures and Propulsion Laboratory, Science and Engineering

*Associate Professor of Mechanical Engineering, Tennessee Technological University, Cookeville, TN.

16. ABSTRACT

This document gives a comprehensive survey of the thermal aspects of phase change material devices. Fundamental mechanisms of heat transfer within the phase change device are discussed. Performance in zero-g and one-g fields are examined as it relates to such a device. Computer models for phase change materials, with metal fillers, undergoing conductive and convective processes are detailed. Using these models, extensive parametric data are presented for a hypothetical configuration with a rectangular phase change housing, using straight fins as the filler, and paraffin as the phase change material. These data are generated over a range of realistic sizes, material properties, and thermal boundary conditions. A number of illustrative examples are given to demonstrate use of the parametric data. Also a complete listing of phase change material property data are reproduced herein as an aid to the reader.

17. KEY WORDS	18. DISTRIBUTION STATEMENT
	STAR Category 34

19. SECURITY CLASSIF. (of this report)	20. SECURITY CLASSIF. (of this page)	21. NO. OF PAGES	22. PRICE
Unclassified	Unclassified	254	$9.00

* For sale by the National Technical Information Service, Springfield, Virginia 22161

*U.S. GOVERNMENT PRINTING OFFICE: 1977 - 735-078/45